Modelling the Liquid Breakup and Vapour Generation during Accidental Releases of Liquid Fuels

Hany Abdelrahman

Department of Chemical and Biological Engineering

The University of Sheffield, United Kingdom

A thesis is submitted to the University of Sheffield
in partial fulfilment of the requirements for the degree of Doctor of Philosophy

September 2015

Acknowledgements

First and foremost, I wish to give all the praise to Almighty Allah for giving me the strength and time to complete this research.

I would like to express grateful appreciations to my supervisors, Dr. Yajue Wu, for her guidance, advice and encouragement throughout the project.

My special gratitude goes to Dr. Graham Atkinson from the HSE. His valuable experiments and modelling results on flammable liquid release was the mainstay of my model validation.

I sincerely thank my colleague Mahmoud abdelhafiz and my friend Dr. Mahmoud saad for their help and support.

I dedicate this work for my father, mother, mother in law and the spirit of my father in law who prayed for my successful.

I owe my deepest gratitude to my wife, Marwa, and my son, Yassin, for their patience, support, understanding and encouragements.

I am really grateful for the help I got from Dr. Lobna, my sister in law, and also many thanks for my brother and sister.

Finally, I would like to thank the Egyptian Armed Forces for their precious confidence granted to me

This study would not have been possible without the financial support of my sponsor, Technical Research Centre of the Egyptian Armed Forces.

Last but not least, I would like to convey my sincere gratitude to the Egyptian Armed Forces for granting me the chance to fulfil my PhD study in the University of Sheffield.

Summary

In the last few decades, the repeated occurrence of vapour cloud fire and explosion due to the flammable liquid release have demonstrated that safe handling the flammable liquid remains as challenging issue for many industrial fields. There is a lack of numerical models to predict the liquid breakup and flammable vapour cloud formation which could be used for risk assessment of liquid fuel storages.

During the process of liquid release, the bulk liquid could disintegrate into droplets of various sizes. According to the droplet size, liquid properties, temperature and the vapour saturation, a mass fraction of these droplets may transform into vapour during the free-fall. Moreover, the disintegration of the liquid bulk and droplets may induce the development of aerosol fractions which have a significant influence on the vapour generation and vapour cloud dispersion.

This study examines the breakup mechanisms take place during the liquid jet release, and develops models to predict the resulting droplet size distribution and vapour generation from liquid droplets.

The research was aimed at collecting and implementing the numerical and empirical models that describe the different steps of the process of liquid release. All of these models were integrated into a comprehensive numerical package program to describe the process of liquid breakup during fuel release. This package included the primary breakup of liquid jet, the secondary aerodynamic breakup of liquid droplets during free-fall and finally the impingement of falling droplets with solid or wetted surface. The numerical models were validated and verified against the collected results of experimental tests and CFD simulations.

A case study was carried out by analysing the liquid breakup and vapour formation during the devastating incidents that took place in Buncefield, UK, 2005. The estimated results for the proportion of vaporized liquid as calculated by the suggested numerical package were comparable to the estimated results obtained from the survey. The case study demonstrated the influential role of droplet evaporation in overfilling release incidents of fuel storage tanks.

The effect of different parameters on the droplet size distribution and the vaporized fraction during liquid releases were also examined using the developed numerical package. Three different groups of parameters were included in this study. The first group included the release conditions (such as: orifice diameter, the release velocity and the release height). The second group focused on the liquid's physical properties which

include density, viscosity, surface tension, molecular weight and the saturation vapour pressure. The third group was concerned with the environmental conditions which include temperature, relative humidity and vapour saturation.

The analytical results indicated that the liquid's release velocity, temperature, saturation vapour pressure and the vapour saturation are the most predominant factors on both droplet size distribution and the fraction of vaporised liquid. The liquid viscosity, density, molecular weight and surface tension were also important. However, the influence of the release height was limited to low release velocities. The liquid breakup and vapour and vapour formation was less sensitive to orifice diameter and relative humidity.

List of Contents

List of Figures

List of Tables

Nomenclature

Abbreviation

ASTM	American Society for Testing and Materials
ATOM	Atomization
CFD	Computational Fluid Dynamics
CMD	Count Median Diameter
FWI	First Wind Induced
HSE	Health and Safety Executive
LFL	Lower Flammability Limits
MMD	The Mass Median Diameter
RVP	Raid Vapour Pressure
SMD	Sauter Mean (Volume - Surface)
SWI	Second Wind Induced
UFL	Upper Flammability Limits

Symbols

A	Droplet cross-section area, m^2
Cp_{Liq}	Mean heat capacity of the liquid between T_{cont} and T_b, kJ kg^{-1} K^{-1}
C_D	Aerodynamic drag coefficient (dimensionless)
C_c	Dimensionless value of slip correction factor
CC	Monodisperse coagulation coefficient ,m^3/s
$\overline{CC}$	Average coagulation coefficient value
D^*	Equilibrium droplet diameter ,m
D	Droplet diameter ,m
d(D)/dt	Droplet growth rate ,m/s
D_{crit}	Droplet diameter at the instant of equilibrium ,m
D_{ini}	Initial droplet diameter before ,m
D_{mean}	Most probable value of the secondary droplet's diameter ,m
DV	Diffusion coefficient of the vapour molecules ,m^2/s
d_o	Diameter of thin circular tube ,m
D_{10}	Arithmetic Mean (Length)
D_{20}	Surface Mean (Surface Area)
D_{30}	Volume Mean (Volume)
D_{21}	Length Mean (Surface Area - Length)

D_{31}	Length Mean (Volume - Length)
D_{32}	Sauter Mean (SMD) (Volume - Surface)
D_{43}	Herdan Mean (Weight)
D_{peak}	Peak Diameter
$D_{0.999}$	Maximum Diameter
$D_{0.632}$	Characteristic Diameter
$D_{0.1}$	10% of the total droplets volume are smaller than this value
$D_{0.9}$	90% of the total droplets' volume are smaller than this value
E_T	Dimensionless impact energy
f	Vaporized fraction due to flashing
G_{pool}	Evaporation rate from pool, kg m^{-2} s^{-1}
g	Gravity acceleration ,m/s^2
G	Gravitational force on falling spherical droplet, kg m s^{-1}
F	Drag force on falling spherical droplet, kg m s^{-1}
H_v	Mean latent heat of vaporization between T_{cont} and T_b, kJ kg^{-1}
Je	Dimensionless Jet number
K_R	Dimensionless Kelvin ratio
K_n	Knudsen number
K	Splashing Parameter
k	Boltzman contant (1.38×10^{-23} J/K)
L	Breakup length, m
M_{liq}	Liquid molecular weight ,kg $kmo1^{-1}$
m_D	Mass of the formed spherical drop ,kg)
N	Number of resulting droplets from spalshing
n	Particle number concentration ,particle/m^3
n_o	Initial number concentration ,particle/m^3
P_{Sat}	Saturation vapour pressure of the liquid at temperature T, Pascal
P_{Par}	Partial pressure of liquid vapour ,Pascal
P_o	Atmospheric pressure ,Pascal
$P_{par,dry}$	Partial pressures of dry air ,Pascal
$P_{par,wv}$	Partial pressures of water vapour ,Pascal
$P_{par,fv}$	Partial pressures of fuel vapour ,Pascal
$P_{Par,\ drop}$	Vapour partial pressure at the droplet's surface ,Pascal
$P_{sat,wv}$	Saturation vapour pressure of water ,Pascal
$P_{sat,fv}$	Partial pressure of each fuel vapour , Pascal
Q	Exponential growth rate

Q_{max}	Exponential growth rate at the fastest growing disturbances ,s^{-1}
q	Rosin-Rammler distribution parameter.
Re_{ter}	Reynolds number at terminal velocity
r_a	Aerodynamic resistance ,$s.m^{-1}$
r_s	Surface or laminar layer resistance , $s.m^{-1}$
r_t	Transfer resistance dependant on surface characteristics , $s.m^{-1}$
r	Radius or pool side parallel to the wind , m
R	Ideal gas constant , J $kmo1^{-1}$ K^{-1}
Re_{Liq}	Dimensionless liquid Reynolds number
Re_{crit}	Corresponds to the point of change from laminar to transition mode
R_{dry}	Specific gas constants for dry air ,J/kg·K
R_{wv}	Specific gas constants for water vapour ,J/kg·K
R_{fv}	Specific gas constants for fuel vapour ,J/kg·K
$R_{specific}$	Specific gas constant , ,J/kg·K
S_R	Saturation ratio
Sc	Dimensionless Schmidt's number
T	Ambient temperature ,K
T_{cont}	Initial temperature of the liquid before depressurization, ^oK
T_b	Final temperature of the mixture after flashing, ^oK
T_d	Temperature at the droplet's surface , ^oK
t	Acceleration or deceleration time, s
u_w	Wind speed , m s^{-1}
U_L	Liquid velocity at the nozzle exit , $m.s^{-1}$
u_{os}	Threshold velocity for splashing , $m.s^{-1}$
V_{drop}	Instantaneous velocity of the falling droplet, $m.s^{-1}$
V_o	Initial droplet velocities before acceleration or deceleration , $m.s^{-1}$
V_f	Final droplet velocities after acceleration or deceleration , $m.s^{-1}$
V_R	Relative velocity between the droplet and ambient air , $m.s^{-1}$
V_{crit}	Droplet critical velocity of disintegration , $m.s^{-1}$
V_{ter}	Terminal velocity , $m.s^{-1}$
V_d	Dry deposition velocity ,$m.s^{-1}$
v_s	Gravitational settling velocity obtained from Stokes equation , $m.s^{-1}$
v_{bn}	Component of the drop velocity normal to the surface just before impact
VF	Total volume fraction of the droplets smaller than certain diameter
We_{Liq}	Dimensionless liquid Weber number
We_{crit},	Critical Weber's number

We_d	Dimensionless value of the Weber's number at the time of disintegration
We_{Air}	Dimensionless Weber's number of air
W_v	Mass of flashed vapour, kg
W_{il}	Initial mass of liquid before flashing, kg
x	Rosin-Rammler constant
X	displacement of droplets during the same period of time ,m
X_i	Mole fraction of component
Oh	Ohnesorge dimensionless number

Greek Symbols

σ_{Liq}	Liquid surface tension ,N/m
ρ_{Liq}	Liquid density ,kg/m^3
ϕ	Fuchs correction factor.
α_c	Dimensionless condensation coefficient
λ	Mean free path in (µm)
λ_r	Standard value of mean free path equals 0.0664µm
λ_{opt}	Wave length at the fastest growing disturbances ,m
μ_{Liq}	Liquid dynamic viscosity ,kg.s/m^2
μ_{Air}	Viscosity of air , kg.s/m^2
ρ_{Air}	Density of air ,kg/m^3
ν_{Liq}	Kinematic viscosity of liquid ,m^2/s
τ	Relaxation time of aerosol size droplets , s
σ_g	Geometric standard deviation
ψ_{fuel}	Fuel vapour saturation ratio
φ	Relative humidity

Chapter 1: Introduction

1.1 Vapour Cloud Fire and Explosions

Recurrent occurrence of the unanticipated phenomenon of *"dense cloud formation"* preceding the induction of cloud type fires and explosions; have been highly emphasised in the field of research studying the accidental incidents of liquid fuel release. In particular, the likely unforeseen behaviour of the non-volatile liquid fuels. Such phenomenon gave rise to a series of publication studying the industrial incidents reported to the Health and Safety Executive (HSE) in the UK. A statistical overview of more than 14 thousands incidents that took place between 1987 and 2000 revealed that nearly 31% of these incidents were caused by flammable liquid releases (Fowler and Hazeldean, 1998; Fowler and Baxter, 2000; Bradley and Baxter, 2002). In the USA, Wiekema (1984a) conducted a study for 165 vapour cloud accidents found in open literature for the period between 1920 and 1980. In fact, statistical analysis indicated that the total number of minor incident releases was about 8000 around the USA during this period (Badoux, 1985). The aforementioned studies revealed the unexpected recurrence of fuel releases in industrial facilities and storage areas.

1.2 Consequences Due to Loss of Containment

When liquid fuel is accidentally released, liquid vapours might be generated forming hazardous dense vapour clouds. Consequently, the ignition of such clouds may cause fire or explosion incidents. Liquid vapours could be generated in such incidents from either a plane liquid surface, liquid pool, or spherical surface liquid droplets.

In risk assessment frame works, liquid pool is considered the main source of vapours during accidental liquid releases. The formation of liquid pool is a frequent observation despite of the containment cause (tank overfilling, broken pipe, tank wall and valve failure). In addition, evaporation from liquid pool is characterised by relatively long duration and large area of spreading especially when the pool area is unbounded. Although most studies and reports have focused on pool evaporation as a source of vapour generation, the conducted theoretical calculations have proved that this amount of vapour, which may be formed through pool evaporation, is inadequate for many incidents and cannot explain the probably estimated cloud mass that could generate such an intense explosion.

In the last few decades, the generation of liquid vapours from falling liquid droplets are thought to be involved in rationalizing this phenomenon. . These droplets are often formed through different mechanisms of liquid breakup during accidental liquid fuel release. In fact, most researches had focused on liquid releases under superheated conditions (Flash evaporation).This type of release is expected to generate an instantaneous vaporised fraction at the time of release, in addition to the highly efficient liquid fragmentation which produces a large amount of fine droplets. On the contrary, the accidental release of sub-cooled liquids is supposed to be less efficient in generation of vapours due to the relatively large size droplets that result from the mechanical breakup of liquid.

This shallow concept about the non-flashing liquid releases was completely changed since the Buncefield incident took place in 2005 (UK), and afterwards further verifications were based on similar incident scenarios at San Juan (Puerto Rico) in 2009, Jaipur (India) in 2009 and Amuay Refinery (Venezuela)in 2012 (Mishra, Wehrstedt and Krebs, 2014). The vaporisation from liquid cascades during tank overfilling incidents was found efficient to create a flammable vapour cloud (Coldrick, Gant, Atkinson and Dakin, 2011).

In the course of the last ten years, several studies were published in the UK in an attempt to investigate the role of droplet evaporation in the overfilling liquid release induced massive cloud size. An example of these studies is the substantial body of work performed by the Health and Safety Laboratory (HSE) involving a combination of large spill experiments and Computational Fluid Dynamics (CFD) modelling (Atkinson, Coldrick, Gant and Cusco, 2014). The conclusions made from these studies suggested the possible formation of large amount of fuel vapours from cascade droplets. Furthermore, it assured the unique role of droplet splashing in the enhancement of the vaporisation efficiency (Atkinson and Coldrick, 2012a, b).

1.3 Vapour Generation from Liquid Droplets

The evaporation rate from liquid droplet is dependent on large number of factors. These factors include droplet’s diameter, droplet’s velocity, the liquid physical properties, ambient temperature and ambient vapour saturation. In order to quantify the vapour fraction from a large number of droplets in cascade, the most challenging point will be the determination of droplet size distribution resulting from liquid disintegration.

In order to perform this assessment, the mechanisms of liquid breakup and droplet disintegration must be studied in details. Moreover, the estimation of droplet size

distribution and velocity need to be studied as well. The estimation of vaporised fraction from each droplet is characterised by its size and velocity during free-fall.

Accordingly, the mechanisms of liquid bulk breakup and the following droplet disintegration should be taken into consideration when evaluating the potentials of large cloud formation from accidental liquid fuel release. These mechanisms describe three main stages during which liquid droplets might be formed and liquid vapour maybe generated. The first stage is the breakup of bulk liquid into multiple sizes of droplets. The following stage is the free-falling period of time in which liquid droplets may undergo further disintegration often accompanied by droplet evaporation. The final stage, which probably produces additional liquid droplets, is the impingement of falling droplets on either dry or wet surfaces.

The liquid breakup process, especially the droplet splashing process, may lead to the formation of some fine droplets. In presence of air these droplets may further form a colloid known as "aerosols" (Baron and Willeke, 2001).Aerosols are characterised by their ability to float and suspend with air. The formation of aerosols plays an important role in both the generation of liquid vapour and the properties of the formed vapour cloud. The presences of aerosols in addition to the liquid vapour form a "two-phase cloud". Such type of clouds is characterized by different dispersion and flammability behaviour. Furthermore, the formation of airborne aerosol particles could enhances the vaporisation process outside the cascade even when the vaporization inside cascade is lowered due to the high vapour saturation.

1.4 The Absence of Comprehensive Model

Although there is a substantial body of literature associated with released liquid breakup and liquid droplet formation, it has so far failed to produce any well-defined holistic model for droplet formation and liquid vapour generation during accidental liquid fuel releases in industry. Hence, there is a need to implement a comprehensive model in order to estimate the droplet size distribution resulting from liquid breakup and the amount of liquid vapours generated throughout the whole process. Such a model may further assist in studying the main factors affecting these mechanisms and the impact of each factor on the amount of vapour generation. The absence of such a model, which represents a weakness in the risk assessment body construction, spawned the motivation behind the work described in this thesis.

The methodology of this work is based on formulating a comprehensive model package in the form of a computer program. This package will be used to estimate the

liquid droplet size distribution during accidental liquid fuel releases and, subsequently, the amount of liquid vapours generated from liquid droplet evaporation. The results obtained out from this package will be used to perform a sensitivity study on the effect, importance, and role of different parameters affecting the mechanisms of liquid breakup during accidental releases. Conclusions from this study will be expected to express the behaviour of fuel liquids during accidental releases and draw guidelines for implementing and taking into consideration the role of liquid breakup during release incidents in industry.

1.5 Research Objectives and Approach

The aim of this research is to study the mechanism and behaviour of liquid breakup during accidental fuel releases under different conditions. This study will express the influence of droplet size distribution and particularly the presence of fine aerosol droplets on the rate of vapour generation. Thereby, this study is intended to help understand the role of liquid breakup mechanisms in fuel vapour cloud generation which have the potential hazards of fires and explosions.

The objectives of the PhD research project are to:

- Examine the different mechanisms of liquid jet and liquid droplet breakup during accidental fuel release. These mechanisms include the primary breakup of liquid jets, the secondary breakup of liquid droplets during free-fall and the disintegration of liquid droplets caused by impinging on solid or wetted surfaces.
- Implement a comprehensive numerical package to predict the droplet size distribution and the amount of fuel vapour generation during accidental liquid fuel releases.
- Apply the numerical package on the Buncefield incident as a case study, and compare the results with other methods.
- Investigate the effect of different factors on the resulting droplet size distribution and the vapour quantity generated from falling liquid droplets.

The approach of the project will be through:

- Reviewing liquid breakup mechanisms through a literature review.
- Selecting the numerical and empirical equations that describe liquid breakup during the different stages and estimate the resulting droplet size distribution and the amount of vapour generation during liquid release.

- Implementing the numerical package in the form of a computer program and validating the program results with collected experimental and CFD simulation results.
- Applying the numerical package on the Buncefield incident as a case study.
- Executing a sensitivity analysis for the impact of different selected factors on the mechanisms of liquid breakup and vapour generation.

1.6 Thesis Layout

Chapter 1 is a general introduction to the thesis to express the background, motivation, objectives and methodology of the work.

Chapter 2 introduces an overview on the different types of liquid release and the different mechanisms of fuel-air cloud formation. Furthermore, a quick view on the dispersion, flammability and ignition of both vapour clouds and two-phase clouds will be provided.

Chapter 3 illustrates the mechanisms of mechanical liquid breakup. This includes the breakup of liquid jets, the disintegration of liquid droplets and the impinging of liquid droplets on dry or wetted surfaces. In addition, it surveys the numerical and empirical models that describe the droplet distribution. The equations of droplet motion are also discussed.

Chapter 4 discusses the implementation of different models into a comprehensive numerical package, the general structure and the model assumptions.

Chapter 5 presents the detailed steps to convert the implemented numerical package into a visual basic program. The program is designed to estimate the droplet size distribution and the amount of vapour generation during liquid releases.

Chapter 6 discusses the validation and verification of the implemented numerical program. The calculated results are compared with experimental and CFD simulation results.

Chapter 7 introduces a case study of the Buncefield fire and explosion incident. The numerical calculations are used to explain the explosion intensity and the cloud magnitude through the mechanisms of mechanical liquid breakup in such overfilling release incidents.

Chapter 8 presents and discusses the effect of different release conditions on droplet size distribution and rate of vaporisation. The release conditions include liquid release velocity, discharge orifice diameter and release height.

Chapter 9 expresses the effect of liquid physical properties on droplet size distribution and rate of vaporisation. These conditions include liquid density, molecular weight, viscosity, surface tension and vapour pressure.

Chapter 10 presents and discusses the effect of ambient properties on droplet size distribution and rate of vaporisation. These conditions include ambient temperature, relative humidity and fuel vapour saturation. The sensitivity of the breakup mechanism towards each property is studied in this chapter.

Chapter 11 concludes the findings of this work, identifies future research work needed in this field and highlights some useful conclusions for risk assessment methodology in industry.

Chapter 2: Literature Review of Liquid Release and Fuel–air Cloud Formation

2.1 Introduction

Despite the fact that advances in the industrial field have benefited and has facilitated human lives since the Industrial Revolution, industry can create many problems and develop several complications. Pollution and accidents of fires and explosions are considered as critical problems facing industrial countries in the last few decades. For instance, many accidents might happen because of the accidental release of flammable liquids, especially liquid fuels, which are commonly stored and used in industry. Such releases may lead to the formation of an ignitable cloud of fuel and air. For example, Koshy, Mallikarjunan and Raghavan (1995) found that 75% of vapour cloud explosions that took place around the world were in petrochemical units.

This chapter discusses the formation of fuel–air clouds from accidental liquid releases in the following order: Initially, a definition of fuel–air cloud fires and explosions and related definitions will be introduced in Section 2.2. Then, an explanation of the different mechanisms of vapour cloud formation from liquid release will be reviewed in Section 2.3. Finally, a quick overview of the dispersion and ignition of vapour clouds will be summarised in Sections 2.4 and 2.5, respectively.

2.2 Definitions of Fuel–air Cloud Fires and Explosions

2.2.1 General Concept

The release of hazardous materials usually happens due to the loss of process containment, such as failure of pipes, storage vessels or process reactors, or by rapid discharge through a relief system (Crowl, 2003). A fuel–air cloud could be formed when flammable substances (in the form of gas, vapour, fine liquid droplets or solid dust) are released and mix with air, forming a cloud. A part of this cloud may be within the explosion limits. If this part is ignited, the combustion reaction will spread through the whole explosive region of the cloud, rapidly producing energy (Wiekema, 1984b). This phenomenon can be classified into two categories according to the pressure magnitude resulting from the combustion reaction. If the combustion causes a certain overpressure rise, that will produce a fuel–air cloud explosion. If there is no overpressure rise, it is then called a vapour cloud fire or a flash fire (Crowl, 2003). A

fuel–air cloud explosion usually produces a dual destructive effect caused by both a pressure wave and thermal radiation resulting from the produced fireball. The fuel–air explosion becomes "detonation" with devastating effects when the ignition reaction propagates with a velocity of more than 1.5 km/s producing an over-pressure in excess of 1.5 MPa (Moen, 1993). Crowl (2003) summarises the conditions required for the fuel–air to cause a damaging overpressure, saying that the released material must be flammable and the cloud must reach sufficient size and sufficient mixing ratio before ignition takes place. In addition, the flame speed must accelerate during the burning of the cloud. Otherwise, only a fire will be presented and no significant overpressures will be measured.

2.2.2 The Two-phase Fuel–air Cloud

The accidental release of liquid fuels in the air usually forms what are generally called “dense clouds” or “heavier than air clouds”. These clouds are characterised by a density larger than the surrounding environment (Scargiali, Grisafi, Busciglio and Brucato, 2011). The high density of such clouds is caused by the presence of either dense fuel vapours with a molecular weight higher than air, such as most hydrocarbons, or the presence of liquid aerosol droplets.

Liquid aerosol droplets could be described as fine, buoyant droplets within a diameter in a range of 0.001 to 100μm and capable of floating and suspending in a gas medium for an observable period of time (Baron and Willeke, 2001). The term "aerosol" might be applied for any liquid or solid suspended in air for just a few seconds (Vincent, 1995). This characterisation is not so far from that of the solid particles called "dust", which have a typical diameter of less than 76μm (Abbasi and Abbasi, 2007). The liquid aerosol droplets might be formed due to aerodynamic fragmentation (caused by the forces acting on the liquid surface) or thermal fragmentation (caused by rapid evaporation) of the released liquid jet (Razzaghi, 1989).

If the cloud only contains a mixture of fuel vapours with air, it could be called simply a "vapour cloud". Somewhat differently, if the cloud contains a mixture of liquid fuel droplets and fuel vapours, it can be described with the terminology "two-phase cloud" (Makhviladze, Roberts and Yakush, 1999; Tan *et al*., 2012). The general landmark for detecting two-phase cloud formation (*i.e.* the presence of liquid droplets) is the visibility and opaque appearance of such clouds, because most hydrocarbon vapours are colourless and transparent (Nevers, 1992). In some special circumstances, a cloud might be formed of a three-phase mixture, which is known as a "mixed phase cloud" or a

"multiphase cloud". This type of cloud might be rarely formed in case of accidental fuel releases but is typically formed in the upper atmosphere where the environment reaches very low temperatures (Piskunov, Petrov and Golubev, 2003; Long *et al.*, 2010; Yang *et al*., 2003).

The hazards of two-phase clouds containing liquid aerosols are not well understood and are still overlooked (Bowen and Cameron, 1999). Herbert (2010) suggested that vapour cloud explosions studies should take into consideration the factors such as aerosol formation, which might increase the cloud size and density. Analysis of two-phase hazard problems is more difficult and complex than analysis of classical single-phase ones. This complexity is due to the highly transitional nature of the system caused by mechanisms such as evaporation and turbulence (Bowen and Cameron, 1999).

2.3 Mechanisms of Fuel–air Cloud formation from Liquid Release

2.3.1 Overview

Discussion of major accidents happening in industrial and storage areas always refers to the loss of containment of flammable materials. These materials could be found in the gas or liquid state, or as a mixture of liquids and gases. Loss of containment of flammable liquids is one of the reasons for explosion/fire incidents that took place in the last five decades (Chang and Lin, 2006). Such liquid releases are mostly expected to take place through tank holes or broken pipes. The mechanism of liquid release and flammable cloud formation in this case is strongly dependent on the storing and release conditions of the liquid.

When the released liquid is initially stored at conditions above the ambient saturation pressure, the liquid is called "superheated" and this type of release is called "flashing" (Kay, Bowen and Witlox, 2010). Superheated liquid breakup or "flashing breakup" is essentially caused by rapid boiling of a liquid jet and dynamic expansion of the resulting vapours causing shattering of liquid into fine droplets (Cleary, Bowen and Witlox, 2007). However, if this condition does not exist, the released liquid is described as a "sub-cooled" or "non-flashing" liquid jet (Witlox *et al.*, 2010). This type of liquid release is broken-up due to aerodynamic and surface tension forces at the liquid–air interface, and this type of breakup is called "mechanical breakup" (Cleary, Bowen and Witlox, 2007).

Both types of liquid release could subsequently form a single-phase or two-phase dense cloud. This could be a result of vapour and aerosol droplets formation. The liquid droplets resulting from either flashing or mechanical breakup usually appear in the form of a wide range of multi-size droplets. Some of these droplets might be small enough to float and suspend in air, which are the "aerosol droplets". The remaining larger droplets become rainout, forming a liquid pool (Cleary, Bowen and Witlox, 2007). Further fine droplets maybe formed during the free falling of rainout droplets due to aerodynamic fragmentation (Liu, 2000). Furthermore, additional fine droplets might be formed due to impinging of some rainout droplets on surfaces. All the liquid droplets keep interacting with each other and with the surrounding environment during the formation and dispersion of the fuel cloud.

During accidental liquid releases, liquid vapours might be formed instantaneously if the released liquid is superheated. In addition, liquid vapours could be generated in both kinds of release from the evaporation of rainout liquid droplets or evaporation from a liquid pool (Witlox, Harper, Bowen and Cleary, 2007).

The different mechanisms of vapour cloud formation from liquid releases will be reviewed in the next sections. The mechanical breakup of liquid release will be discussed in detail in Chapter 3. Figure 2.1 summarises the different mechanisms of vapour cloud formation from liquid releases.

2.3.2 Flash Release of Superheated Liquids

As mentioned before, the term *flashing* could be used to describe the release of a superheated liquid. The energy produced because of a sudden drop in pressure cannot be contained in liquid in the form of heat. Part of this energy is converted to latent heat of vaporisation (Saury, Harmand and Siroux, 2005). In this case, the resulting liquid jet is usually subjected to rapid boiling, which produces a vapour fraction. The dynamic expansion of these vapours could disintegrate the liquid jet into a range of fine droplets (Cleary, Bowen and Witlox, 2007). The term flashing could also be used to describe the phenomenon whereby liquefied gas stored under pressure is released to normal atmospheric pressure. In this case, part of the liquid will boil to vapour whereas the remaining liquid will be cooled down to its boiling point at atmospheric pressure (Lautkaski, 2008).

The flash fraction is often determined assuming isenthalpic depressurisation. Hence, any form of energy transfer between the liquid jet and the surrounding environment is neglected (Bricard and Friedel, 1998). The initial percentage of liquid flashed into

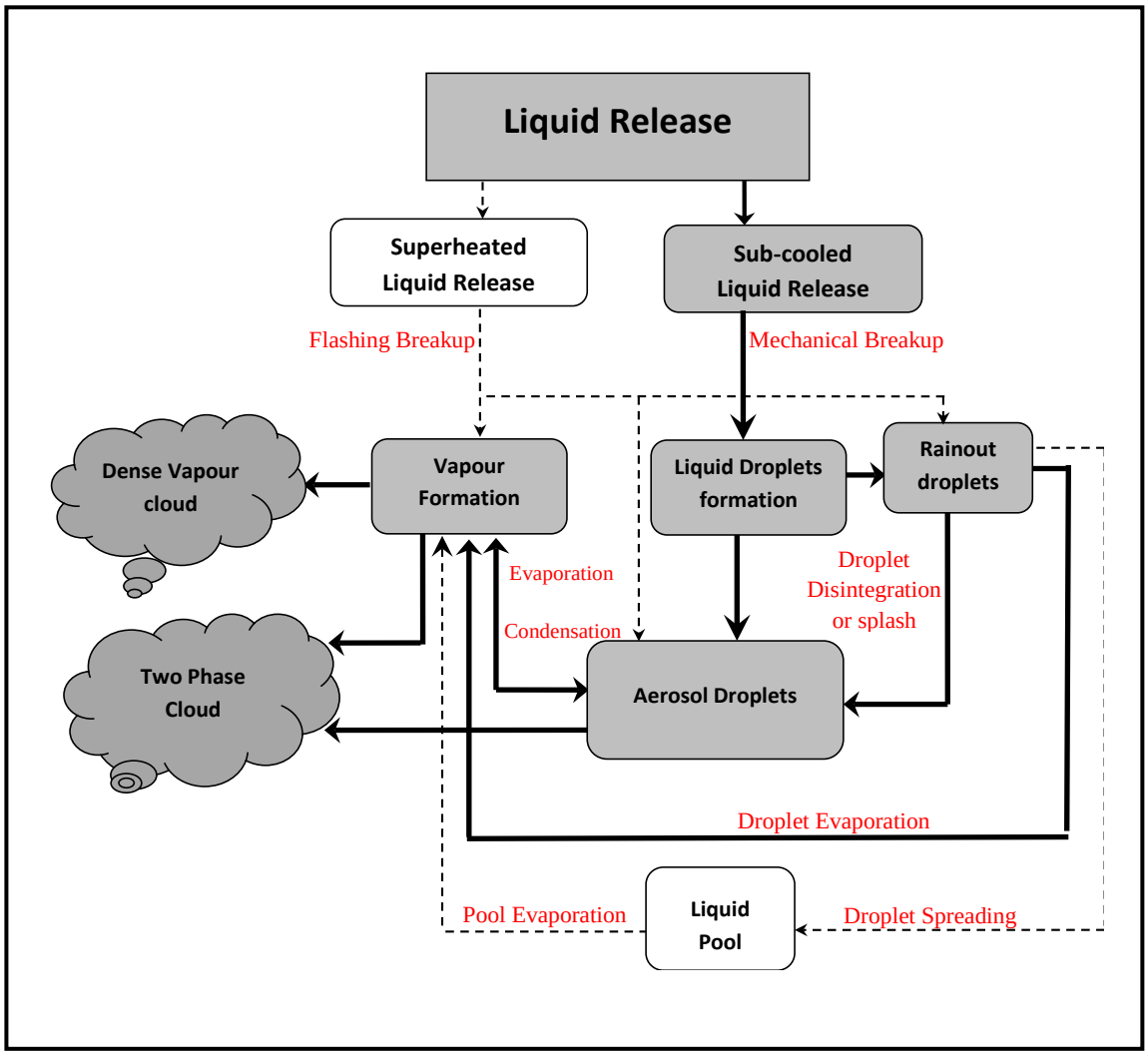

Figure 2.1 Different mechanisms of vapour cloud formation from liquid release

Vapour is called the "vaporisation fraction". The mass transfer rate due to flashing might reach 10 to 12 times the usual rate due to normal evaporation (Petekson, Grewal and EL-Wakil, 1984). The value of this fraction (f) could be estimated as follows (Casal, 2008):

$$f = \frac{W_v}{W_{il}} = 1 - e^{\frac{Cp_{Liq}\left(T_{cont} - T_b\right)}{\Delta H_v}} \qquad \text{eq 2.1}$$

Where f is the vaporization fraction, T_{cont} is the initial temperature of the liquid before depressurization (^oK), T_b is the final temperature of the mixture (^oK), W_v is the mass of vapour (kg), W_{il} is the initial mass of liquid (kg), H_v is the mean latent heat of vaporization between T_{cont} and T_b ($kJ.kg^{-1}$) and Cp_{Liq} is the mean heat capacity of the liquid between T_{cont} and T_b ($kJ\ kg^{-1}\ K^{-1}$).

A few decades ago, modelling of liquid flash vaporisation assumed that the flash vapour fraction is the only contributor to the cloud. The remaining liquid was supposed to fall down forming a liquid pool (Lautkaski, 2008). On the contrary, contemporary experimental studies prove that most of the formed liquid droplets are presented as an aerosol, and rarely are rainout droplets expected. These fractions of floating droplets also contribute to the cloud and later it might be completely vaporised. For this reason, the real value of the flash fraction is expected to be higher and is sometimes suggested to be double the value calculated from classical models (Casal, 2008).

The flashing process is generally caused by a sudden pressure drop, turning the liquid vigorously into a superheated state. This change is more violent at the surface layer, creating a very heterogeneous temperature profile composed of superheated, saturated and sub-cooled liquid (Petekson, Grewal and EL-Wakil, 1984). The breakup of the liquid jet into droplets during the flashing process might take place through mechanical and thermal fragmentation mechanisms. The type of thermal fragmentation is caused by vapour bubbles that spread the liquid into thin layers. When these bubbles are ruptured, liquid layers could be split into fine droplets (Razzaghi, 1989).

Brown and York (1962) studied the sprays formed when hot water is released at pressures up to 1 MPa and different temperatures ranging from 360 to 378 K compared to the atmospheric conditions. The empirical correlation achieved from their results implies that both aerodynamic and thermal effects are important in determining droplet sizes.

Liquid breakup through the thermal fragmentation process usually produces a relatively high population of small droplets (<150μm); these droplets are usually entrained by aerosol droplets (Witlox and Bowen, 2001). Bigot, Touil, Bonnet and Lacôme (2005) performed two pilot-scale experiments and found that most of the droplet population are smaller than 150μm. On the other hand, some large droplets unexpectedly have a count of more than 85% of the liquid mass.

2.3.3 Evaporation from a Liquid Pool

The rainout droplets that fall to the ground during accidental liquid releases, either superheated or sub-cooled liquid fuel, usually form a liquid pool. Heat conduction to this pool from the ground, atmosphere or even radiation from solar energy may cause the liquid to start vaporising. The mechanism of pool evaporation is supposed to participate in vapour cloud formation in many accidents.

In order to estimate the evaporation rate from this mechanism, the pool surface area must be calculated in accordance to release type and the presence of dikes. Then, the mass evaporation rate can be determined depending on the pool area and physical properties of both the released liquid and the surrounding environment. If the liquid pool is surrounded with a bund or dike, the pool area can be directly calculated depending on the shape of the bund. If not, the pool spreading area should be estimated numerically with time. Kim, Do, Choi and Han (2011) have simplified a physical model for liquid pool spreading during instantaneous and continuous spills. In addition, the mass evaporation rate depends on whether the released liquid is boiling or not. When the spilled liquid is at boiling point and it is colder than the surrounding temperature, it is called a boiling liquid. In this case, the liquid will gain energy by conduction from the ground as long as the temperature difference between the liquid and the ground is noticeable. With the progress of time, the influence of heat conduction from the ground decreases and the role of solar heat radiation becomes dominant (Brambilla and Manca, 2009). On the other hand, when the spilled liquid is non-boiling (*i.e.* both ambient and storing temperature are lower than the liquid's boiling point), liquid evaporation will take place through vapour diffusion. This diffusion happens due to the difference between the saturated vapour pressure and the partial pressure of the liquid vapour. Liquid vapour diffusion above the pool surface can be enhanced with higher wind speed and is strongly dependent on temperature. The evaporation rate can be estimated from the following equation (Casal, 2008):

$$G_{pool} = 2\times10^{-3}\, u_w^{0.78}\; r^{-0.11}\, \frac{M_{liq}\, P_o}{R\, T} \ln\left(1+\frac{P_{Sat}-P_{Par}}{P_o-P_{Sat}}\right) \qquad \text{eq2.2}$$

Where G_{pool} is the evaporation rate (kg m $^{-2}$ s $^{-1}$), u_w is the wind speed (m s $^{-1}$), r is the radius of the circular pool or the length of the side of the rectangular pool parallel to the wind (m), M_{liq} is the liquid molecular weight (kg kmo1^{-1}), R is the ideal gas constant (expressed in J kmo1^{-1} K $^{-1}$), T is the ambient temperature (K), P_{Sat} is the saturation vapour pressure of the liquid at temperature T (Pa), P_{Par} is the partial pressure of liquid vapour (Pa) and P_o is the atmospheric pressure (Pa).

If $P_{par} < 2.104$ Pa, the above equation could be simplified as follows:

$$G_{pool} = 2\times10^{-3}\, u_w^{0.78}\; r^{-0.11}\, \frac{M_{liq}}{R\, T} \ln\left(P_{liq}-P_{amb}\right) \qquad \text{eq 2.3}$$

2.3.4 Aerosol Formation Due to Vapour Condensation

2.3.4.1Basic Principles

In a fuel–air cloud, the fuel vapours could occupy part of the volume in addition to the normal air components and possibly some water vapour. The percentage of this part is typically the partial pressure (P) of these vapours in this gaseous mixture. At certain ambient conditions of pressure and temperature, each gaseous component has a pressure value at which the vapour is in mass equilibrium with the condensed vapour. This value is called the "saturation vapour pressure" (P_s). The value of the saturation vapour pressure for each vapour constituent can be estimated from Antoine's equation (Appendix A1). The ratio between vapour partial pressure and the value of saturation vapour pressure is called the saturation ratio "S_R" (Hinds, 1999), as seen in Equation 2.4:

$$S_R = \frac{P_{Par}}{P_{sat}} \qquad \text{eq 2.4}$$

Where S_R is the saturation ratio.

If the value of the saturation ratio is larger than unity, the gaseous mixture is then called "super-saturated" with vapour. In this case, the number of molecules moved from the gaseous to the condensed phase is larger than the number of molecules moved in the opposite direction. If the value of the saturation ratio is smaller than unity, the vapour is unsaturated.

2.3.4.2Types of Aerosol Formation

Formation of liquid aerosol droplets by condensation is the common principle of aerosol formation in nature. In most cases, this process requires the presence of nuclei or an ion particle and the existence of a super-saturation condition (Hinds, 1999). This condition could be achieved by adiabatic expansion or simultaneous processes of heat and mass transfer (Hidy, 1984). Mist, for example, is formed by sudden expansion or cooling of a high saturation vapour cloud (Eckhoff, 2005).

The formation of liquid droplets through vapour condensation could be created by two different mechanisms. First is the homogeneous condensation or self-nucleation, in which condensation takes place at high saturation ratios (usually 2–10) without the presence of any condensation nuclei or ion. This type can occur for gases and vapours, but rarely in water. The super-saturation condition required for homogeneous

condensation for a certain liquid at a given temperature is known as the "critical saturation ratio" (Hinds, 1999).

The other mechanism for vapour condensation is "nucleated condensation" or "heterogeneous nucleation". This type of condensation is promoted by the presence of small soluble nuclei, insoluble nuclei or ions. Unlike homogeneous condensation, nucleated condensation could take place at super saturation ratios of only a few percent. Heterogeneous condensation on soluble nuclei is supposed to be the most common mechanism of vapour condensation. In this case, condensation can happen even in unsaturated conditions (Hinds, 1999). Soluble nuclei are the type responsible for the formation of water droplets in the atmosphere, where the nuclei are supposed to be the sodium chloride formed by the action of oceans waves and bubbles.

2.3.5 Growth and Diminution of Liquid Droplets

2.3.5.1 Basic Principle of Droplet/vapour Equilibrium

The process of evaporation and condensation is the most important relation between liquid droplets and the surrounding environmental gas mixture. At equilibrium conditions, 10^{23}gas moleculescm^{-2}sec^{-1}usually impinges the droplet surface. At the same time, the same number of molecules leaves the surface for the gaseous environment (Williams and Loyalka, 1991).

Once they have been formed, the process of interaction with the surrounding gas will start. The magnitude and direction of such a process are dominated by many factors such as the partial pressures of the gas constituents, the molecular properties of each constituent, the particle sizes and the ambient temperature (Williams and Loyalka, 1991).

The saturation ratio (S_R) might be the most important factor controlling the mechanisms of aerosol particle formation, which is called the “nucleation”. Subsequently, it controls the growth and diminution of the formed liquid droplets. In homogeneous condensation, typically an $S_R > 4$ is required to form the liquid droplets in the absence of condensate nuclei (Vincent, 1995), and this value is inversely proportional to temperature (Hinds, 1999). On the contrary, nucleated condensation could take place at much lower saturation ratios.

As previously discussed, liquid and vapour phases come into mass equilibrium at a unity saturation ratio. This statement is not completely accurate when describing the case of liquid droplets. The droplet surface curvature could slightly modify the

attractive forces between surface molecules (Hinds, 1999). Therefore, it always needs higher partial pressure values to reach the equilibrium condition. This amount of pressure increase is inversely proportional to the droplet size (Baron and Willeke, 2001). Thisis called the Kelvin effect. The modified saturation ratio required for the mass equilibrium of spherical droplets could be estimated from the Kelvin or Thomson–Gibbs equation (Hinds, 1999):

$$S_R \text{ required for mass equilibrium for size } D^* = K_R = \frac{P_d}{P_s} = \exp\left(\frac{4\,\sigma_{Liq}\,M_{Liq}}{\rho_{Liq}\,R\,T\,D^*}\right) \quad \text{eq 2.5}$$

In Equation 2.5, D^* is the equilibrium droplet diameter (m), σ_{Liq} is the liquid surface tension, ρ_{Liq} is the liquid density (kg/m^3) and K_R is the dimensionless Kelvin ratio.

2.3.5.2Liquid Droplet Growth by Condensation

Once a liquid droplet is formed, either by homogeneous or heterogeneous mechanism, and the droplet diameter has passed the equilibrium diameter for the existing saturation ratio, the droplet will start to grow by condensation. The growth rate in this case is dependent on droplet diameter and the saturation ratio. In addition, the relation between droplet diameter and the mean free path can also affect the arrival rate of vapour molecules to the droplet's surface (Hinds, 1999). For ultra-fine droplets of diameter smaller than the mean free path, the vapour molecules' arrival rate is governed by the kinetic theory of gases. On the contrary, the rate of molecular diffusion to the droplet surface governs the arrival rate if the droplet's diameter is larger (Baron and Willeke, 2001). The rate of growth in both cases could be estimated according to the following equations:

$$\frac{d(D)}{dt} = \frac{2\,\alpha_c\left(P_{Par} - P_{Par,\,drop}\right)}{\rho_{liq}\sqrt{2\,\pi\,R\,T/M_{Liq}}} \qquad \text{for } D < \lambda \qquad \text{eq 2.6}$$

$$\frac{d(D)}{dt} = \frac{4\,DV\,M_{Liq}}{R\rho_{liq}D}\left(\frac{P_o}{T} - \frac{P_{Par,\,drop}}{T_d}\right)\phi \qquad \text{for } D > \lambda \qquad \text{eq 2.7}$$

Here d(D)/dt is the growth rate (m/s), α_c is the dimensionless condensation coefficient, P_{Par} is the vapour partial pressure in the neighbourhood of the droplet (Pa), $P_{Par,\,drop}$ is the vapour partial pressure at the droplet's surface (Pa), P_o is the pressure refers to conditions removed from the droplet (Pa), T_d is the temperature at the droplet's surface (^{o}K), DV is the diffusion coefficient of the vapour molecules (m^2/s), λ is the mean free path (μm), ϕ is the Fuchs correction factor and D is the droplet diameter (m).

The condensation coefficient (α_c) could be approximately 0.04, which represents the fraction of sticking molecules in the total arriving molecules (Barrett and Clement, 1988). Where the Fuchs factor (ϕ) is a correction value to solve the complications of mass transfer governed by diffusion within one free path from the droplet surface (Baron and Willeke, 2001), the value of the Fuchs correction factor could be estimated as follows (Davies, 1978):

$$\phi = \frac{2\lambda + D}{D + 5.35\left(\lambda^2/D\right) + 3.42\lambda} \qquad \text{eq 2.8}$$

Under the condition of slow droplet growth, $S_R < 1.05$, droplet temperature is expected to be similar to ambient temperature ($T_d = T_\infty$), and Equation 3.31 should be more simple. For the growing faster droplets, the difference between droplet and ambient temperatures becomes significant and should be taken into account. In this case, droplet temperature could be estimated by the following simplified empirical equation (Hinds, 1999):

$$T_d = T_\infty + \frac{\left(6.65 + 0.345\,T_\infty + 0.0031\,T_\infty^2\right)\left(S_R - 1\right)}{1 + \left(0.082 + 0.00782\,T_\infty\right)S_R} \qquad \text{eq 2.9}$$

Here T_d and T_∞ are expressed in °C. This equation is valid for saturation ratios ranging from 0 to 5, and ambient temperatures from 0 to 40°C.

Furthermore, the time required for growth from d_1 to d_2 could be estimated from Equation 2.7 by integration over the size limit as follows (Boron and Willeke, 2001):

$$t = \frac{R\,\rho_{Liq}\left(D_2^2 - D_1^2\right)}{8\,DV\,M_{Liq}\left(\frac{P_o}{T_\infty} - \frac{P_{Par,\,drop}}{T_d}\right)} \quad \text{for } D_1 >> \lambda \qquad \text{eq 2.10}$$

2.3.5.3Vapour Generation from Droplet Evaporation

The evaporation process is typically the reverse process of condensation since the number of molecules leaving the droplet's surface is larger than the number merging. Another fundamental difference between the two processes is that the evaporation has no stopping condition similar to the starting condition in the case of condensation. Therefore, once the droplet starts to evaporate, the process will continue until the droplet evaporates completely (Hinds, 1999).

The rate of evaporation could be estimated from the same equation that governs the condensation growth rate. The value of the diminution rate will have a negative sign

indicating the size decrease. Equation 2.10 could also be used for estimating the evaporation time. Presently, it should be called the “life time” or “drying time”. The equation should be modified by exchanging the positions of pressures and temperatures, and assuming that the final diameter equals zero. The final equation form is expressed as:

$$t = \frac{R\,\rho_{Liq} D^2}{8\,DV\,M_{liq}\left(\frac{P_{Par,drop}}{T_d} - \frac{P_o}{T_\infty}\right)} \quad \text{for } D > 1.0\,\mu m \qquad \text{eq 2.11}$$

In 1959, Fuchs examined the evaporation of the moving droplets theoretically and experimentally. For the droplets moving in the Stokes’ region, it was found that evaporation increases on the droplet’s front face. This amount of increase is usually balanced with another amount of decrease on the rear. Therefore, the conclusion was that overall evaporation rate is not affected by a droplet’s motion.

2.4 Dispersion of a Fuel–air Cloud

2.4.1 Vapour Cloud Dispersion

When a toxic or flammable cloud is formed from liquid release, the constituents of this cloud will be transported under the effect of both diffusion and wind motion. This motion causes a development in cloud shape, size and particle distribution inside the cloud. This process is called "cloud dispersion".

In general, gases or vapours can be heavier than air because of their higher density. The air density is 1.2041 kgm^{-3} At 20 °C and 101.325 kPa. There are many reasons that can lead to a substance being heavier than air. Alp and Matthias (1991) summarised the reasons that can lead substances to be described as heavier than air. The first reason is simply that the substance itself could have a larger-than-air molecular weight. In fact, most hydrocarbon fuels have a larger molecular weight than air, which is 28.97 $gmol^{-1}$. The second reason is the increase of density because of cooling, and the reason for this cooling might be the flashing process. Another important reason might be the presence of aerosol liquid droplets, which will directly increase the cloud average density according to the high density of liquids relative to gases. Another reason expressed by Koopman, Ermak and Chan (1989) is the incidence of some types of chemical reactions that produce heavy molecular weight gaseous or liquid products. For example, when N_2O_4 gas is released, it will disintegrate directly to NO_2, which reacts with water vapour forming fine droplets of liquid nitric acid. Similar to this case is the behaviour of

hydrogen fluoride gas. Although its molecular weight seems to be lower than air, HF usually forms polymers up to $(HF)_8$, which means that the molecular weight is up to 160 $gmol^{-1}$ (Puttock*et al*., 1991).

The dispersion and spreading of heavier than air clouds have different behaviours. Such clouds can displace the atmospheric flow field and spread both in upwind and lateral directions. In addition, these clouds can resist atmospheric turbulence dilution by forming stable and dense layers (Spicer and Havens, 1996). A large number of mathematical models have been developed to describe the dispersion of such dense clouds (Blackmore, 1982).

2.4.2 Two-phase Cloud Dispersion

The dispersion modelling of two-phase clouds is more complicated than the dispersion of normal single-phase dense clouds. This complication may result from the continuous interaction between the airborne liquid droplets and the surrounding vapour. The interaction of evaporation and condensation processes may cause tangible and continuous changes in the temperature and composition of the cloud (Pattison, Martini, Banerjee and Hewitt, 1998).

Contrary to gas behaviour, the motion of aerosol droplets is controlled by inertial forces rather than random molecular motion. The role of these forces is directly proportional to both droplet size and liquid density (Eckhoff, 2005). Furthermore, the turbulence and other convective movements have a tangible effect on aerosol particles through increasing their floating time. The presence of a liquid aerosol seems to extend the hazardous range where clouds could for persist longer and extend further (Woodward, 1989; Bowen and Cameron, 1999). Bricard and Friedel (1998) expressed the role of aerosols in extending the range and duration of two-phase clouds. One of the influencing effects is the evaporating process of aerosol droplets, which might dramatically cool down the environment and even the liquid jet itself. When a liquid jet is cooled down, the density increases and thus the discharge mass flow-rate becomes higher. On the other hand, cooling down the cloud makes the vapour density higher; even small molecular weight gases may become heavier than air. Furthermore, the cooling process may push the air humidity to condensate or, sometimes, to form ice particles. Finally, the presence of aerosol droplets could enhance the turbulent structure of the jet bringing more breakup quality and higher evaporation quality.

2.5 Flammability and Ignition of Fuel–air Cloud

2.5.1 General

The ignition probability of a fuel–air cloud depends on many factors, such as fuel type, fuel concentration and strength of the ignition source. In general, ignition takes place when an ignition source with sufficient strength interacts with a flammable fuel–air cloud with a suitable fuel concentration in air. Each type of fuel has an upper and lower limit of concentration called the flammability limit or flammability concentration limit. If the concentration is below the lower flammability limit (LFL), the amount of fuel is not enough to support the ignition process. On the other hand, if the concentration is above the upper flammability limit (UFL), the oxygen level is too low for the ignition to take place (Casal, 2008). Flammability limits are usually obtained experimentally (Bjerketvedt, Bakke and Wingerden, 1997), and these limits are highly dependent on both pressure and temperature. In general, the flammability range becomes wider when either pressure or temperature increases (Kondo, Takizawa, Takahashi and Tokuhashi, 2011).

The required ignition source strength is highly dependent on fuel type and fuel concentration. Therefore, some ignition sources of a specific strength may sufficiently ignite a cloud with a certain concentration while other sources do not (Bjerketvedt, Bakke and Wingerden, 1997). For example, when the ignition source is strong enough, the gas cloud will be ignited when the edge of the cloud reaches the ignition source. However, if the source is weak, it may fail to ignite the cloud at an early stage of dispersion or ignite only a small part of the cloud.

2.5.2 Flammability and Combustion of Liquid Aerosols

The presence of a liquid aerosol is believed to have a great impact on a cloud's flammability and burning properties. Kletz (1999) argued that clouds containing aerosols can explode under different conditions. This conclusion is dependent on experiments performed by Kohlbrand (1991), which have confirmed that fine droplet explosionstake place in conditions considered completely safe for fuel–air mixtures with the absence of such droplets. Regardless of the liquid boiling point, the fine combustible liquid droplets of diameter smaller than 100μm and droplet mass concentration ranging between 100 and 500gm^{-3} are generally explosive (Eckhoff, 2005).

The aerosol flammability is mainly dependent on aerosol droplet size and droplet volume concentration. Bowen and Cameron (1999) believe that fine liquid droplets in the range of 7 to 15μm can burn faster than vapours. The mechanism of flame propagation was found to be completely different between droplet sizes smaller than 7μm and larger than 40μm (Burgoyne and Cohen, 1954). Further experiments have indicated that the presence of droplets may develop the propagation velocity through combustible homogeneous mixtures (Mizutani and Nakajima, 1973a; Mizutani and Nakajima, 1973b; Polymeropoulos and Das, 1975). In general, the flammability of aerosols usually increases when the droplet volume concentration increases or the aerosol droplet size decreases (Lian, Mejia, Cheng and Mannan, 2010).

Chapter 3: Literature Review of the Mechanisms of Mechanical Liquid Breakup

3.1 Introduction

Mechanical breakup is the process in which a liquid might disintegrate into various sizes of droplets due to the effect of mechanical forces. When a liquid is accidentally released, liquid droplets of various sizes maybe formed through different and successive disruptive mechanisms. These mechanisms are strongly dependent on the features of liquid geometry and release conditions. The liquid dripping might be the simplest mechanism of liquid drop formation; this usually happens when a liquid slowly flows from a small diameter outlet (Liu, 2000).

One of the most prevalent forms of mechanical breakup is the breakup of a liquid jet into liquid droplets. The mechanism happens due to interaction between the liquid bulk (dispersed phase) and the surrounding medium (continuous phase). In the absence of any external forces, two forces affect the stability of a releasing liquid bulk. The liquid surface tension always tries to pull the liquid into the form of sphere, which has the lowest surface energy. On the other hand, the liquid viscosity tries to oppose and stand against any deformation in liquid geometry (Lefebvre, 1989). The liquid breakup takes place when the external disruptive forces exceed the internal liquid surface tension forces. The effect of aerodynamic forces on the liquid surface may outweigh the balance toward the deformity of the liquid bulk. This lack of balance may appear in the form of disturbed oscillations. In certain circumstances, these oscillations may reach a certain limit at which the liquid bulk is capable of disintegrating into droplets. This process is often called primary breakup, primary disintegration or primary atomisation (Liu, 2000). The comprehension of the physics of this type of breakup is still incomplete, and exact correlations describing the mechanism are still debatable (Eckhoff, 2005).

Another form of liquid mechanical breakup is the breakup of liquid drops due to dynamic pressure, surface tension and viscous forces. This kind of breakup could take place when liquid droplets move with sufficient velocity through another fluid. The breakup is achieved when the aerodynamic drag forces equalise the surface tension forces (Lefebvre, 1989). For each liquid droplet falling with a certain velocity into a gaseous environment, there exists a maximum stable size. After the primary step of liquid breakup into various droplet sizes, some of these droplets may become

aerodynamically unstable because of their sizes. As a result of the aerodynamic forces on such droplet surfaces, these droplets may undergo further disintegration into smaller ones (Lefebvre, 1989). This process is called the secondary breakup, secondary disintegration, or the secondary atomisation of liquid droplets (Liu, 2000).

The primary breakup of a liquid jet and the secondary breakup of the resulting droplets could be described as synchronous or inseparable processes. Therefore, the first stable droplet size distribution resulting from the liquid jet release always appears after both steps take place (Lefebvre, 1989). In this work, the term "primary stage" is used to indicate the whole process of the primary breakup of a liquid jet and the instantaneous secondary breakup of liquid droplets.

After this stage, the falling liquid droplets may show some evolution in size due to evaporation, condensation, coalescence or coagulation. Moreover, the droplet velocity may express some changes due to acceleration or deceleration. Because of these changes, some of the droplets may undergo disintegration due to aerodynamic instability.

Another form of mechanical breakup of liquid droplets is breakup due to collision. The collision of liquid droplets may take place between two or more droplets, or between droplets and a solid or wetted surface (Liu, 2000). The phenomenon of collision between falling droplets is rare and unlikely to happen (Baron and Willeke, 2001). In most cases, falling droplets collision leads to coalescence or coagulation rather than droplet breakup. In addition, this type of collision is a very complicated process and extremely difficult to be described theoretically (Brenn, 2011). When a liquid droplet impinges on a surface, it could spread or bounce. Under certain conditions of impact velocity and impinging surface characteristics, the impinging droplet may disintegrate, producing smaller droplets. This type of droplet breakup is called "splashing" (Liu, 2000).

Each mechanical breakup mechanism, including liquid bulk breakup and liquid droplet breakup, produces multiple sizes of liquid droplets, including droplets of floating aerosol sizes. Therefore, it is very important to estimate the droplets' size distribution after each step during the whole scenario of accidental liquid releases. This quantitative analysis provides information about the liquid fractions incorporated into the gaseous cloud in the form of aerosol droplets. In addition, estimating the sizes of falling droplets is essential to estimating the fraction of generated vapours.

This chapter presents the different mechanisms of mechanical liquid breakup. This includes liquid dripping in Section 3.2, the primary breakup of liquid jets in Section 3.3,

secondary breakup of liquid droplets in Section 3.4 and the impinging of falling droplets on surfaces in Section 3.7. The numerical and empirical equations for estimating the resulting particle size distribution after each process are also discussed throughout the chapter. In addition, the equations describing the motion of falling liquid droplets are reviewed in Section 3.5, and the phenomenon of droplets coagulation is highlighted in Section 3.6.

3.2 Liquid Dripping

Liquid dripping is the simplest mode of droplet formation. This kind of breakup is characterised by individual and large droplets output. In general, this phenomenon could happen by two different mechanisms. The first mechanism occurs when liquid flows slowly from the end of a thin tube. In this case, the droplets appear to be hanging due to the effect of surface tension forces. At a certain droplet mass, gravity forces can exceed the cohesive forces and the droplets are pulled away (Liu, 2000). If the liquid velocity is increased to a certain value, the dripping mechanism transfers to a continuous laminar jet flow (Liu, 2000). The mass and diameter of such formed droplets are estimated from the following equations (Lefebvre, 1989):

$$m_D = \frac{\pi d_o \sigma_{Liq}}{g} \qquad \text{eq 3.1}$$

$$D = \left(\frac{6 d_o \sigma_{Liq}}{g \rho_{Liq}} \right)^{1/3} \qquad \text{eq 3.2}$$

Where d_o is the diameter of thin circular tube (m), m_D is the mass of the formed spherical drop (kg) and g is the gravity acceleration (m/s^2) .

The other form of dripping mechanism is the formation of liquid drops from a liquid film gliding on the bottom of a flat horizontal surface. This mechanism is also stimulated by the effect of gravity force against the liquid surface tension force. The size of the formed drops in this case can be estimated from the balance between gravity and surface tension forces using the following expression (Lefebvre, 1989):

$$D = 3.3 \left(\frac{\sigma_{Liq}}{g \rho_{Liq}} \right)^{0.5} \qquad \text{eq 3.3}$$

3.3 The Primary Breakup of Liquid Jets

The process in which bulk liquid disintegrates into drops is generally called the "atomisation" process. This approach is usually motivated under the influence of the

development of waves on a liquid surface (Bayvel and Orzechowski, 1993). These waves could be generated due to both internal and external causes (Lefebvre, 1989). The internal causes may proceed due to the disturbances inside the atomizer, liquid expansion due to pressure drop and liquid motion on the orifice edge. The external causes always refer to the aerodynamic forces caused by the liquid's interaction with the surrounding gaseous environment. The amplitude of such forces is dependent on many factors, such as relative velocity between liquid and gas, the gas density and the nozzle dimensions. The disintegration of bulk liquid is more liable when the liquid is in the form of a jet or sheet because these forms are characterised by the highest surface energy (Bayvel and Orzechowski, 1993).

3.3.1 The Theory of Jet Breakup

The first model for solving the breakup of liquid jets was expressed by Lord Rayleigh in 1878. The solution only took into consideration the effect of surface tension forces on axisymmetrical wave disturbance. The model was limited only to the breakup of a cylindrical jet of non-viscous liquids under laminar flow conditions in a vacuum. Later on, Rayleigh extended his work to account for the effect of the liquid viscosity as well (Bayvel and Orzechowski, 1993). The jet instability is generally caused by interfacial tension in the form of long disturbance waves (Kinoshita, Teng and Masutani, 1994). In his work, Lord Rayleigh assumes that the liquid jet becomes unstable only if the axisymmetrical disturbance wavelength develops to exceed the value of the jet perimeter (Liu, 2000).

Rayleigh's contribution assumed that the jet breakup is a dynamic problem; hence the rate of collapse is important (Lefebvre, 1989). The axisymmetric jet disturbances grow in time with an exponential rate called the exponential growth rate of disturbances "q" (Lin, 2003). At the fastest growing disturbances, the exponential growth rate (q_{max}) and the corresponding wavelength (λ_{opt}) could be estimated from the simplified model of Rayleigh as follows (Liu, 2000; Lefebvre, 1989):

$$Q_{max} = 0.97\left(\frac{\sigma_{Liq}}{\rho_{Liq}\, d_o^3}\right)^{0.5} \qquad \text{eq } 3.4$$

$$\lambda_{opt} = 4.51\, d_o \qquad \text{eq } 3.5$$

Where Q is the exponential growth rate (s^{-1}), Q_{max} is the exponential growth rate at the fastest growing disturbances (s^{-1}) and λ_{opt} is the wavelength at the fastest growing disturbances (m).

The liquid jet breakup in this case is supposed to generate uniform size droplets of nearly 1.89 times the value of jet diameter at uniform spacing (Liu, 2000; van Rijn, 2004). Another study performed by Lee *et al*. in (1979) considers a smaller wavelength value of nearly $3.14d_o$ at the maximum growth rate.

Due to the significant limitations of the Rayleigh model, many researchers afterwards tried to expand the model's scope in order to generalise the theory for viscous liquids. In addition, the surrounding gaseous medium is supposed to affect the process of liquid jet breakup.

The first extension for the original theory was achieved by Weber in 1931. In his theory, Weber considered the effect of aerodynamic forces on jet instability. Furthermore, the theory involves both viscous and non-viscous liquids in order to investigate the effect of liquid viscosity on the breakup of liquid jets. In addition, Weber suggested that small wavelength disturbances "λ_{min}", which are equal to the jet circumference, maybe amplified to cause a jet breakup. The dynamic viscosity was found to increase the optimum wavelength and has no effect on the minimum wavelength. The relative velocity between the jet and the surrounding air shortens both the minimum wavelength and the optimum wavelength. The optimum wavelengths for viscous and non-viscous liquids were expressed as follows (Liu, 2000):

$$\lambda_{opt} = \sqrt{2\pi}\, d_o \left(1 + \frac{3\mu_{Liq}}{\sqrt{\rho_{Liq}\sigma_{Liq}\, d_o}}\right)^{0.5} \quad \text{For viscous liquid} \qquad \text{eq 3.6}$$

$$\lambda_{opt} = 4.44\, d_o \quad \text{For non-viscous liquid} \qquad \text{eq 3.7}$$

Here μ_{Liq} is the liquid dynamic viscosity ($kg.s/m^2$).

The ideal droplet diameter formed within the wavelength of the jet is expressed as follows:

$$D = (1.5\,\lambda_{opt} d_o)^{1/3} \qquad \text{eq 3.8}$$

In order to study the jet breakup that occurs under the influence of relatively large amplitude disturbances, non-linear equations need to be solved (Bayvel and Orzechowski, 1993). Such consideration was utilised by Rutland and Jameson in 1970. Calculating the volume of large and satellite droplets was studied theoretically and experimentally using a non-linear model calculation. Later on, the non-linear solution was applied on viscous liquids and the results were harmonious with experimental data (Novikov, 1977).

3.3.2 Classification of Jet Breakup Regimes

Many research studies were carried out to extend Weber's theory and consider the effect of ambient conditions on jet breakup at high-velocity releases. According to these studies, jet breakup can be classified into four breakup regimes depending on the magnitude of the proposed dimensionless numbers (Liu, 2000). In general, these dimensionless numbers depend on the values of jet velocity, nozzle diameter and the properties of both released liquid and the surrounding media (Liu, 2000). The Reynolds dimensionless number "Re" expresses the ratio between inertia forces acting on fluid and liquid viscosity, where the Weber's dimensionless number "We" expresses the relation between the forces of inertia and liquid surface tension forces (Savic, 2000).

In 1936, Ohnesorge introduced his dimensionless number "Oh" which defines the ratio of internal viscous forces to interfacial surface tension forces. Furthermore, Ohnesorge's study expressed the most common quoted criteria for the jet breakup regime classification (Liu, 2000). Later on, further studies were carried out by Miesse (1955) and Reitz (1978) to identify the different regimes of circular jet breakup, and to express the relative importance of surface tension, viscosity and aerodynamic forces. The proposed classification shows the differences in jet appearance in each case, and identifies the dominant forces leading to jet breakup at different operation conditions. The following equations represent the values of the different proposed dimensionless numbers (Liu, 2000):

$$Re_{Liq} = \rho_{Liq} U_L \frac{d_o}{\mu_{Liq}} \qquad \text{eq 3.9}$$

$$We_{Liq} = \rho_{Liq} U_L^2 \frac{d_o}{\sigma_{Liq}} \qquad \text{eq 3.10}$$

$$Z = Oh = We_{Liq}^{0.5} Re_{Liq}^{-1} = \mu_{Liq} / \left(\rho_{Liq} \sigma_{Liq} d_o\right)^{0.5} \qquad \text{eq 3.11}$$

Where U_L is the liquid velocity at the nozzle exit (m/s), We_{Liq} is the dimensionless liquid Weber number, Re_{Liq} is the dimensionless liquid Reynolds number, Z or Oh is known as the Ohnesorge dimensionless number, We_{Air} is the dimensionless Weber's number of air and ρ_{Air} is the density of air (kg/m^3).

$$We_{Air} = \rho_{Air} U_L^2 \frac{d_o}{\sigma_{Liq}} \qquad \text{eq 3.12}$$

Table 3.1 Classification and Criteria of Breakup Regimes of Round Liquid Jets in Quiescent Air

Regime	Predominant Breakup Mechanism	Criteria
Rayleigh jet breakup	Surface tension force	$We_A < 0.4$ or $We_A < 1.2+3.41\ Oh^{0.9}$
First wind induction	Surface tension force Dynamic pressure of ambient air	$1.2+3.41\ Oh^{0.9} < We_A < 13$
Second wind induced	Dynamic pressure of ambient air	$13 < We_A < 40.3$
Atomization	Unknown but plausible: Aerodynamic interaction, turbulence, cavitation, bursting effect	$We_A > 40.3$

The Rayleigh jet breakup regime is the simplest form of jet breakup, which is motivated by the surface tension forces causing axisymmetrical disturbances. The inertial forces in this case are in balance with the surface tension forces (Reitz and Bracco, 1986). The liquid droplets are formed a few nozzle diameters below the orifice, and this distance is usually called the "breakup length". In the Rayleigh regime, the formed droplets are uniform with a typical diameter being larger than the jet's diameter. At higher release velocities, the droplet's diameter becomes nearly equal to the jet's diameter and the aerodynamic effect becomes influential. The breakup length and time are found to be directly proportional to the liquid release velocity (Liu, 2000).

When the liquid release velocity increases, the effect of aerodynamic forces on jet breakup becomes more and more predominant and the effect of liquid surface tension is minimised. The droplets are formed a few orifice diameters downstream of the nozzle and the average droplet size is smaller than the jet diameter. The breakup in this regime is called first wind-induced breakup (Liu, 2000).

Another breakup regime becomes dominant when the maximum growth rate and the optimum wavelength become completely independent on jet diameter (Reitz and Bracco, 1986). This regime is called second wind-induced breakup. In this case, the formed droplets become typically smaller than jet diameter and are generally characterised by a wide size range (Liu, 2000).

At higher jet velocities, the breakup distance becomes very short and the liquid bulk is completely transformed into a wide range of spray droplets. This regime is called atomisation breakup (Liu, 2000).

The classification, suggested by Ohnesorge (1936), Miesse (1955) and Reitz (1978), expressed the role of aerodynamic effect on the mechanism of liquid jet breakup.

Breakup length and droplet size distribution are quite dependent on liquid release velocity, which subsequently aggravates the aerodynamic forces (Liu, 2000).

In addition to the aerodynamic force as an external stimulant, further different factors could affect the jet breakup process (Hiroyasu, Shimizu and Arai, 1982; Reitz, 1986). Jet turbulence, for example, plays an important role due to increasing the jet's surface, which makes it more susceptible to aerodynamic effects (Shavit and Chigier, 1996). The initiation of liquid disturbances could be excited due to one or more of the following (Chigier, 1991):

a- The atomiser disturbances caused by liquid or air.
b- The presence of sharp edges causing flow separation.
c- The effect of wall surface roughness.
d- The turbulence and cavitations generated inside the atomiser.
e- The growth of a boundary layer.
f- The interaction between the liquid and the surrounding gaseous environment (aerodynamic effect).

Another regime classification was presented by Tanasawa and Toyoda (1955). According to their high-speed imaging, the mechanisms of jet breakup are classified into four regimes: laminar flow, transition flow, turbulent flow and spray. A new dimensionless number was proposed to classify the different breakup modes. This number, called the "jet number", is a combination of the aerodynamic Weber number and the density ratio between gas and liquid. According to the value of the jet number, the general appearance of jet breakup can be classified as follows (Liu, 2000):

a- Laminar flow: Je < 0.1: Dripping
b- Transition flow: Je =0.1–10: Jet breaks up into droplets due to longitudinal oscillations
c- Turbulent flow: Je =10–500: Jet breaks up into droplets due to lateral oscillations with additional effect of air friction
d- Spray: Je > 500: Jet breaks up into multitude of droplets due to membrane formation.

$$Je = \frac{\rho_{Air} U_L^2 d_o}{\sigma_{Air}} \left(\frac{\rho_{Liq}}{\rho_{Air}} \right)^{0.45} \qquad \text{eq 3.13}$$

This classification is quite comparable with the first one. The average ratio between air density and liquid density is nearly 1:640 for the most commonly used liquid fuels. This means that the jet number is nearly 18 times the value of the aerodynamic Weber's

number. A semi-convergence appears when substituting the jet number values with the corresponding Weber's numbers. Figure 3.1 compares the Weber's number values in both types of breakup regime classifications.

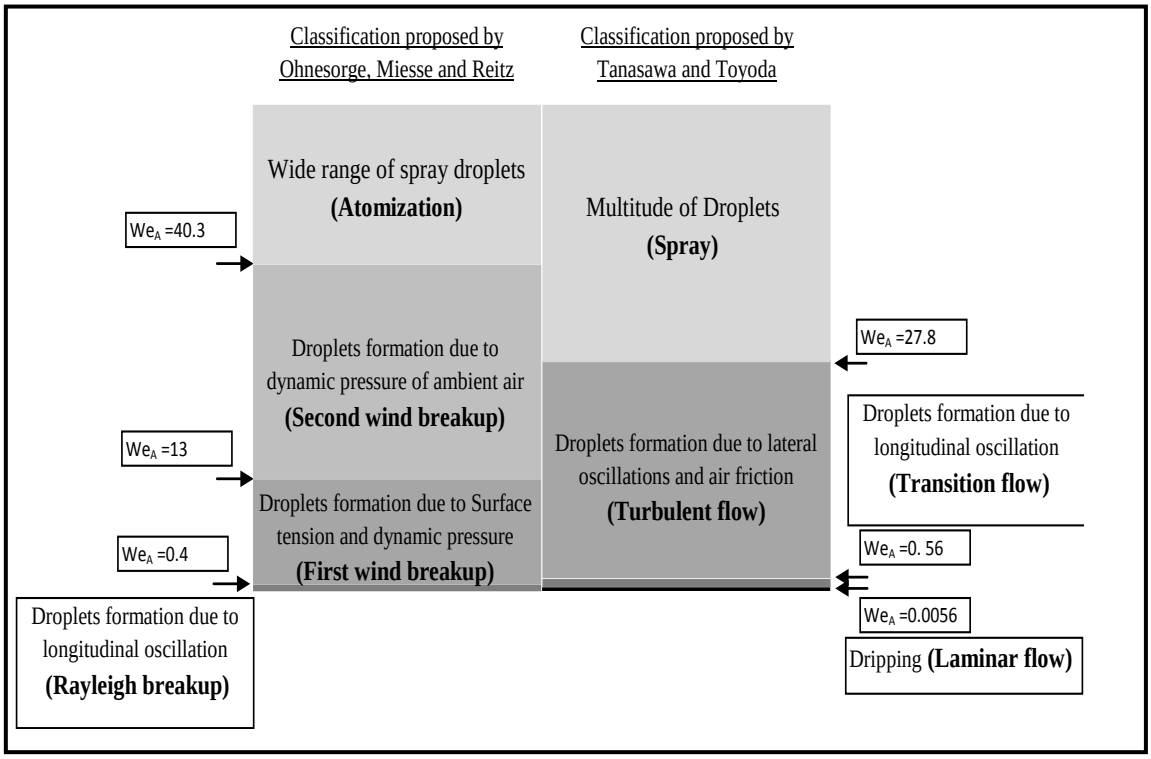

Figure 3.1 Comparison between the different types of breakup regime classifications

3.3.3 The Correlations of Jet Breakup Length

The jet breakup length is defined as the length of the continuous portion of the jet, measured from the nozzle to the droplets formation point (Lefebvre, 1989). In general, the breakup length increases to a maximum value with the increase of the jet's velocity (Hiroyasu, Shimizu and Arai, 1982; Arai, Shimizu and Hiroyasu, 1985), and then starts to decrease with further velocity increase. Tanasawa and Toyoda (1955) argued that the breakup length starts to increase in laminar flow until reaching a maximum value at nearly Re ≈ 1400. Grant and Middleman (1966) suggested a special correlation for this point as follows:

$$Re_{crit} = 3.25\,Oh^{-0.28} \qquad \text{eq } 3.14$$

Where Re_{crit} corresponds to the point of change from laminar to transition mode.

In the transition region, the value of breakup length starts to decrease until reaching a minimum value at Re =1800–2400. At this point, the turbulence flow region starts and the breakup length begins to increase again (Tanasawa and Toyoda, 1955). For viscous

liquids, the transition flow begins earlier and the transition region becomes wider. For the transition region in which the flow transfers from laminar to turbulent, the following expression was proposed by Van de Sande and Smith (1976):

$$Re_{crit} = 12{,}000\left(\frac{1}{d_o}\right)^{-0.3} \qquad \text{eq 3.15}$$

Grant and Middleman (1966) suggested an empirical correlation for calculating the jet breakup length in laminar and turbulent flow regions as follows:

$$L = 19.5\, d_o\, We_{Liq}^{0.5}\left(1+3\,Oh\right)^{0.85} \quad \text{in laminar flow} \qquad \text{eq 3.16}$$

$$L = 8.51\, d_o\, We_{Liq}^{0.32} \quad \text{in tubulent flow} \qquad \text{eq 3.17}$$

3.3.4 Droplet Size Distribution after Primary Breakup

In the atomisation process, the liquid droplets are always generated with various sizes over a wide spectrum (Liu, 2000). In order to describe the size distribution of the resulting droplets, a number of empirical and probability functions have been proposed (Lefebvre, 1989). For example, Déchelette, Babinsky and Sojka (2011) enumerated some common empirical functions that are used to express the droplet size distributions. Their discussion includes: log-normal number distribution, upper-limit distribution, root-normal volume distribution, Nukiyama–Tanasawa number distribution and the Rosin–Rammler distribution. In fact, none of these functions can describe the size distribution in all cases. therefore, several trials should be performed to find the function that is most compatible with the experimental results (Lefebvre, 1989).

In order to depict the size distribution function for any droplets array, it is necessary to determine the value of a representative droplet's diameter, such as the mean droplet size. In addition, a certain measure value is needed to present the width of the distribution range, such as the standard deviation or q (Liu, 2000). Table 3.2 represents the different types of droplet mean diameters as suggested by Mugele and Evans (1951).

The Rosin–Rammler distribution function (Rosin and Rammler, 1933) is the most prevalent distribution function nowadays (Liu, 2000). The following equation represents the general form of the Rosin–Rammler function:

$$VF = 1 - \exp\left[-\frac{D}{x}\right]^{q} \qquad \text{eq 3.18}$$

Where VF is the total volume fraction of the droplets smaller than D, x is constant and q is the Rosin-Rammler distribution parameter.

Table 3.2 Definitions of Mean Droplet Diameters and Their Applications

Quant	Common name	Application
D_{10}	Arithmetic Mean (Length)	Comparison
D_{20}	Surface Mean (Surface Area)	Surface Area
D_{30}	Volume Mean (Volume)	Volume Control
D_{21}	Length Mean (Surface Area - Length)	Absorption
D_{31}	Length Mean (Volume - Length)	Evaporation - Molecular
D_{32}	Sauter Mean (SMD) (Volume -	Mass Transfer Reaction
D_{43}	Herdan Mean (Weight)	Combustion - Equilibrium

Table 3.3 expresses the different representative droplet diameters that can be used to specify distribution functions (Liu, 2000). The relationships between these diameters are based on the function of the Rosin–Rammler distribution in which each relation is dependent on the Rosin–Rammler distribution's parameter (q).

Table 3.3 Definitions of Representative Droplet Diameters

Symbol	Definition	Relationship
$D_{0.1}$	10% of the total droplets volume are smaller than this value	$\frac{D_{0.1}}{X} = (0.1054)^{\frac{1}{q}}$ $\frac{D_{0.1}}{MMD} = (0.152)^{\frac{1}{q}}$
$D_{0.5}$ (MMD)	"The Mass Median Diameter" 50% of total droplets volume are smaller than this value	$\frac{MMD}{X} = (0.693)^{\frac{1}{q}}$ $\frac{MMD}{SMD} = (0.693)^{\frac{1}{q}}\Gamma\left(1-\frac{1}{q}\right)$
$D_{0.632}$	"The Characteristic Diameter" 63.2% of the total droplets' volume are smaller than this value	X in Rosin - Rammler distribution function
$D_{0.9}$	90% of the total droplets' volume are smaller than this value	$\frac{D_{0.9}}{X} = (2.3025)^{\frac{1}{q}}$ $\frac{D_{0.9}}{MMD} = (3.32)^{\frac{1}{q}}$
$D_{0.999}$	"The Maximum Diameter" 99.9% of the total droplets' volume are smaller than this value	$\frac{D_{0.999}}{MMD} = (9.968)^{\frac{1}{q}}$
D_{peak}	"The Peak Diameter" The D value corresponds to the peak of the drop's size curve	$\frac{D_{peak}}{X} = \left(1-\frac{1}{q}\right)^{\frac{1}{q}}$ $\frac{D_{peak}}{MMD} = \left(1.4428-\frac{1.4428}{q}\right)^{\frac{1}{q}}$ $\frac{D_{peak}}{SMD} = \left(1-\frac{1}{q}\right)^{\frac{1}{q}}\Gamma\left(1-\frac{1}{q}\right)$

Regarding the relation between the representative diameters, the larger value of exponent *q* represents a higher degree of droplet uniformity (Liu, 2000). The value of

the *q* exponent may vary between 1.2 and 4 for many applications, and it can reach 7 in case of rotary atomisation (Lefebvre, 2000). According to the unique relationships between any two different diameters, the Rosin–Rammler distribution function can be rewritten according to the following form:

$$VF = 1 - \exp\left[-0.693\left(\frac{D}{MMD}\right)^{q}\right] = 1 - \exp\left[-\Gamma\left(1-\frac{1}{q}\right)^{-q}\left(\frac{D}{SMD}\right)^{q}\right] \qquad \text{eq 3.19}$$

Based on Equation 3.19, the droplets' size distribution can be quantified once the exponent *q* and a representative diameter have been determined. The value of exponent *q* is usually estimated graphically from the experimental results. This value is the slope of straight line of plotting $\ln(1\text{-}v)^{-1}$ *vs*. droplet diameter (Liu, 2000). On the other hand, different correlations have been proposed to estimate the values for mean, minimum and maximum droplet sizes generated from the liquid jet atomisation. Merrington and Richardson (1947) derived a correlation to estimate the Sauter mean diameter value for the droplets generating from liquid jet disintegration as follows:

$$SMD = \frac{500 \times d_o^{1.2} \nu_{Liq}^{0.2}}{U_L} \qquad \text{eq 3.20}$$

Where ν_{Liq} is the kinematic viscosity of liquid (m^2/s).

This correlation is typically for liquid jets releasing from a plain orifice diameter into quiescent air where d_0 is the diameter of discharge orifice (m) and ν_L is the kinematic viscosity of a liquid (m^2s^{-1}).

Another correlation has been derived by Miesse (1955) for the maximum diameter resulting from the liquid jet disintegration:

$$D_{0.999} = d_o \, We_{Liq}^{-0.333}\left(23.5 + 0.000395 \, Re_{Liq}\right) \qquad \text{eq 3.21}$$

3.4 The Secondary Breakup of Liquid Droplets Due to Aerodynamic Forces

3.4.1 Theory of Liquid Droplet Breakup

The secondary breakup of liquid droplets is the process in which a droplet disintegrates into smaller droplets due to interaction with the surrounding medium (Liu, 2000). The disintegration of liquid droplets is highly dependent on the effect of aerodynamic forces (McCarthy, 1974). Each falling droplet is always subjected to vibration, deformation and liquid circulation. However, liquid surface tension forces can

retain the droplet's unity until the influence of external aerodynamic forces reaches a sufficient magnitude (Bayvel and Orzechowski, 1993).When gas flows around a liquid droplet, the distribution of aerodynamic pressure on the droplet's surface may vary. The influence of such variation could result in the droplet's deformation. Under certain conditions of forces equilibrium, further deformation could lead to droplet breakup (Lefebvre, 1989).

In general, droplet breakup is governed by surface tension forces, viscous forces and aerodynamic forces (Liu, 2000). For liquids characterised by relatively low viscosity, droplet disintegration takes place if the balance between aerodynamic forces and surface tension forces is disturbed toward the first one. The balance equation between the two forces is suggested as follows (Bayvel and Orzechowski, 1993):

$$C_D \frac{\pi D^2}{4} \frac{\rho_{Air} V_R^{\ 2}}{2} = \pi D \sigma \qquad \text{eq 3.22}$$

Where V_R is the relative velocity between the droplet and ambient air (m/s).

In order to derive relations for the droplet's size, velocity and Weber's number at the instant of such equilibrium, the following relations can be derived from Equation 3.22:

$$We_{crit} = \frac{\rho_{Air} V_R^{\ 2} D}{\sigma} = \frac{8}{C_D} \qquad \text{eq 3.23}$$

$$D_{crit} = \frac{8\sigma}{C_D \rho_{Air} V_R^{\ 2}} \qquad \text{eq 3.24}$$

$$V_{crit} = \left(\frac{8\sigma}{C_D \rho_{Air} D} \right)^{0.5} \qquad \text{eq 3.25}$$

Where We_{crit}, D_{crit} and V_{crit} are subsequently the critical Weber's number, droplet diameter and droplet velocity at the instant of equilibrium.

This means, at the proposed physical properties (air density and liquid surface tension) and droplet diameter, disintegration takes place if the droplet's velocity passes the critical velocity value. The same principle can be applied for the critical droplet diameter. It is well known that liquid droplets of a diameter larger than 1mm are generally unstable in a gas stream (Woodward, 1989).

In addition to the liquid surface tension, liquid viscosity can also reduce the prospect of droplet disintegration. If the liquid viscosity is significant, both liquid properties can be expressed using the Ohnesorge number (Guildenbecher, Rivera and Sojka, 2011)

3.4.2 Regimes of Liquid Droplet Breakup

A liquid droplet's disintegration can take place through different manners (modes or regimes). According to Hinze (1955) droplet breakup may occur in three basic modes:

a- The droplet is initially flattened to an oblate ellipsoid. This ellipsoid can be converted into a torus, which is finally stretched and then disintegrates into droplets.

b- The droplet is elongated to form a cylindrical thread or ligament and finally fragmented into small droplets.

c- Some protuberances may be created on a droplet's surface due to local deformations. Under favourable conditions, these bulges detach from the droplet and disintegrate into smaller droplets.

In recent studies, four regimes have been mainly used to describe the scenario of the liquid droplets secondary breakup (Guildenbecher, Rivera and Sojka, 2009).Each regime is specified for a distinct range of Weber's number values. Table 3.4 expresses the different modes of droplet breakup and the typical Weber's number range for each one (Guildenbecher, Rivera and Sojka, 2011).

Table 3.4 Transition We for Newtonian Drops with Oh < 0.1

Vibrational (no breakup)	$0 < We < 11$
Bag	$11 < We < 35$
Multimode	$35 < We < 80$
Sheet thinning	$80 < We < 350$
Catastrophic	$We > 350$

In addition to the Weber's number, the actual breakup modes also depend on whether a droplet is subjected to steady acceleration, or is suddenly exposed to a high-velocity gas stream (Lane, 1951; Hinze, 1955). Taylor (1934) argued that the critical Weber's number value for drops subjected to a steady stream is twice the value for those subjected suddenly to airflow at a constant speed.

The bag breakup mode is the most likely to take place since it occurs at low Weber numbers (Guildenbecher, Lopez-Rivera and Sojka, 2009). The mechanism of the bag breakup mode first starts when the droplet is flattened due to its subjection to steady acceleration. After a critical velocity, the breakup process takes place in two stages

(Grover and Assanis, 2004). In the first stage, a pressure difference arises between the leading stagnation point and the wake (Han and Tryggvason, 2001). In the second stage, the flattened drop is blown to form a hollow bag connected with a circular rim that contains more than 70% of the droplet mass. The liquid bag continues stretching until the rupture takes place producing a number of very fine droplets (Kennedy and Roberts, 1990). In conjunction with this section, the circular rim itself disintegrates due to Rayleigh instability and forms comparatively larger droplets (Grover and Assanis, 2004).

3.4.3 Droplet Size Distribution for Liquid Droplets' Breakup

As previously discussed, the atomisation process contains both the primary breakup and the secondary breakup. In order to quantify the droplet size distribution for the whole process of atomisation, it is very important to estimate the distribution of the droplets resulting from secondary droplet breakup. Many researchers surmised that the daughter droplets resulting from secondary breakup should be multi-sized due to the combination of breakup regimes (Liu, 2000).

Many experimental and theoretical approaches have been conducted to estimate a representative diameter for the secondary disintegration of liquid droplets. For example, the experiments done by Grover and Assan in (2004) suggest that the SMD of the rim drops is approximately 36% of the original drop diameter, while this percentage is just about 4% for the fine droplets resulting from the bursting of the bag. The average SMD for all the resulting droplets is nearly 11% of the original drop's diameter. In another study (Chou and Faeth, 1998), the mean diameter of the fragments formed from the ring's breakup was 30% of the original drop's diameter while the mean diameter of the fragments formed from bag disintegration was approximately 4% of the original drop's diameter.

Simmons (1977a, b) studied drop-size distributions and found that the relation MMD/SMD is nearly 1.2, where the maximum diameter is nearly 3 times the MMD. Simmons found that the droplets' volume distribution can obey root-distribution, while O'Rourke and Amsden (1987) used the c-square distribution function for determining the size distribution of the secondary droplets. Hsiang and Faeth (1992, 1993) used holography to measure the droplet size distributions in the bag and multimode regimes. In their experiments, the root-normal distribution was found to fit and the relation MMD/SMD = 1.2 was confirmed. A later study on drops produced by shear breakup (Chou, Hsiang and Faeth, 1997) found the distribution results to satisfy the universal

root normal drop size distribution function, and a similar relation between MMD and SMD was ascertained. Hsiang and Faeth (1992) derived a correlation for the SMD value based on their experimental measurements as follows:

$$\rho_{Air}\ SMD\ V_R^2/\sigma_{Liq} = 6.2\left(\rho_{Liq}/\rho_{Air}\right)^{1/4}\left[\mu_{Liq}/\left(\rho_{Liq}\ D_{ini}\ V_R\right)\right]^{1/2}\ We_d \qquad \text{eq 3.26}$$

Where SMD is the Sauter mean diameter of the resulting daughter droplets (m),V_R is the relative velocity between droplet and the surrounding air (m/s), D_{ini} is the initial droplet diameter (m) and We_d is the dimensionless value of the Weber's number at the time of disintegration.

3.5 Liquid Droplet Motion

3.5.1 General

The motion of liquid droplets after formation is mainly a result of the competition between two opposite forces: the constant gravitational force and the opposing drag force. When these forces are in equilibrium, the droplet motion is then called "steady straight line" motion. This type of motion is probably the best choice to describe the motion of aerosol droplets (Hinds, 1999).

Since the force of gravity has a constant value at a certain height level, the drag force is always the master in controlling droplet motion. The magnitude of this force is dependent on many factors, such as droplet size, shape and orientation, and dramatically the physical properties of the gaseous mixture (Williams and Loyalka, 1991). Hence, estimating the physical properties of the gaseous mixture around the falling droplets is very important for studying the motion of droplets. The aerodynamic drag force (F) could be estimated from the general form of Newton's resistance equation (Equation 3.27), where this form is valid for all droplets moving through a gas in the subsonic domain (Hinds, 1999). This equation is suitable for particles moving with Reynolds numbers greater than 1000.

$$F = C_D \frac{\pi D^2}{4} \frac{\rho_{Air} V_R^2}{2} \qquad \text{eq 3.27}$$

Here C_D is the aerodynamic drag coefficient (dimensionless).

Gravitational force (G) on falling spherical droplet could be calculated from equation 3.28:

$$G = g \frac{\pi D^3}{6}\left(\rho_{Liq} - \rho_{Air}\right) \qquad \text{eq 3.28}$$

Here g is the gravity acceleration ($m.s^{-2}$).

In general, the field study of droplet motion is not easy to analyse. The domain that contains moving liquid droplets is usually subjected to various physical changes. Bayvel and Orzechowski (1993) summarised the most prominent manifestations of complexity as follows:

- The moving liquid droplets are usually subjected to multi variable forces such as drag forces and wind forces.
- The motion of a jet of droplets does not obey the same rules that describe the motion of a single droplet.
- The two-phase cloud always contains multi-size liquid droplets of different characteristics.
- Liquid droplets moving in a gaseous medium are always subjected to mass and velocity changes.

3.5.2 Droplet Terminal Settling Velocity

Depending on the drag resistance force of the air mixture on falling droplets, each droplet could reach a specific steady velocity called the "terminal settling velocity". This velocity could be reached when the drag force reaches equilibrium with gravitational forces. The general form for calculating terminal settling velocity (Equation 3.29) is obtained from Equations 3.27 and 3.28. To insure accurate measurement of droplet terminal velocity, the surrounding air mixture should be stagnant and the droplet concentration must be very small to avoid any mutual influences between neighbouring droplets (Bayvel and Orzechowski, 1993).

$$V_{ter} = \sqrt{\frac{4\,g\left(\rho_{Liq} - \rho_{Air}\right) D}{3\,\rho_{Air}\ C_D}} \qquad \text{eq 3.29}$$

Since the density of the air mixture is very low compared to the density of liquids, Equation 3.29 could be simplified to the following form:

$$V_{ter} = \sqrt{\frac{4\,g\,\rho_{Liq}\,D}{3\,\rho_{Air}\,C_D}} \qquad \text{eq 3.30}$$

Terminal settling velocity measurements have been a field of interest for many researchers. Many investigators since the early twentieth century estimated the terminal velocity of different droplet sizes experimentally. In addition, empirical models have been developed for this purpose. For example, Gunn and Kinzer (1949) determined the terminal velocity of distilled water droplets falling through stagnant air accurately using an electronic techniques method. The velocity of droplet sizes from 0.2 to 100,000 micrograms was determined with accuracy better than 0.7%.

3.5.3 Aerodynamic Drag Coefficient

The key to the terminal velocity determination is the drag coefficient estimation. Generally, the drag coefficient value is a function of the Reynolds number, Re_{ter}:

$$Re_{ter} = \frac{\rho_{Air} V_R D}{\mu_{Air}} \qquad \text{eq 3.31}$$

Where μ_{Air} is the dynamic viscosity of air mixture.

The drag coefficient for spherical droplets was obtained experimentally over a wide range of Reynolds number. Empirical equations have been established to estimate the drag coefficient in laminar, transient and turbulent ranges of motion. These equations are dependent on the value of Reynolds number varying between 1×10^{-4} and 2×10^{5}. Beyond the value of 2×10^{5}, the relation between drag coefficient value and Reynolds number value seems to be too complicated to be described by an equation (Bayvel and Orzechowski, 1993):

a- Laminar range, $1\times10^{-4} < Re_{\infty} < 0.4$

b- Transient range, $0.4 < Re_{\infty} < 1\times10^{3}$

c- Turbulent range, $1\times10^{3} < Re_{\infty} < 2\times10^{5}$

In the laminar region, sometimes called the Stokes' region (Hinds, 1999), the relation between drag coefficient and Reynolds number is linear and the coefficient value could be estimated according to the following relation:

$$C_D = \frac{24}{Re_{ter}} \qquad \text{eq 3.32}$$

Using Equations 3.31 and 3.32 and substituting in Equation 3.2, the value of drag forces in this case could be estimated from the following equation.This equation indicating the laminar flow is called the Stokes' equation, and it could be applied for small rigid spheres including liquid droplets (Bayvel and Orzechowski, 1993). This equation represents a special case of Newton's resistance law (Hinds, 1999).

$$F = 3\pi\mu_{Air} D V_R \qquad \text{eq 3.33}$$

For droplets moving with a Reynolds number larger than 1000, the dimensionless coefficient of drag always has a constant value of nearly 0.44. This value could be applied to all particles moving in a turbulent region and with a Reynolds value up to 20,000.

As for the middle transient region, many scientists have put forth an effort to formulate an equation describing the relation between drag coefficient and Reynolds number in this range. One of the most useful equations in this field is the Allen equation (Equation 3.34), which is particularly active for droplets moving with a Reynolds value between 2 and 500 (Bayvel and Orzechowski, 1993).

$$C_D = \frac{18.5}{Re_{ter}^{0.6}} \qquad \text{eq 3.34}$$

Another relation expressed in Equation 3.10 gives results coherent with the experimental correlations of Clift, Grace and Weber (1978). The deviation from experimental results is not more than 4% for $Re_\infty < 800$ and within 7% for $Re_\infty < 1000$ (Hinds, 1999).

$$C_D = \frac{24}{Re_{ter}}\left(1 + 0.15\,Re_{ter}^{0.687}\right) \qquad \text{eq 3.35}$$

Further formulas for exploring the relation between drag coefficient and Reynolds number in the transient range of motion are expressed by Equations 3.36, 3.37 and 3.38. Vincent (1995) argued that the relation expressed in Equation 3.36 covers the interval for Reynolds values from 1 to 2000 within 2% of the experimental data. Previously, Sartor and Abbott (1975) and Friedlander (1977) developed their empirical relations expressed by Equations 3.37 and 3.38, respectively. The equation of Sartor and Abbott only covers the region for Reynolds numbers from 0.1 to 5, whereas the Friedlander equation covers most of the transient region for Reynolds from 5 to 1000:

$$C_D = \left(\frac{24}{Re_{ter}}\right)\left\{1 + \left(\frac{Re_{ter}^{2/3}}{6}\right)\right\} \qquad \text{eq 3.36}$$

$$C_D = \frac{24}{Re_{ter}}\left(1 + 0.0196\,Re_{ter}\right) \qquad \text{eq 3.37}$$

$$C_D = \frac{24}{Re_{ter}}\left(1 + 0.0158\,Re_{ter}^{2/3}\right) \qquad \text{eq 3.38}$$

3.5.4 Terminal Settling Velocity of Aerosol Droplets

Liquid aerosol droplets of a size smaller than 100μm are most probably obeying Stokes' law. The gravitational terminal settling velocity of such droplets could be estimated from the balance between gravity force and drag force under Stokes' considerations as follows (Hinds, 1999).

$$3\pi\mu_{Air}D\,V_{ter} = \frac{\pi D^3}{6}\left(\rho_{Liq} - \rho_{Air}\right) \qquad \text{eq 3.39}$$

The terminal settling velocity of an aerosol droplet under this condition could be estimated from the following equation:

$$V_{ter} = \frac{g\,D^2\left(\rho_{Liq} - \rho_{Air}\right)C_c}{18\,\mu_{Air}} \qquad \text{for } Re_{Air} < 1 \qquad \text{eq 3.40}$$

Where C_c is the dimensionless value of slip correction factor

3.5.4.1Slip Correction Factor

When liquid droplets fall down due to gravitational force, each droplet will be subjected to gas molecule collision from all directions. In fact, this collision is the real source of drag. Stokes' law assumes that the relative velocity of the gas molecules right at the falling particle's surface is zero (Hinds, 1999), but this assumption might be not valid in all cases.

The scientists found that the settling velocity of droplets smaller than 1μm could be higher than that predicted by Stokes' law. For these fine droplets, gas molecules moving around may irregularly miss the droplet surface and this would make the drag resistance somewhat smaller. This phenomenon is called the "slip", and the amount of velocity deviation that occurs is usually corrected by a "slip correction factor".

The value of the slip correction factor was derived by Cunningham in 1910; this Cunningham correction factor (Equations 3.41 and 3.42) is always equal to or greater than one (Reist, 1984). The use of this factor extends the range of application for the Stokes' equation to droplets of 0.1μm in diameter (Hinds, 1999).

$$C_c = 1 + \frac{2.52\lambda}{D} \qquad \text{when } D > 2\lambda \qquad \text{eq 3.41}$$

$$C_c = 1 + \frac{3.31\lambda}{D} \qquad \text{when } D < 2\lambda \qquad \text{eq 3.42}$$

The mean free path could be defined as "the mean distance a molecule travels before colliding with another molecule" (Baron and Willeke, 2001). The value of the gas mean free path could be estimated at any pressure and temperature conditions according to the following equation (Willeke, 1976):

$$\lambda = \lambda_r\left(\frac{101}{P}\right)\left(\frac{T}{293}\right)\left(\frac{1+110/293}{1+110/T}\right) \qquad \text{eq 3.43}$$

This equation is true when: P is the current pressure in (kPa), T is the current temperature in (^{o}K) and λ_r is the standard value of mean free path equals 0.0664µm at an ambient pressure of 101kPa and an ambient temperature of 293^{o}K.

The numerical relation between mean free path and droplet dimension is referred to as a dimensionless number called the Knudsen number "K_n", where:

$$K_n = \frac{\lambda}{r} = \frac{2\lambda}{d} \qquad \text{eq 3.44}$$

Where K_n is the Knudsen number.

Further correlations have been achieved to estimate the value of the slip correction factor. For example, Allen and Raabe suggested two formulas for estimating the correction factor for oils (Allen and Raabe, 1982) and for solid particles (Allen and Raabe, 1985):

$$C_c = 1 + \frac{\lambda}{D}\left[2.31 + 0.942\exp\left(-0.298\frac{D}{\lambda}\right)\right] \quad \text{for oil droplets} \qquad \text{eq 3.45}$$

$$C_c = 1 + \frac{\lambda}{D}\left[2.284 + 1.116\exp\left(-0.499\frac{D}{\lambda}\right)\right] \quad \text{for solid particles} \qquad \text{eq 3.46}$$

Not so far from their results, another correlation presented by Hinds in (1999) could be used to estimate the slip correction factors for droplets smaller than 0.1µm:

$$C_c = 1 + \frac{\lambda}{D}\left[2.34 + 1.05\exp\left(-0.39\frac{D}{\lambda}\right)\right] \qquad \text{eq 3.47}$$

3.5.4.2Dry Deposition of Ultra-fine Droplets

The relatively large aerosol liquid droplets could be settled down with appreciable gravitational settling speed. The value of such deposition could be dominated by the simple gravitational settling Stokes' equation (AIChE, 1996).

In the case of ultra-fine aerosols, deposition on the surface could be also dominated by a process called dry deposition. This process takes place due to a combination of chemical reactions and physical interception caused by the ground and vegetation (Sehmel, 1984). Dry deposition can also occur by the absorption and collection of rain drops and snowflakes (Slinn, 1984).

EPA (1995) expressed a detailed model to estimate the dry deposition velocity. In this model, the velocity is assumed to be dependent on three types of resistances:

$$v_d = \frac{1}{r_a + r_s + r_t} + v_s \qquad \text{eq 3.48}$$

In which case, r_a is the aerodynamic resistance ($s.m^{-1}$), r_s is the surface or laminar layer resistance ($s.m^{-1}$), r_t is the transfer resistance dependant on surface characteristics ($s.m^{-1}$), v_s is the gravitational settling velocity obtained from Stokes equation ($m.s^{-1}$) and V_d is the dry deposition velocity ($m.s^{-1}$).

3.5.5 Acceleration/Deceleration Motion of Falling Liquid Droplets

Estimating the velocity change with time and displacement for falling liquid droplets is a very important parameter. In general, Newton's second law of motion should be applied on any droplet accelerating or decelerating under the effect of external acting force (Hinds, 1999). Therefore, the instantaneous velocity of a known mass of liquid droplets falling under the effect of gravity and drag forces could be estimated easily using Equation 3.49:

$$G - F = \frac{m_D \left(V_f - V_o\right)}{t} \qquad \text{eq 3.49}$$

Here G and F are respectively the gravity and drag forces estimated from equations 3.2 and 3.3 ($kg.m.s^{-2}$), m_o is the droplet mass (kg), t is the acceleration or deceleration time (s), where V_o and V_f are the initial and final droplet velocities before and after acceleration or deceleration ($m.s^{-2}$).

The displacement of droplets during the same period of time could also be estimated from the equation of motion:

$$X = V_o\, t + \frac{0.5\, t^2 (G - F)}{m_D} \qquad \text{eq 3.50}$$

Where X is the displacement of droplets during the same period of time.

In case of fine aerosol droplets, these parameters become very small. The falling droplets of size 100μm or less could accelerate or decelerate very fast towards the terminal settling velocity. When the problem domain is relatively large (such as in case of industrial fuel release incidents), the time and displacement needed to reach the settling velocity could be negligible.

An important quantity in studying the motion of aerosol size droplets is the relaxation time (τ). It could be defined as "the characterisation of the time required for a particle to adjust or relax its velocity to a new condition of forces"(Hinds, 1999). According to the aerosol equation of motion, this quantity could be simply estimated from the following equation:

$$\tau = \frac{D^2\left(\rho_{Liq} - \rho_{Air}\right)C_c}{18\,\mu_{Air}} = \frac{V_R}{g} \qquad \text{for } Re_{Air} < 1 \qquad \text{eq } 3.51$$

Where τ the relaxation time of aerosol size droplets (s)

This means, the relaxation time is directly dependent on the air mixture viscosity and the slip correction factor, which is in turn dependent on the ambient temperature and pressure (Hinds, 1999).

The equations of motion that could be used for estimating the instantaneous velocity and displacement of any accelerating or decelerating aerosol droplet are expressed as follows:

$$V(t) = V_f - (V_f - V_o)e^{-\frac{t}{\tau}} \qquad \text{eq } 3.52$$

$$X(t) = V_f t - (V_f - V_o)\tau\left(1 - e^{-\frac{t}{\tau}}\right) \qquad \text{eq } 3.53$$

According to equation (3.52), if a liquid droplet is released from rest through stagnant air reaching the terminal settling velocity, the droplet will need a time equal to the relaxation time to reach 63% of its terminal settling velocity. In addition, after three times the relaxation time, the droplet could reach about 95% of the estimated settling velocity (Hinds, 1999).

Regarding the decelerating aerosol droplets, when a droplet is released with higher than settling velocity, it will decelerate rapidly toward reaching the stable settling velocity value. The distance needed to reach this target is called the stopping distance "S". Theoretically, the droplet will need an infinite time to travel through this distance. However, in fact, after three times the relaxation time, 95% of this distance will be travelled (Hinds, 1999). If a liquid droplet is injected into a moving air stream, the falling droplet could reach a steady-state condition at a velocity similar to the air flow within a time equals 7τ (Reist, 1984). Table 3.5 represents the values of the different parameters of motion for aerosol size droplets at standard density and ambient conditions.

Table 3.5 Different motion parameters for aerosol sized droplets

Droplet Diameter (μm)	Relaxation time (s)	Time need to reach the terminal settling velocity (s) [assumed as 3τ]	Stopping distance from V_o=10m/s (mm)	Time to travel 95% of stopping distance (s)
0.01	7×10^{-9}	2×10^{-8}	7×10^{-5}	2×10^{-8}
0.1	9×10^{-8}	2.7×10^{-7}	9×10^{-4}	2.7×10^{-7}
1	3.5×10^{-6}	1.1×10^{-5}	0.035	1.1×10^{-5}
10	3.1×10^{-4}	9.4×10^{-4}	2.3	8.5×10^{-4}
100	7×10^{-2}	9.2×10^{-2}	127	0.065

3.6 Coagulation and Coalescence of Liquid Droplets

For liquid droplets in general and aerosol droplets in particular, the growth and diminution of such droplets after the formation and during the free-falling period always occur continuously. Because of these changes in mass and volume, droplet size distribution and aerosol mass concentration are always developing (Vincent, 1995).

Various mechanisms could be accounted as evolutionary mechanisms for droplets mass and volume. Droplets mass could increase or decrease by thermal methods through evaporation or condensation, as discussed in Chapter 2. On the other hand, growth and diminution may take place through mechanical methods. These methods include the growth of liquid droplets through coagulation and coalescence, or the diminution of colliding droplets through disintegration (Vincent, 1995). Furthermore, droplet disintegration may occur because of aerodynamic forces (as discussed in Section 3.4), or because of the droplet impinging on a solid or wetted surface (Bayvel and Orzechowski, 1993).

When droplets are accidentally released or atomised, there is always a possibility of their colliding with each other. Since the droplets are moving in parallel directions, the potential of such a collision becomes very low (Baron and Willeke, 2001). On the other hand, the relative motion caused by the different settling velocities may drive some larger droplets to catch-up with smaller ones and this will lead to some potential of collisions (Bayvel and Orzechowski, 1993). In addition, small aerosol droplets may also be subjected to collisions caused by Brownian motions and turbulence (Williams and Loyalka, 1991).

Droplets collision does not always give the same result. Although sometimes droplet disintegration could take place, in other cases droplets may combine with each other,

forming a larger drop. Such an outcome is dependent on impact parameter, colliding droplet sizes and fluid properties (Melean and Sigalotti, 2005). Table 3.6 expresses five different possibilities for droplets collision depending on different droplets' masses and relative velocities (Bayvel and Orzechowski, 1993).

Table 3.6 Types of drops collision according to We number

Collision case	Expected consequence
$0.35<W_e< 0.75$	Smaller drop rebounds from the big one
$1<W_e< 7.5$	Weak coalescence follows by disintegration when aerodynamic interaction occurs
$7.5<W_e< 20$	-Momentary coalescence occurs - after disintegration, same drop diameter formed again
$W_e> 25$	Puncture of the larger drop occurs
$W_e> 50$	Explosion breaks up of the large drop into a number of small droplets

Where W_e is the Weber number = $\rho_{Liq} V^2 D / \sigma$

Aerosol droplets collision will most probably take place in the coagulation process. In this process, two aerosol droplets or more will combine to form large particles called "clusters" (Hinds, 1999). In the case of solid particles, the same process might be called "agglomeration" and subsequently the resulting clusters are called "agglomerates" (Vincent, 1995). Another term that could be used for such a process is "coalescence". This term is more commonly used for spherical droplets merging together (Hinds, 1999). The collision process usually results in a larger particle size and lower aerosol number concentration (Baron and Willeke, 2001). Furthermore, the main goal of any coagulation study is to discover the change of both parameters over time (Hinds, 1999).

The collision of aerosol liquid droplets could be classified into two main types. If the collision is motivated by Brownian motion, the process is then called "thermal coagulation" or "Smoluchowski coagulation" (Hinds, 1999). Otherwise, if the collision is motivated by an external force, such as gravity, the coagulation could be described as "kinematic coagulation" (Baron and Willeke, 2001).

3.6.1 Simple Monodisperse Coagulation

According to the high complexity of the coagulation process, simple assumptions of monodisperse coagulation might be resorted to for easier model calculations. In this model, aerosol droplets are supposed to stick once they contact each other. In addition, the resulting clusters are assumed to grow slowly. The coagulation model of aerosols, such as for the motion of gases, is basically dependent on diffusion kinetics. However, in fact, aerosol droplets diffusion is much slower (Baron and Willeke, 2001). According

to the essential model developed by Smoluchowski, the decrease rate in aerosol number concentration could be estimated from the following equation (Hinds, 1999):

$$\frac{Dn}{Dt} = -CC\,N^2 \qquad \text{eq 3.54}$$

Where N is the particle number concentration (particle/m^3) and CC is the monodisperse coagulation coefficient (m^3/s).

For particles larger than the gas mean free path, the coagulation coefficient could be estimated as follows (Baron and Willeke, 2001):

$$CC = 4\pi\,D\,DV = \frac{4kTC_c}{3\mu_{Air}} \quad \text{for } D > \lambda \qquad \text{eq 3.55}$$

Where μ_{Air} is the gas viscosity (Pa.s), k is the Boltzman contant (1.38 x 10^{-23} J/K) and DV is the particle diffusion cofficient (m^2/s).

According to Equation 3.54, the change in aerosol number concentration and droplet size over time could be integrated as follows:

$$n(t) = \frac{n_o}{1 + n_o \overline{CC}\,t} \qquad \text{eq 3.56}$$

$$D(t) = D_o\left(\frac{n_o}{n(t)}\right)^{1/3} = D_o\left(1 + n_o CC\,t\right)^{1/3} \qquad \text{eq 3.57}$$

Where D_o is the initial diameter of monodisperse aerosol droplets (m), n_o is the initial number concentration (particle/m^3), D is the droplet diameter after time t in (m), n is the final number concentration (particle/m^3) and t is the time (s).

3.6.2 Polydisperse Coagulation

In reality, the simplified monodisperse model cannot be considered as a case of aerosol coagulation. Liquid aerosols are usually found as a mixture of multi-sized droplets. According to diffusion theory, the Brownian motion of smaller droplets is more vigorous. Therefore, the diffusion coefficient should be inversely proportional to droplet size (Hinds, 1999).

$$D = \frac{kTC_c}{3\mu_{Air}\pi\,D} \qquad \text{eq 3.58}$$

In the case of multi-sized droplets collisions, the coagulation for each combination of droplet sizes should be estimated using a particular diffusion coefficient (Zebel, 1966).

Because a very large number of different droplet sizes could be found in any sample, this model procedure should be much more complicated.

Lee and Chen (1984) derived an equation to estimate the average coagulation coefficient for multi-size droplets coagulation problems. The formula expressed in Equation 3.41 could be used for aerosols with a lognormal size distribution having a count median diameter (CMD) and a geometric standard deviation (σ_g).

$$\overline{CC} = \frac{2kT}{3\mu_{Liq}}\{1 + \exp\left(\ln^2\sigma_g\right) + \left(\frac{2.49\lambda}{CMD}\right)\left[\exp\left(0.5\ln^2\sigma_g\right) + \exp\left(2.5\ln^2\sigma_g\right)\right]\} \qquad \text{eq 3.59}$$

Where $\overline{CC}$ is the average coagulation coefficient value, CMD is the count median diameter and $\sigma_{g\ is\ the}$ geometric standard deviation.

3.7 Droplets Impinging on Surfaces

The secondary disintegration of liquid drops can also occur due to the drops impinging on solid or liquid surfaces. In fact, such a collision does not always lead to droplet disintegration (Bayvel and Orzechowski, 1993). Droplets impinging on such surfaces may stick, spread, splash or rebound (Liu, 2000).

Although a lot of theoretical and experimental work has addressed the details of the droplet breakup mechanism, unfortunately very little work has attempted to provide a predictive model for the size distribution of the 'daughter' droplets formed by the shattering of a single 'mother' droplet (Cohen, 1991). Kletz (1999) advised that a flammable liquid splashing during filling produces a lot of mist droplets that can be ignited at any temperature.

3.7.1 Droplets Splashing Criteria

The splashing process is the phenomenon in which the droplet is shattered into a number of smaller daughter droplets due to impinging on solid or wetted surface (Liu, 2000). A study performed by Hinkle (1989) on the impact of droplets on a surface revealed that splashing occurs only if the surface is rough or wet. In other words, droplets colliding with flat, smooth and dry surfaces are not expected to splash. In spite of this conviction, other researchers allowed that splashing may occur even at these conditions if the droplet's impact velocity reaches a certain critical value (Stow and Hadfield, 1981) or if the droplet is subjected to a phase change during the impact (Dykhuizen, 1994).

Regarding the factors affecting the splash parameters, many studies have demonstrated that the splash mass is directly proportional to impact velocity, droplet size and the roughness height of the impact surface (Liu, 2000). By dropping a ball into a suitably deep container of water and collecting the resulting splash mass, Sampson, Chung and Lozowski (1996) found that the splash mass varied with the impact velocity raised to the power 2.67 ±0.06. The impact angle seems to be insignificant to splash mass (Berg and Ulrich, 1997), but only affects the final splash geometry (Madejski, 1979).

Moita and Moreira (2007) argued that the mean roughness decreases the critical velocity for disintegration, where the wet-ability determines the mechanism of breakup at small rough surfaces. The most apparent factor influencing the secondary atomisation is the increase in liquid viscosity. In another experimental study, Shakeri and Chandra (2002) found that increasing the substrate roughness to a certain limit could increases the tendency to splash. After this limit, the splashing probability may be reduced.

Many studies have found that the impact dynamics are characterised by a combination of Weber's and Reynolds numbers (Liu, 2000). Hence, an innovative mixed dimensionless parameter called the splashing parameter "K" has been proposed for this purpose. Table 3.7 reviews some examples for the proposed value of the dimensionless splashing parameter. In addition, a correlated figure for the relation between the Weber number and the Ohnesorge number has been suggested by Stow and Hadfield (1981). This relation, expressed in Equation 3.60, could be used to discriminate between spreading and splashing regions.

$$We_{Liq} = 7.9 \times 10^{10} Oh^{2.8} \qquad \text{eq } 3.60$$

If the Weber's number (the right hand side) is smaller than the value expressed by the left hand side, the droplets are expected to undergo spreading rather than splashing and vice versa. Additionally, the threshold velocity for splashing could be estimated using the following equation (Stow and Hadfield, 1981):

$$u_{os}^{8} = const \times \left(\sigma_{Liq}/\rho_{Liq}\right)^{2} \nu_{Liq} \left(u_{o}/D\right)^{3} \qquad \text{eq } 3.61$$

Here u_{os} the threshold velocity for splashing.

Another correlation for the transition Weber number was suggested by Bai and Gosman (1995) according to the following equation:

$$We_{Liq} > 1320 \left(\frac{\rho_{Liq}\, \sigma_{Liq}\, D}{\mu_{Liq}} \right) \qquad \text{eq } 3.62$$

Table 3.7 Examples for Splashing Parameter Equations

$K = Re_{Liq}^{0.31} We_{Liq}^{0.69}$	Stow and Hadfield (1981)
$K = \left(Re_{Liq}^{1/2} We_{Liq}\right)^{4/5}$	Cossali, Coghe and Marengo (1997)
$K = \left(Re_{Liq}^{1/2} We_{Liq}\right)^{1/2} = 57.7$	Mundo, Sommerfield and Tropea (1995)

Where K is Splashing Parameter

3.7.2 Droplets Splash Modelling

A lot of experiments have been done in order to formulate a model for the droplets' impact. The early experiments performed by Wachters and Westerling (1966) suggested a value of≈ 80 for the critical Weber number. The original model developed by Watkins and Wang in 1990 got used with the result as a threshold between droplets rebounding below the value and droplets splashing when the Weber number is above the value. This model for the impact of single droplets on solid or liquid surfaces was effective in the near wall-spray, where the critical Weber can be defined as follows:

$$We_{Liq} = \rho_{Liq} v_{bn}^2 \frac{D}{\sigma_{Liq}} \qquad \text{eq 3.63}$$

Where v_{bn} is the component of the drop velocity normal to the surface just before impact

This model was later developed by Wang (1992) and Wang and Watkins (1993). The later model has a disadvantage of being implemented very near the impinging wall surface (Park and Watkins, 1996).

Another model taking into account the data of Wachters and Westerling was developed by Park (1994). The model looked at the rebound and breakup regimes for drop impact on hot surfaces only and estimated the number of resulting droplets "N" as a linear function of We_b (Equation 3.64). This model was applied later by Park (1994) and Park and Watkins (1996) to both hot and cold surfaces and for higher Weber number values. This equation follows:

$$N = 0.187 We_b - 14.0 \qquad \text{eq 3.64}$$

Bai and Gosman (1995) also implemented their own function of N on We_b as follows:

$$N \approx 0.016\, We_b - 5.0 \qquad \text{eq 3.65}$$

Where N the number of resulting droplets from splashing

Another experimental study (Mundo, Sommerfeld and Tropea, 1995) found the values of N as a nonlinear function of We_b, and obeying Park's equation better than Bai and Gosman's equation.

Cohen (1991) formulated a statistical framework model to predict the size and number of the droplets generated from a spherical liquid drop subjected to a sudden uniform impact. According to Cohen's model, the following numerical relations were derived:

$$N \approx 0.19\,\hat{E}_T^{2.84} \qquad \text{eq 3.66}$$

In Cohen's model, N is the daughter droplet population and E_T is the dimensionless impact energy, which could be expressed as follows:

$$\tilde{E}_T = E_T / \sigma_{Liq}\,\pi\,d_o^2 \qquad \text{eq 3.67}$$

Where E_T is the droplet impact energy. Another relation expressed by Cohen for the daughter droplet's maximum size, minimum size and Sauter's mean diameter is the following:

$$D_{max}/d_o \approx 2.3\,\hat{E}_T^{-0.943} \qquad \text{eq 3.68}$$

$$D_{min}/d_o \approx \left(1+\hat{E}_T\right)^{-1} \qquad \text{eq 3.69}$$

$$d_{32} \approx 1.78\,\hat{E}_T^{-0.946} \qquad \text{eq 3.70}$$

The size distribution of the daughter droplets resulting from crown splashing was studied theoretically and experimentally by Wu (2003). The proposed distribution satisfied the log-normal distribution function, which contains two parameters: the most probable diameter "d_s" and the distribution width "λ". The value of distribution width was estimated to be nearly 0.41. Hence, the distribution function according to the log-normal law expressed by Wu is as follows:

$$f(D) = \frac{\sqrt{3}}{\sqrt{\pi}d}\exp\left(-3\left(\ln\frac{D}{D_{mean}} - \frac{1}{6}\right)^2\right) \qquad \text{eq 3.71}$$

Where f (D) is the fraction of the droplet size d, D_{mean} is the most probable value of the secondary droplet's diameter (equivalent to mean diameter) estimated as follows:

$$\frac{D_{mean}}{D_{ini}} = 4.23\left(\sqrt{9+\frac{2\,We(We+12)}{Re}}+3\right)(We+12)^{-1} \qquad \text{eq 3.72}$$

Here D_{ini} is the mother droplet's diameter. The results of this distribution fit well with much of the experimental data.

Chapter 4: Implementing Numerical Package to estimated Droplet size distribution and vapour Generation during Liquid Release

4.1 Introduction

This chapter presents the integration of different numerical and empirical equations into a comprehensive numerical package. Such a package may be implemented to describe the process of liquid breakup during accidental release. In particular, the assessment of droplet size distribution and the amount of vapour generation during the successive stages of the entire scenario.

The numerical calculations were divided in to four main stages. The first stage expressed the numerical model calculations of the liquid jet primary breakup. Moreover, it provided an estimate for both the breakup length and the resulting droplet size distribution. The second stage examined the stability of each droplet size and the possibility to disintegrate due to aerodynamic forces. The third stage was concerned with the application of numerical calculations for droplet velocity change, mass loss due to evaporation and the probability of further aerodynamic disintegration on each size of the falling liquid droplets. The final calculation stage assessed the probability of impinging droplets for splashing and formation of smaller daughter droplets. Hence, this calculation package aimed to describe the variation of droplet size distribution during the different release stages. Accordingly, this characterization is essential to estimate the amount of vapour and airborne liquid droplets which might contribute to the formation of fuel-air cloud.

Several aspects will be covered throughout this chapter. Section 4.2 illustrates the general structure of the numerical package. Section 4.3 explains the calculations related to the primary breakup of liquid jet. The calculations defining different droplet changes during free-falling are spread over Section 4.4. Finally, section 4.5 is focused on the droplets impinging and probability of further disintegration.

4.2 General Structure of the Numerical Package

4.2.1 Summary of liquid release mechanisms

The liquid jet release may incorporate various mechanisms. involving the types of mechanical liquid disintegration as well as other conjugated mechanisms might be included. The sequence of such mechanisms could be summarized as follows:

1- The surface tension forces and the aerodynamic forces at the begging of the liquid jet release may succeed to break the liquid bulk into liquid droplets with various sizes. This mechanism is called the primary breakup of liquid jet. The breakup type, the resulting droplet size distribution and the distance with which the jet breakup takes place could be estimated from numerical equations. These above mentioned parameters are dependent on the release conditions, environmental conditions and properties of the released liquid.

2- After the primary breakup takes place, some of the resulting liquid droplets may be aerodynamically unstable due to their size and velocity. Those droplets will directly undergo further disintegration producing smaller droplets. This mechanism is called the secondary breakup of liquid droplets. The droplet size distribution should develop after this process.

3- Droplets resulting from the previous stage will fall down under the effect of gravity forces. During the free-falling distance, liquid droplets may undergo different velocity and mass changes. These potential changes are illustrated as follows:

   a- According to the initial droplet velocity and the terminal settling velocity of each droplet’s size, it may accelerate or decelerate approaching its terminal velocity. The final velocity reached will depend on the available falling distance.

   b- When droplets accelerate, some of the droplet sizes may reach their critical velocity of disintegration. This will lead to further disintegration of liquid droplets.

   c- Liquid droplets may lose or gain mass through evaporation or condensation process. This process is strongly dependent on vapour saturation level of the surrounding medium and the physical properties of released liquid.

d- During free-fall, liquid droplets may be subjected to collision with each other. In some cases, this collision could result in coagulation of droplets or disintegration of large droplets.

4- At the end of falling distance, liquid droplets will impinge on either solid or wetted surface. The droplet impinging may cause spreading or splashing. If splashing takes place, the droplet will disintegrate forming smaller daughter droplets.

During the successive mechanisms, the resulting droplet size distribution and droplets velocity are constantly changing. In order to estimate the amount of generated vapour, these two variants must be well tracked. Fig (4.1) illustrates the different mechanisms that might take place during the vertical flow of liquid release at an initial velocity governed by the force of gravity.

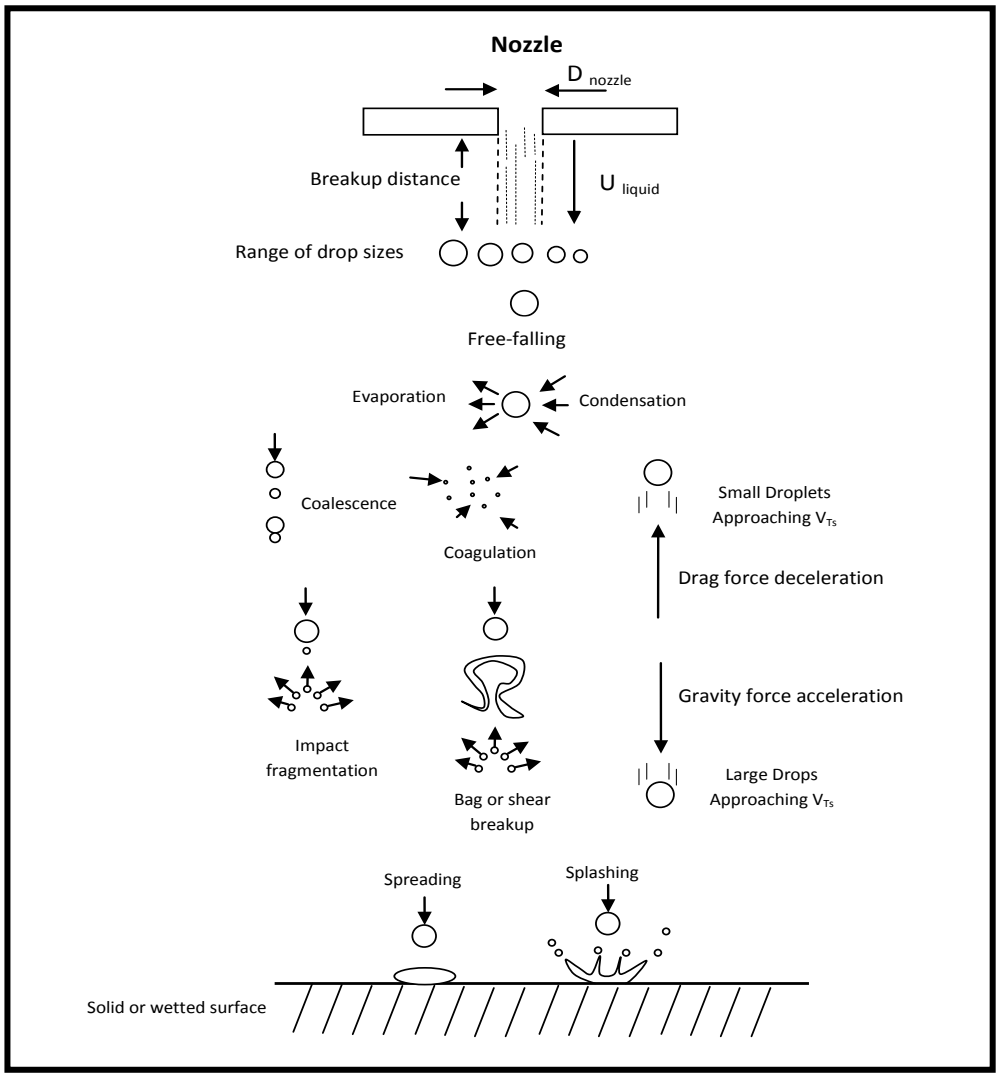

Figure 4.1 Different mechanisms during accidental liquid release

4.2.2 Numerical Package Assumptions

The liquid release mechanisms are pretty complicated and significantly overlapped, thus, some assumptions are imposed for the purpose of simplification. The numerical package was built-up based on the following assumptions:

1- The numerical calculations are limited to the case of liquid jet releasing vertically with initial release velocity and under the effect of both gravity and drag forces. The numerical calculations consider the release velocity as an initial condition rather than pressure difference to simplify the calculations of fluid mechanics inside pipe or tank.

2- The release is assumed to take place in a fully quiescent environment, where the wind velocity is presumed to be negligible.

3- The liquid is supposed to be released from plain round orifice, and orifice geometry effect on release mechanism is neglected.

4- The numerical package doesn't take into account the changes in droplets population and the variable size distribution resultant from coalescence, coagulation and collision-induced fragmentation.

5- Temperature changes due to evaporation and heat transfer are also over looked.

6- The numerical package applies droplets impinging only on solid and wetted surfaces and doesn't apply for impinging on deep liquid layers.

7- The initial velocity of the formed liquid droplets will be equal to the jet velocity at the nozzle. The acceleration of liquid jet along the breakup length will not be considered.

8- The properties of impact surface such as surface roughness and temperature will not be considered when modelling the splash criteria.

4.3 Primary Breakup of Liquid Jet

When liquid is initially released, the variables such as (breakup regime, breakup length and particle size distribution) are dependent on the release conditions (exit diameter and liquid release velocity), the air mixture properties (air mixture density and air mixture viscosity) and the physical properties of the released liquid (density, viscosity, surface tension...etc).

In order to determine these variables, the physical properties of both air mixture and released liquid are need to be determined at the existing temperature. Afterwards, both the Weber's and Reynolds number for the released liquid and ambient air maybe calculated.

4.3.1 Calculating Ambient Air Properties

4.3.1.1 Calculating air density

The density of humid air which may contain some fuel vapours will be calculated from the following equation:

$$\rho_{air} = \frac{P_{par,dry}}{R_{dry}T} + \frac{P_{par,wv}}{R_{wv}T} + \frac{P_{par,\,fv}}{R_{fv}T} \qquad \text{eq 4.1}$$

This illustration is valid when $P_{par,dry}$, $P_{par,wv}$ and $P_{par,fv}$ are the partial pressures of dry air, water vapour and fuel vapour respectively (Pascals), R_{dry}, R_{wv} and R_{fv} are the specific gas constants for dry air, water vapour and fuel vapour respectively (J/kg·K) and T is the ambient temperature (K).

(a) The partial pressure of water vapour (P_v) could be calculated from the saturation vapour pressure and relative humidity according to the following equation:

$$P_v = \varphi P_{sat,v} \qquad \text{eq 4.2}$$

Here φ is the relative humidity (values between 0 and 1), and $P_{sat,v}$is the saturation vapour pressure of water (Pa). At any given temperature, the saturation vapour pressure of water could be estimated directly from the following equation,

$$P_{sat,wv} = 6.1078 \times 10^{\frac{7.5T-2048.625}{T-35.85}} \qquad \text{eq 4.3}$$

This will give a result in (mbar) and must be multiplied by 100 to transform into Pascal.

(b) The partial pressure of each fuel vapour ($P_{sat,fv}$) could be estimated from the saturated fuel vapour pressure and relative fuel vapour saturation as follows:

$$P_{fv} = \Psi_{fuel} P_{sat,fv} \qquad \text{eq 4.4}$$

Where ψ_{fuel} is the fuel vapour saturation (value between 0 and 1).

The saturated vapour pressure could be estimated from Antoine's equation as follow:

$$\log P_{sat,fv} = A - \frac{B}{C+T} \qquad \text{eq 4.5}$$

In this equation, T is the temperature (K), $P_{sat,fv}$ is the saturated vapour pressure of fuel (bars), A, B and C are the Antoine's coefficients. Values of the Antoine's coefficients for different liquid fuels are represented in Appendix (A6).

(**c) The partial pressure of dry air (P_{dry})** is then calculated as the remaining partial pressure,

$$P_{par,dry} = 101325 - \sum P_{par,fv} - P_{par,wv} \qquad \text{eq 4.6}$$

(d) The specific gas constant ($R_{specific}$) for each material could be calculated from the molar constant (R), divided by the molar mass (M),

$$R_{specific} = \frac{R}{M} \qquad \text{eq 4.7}$$

where, $R_{specific}$ in (J/kg·K), R= 8.3144621in (J/mol.K) and M is the molecular weight of fuel vapour in (Kg/mol). Molecular weights of different liquid fuels are represented in Appendix (A1).

4.3.1.2Calculating Air Viscosity

Air mixture viscosity is calculated according to the following equation (Riazi, 2005),

$$\mu_{Air} = \frac{\sum_{i=1}^{N} X_i \, i \, \mu_i}{\sum_{i=1}^{N} X_i \, i} \qquad \text{eq 4.8}$$

Where $\mu_{Air}$is the viscosity of the air mixture (Pa.s), i is the mole index of the component (i= $M_i^{0.5}$), Nis the number of mixture components, X_i is the mole fraction of component i and $\mu_i$is the viscosity of component i (Pa.s).

Viscosity of each component is calculated according to the viscosity coefficients of pure vapour compounds (listed in Appendix.A3) and the existing ambient temperature.

4.3.2 Calculating Released Liquid Properties.

Density, viscosity and surface tension of the released liquid fuel could be estimated from empirical equations specific for each type of liquid fuels. These equations utilize specific coefficients for each type of liquid fuels. The Appendices A.2, A.4 and A.7 present the empirical equations used for estimating liquid properties, and also present

the tables of coefficients for different fuel liquids. Each equation is dependent on liquid temperature in (Kelvin).

4.3.3 Calculating Dimensionless Numbers

After estimating the physical properties of both the released liquid and the air mixture, the dimensionless numbers could be calculated from equations 3.9, 3.10, 3.11, 3.12, 3.13 and 3.31 for the values of Re_{liq}, We_{liq}, Oh_{liq}, We_{Air}, Je and Re_{Air} respectively.

4.3.4 Breakup Regime Classification.

According to the discussion presented in section (3.3.2), the liquid jet breakup could be classified into five breakup regimes depending on the value of the air Weber number (We_A) and the jet number (Je) as follows:

Table 4.1 Classification of liquid breakup regimes

Dimensionless number	breakup Regime
$Je_{Liq} < 0.1$	Liquid Dripping
$We_{Air} < 0.4$ or	Rayleigh jet Breakup
$0.4 < We_{Air} < 13$	First Wind induced breakup
$13 < We_{Air} < 40.3$	Second Wind induced breakup
$We_{Air} > 40.3$	Atomization

4.3.5 Calculating Breakup Length and Mean Droplet Diameter

Based on the proper choice of the jet breakup regime, the breakup length and droplets size distribution could be estimated for each case as follows:

4.3.5.1Dripping Regime

In this case the liquid drops are completely formed under the effect of gravity force. The drops are formed exactly at no distance from the nozzle and start free-falling from the rest. Hence, breakup length and initial droplets velocity will be assumed to be zero. The average value for droplet diameter are estimated from equation (3.2)

4.3.5.2Rayleigh Breakup Regime

Most of the transportation fuels utilized in this model are assumed to be non-viscous. Subsequently the wave length (λ_{opt}) of the fastest-growing disturbance will be estimated from equation (3.7) and then the droplet average diameter could be estimated from equation (3.8). The breakup length is estimated from equation (3.16) for laminar flow (Re_{Air}< 2000) and from equation (3.17) for turbulent flow (Re_{Air} > 2000).

4.3.5.3Other Regimes

For the first and second wind induced regimes, the breakup length (L) is calculated from equation (3.16) for laminar flow (Re_{Air}< 2000) and from equation (3.17) for turbulent flow (Re_{Air} > 2000). However, for the atomization regime, breakup length is assumed to be zero according to the principles of disintegration theory.

The Rosin-Rammler distribution function, expressed in equation (3.19), will be used to estimate the resulting droplet size distribution of the formed droplet. The value of distribution coefficient (q) will be assumed as 2 to indicate indicates the non-uniform distribution during accidental fuel releases.

The maximum diameter of the resulting droplets ($D_{0.999}$) will be estimated from equation (3.21). Then, the median mean diameter value (MMD) will be estimated relatively according to the basis of the Rosin-Rammler distribution function as following:

$$\frac{D_{0.999}}{MMD} = (9.968)^{1/q} \qquad \text{eq4.9}$$

For q = 2,

$$MMD = \frac{3.1572}{D_{0.999}} \qquad \text{eq4.10}$$

4.4 Free-Falling and Secondary Breakups of Droplets

As mentioned earlier in this chapter, some of the formed liquid droplets may undergo further disintegration if they exceeded their critical velocity of disintegration. This characteristic velocity depends on droplet size, air mixture and the liquid physical properties. For some droplet sizes, this could happen directly after the formation. In other cases, droplets may reach their critical velocity due to acceleration.

During free-falling, liquid droplets are usually exposed to different velocity and mass changes. The droplets may accelerate or decelerate depending on the mutual relation between the motion velocity and the settling velocity concerning each droplet. While the droplets' mass may change due to evaporation or disintegration.

The probability to disintegrate is overshadowed by both the terminal settling velocity and the critical velocity of disintegration for each size. Consequently, the characteristics of each droplet size must be updated regularly during free-fall to ensure accurate estimates. The calculation during free-fall period will be discussed in details in the next sections.

4.4.1 Settling Velocity of Liquid Droplets.

During the free-fall of liquid droplets, all droplet sizes will accelerate or decelerate to reach the terminal settling velocity. The terminal velocity (V_{ter}) will be calculated for various droplets as follows,

1- For the slow moving droplet ($Re_{Air} < 1$), Terminal velocity will be calculated from equation (3.40) according to Stokes' law. The value of slip correction factor (C_c) and mean free bath (λ) will be estimated respectively from equation (3.41) and equation (3.43).

2- For the faster moving droplet ($Re_{Air} > 1$), terminal velocity is calculated from the Newton's law expressed in equation (3.30).

The drag coefficient (C_D) will be estimated from equation (3.32), equation (3.35) according to the value of Reynolds number (Re_{Air}). If the value of Reynolds number is larger than 1000, then the value of drag coefficient will equal 0.44.

In order to determine C_{Drag}, the Reynolds' number must be calculated first. The value of the Reynolds' number at that moment is dependent on the terminal velocity of the droplet. To solve this dilemma, the following steps will be performed (Hinds, 1999):

a) Terminal velocity is always to be calculated first according to Stokes' law (assuming that $Re_{Air}<1$).

b) Reynolds' number then is calculated using the value of terminal velocity calculated in step (1).

c) If the calculated value of Reynolds' number is larger than 1, then using Stokes' law is wrong in that case.

d) To calculate terminal velocity according to Newton's law independently on the value of drag coefficient, the equation of drag coefficient in the transition region is substituted in the equation of Newton's law of terminal velocity as follows:

$$V_{ter} = \left(\frac{4\,\rho_{Liq}\,g\,D}{3\,\rho_{Air}\,\frac{24}{Re_{Air}}\left(1+0.15\,Re_{Air}^{0.687}\right)} \right)^{0.5} \qquad \text{eq4.11}$$

By substituting the value of the drag coefficient from equation (3.32) then,

$$V_{ter}^2 = \frac{4\,\rho_{Liq}\,g\,D}{\frac{72\rho_{Air}}{Re_{Air}} + \frac{10.8\ \rho_{Air}}{Re_{Air}^{0.313}}} = \frac{4\rho_{Liq}\,g\,D\ Re_{Air}}{72\rho_{Air} + 10.8\ \rho_{Air} Re_{Air}^{0.687}} \qquad \text{eq4.12}$$

By substituting the value of the air mixture Reynolds number from equation (3.31) then,

$$V_{ter}^2 = \frac{4\,\rho_{Liq}\rho_{Air}\,g\,D\,D}{\mu_{Air}\left(72\rho_{Air} + 10.8\ \rho_{Air} Re_{Air}^{0.687}\right)} \qquad \text{eq4.13}$$

$$V_{terl}^2 = \frac{4\,\rho_{Liq}\rho_{Air}\,g\,D^2\,V_{ter}}{72\mu_{Air}\rho_{Air} + \frac{10.8\rho_{Air}\rho_{Air}^{0.687}\mu_{Air}V_{ter}^{0.687}D^{0.687}}{\mu_{Air}^{0.687}}} \qquad \text{eq4.14}$$

$$V_{ter}^2 = \frac{4\,\rho_{Liq}\rho_{Air}\,g\,D^2\,V_{ter}}{72\mu_{Air}\rho_{Air} + 10.8\,\rho_{Air}^{1.687}\,\mu_{Air}^{0.313}\,D^{0.687}\,V_{ter}^{0.687}} \qquad \text{eq4.15}$$

$$72\,\mu_{Air}\rho_{Air}V_{ter}^2 + 10.8\,\rho_{Air}^{1.687}\,\mu_{Air}^{0.313}\,D^{0.687}\,V_{terl}^{2.687} = 4\,\rho_{Liq}\rho_{Air}\,g\,D^2\,V \qquad \text{eq4.16}$$

$$72\,\mu_{Air}V_{ter} + 10.8\,\rho_{Air}^{0.687}\,\mu_{Air}^{0.313}\,D^{0.687}\,V_{ter}^{1.687} = 4\,\rho_{Liq}\,g\,D^2 \qquad \text{eq4.17}$$

Equation 4.17 will be solved using the trial-and-error method to estimate the accurate value of terminal settling velocity.

e) The Reynolds number is calculated again using the resulting terminal settling velocity obtained at step 4. If the value of Reynolds number is greater than 1,000 then thecalculations of terminal velocity in step (d) are wrong. Terminal velocity

must be recalculated assuming that the motion is in the Newton's law region and using the value of the drag coefficient (C_D) = 0.44.

4.4.2 The Velocity Change of Liquid Droplets

As previously mentioned, liquid droplets during free fall may accelerate or decelerate. The limiting factor controlling this process is the ratio between the actual droplet velocity and the terminal velocity. Each droplet falling freely under the influence of the gravity force tends to reach its terminal velocity. Droplet moving with velocity lower than the terminal velocity will accelerate, while the droplet moving with velocity higher than the terminal velocity will start to decelerate. Multiple equations are manipulated to estimate the velocity changes. These equations vary according to whether the droplet is moving in Stokes region or Newton's region.

4.4.2.1Drplets Moving in Stokes' Region.

The fine droplets (D < 100μm) are expected to decelerate rather than accelerate. The terminal velocity of such droplets in most cases is less than 0.3 m/s, which is most likely lower than the liquid jet release velocity. In general, the instantaneous velocity and displacement will be calculated from equation (3.52) and equation (3.53) respectively, and the value of relaxation time will be estimated from equation (3.51).

For the small droplets accelerating from $V_o < V_{ter}$ to reach terminal velocity:
V_f is assumed as V_{ter}, V is assumed to be $0.95V_{ter}$, and $\tau = V_{ter}/9.81$.
Therefore, the above formulas are rearranged in the following forms,

$$0.95\,V_{ter} = V_{ter} - \left(V_{ter} - V_o\right)e^{-\frac{t}{\tau}} \qquad \text{eq4.18}$$

$$0.05\,V_{ter} = \left(V_{ter} - V_o\right)e^{-\frac{t}{\tau}} \qquad \text{eq4.19}$$

$$\ln\frac{0.05\,V_{ter}}{V_{ter} - V_o} = e^{-\frac{t}{\tau}} \qquad \text{eq4.20}$$

$$t = -\tau \ln\frac{0.05\,V_{ter}}{V_{ter} - V_o} \qquad \text{eq4.21}$$

$$\left[X = V_{ter}\,t - \left(V_{ter} - V_o\right)\tau\left(1 - e^{-\frac{t}{\tau}}\right)\right] \qquad \text{eq4.22}$$

For small droplets decelerating from $V_o > V_{ter}$ to reach terminal velocity:

V_f is assumed as V_{ter}, V is assumed to be $0.05V_{ter}$, and $\tau = V_{Ts}/9.81$.

The above formulas are rearranged in the following forms:

$$0.05\,V_{ter} = V_{ter} - (V_o - V_{ter})e^{-\frac{t}{\tau}} \qquad \text{eq4.23}$$

$$0.95\,V_{ter} = (V_o - V_{ter})e^{-\frac{t}{\tau}} \qquad \text{eq4.24}$$

$$\ln\frac{0.95\,V_{Terminal}}{V_o - V_{Terminal}} = -\frac{t}{\tau} \qquad \text{eq4.25}$$

$$t = -\tau \ln\frac{0.95\,V_{ter}}{V_o - V_{ter}} \qquad \text{eq4.26}$$

$$\left[X = V_{ter}\,t - (V_o - V_{ter})\tau\left(1 - e^{-\frac{t}{\tau}}\right)\right] \qquad \text{eq4.27}$$

In general, the time and distance needed for the small like aerosl droplets to reach their terminal settling velocity are relatively very small and could be neglected. Table (4.2) provides the time and distance needed for different aerosol droplet sizes to reach terminal velocity.

Table 4.2 Time and displacement needed for aerosol droplets to reach terminal velocity

D (μm)	V_{ter} (m/s)	Acceleration			Deceleration		
		V_o (m/s)	T (sec)	X (m)	V_o (m/s)	T (sec)	X (m)
1	0.00004	0	1.1×10^{-5}	3.6×10^{-10}	1	4.7×10^{-5}	3.6×10^{-6}
10	0.00307	0	9.4×10^{-4}	2.8×10^{-06}	1	2.7×10^{-3}	3.2×10^{-4}
20	0.01219	0	3.7×10^{-3}	4.5×10^{-5}	1	9.2×10^{-3}	1.3×10^{-3}
50	0.07584	0	2.3×10^{-2}	1.7×10^{-3}	1	4.2×10^{-2}	1.0×10^{-2}
100	0.30288	0	9.2×10^{-2}	2.7×10^{-2}	1	1.2×10^{-1}	5.6×10^{-2}

4.4.2.2Droplets moving in Newton's Region

The relatively larger droplets may accelerate or decelerate depending on the relation between the instantaneous velocity and the terminal velocity.

For accurate calculations of the falling time, the distance and the drag acceleration should be estimated continuously during free fall, where the value of the drag

coefficient is dependent on the instantaneous droplet velocity. The drag acceleration could be estimated as follows:

$$a_{Drag} = \frac{F}{m} = \frac{\rho_{Air}\, C_D\, A\, V_{Drop}^2}{2m} \qquad \text{eq4.28}$$

Here, a_{Drag} is the drag acceleration (m/s^2) acting on the liquid droplet falling with velocity V_{Drop} (m/s), A is the droplet's cross-section area (m^2):C_D is the instantaneous dimensionless drag coefficient for the falling droplet and m is the droplet's mass (kg).

$$A = \pi r^2 \qquad \text{eq4.29}$$

$$m = \frac{\rho_{Liq}\, \pi\, D_D^3}{6} \qquad \text{eq4.30}$$

By substituting eq 4.29 and 4.30 in equation 4.28 then,

$$a_{Drag} = \frac{3\ \rho_{Air} C_D V_{Drop}^2}{4\,\rho_{Liq}\, D} \qquad \text{eq4.31}$$

In the Stokes region,

$$C_D = \frac{24}{Re_{Air}} = \frac{24\,\mu_{Air}}{\rho_{Air}\, V_{Drop}\, D} \qquad \text{eq4.32}$$

$$a_{Drag} = \frac{3\rho_{Air}\, 24\,\mu_{Air} V_{Drop}^2}{4\,D\ \ \rho_{Liq}\,\rho_{Air}\, V_{Drop}\, D} = \frac{18\, V_{Drop}\,\mu_{Air}}{\rho_{Air}\, D^2} \qquad \text{eq4.33}$$

In each time step, drag acceleration is calculated according to the instantaneous falling velocity. Total acceleration (gravity acceleration + drag acceleration) will be used to predict the droplet's velocity in the next time interval.

4.4.3 Critical Velocity and Secondary Breakup of Liquid Droplets

During free-falling, if a liquid droplet reaches its critical velocity it will disintegrate. Therefore, the droplet's velocity must be continuously compared with the specific critical velocity of disintegration throughout the whole process of free-falling. The critical velocity of disintegration for each droplet size (m/s) will be calculated from the following equation (Liu, 2000),

$$V_{Crit} = \left(\frac{8\,\sigma_{liq}}{\rho_{Air}\,D\,C_{Drag}} \right)^{0.5} \qquad \text{eq4.34}$$

Coefficient C_D is calculated according to the value of Re_{Air}. In order to calculate the critical velocity independently on the value of drag coefficient, the following steps are performed:

1- Droplet sizes with $Re_{Air} < 1$ are not expected to disintegrate. To prove that, the drag coefficient equation in Stokes region is substituted in the critical velocity equation. Terminal velocity is then calculated using the following form:

$$V_{Crit}^2 = \frac{8\,\sigma_{liq} Re_{Air}}{24\,\rho_{Air}\,D} = \frac{\sigma_{liq}\,\rho_{Air}\,D\,V_{Crit}}{3\,\rho_{Air}\,D\,\mu_{Air}} \qquad \text{eq4.35}$$

$$V_{Crit} = \frac{\sigma_{liq}}{3\,\mu_{Air}} \qquad \text{eq4.36}$$

Table (4.3) presents the critical velocities and the corresponding droplet diameters for different liquids Where $Re_{Air}<1$, $\rho_{Air} = 1.2$ kg/m^3.

Table 4.3 Critical velocity and corresponding diameter for different liquid droplets at $Re_{Air} < 1$

Liquid Type	Surface Tension (N/m)	V_{crit} (m/s)	Corresponding Diameter (μm)
Water	72×10^{-3}	1333.3	$<1.1 \times 10^{-2}$
Ethanol	21.9×10^{-3}	405.5	$<3.7 \times 10^{-2}$
Ethanediol	48×10^{-3}	888.8	$< 1.7 \times 10^{-2}$
Acetone	23.3×10^{-3}	413.5	$< 3.6 \times 10^{-2}$
Benzene	28.9×10^{-3}	535.2	$< 2.8 \times 10^{-2}$
Gasoline	19.7×10^{-3}	364.8	$< 4.1 \times 10^{-2}$

The results provided in table (4.3) show that the disintegration conditions for liquid droplets with the Reynolds number < 1 are very difficult to achieve during free-fall.

2- Terminal velocity is calculated by substituting equation 3.35 in equation 4.34 as follows:

$$V_{Crit}^2 = \frac{8\,\sigma_{liq}}{\rho_{Air}\,D\left(\frac{24}{Re_{Air}} + \frac{3.6}{Re_{Air}^{0.313}} \right)} = \frac{8\,\sigma_{liq}}{\frac{24\,\rho_{Air}\,D}{Re_{Air}} + \frac{3.6\,\rho_{Air}\,D}{Re_{Air}^{0.313}}} \qquad \text{eq4.37}$$

$$V_{Crit}^2 = \frac{8\,\sigma_{liq}\,Re_{Air}}{24\,\rho_{Air}\,D\ + 3.6\,\rho_{Air}\,D\ \ Re_{Air}^{0.687}} \qquad \text{eq4.38}$$

$$V_{Crit}^2 = \frac{8\,\sigma_{liq}\rho_{Air}V_{Crit}D}{\mu_{Air}\left(24\,\rho_{Air}\,D\ + \dfrac{3.6\ \rho_{Air}\,D\ \ \rho_{Air}^{0.687}D^{0.687}V_{Crit}^{0.687}}{\mu_{Air}^{0.687}}\right)} \qquad \text{eq4.39}$$

by substituting the value of Reynolds number for air mixture from equation 3.31

$$V_{Crit}^2 = \frac{8\,\sigma_{liq}\,\rho_{Air}\,V_{Crit}\,D}{24\,\rho_{Air}\,D\ \ \mu_{Air} + 3.6\,\rho_{Air}^{1.687}\ \mu_{Air}^{0.313}\ D^{1.687}\ V_{Crit}^{0.687}} \qquad \text{eq4.40}$$

$$24\,\rho_{Air}\,D\ \ \mu_{Air}V_{Crit}^2 + 3.6\,\rho_{Air}^{1.687}\ \mu_{Air}^{0.313}\ D^{1.687}\ V_{Crit}^{2.687} = 8\,\sigma_{liq}\,\rho_{Air}\,V_{Crit}\,D \qquad \text{eq4.41}$$

$$24\ \ \mu_{Air}V_{Crit} + 3.6\,\rho_{Air}^{0.687}\ \mu_{Air}^{0.313}\ D^{0.687}\ V_{Crit}^{1.687} = 8\,\sigma_{liq} \qquad \text{eq4.42}$$

This equation will be solved using the trial-and-error solution for the accurate value of droplet critical velocity.

3- The Reynolds number is calculated again using the resulting terminal settling velocity from step 4. If the value of Re_{Air} number is greater than 1,000, the terminal velocity is calculated again using the value of the drag coefficient (C_{Drag}) = 0.44.

The Sauter mean diameter for a daughter droplet resulting from secondary breakup is estimated from equation (3.26). the equation could be rearranged into the following form:

$$SMD = 6.2\left(\frac{1}{\rho_{Liq}\,\rho_{Air}}\right)^{1/4}\left(\frac{D_{ini}\,\mu_{Liq}}{V_R}\right)^{1/2} \qquad \text{eq4.43}$$

The Rosin-Rammler distribution function is used to describe the daughter droplet's size distribution. The median mean diameter is then estimated from the following ratio (Simmons, 1977a, b):

$$MMD = SMD \times 1.2 \qquad \text{eq4.44}$$

After secondary breakup disintegration calculations, the volume fraction of each droplet's size is modified according to the disintegration and formation process of secondary breakup.

4.4.4 Evaporation of Liquid Droplets

Droplets evaporation during free-fall is the second phenomenon in which mass change may take place. At the begging of accidental releases, the fuel vapour concentration is expected to be very low. Evaporation from droplets' surfaces at that time will take place. As the release continues, the concentration may increase depending on vaporisation rate and dilution rate. As soon as the surrounding media reach the saturation conditions, evaporation from droplets could stop.

The following procedure will be performed to estimate the droplets' mass loss due to evaporation:

- All droplets will be assumed with diameter larger than 1μm. Therefore, the saturation ratio (S_R) will be calculated from equation (2.4). the change in droplet diameter with time will be estimated from the following equation (Holterman, 2003; Hinds, 1999),

$$\frac{d(D)}{dt} = \frac{4\ DV\ M_{Liq}}{R\,\rho_{Liq} D}\left(\frac{P_o}{T} - \frac{P_{par,drop}}{T_d}\right)\left(1 + 0.276\,Re_{Air}^{1/2}\,Sc^{1/3}\right)\phi \qquad \text{eq4.45}$$

Here the droplet diameter D is > 0.066 μm (the mean free bath).

Where, DV is the diffusion coefficient of the vapor molecules (m^2/s), P_o and T are the pressure and temperature away from droplet's surface in (Pa and K), $P_{par,drop}$ and T_d are the pressure and temperature right at the drop's surface in (Pa and K), M_{Liq} is the molar mass (gm/mole), R is the universal gas constant (J/K. mole), ϕ is the Fuchs correction factor, and Sc is the dimensionless Schmidt's number. The value of the vapour diffusion coefficient and Schmidt's number can be expressed by the following equations:

$$DV = \frac{k\,T\,C_c}{3\,\pi\,\mu_{Air}\,D} \qquad \text{eq4.46}$$

$$Sc = \frac{\mu_{Air}}{\rho_{Air}\,DV} \qquad \text{eq4.47}$$

Here it is understood that k is the Boltzmann constant = 1.38 $x10^{-23}$ N.m/K

- D > 1μm, then the Fuchs' correction factor is neglected.

If $S_R > 0.95$, then $T_d = T_\infty$. Otherwise the temperature difference will be calculated from equation (2.9).

4.5 Droplet Impingement

4.5.1 Impinging Model Selection

A few models have been developed to describe the process of the liquid droplet impact on solid or wetted surfaces. Two main criteria should be taken into consideration when choosing such a model. First, the model needs to determine the regime and if splashing will take place or not. Second, the model has to predict the size distribution of the resulting daughter droplets when splashing takes place. The impact angle is assumed to be negligible because the surface is far from the release nozzle and the droplets are assumed to fall vertically.

4.5.1.1 The Transition from Spreading to Splashing

The following equations express different correlations to estimate the critical Weber number for the transition from spreading to splashing:

$$a - We_{impact} > 7.9\times10^{10}\times Oh_{Liq}^{2.8} \quad \text{(Stow and Hadfield,1981)} \quad \text{eq4.48}$$

$$b - We_{impact} > 1320\left(\frac{\rho_{Liq}\,\sigma_{Liq}\,D_{Drop}}{\mu_{Liq}^{2}}\right)^{-0.18} \quad \text{(Bai and Gosman,1995)} \quad \text{eq4.49}$$

$$c - We_{impact} > 80 \quad \text{(Wachters and Westerling, 1966)} \quad \text{eq4.50}$$

$$d - We_{impact}^{0.5}\,Re_{Liq}^{0.25} > 57.7 \quad \text{(Mundo, Sommerfield and Tropea ,1995)} \quad \text{eq4.51}$$

A comparison between the different correlations has been presented in Figure 4.2. The results were estimated for water droplets with D=1mm at temperature = 25°C.

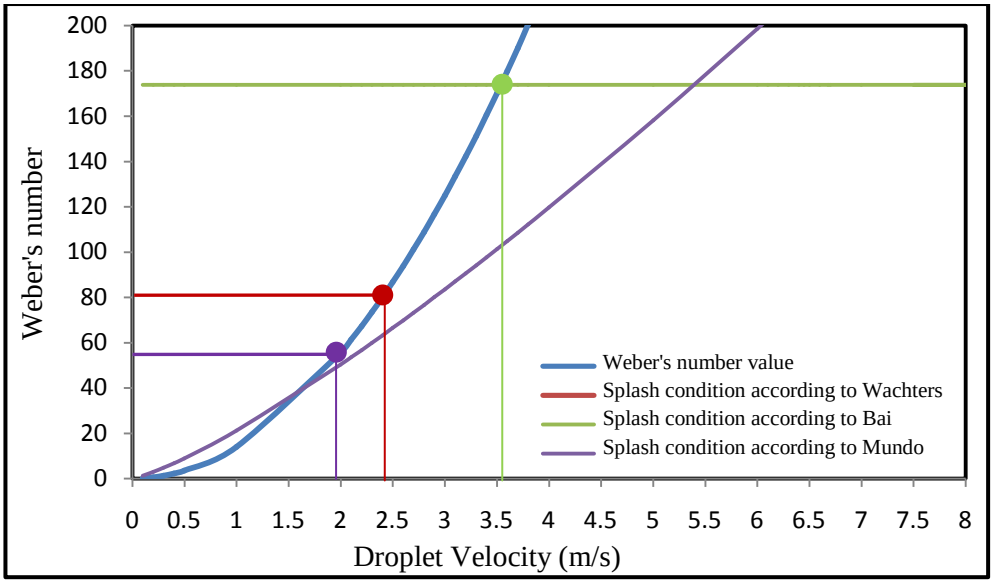

Figure 4.2 Different correlations for the transition from spreading to splashing

The conclusions from figure 4.2 are summarized as follows:

a) The correlation of Stow and Hadfield is not shown in figure 4.2 because the value of We_{impact} is out of range. According to this correlation, the transition from spreading to splashing was achieved at droplet velocity =28.5 m/s. In fact, this velocity is impossible to reach by such droplet size during free-fall.

b) The three other correlations have achieved relatively close results. The transition from spreading to splashing took place at droplet velocity equals 1.9, 2.4 and 3.6 m/s from the correlation of Mundo, Wachter and Bai respectively.

c) The correlation presented by Mundo has the minimum Weber number to achieve splashing and incorporates a wide range of droplet impaction in the splashing regime. Hence, it will be selected to allow the splashing of the widest range of droplets.

4.5.1.2 The Mean Diameter of the Resulting Daughter Droplets

The following equations express different correlations for estimating the daughter droplets mean diameter:

$$a\text{-}\,d_{mean} \approx 1.78\,\hat{E}_T^{-0.946} \quad \text{(Cohen,1991)} \qquad \text{eq4.52}$$

$$\text{Where, } \hat{E}_T = \frac{\rho_{Liq}\, V_{Drop}^2\, D}{12\,\sigma_{Liq}} \qquad \text{eq4.53}$$

$$b\text{-}\,d_{mean} = 4.23\,d_o\left(\sqrt{9+\frac{2\,We_{Liq}\left(We_{Liq}+12\right)}{Re_{Liq}}}+3\right)\left(We_{Liq}+12\right)^{-1} \text{ (Wu, 2003)} \qquad \text{eq4.54}$$

c- d_{mean}/d_o has been estimated graphically from the results curve (Mundo, 1995)

A comparison between these correlations is presented in Table (4.4)

Conclusions from table (4.4) are summarized as follows:

The estimated values for (d_{mean}/ d_o) from Cohen's and Wu's correlations are completely divergent.

The results obtained from Wu's correlation are more accepted when compared with the experimental results.

Table 4.4 Estimated Droplets' Mean Diameter for Different Impact Weber Numbers

V_{drop} (m/s)	We_{impact}	d_{mean} / d_o		
		Experimental results expressed by Mundo	Estimated by Cohen's correlation	Estimated by Wu's correlation
6	500	-	52.3	0.282
6.45	579.5	0.16	45.6	0.271
6.5	586.8	-	44.9	0.269
6.68	620.1	0.14	42.6	0.265
7	680.6	-	39.1	0.258
7.5	781.25	-	34.3	0.248
8	888.9	-	30.3	0.239
8.01	891.2	0.08	30.2	0.239
8.5	1003.5	-	27.1	0.230
9	1125	-	24.3	0.224
9.23	1183.2	0.06	23.1	0.220

4.5.2 Estimating Droplet Size Distribution from the Selected Model

For each droplet satisfying the critical Weber number, the mean diameter of the resulting daughter droplets will be estimated from equation (4.54). The droplet size distribution of the resulting daughter droplets will be estimated from the log-normal law as follows:

$$f\left(d_{daughter}\right)=\frac{\sqrt{3}}{\sqrt{\pi d_{daughter}}}\exp\left(-3\left(\ln\frac{d_{daughter}}{d_{ini}}-\frac{1}{6}\right)^2\right) \qquad \text{eq4.55}$$

Where f ($d_{daugther}$) is the function value of a daughter droplet of size $d_{daughter}$, and d_{ini} is the diameter of the splashed mother droplet.

The function values for the different daughter droplets' sizes are not a mass percentage values. These values need to be transformed into percentage values according to the following equation:

$$X_i=\frac{f\left(d_i\right)}{\sum_{i=1}^{N} f\left(d_i\right)} \qquad \text{eq4.56}$$

Where X_i is the mass fraction of a daughter droplet with size i, f (d_i) is the function value of a daughter droplet with size i.

Chapter 5: Numerical Package Programming

The aim of this chapter is to simulate the progress consequences of liquid fuel releases as a function of time. In other words, the target is to estimate the amount of fuel vapours and aerosol droplets generated in each release-time step, taking into account the ambient conditions development.

During continuous releases, if all the conditions, such as release orifice diameter, release velocity and fuel composition, are supposed to be stable, there will be two main factors which might possibly develop some changes due to release consequences. These factors are the fuel vapour fraction in the air mixture and the ambient temperature, which both have a great impact on liquid breakup and liquid evaporation mechanisms. Continuing liquid evaporation will increase the amount of vapour in the air mixture. Also, because of heat transfer during this process, the ambient air mixture temperature may fall. Therefore, ambient conditions are expected to change continuously during the release process, and this will overshadow the overall scenario.

Section 2 of this chapter describes the program development which is performed to solve this problem. In section 3, the effect of temperature and saturated vapour pressure on cloud flammability is under scope. Furthermore, some examples are presented in section 4 to investigate the effect of vapour saturation increase rate on liquid droplets evaporation quality during free-fall.

5.1 Model General Construction and Building up Flowchart

In order to apply the mathematical model in an easy way, a numerical programme is developed using the visual basic programming. The detailed contents of this programmeare given in (Appendix B). This chapter presents the general structure of the numerical programme and the detailed considerations used in the programme's development.

In general, the programme is divided into the following sections. The programme flow chart is presented in figure (5.1).

- Getting user's assumptions and checking inputs acceptance.
- Calculating physical properties of both released liquid and air mixture.
- Calculating dimensionless factors.
- Determining jet breakup regime.

- Estimating breakup length, median and maximum droplets diameter and resulting particle size distribution from liquid jet breakup.
- Checking instantaneous secondary breakup for resulting droplets and redistributing droplets mass fractions.
- Estimating changes in droplets velocity due to acceleration and deceleration during free falling and possibility for disintegration.
- Estimating changes in droplets mass due to evaporation during free falling and redistributing droplets' mass fractions.
- Evaluating falling droplets' possibility to splash.
- Estimating droplets size distribution for splashed daughter droplets.

5.2 Checking the Acceptance of Users' Inputs

The programme allows the user to define the following initial conditions:

1- Release nozzle diameter (supposed to be rounded) in (mm).
2- Liquid release flow velocity in (m/s).
3- Release falling height measured from the ground in (m).
4- Selecting released liquid type from the available list.
5- Ambient temperature in (^{o}C).
6- Liquid temperature in (^{o}C).
7- Atmospheric relative humidity in (%).
8- Fuel vapour saturation in (%).

Figure (5.2) shows the program's main window interface which is used to enter the user's assumptions (input frame) and also contains the operational keys available for the user.

Once the input data is inserted, the program is then ready to start calculations. The first step of the program is to carry out determine if the inputs lie within the acceptable regimes defined by the programme. Details of this step can be found in (Appendix B1 – Part B). The initial assumptions of the program are limited as follows,

- Orifice diameter [1 to 50 mm)
- Release velocity [1 to 30 m/s]
- Falling height [1 to 15 m]
- Temperature range [-20 to +50^{o}C]
-Relative humidity and fuel vapour saturation [0 to 100%]
- The program is able to consider 5 different fuel liquids [Ethanol - Benzene - Toluene - n-Hexane and n-Pentane].

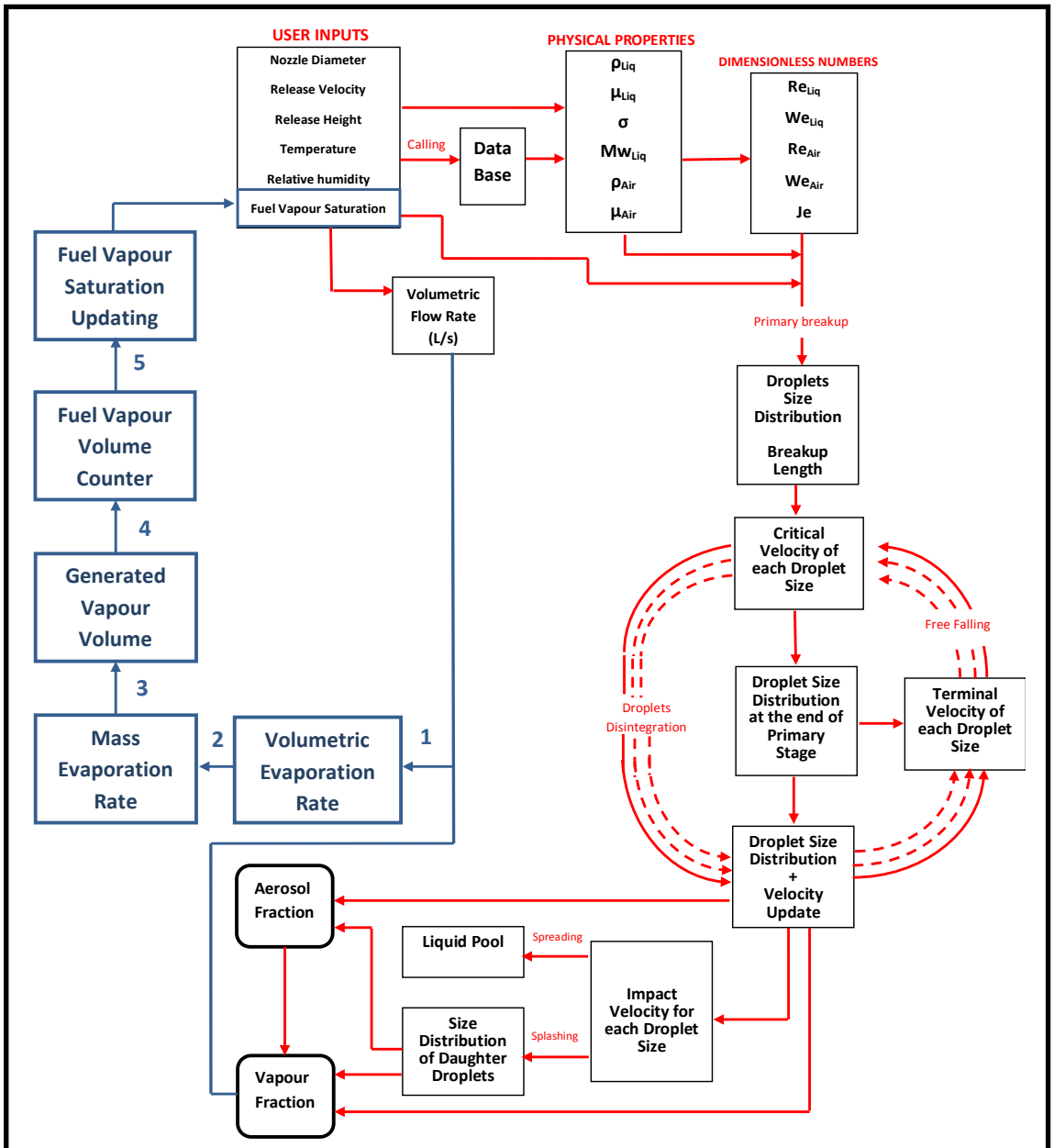

1- VER (L/min) = Vapours Fraction (%) x Liquid Flow Rate (L/s) x 60

2- MER (kg/min) = VER (L/min) x ρ_{Liq} (kg/m^3) x 1000

3- VVGR (m3/min) = MER (kg/min)/ ρ_{FV} (kg/m3)

4- $VV = \sum_{1}^{n} VVGR_n$

5-AV=DA - VV

AM = AV x ρ_{Air}

FVM = VV x ρ_{FV}

FVS = FVM / (FVM + AM)

Where VER is the volumetric liquid evaporation rate (Litre/min), MER is the mass evaporation rate (kg/min), VVGR is the fuel vapour generation rate (m^3/min), VV is the total vapour volume added to the cloud (m^3), AV is the dry or humid air volume in the cloud (m^3), DA is the total cloud dispersion volume (m^3), AM is the dry or humid air mass (kg), FVM is the total mass of fuel vapour (kg) and FVS is fuel vapour saturation (%).

Figure 5.1 The detailed programming flow chart

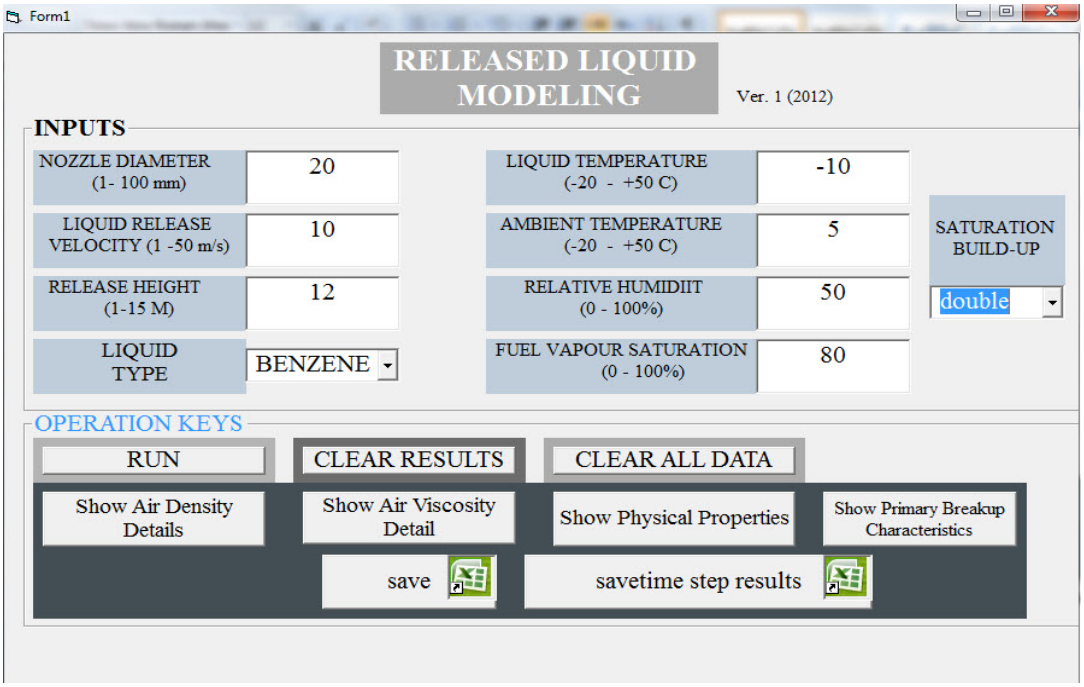

Figure 5.2 The programs main interface windows

5.3 Calculating Physical Properties

In this step of the program, all needed physical properties of both released liquid and air mixture are calculated relative to release temperature using the equations from equation 4.1 to equation 4.8. These calculations are carried out in a separate calling function. This calling function contains the data base and all coefficients needed to calculate the density, viscosity and surface tension of the released liquid, and the density and viscosity of air mixture. Program data base and calculation steps for calculating physical properties are presented in Appendix B1 – Part E and Appendix B2.The results of these calculations are available to display in three different interface windows shown in figures 5.3, 5.4 and 5.5.

5.4 Calculating Dimensionless Factors

After the physical properties are calculated, the dimensionless factors such as Re_{liq}, We_{liq}, Oh_{liq}, We_{Air}, Je and Re_{Air} are calculated depending on these values using equations from 3.9, 3.10, 3.11, 3.12, 3.13 and 3.31.The values of the dimensionless factors are expressed in a separate interface window shown in figure (5.6). Details of this step are given in Appendix B1 – Part F.

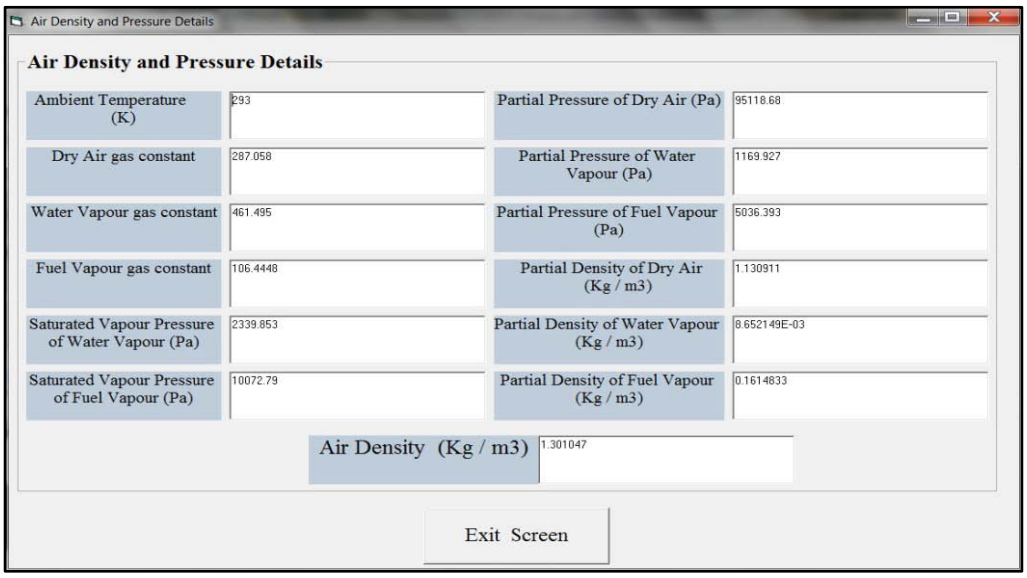

Figure 5.3 The program interface windows for density and pressure

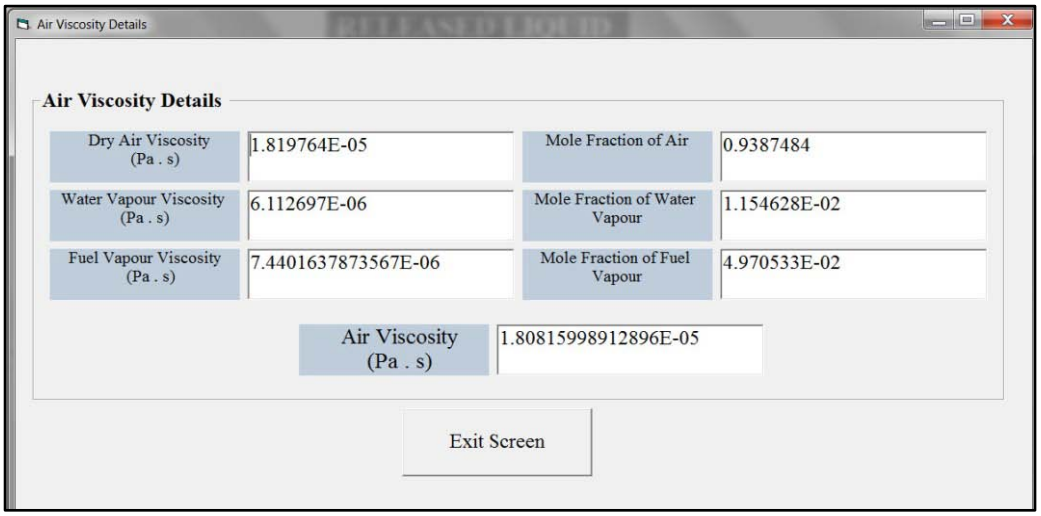

Figure 5.4 The program interface windows for viscosity

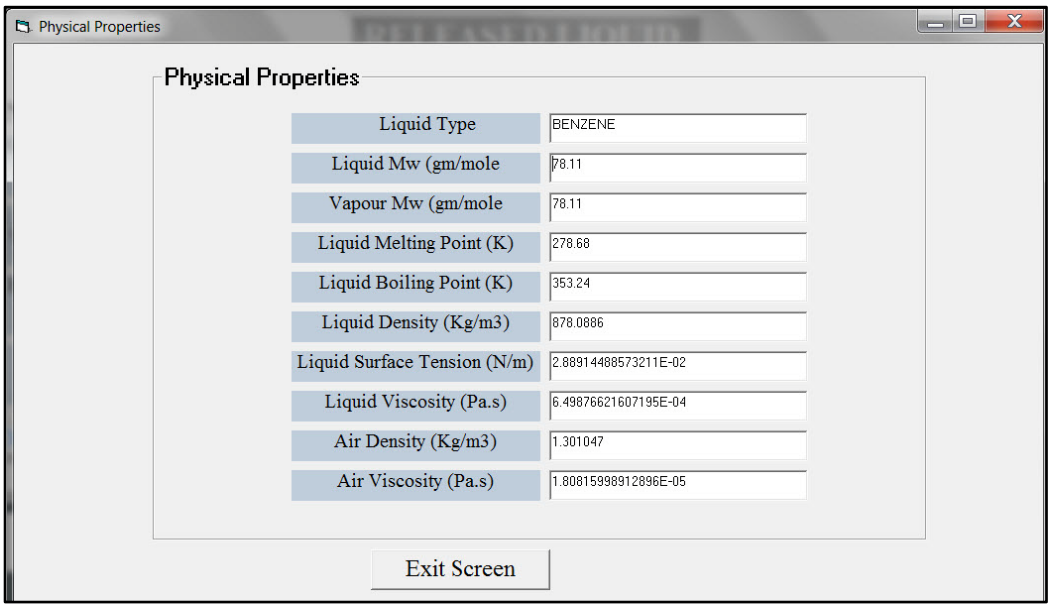

Figure 5.5 The program interface windows for physical properties

5.5 Determining the Jet Breakup Regime

The breakup regimes must be classified before calculation of droplet sizes generated from jet breakup. According to the formulated model represented in chapter 4, the jet breakup is classified as one of five possible regimes (liquid dripping, Rayleigh breakup, first wind induced breakup, second wind-induced breakup and atomization). Appendix B1 – Part F expresses the steps by which breakup regime is classified and named.

5.6 Estimating Droplet Size Distribution and Breakup Length

Droplet size distribution and breakup length estimation are performed in these three steps. First, the size distribution matrix is formed to accommodate all droplet sizes which may appear as a result of jet disintegration and in accordance to the limits of program inputs. In the second step, the median and maximum values of generated droplet sizes are estimated depending on the breakup regime which is already identified in the previous step. In addition, the breakup length is also estimated. Finally, the droplets size distribution is determined in the matrix.

5.6.1 Creating Size Distribution Matrix

The droplet size distribution matrix contains 20010 rows and 6 columns; it can theoretically accommodate droplet diameters up to 2 meters. The first ten rows are concerned with droplet diameters which are usually proposed as aerosol droplets ($0 < D_{Drop} < 100$ μm). Each row covers a domain of 10 microns wide, and the intermediate diameter value symbolizes this domain. The remaining rows represent wider domains of 100 microns. Columns from 1 to 3 in each row contain respectively the lower diameter, the upper diameter and the average diameter for each row diameters domain. Table (5.1) represents how the size distribution matrix is formed.

5.6.2 Estimating Droplet Size Margins

According to the model illustrated in the previous chapter, if the breakup regime is found as dripping or Rayleigh breakup, an average droplet diameter's value will be calculated from equation 3.2 or equation 3.8 as the droplets are supposed to be of the same diameters. For the three other breakup regimes, the values for maximum and median diameters are estimated from equation 3.21 and equation 4.10.The breakup length is estimated from equation 3.16 or equation 3.17 depending on whether the flow

is laminar or turbulent. This is true for the three cases of Rayleigh breakup, first wind breakup and second wind breakup regimes, whereas in a dripping and atomization case, the breakup length could be neglected and would be assumed to be zero.

5.6.3 Distributing Droplet Sizes along the Matrix

After the maximum and the mean diameter for the formed droplets are estimated, the droplet size distribution is determined according to the Rosin-Rammler distribution function (equation 3.19) along with the size distribution matrix. According to this function, the fractions of lower and upper domain size limits are calculated by the equation function and placed in columns number 4 and 5 respectively. The difference between these fractions represents the fraction of the droplet sizes lying between these two limits and is placed in column number 6.

For example, when calculating the fraction of droplet sizes between 100 and 200μm, the fraction of 200μm gotten from the equation is the percentage of droplets which are smaller than 200μm, and the same process for the value of 100μm. The difference between these two fractions, arrived at by subtraction, represents the percentage of droplets which are larger than 100μm and smaller than or equal 200μm. Table (5.1) gives an example of how these calculations are performed. The program steps performed for creating and filling the droplet distribution matrix are expressed in Appendix B1 – Part G, H, I and J. Main parameters calculated for primary breakup of the liquid jet are displayed in the program display window shown in figure (5.6).

Table 5.1 An example of the formation of size distribution matrix

Columns	**1**	**2**	**3**	**4**	**5**	**6**
Rows	**$D_{Lower\ limit}$**	**$D_{upper\ limit}$**	**$D_{average}$**	**Fraction of $D_{Lower\ limit}$**	**Fraction $D_{upper\ limit}$**	**Δfraction**
1	0	10	5	0	$2.3*10^{-5}$	$2.3*10^{-5}$
2	10	20	15	$2.3*10^{-5}$	$4.8*10^{-5}$	$2.5*10^{-5}$
3	20	30	25	$4.8*10^{-5}$	$6.2*10^{-5}$	$1.4*10^{-5}$
	↓	↓	↓	↓	↓	↓
9	80	90	85	$1.8*10^{-4}$	$3.5*10^{-4}$	$1.7*10^{-4}$
10	90	100	95	$3.5*10^{-4}$	$6.8*10^{-4}$	$3.3*10^{-4}$
11	100	200	150	$6.8*10^{-4}$	$1.3*10^{-3}$	$6.2*10^{-4}$
12	200	300	250	$1.3*10^{-3}$	$5.3*10^{-3}$	$4.0*10^{-3}$
	↓	↓	↓	↓	↓	↓
	↓	↓	↓	↓	↓	↓
20000	2000000	2000100	2000050	0.984	0.999	$1.5*10^{-2}$

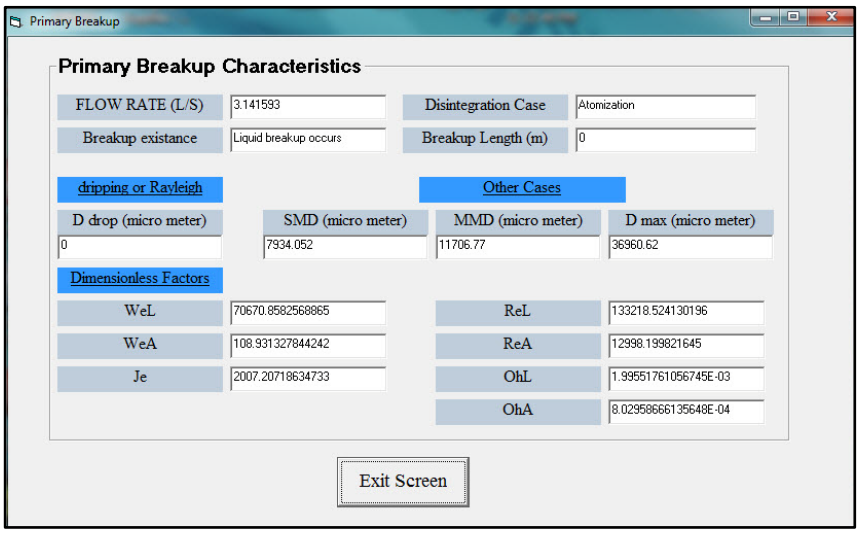

Figure 5.6 The primary breakup characteristics and dimensionless factors interface windows

5.7 Checking Instantaneous Secondary Breakup

In this part of the program, the critical velocity of disintegration for each droplet size in the size distribution matrix is calculated according to equation 4.42 using nested loop iterations. The programming steps for these calculations are illustrated in (Appendix B3 – Part C). The motion velocity of all droplet sizes is assumed to be equal to the jet release velocity. Droplets which have a critical velocity lower than the motion velocity are subjected to instantaneous disintegration. The Sauter mean diameter of those droplets is calculated according to equation 4.43, and then the size distribution of the resulting droplets is distributed according to the Rosin-Rammler distribution function (equation 3.19). Each fraction of the resulting daughter droplets is added to the fraction of similar droplet size. On the other hand, the fraction of each disintegrated droplet size disappears after the secondary disintegration process. Detailed programming steps could be found (Appendix B3 – Part E).

Table (5.2) shows a simplified example for this process. In this example, liquid droplets from 5 to 550µm were generated with the initial mass fractions and subjected to 25 m/s jet release velocity. According to the critical velocity of each droplet, droplets with 550µm diameters ware the ones subjected to disintegration. The maximum and mean sizes of daughter droplets resulting from this disintegration were calculated and the mass fractions of daughter droplets were distributed in column number 5. These fractions were multiplied by the initial fraction of the 550µm droplet (0.000537%), and the total fractions of the resulting daughter droplets, compared to the total mass of liquid

droplets appear in column number 6. The new fraction is then added to the initial fraction of each droplet size giving the new final fraction of each droplet size. The fraction of the 550μm disintegrated droplet finally disappeared. This procedure is carried out for each droplet size subjected to disintegration, starting with larger droplets.

5.8 Estimating the Changes in Droplets Mass and Velocity during Free-Falling and Possibility for Disintegration

The free-falling distance of liquid droplets is the release height after deducting the jet breakup length. To simplify the calculations of the developments taking place during this process, estimation is applied for mass and velocity after each meter of fall. The parameters of each droplet size are recalculated after each meter and the possibility for disintegration is rechecked.

Table 5.2 Illustration for secondary breakup of liquid droplets

D_{Drop} (μm)	Mass Fraction (%)	Motion Velocity (m/s)	Critical Velocity (m/s)	Fractions of daughter droplets from 550μm droplet disintegration	Total fractions of daughter droplets	Final mass Fraction
5	$4.89x10^{-07}$	25	132.66	0.02	0.00001074	$1.12\ x10^{-05}$
15	$1.47x10^{-06}$	25	92.28	0.03	0.00001611	$1.76\ x10^{-05}$
25	$2.45\ x10^{-06}$	25	77.14	0.05	0.00002685	$2.93\ x10^{-05}$
35	$3.42\ x10^{-06}$	25	68.35	0.08	0.00004296	$4.64\ x10^{-05}$
45	$4.4\ x10^{-06}$	25	62.36	0.12	0.00006444	$6.88\ x10^{-05}$
55	$5.38\ x10^{-06}$	25	57.92	0.16	0.00008592	$9.13\ x10^{-05}$
65	$6.36\ x10^{-06}$	25	54.44	0.14	0.00007518	$8.15\ x10^{-05}$
75	$7.34\ x10^{-06}$	25	51.61	0.11	0.00005907	$6.64\ x10^{-05}$
85	$8.32\ x10^{-06}$	25	49.25	0.09	0.00004833	$5.67\ x10^{-05}$
95	$9.29\ x10^{-06}$	25	47.23	0.07	0.00003759	$4.69\ x10^{-05}$
150	0.000147	25	39.71	0.04	0.00002148	$1.68\ x10^{-04}$
250	0.000245	25	32.63	0.035	$1.8795\ x10^{-05}$	$2.64\ x10^{-04}$
350	0.000342	25	28.64	0.03	0.00001611	$3.58\ x10^{-04}$
450	0.00044	25	25.96	0.025	$1.3425\ x10^{-05}$	$4.53\ x10^{-04}$
550	0.000537	25	24	0	0	0

5.8.1 Calculating the terminal settling velocity

To estimate the accurate settling velocity of each droplet size, the value of Re_{Air} is recalculated after each falling distance in order to determine the suitable velocity equation. Droplet sizes with $Re_{Air}<1$ are calculated using equation 3.40. The specific slip correction factor is calculated for each droplet diameter. If the value of the

Reynolds number is larger than 1, equation 4.17 is used instead. The calculations are performed using the nested loop iterations similar to the procedure for calculating the droplets critical velocity. If the value of Reynolds is larger than 1000, the terminal velocity will be estimated directly from equation 3.30 assuming the value of drag coefficient equals to 0.44. Details for droplets terminal velocity calculations are given in (Appendix B3- Part D).

5.8.2 Estimating Change in Droplets Velocity

The main part of calculations during each falling meter is the development in droplets velocity. According to the values of motion velocity (V_{Drop}), terminal velocity ($V_{Terminal}$) and critical velocity ($V_{Critical}$), each droplet size will be classified to one of the following classes:

1- Droplet size with $[\, V_{Drop} < V_{Terminal} \text{ and } V_{Critical} < V_{Terminal} \,]$

These droplet sizes will accelerate and may disintegrate.

2- Droplet size with $[\, V_{Drop} < V_{Terminal} \text{ and } V_{Critical} > V_{Terminal} \,]$

These droplet sizes will accelerate and may disintegrate.

3- Droplet size with $[\, V_{Drop} > V_{Terminal} \,]$

These droplet sizes will decelerate and also will never disintegrate.

4- Droplet size with $[\, V_{Drop} = V_{Terminal} \,]$

These droplet sizes will have no velocity change.

Each droplet size found in the distribution matrix is tagged with a value indicating its class and therefore the procedure is performed for each droplet size according to this tag. For cases of either acceleration or deceleration, the velocity development during each falling distance is performed every 10ms. The falling distance during each 10ms is estimated using equation 4.22 for accelerating droplets and equation 4.27 for decelerating droplets. Then, new velocity is calculated from the motion equation. This step is repeated consecutively for each droplet size until the end of 1 meter falling distance is reached or the droplet reaches its terminal velocity or the droplet reached its critical velocity. After each falling meter, falling time and final falling velocity are

stored in the results matrix. The programming procedure of these steps is presented in (Appendix B4 - Part C) and (Appendix B5 - Part C).

5.8.3 Applying Secondary Droplets Disintegration

The droplets which reach their critical velocity during acceleration will disintegrate. The programming procedure for this step is similar to that performed directly after jet breakup. Droplet sizes redistribution is carried out similarly to the procedure discussed in table (5.2). The programming procedure for this part is given in (Appendix B4 - Part D) and (Appendix B5 - Part D).

5.8.4 Estimating the Change in Droplets' Volume

The second mechanism controlling the change in droplet mass during free-falling is the droplets evaporation. The rate of evaporation for each droplet size is estimated according to equation 4.45. The values of saturated vapour pressure and partial pressure of fuel vapour are already estimated previously and stored in the data matrix. The values of diffusion coefficient and dimensionless Schmidt's numbers are calculated for each droplet size using equation 4.46 and equation 4.47. If the vapour saturation is less than 95%, the ambient temperature near the droplet's surface is estimated using equation 2.9. The falling time for each droplet size is called from previously stored data and multiplied by the evaporation rate to estimate the total amount of vapour generated from each droplet. This amount of vapour could be transformed into mass lose and hence change in diameter. After estimation of the new diameter for each droplet size, fractions of these droplets will be redistributed along the droplet distribution matrix. In addition, the amount of vapour collected from each droplet size are added together to get the total amount of fuel vapour generated during each falling meter. The detailed programming procedure for estimating droplets evaporation is presented in (Appendix B4 – Part E) and (Appendix B5 – Part E).

5.9 Droplet Impingement

As previously discussed in chapter 4, the mechanism of droplets impingement consists of two main parts:

1- Evaluating falling droplets possibility of splashing.

2- Estimating daughter droplets size distribution for each splashed droplet size.

The first part is performed by applying the splashing conditions on each droplet size using equation 4.51. Both Weber's and Reynolds numbers are calculated according to

the final droplet velocity reached just before impinging. In addition, the mean daughter droplet diameter for each impinging droplet size has the ability to splash is calculated according to Wu's model calculations and using equation 4.54. The programming procedure of this part is given in (Appendix B6 - part B).

The second part is performed in a separate calculating matrix. Each droplet size which satisfies the splashing condition is called separately to this matrix in order to apply fragmentation calculations according to the log-normal distribution (equation 4.55). A mathematical procedure is applied for estimating the actual size distribution and transformed into percentage values using equation 4.56.This procedure is simplified in table (5.3) using an example of 150μm splashed droplet. In this example, the droplets with a 150μm diameter and a fraction of 0.002% (column number 3) have satisfied the condition for transition from spreading to splashing. The mean diameter for resulting daughter droplets has been estimated as 22μm (column number 2). Then, the fraction of each daughter droplet size is estimated from equation 4.55 (column number 4). These fractions are transformed into percentage values using equation 4.56 (column number 5), and finally these fractions are added to the existing fractions of droplets (column number 6). These steps are repeated for splashing droplet starting from larger droplets and continuing towards the smaller droplets. Each time, the new resulting droplet fractions are added to the initial values and the splashed droplet size will disappear. More details for programming steps are presented in (Appendix B6 – part C).

Table 5.3 Mathematical procedure for estimating size distribution from 150 μm drop

Columns	1	2	3	4	5	6
Rows	$D_{Daughter}$	D_{mean}	fraction of (d=150μm)	F ($D_{Daughter}$)	Fractions of $D_{Daughter}$ ($F(D_{ave})/ \sum f(D_{ave})$)	Final Fractions
1	5	22	0.002	2	0.0469	0.000098
2	15	22	0.002	4	0.0938	0.0001878
3	25	22	0.002	9	0.2112	0.0004225
4	35	22	0.002	7	0.1643	0.0003286
5	45	22	0.002	6	0.1408	0.0002817
6	55	22	0.002	4.5	0.1056	0.0002113
7	65	22	0.002	4	0.0938	0.0001878
8	75	22	0.002	2.8	0.0657	0.0001315
9	85	22	0.002	2.1	0.0492	0.0000859
10	95	22	0.002	1.2	0.0281	0.0000634

5.10 The Ratio between Vapour Concentration inside and Outside the Cascade

Vapour saturation inside the cascade region might reach high saturation level in a short time. This depends on both the vapour generation rate and the vapour dilution rate. This means, the fuel vapour concentration is not equally distributed through the whole cloud, and might be concentrated inside the cascade region. If the release area is well ventilated and the wind speed is enough, the fuel vapours may spread well through the fuel/air cloud and become homogeneously distributed. If this does not happen, the fuel vapour concentration adjacent to the source might be higher than the far field of the formed vapour cloud.

In this part of the program, the release time (received from the user input) will be divided into seconds / minutes of time. After each time interval, the air mixture characteristics (density, viscosity and surface tension) will be recalculated using different air mixture composition. The amount of vapours and possibly the aerosol generated during the elapsed minute will be used to restore the composition of the surrounding air mixture. The new programming steps formulated for this purpose are described through the following procedure, and the detailed programming step are presented in Appendix B-1/part O:

a- The initial air mixture composition is assumed to be dry or humid air and fuel-vapour free.

b- Release time and fuel-air cloud volume must be provided as program inputs.

c- After each minute, the program estimates will estimate the amount of vapours and aerosols which might be incorporated in the fuel-air cloud.

d- The mass and volume of vapours added to the cloud each minute will be collected in counter cells. The value inside these cells will indicates the total amount of vapours generated until that time.

e- The volume of dry or humid air will be the remainder of the cloud volume after subtracting vapours volume.

f- According to these results, volume and mass percentages of fuel vapours in cloud can be re-estimated after each minute.

g- Vapour saturation at any time is the instantaneous vapour volume percentage divided by the vapour volume percentage at saturated conditions.

h- The vapour concentration value inside the release region will be chosen as similar, 1.25 times, 1.5 times, 1.75 times, and double the concentration through the remaining

cloud volume. In addition, the program will be provided with the ability of solving multi-point releases which will be used in (chapter 6,7).

The program's output file will express detailed results after each minute of release. This data will include the generated amount of fuel vapours and aerosol droplets, the vapour mass and volume, the vapour volume fraction in cloud, the vapour mass fraction in cloud, and the vapour saturation level in both the vapour cloud and the release area. Programming details for this development are expressed in (Appendix B1 - section O).

During liquid release, the liquid mass can be divided into different forms. Liquid bulk disintegrates into large and small droplets during the primary breakup of liquid jet and the secondary breakup of falling liquid droplets. Some of these droplets are small enough to float and merge into the vapour cloud, whereas others will directly fall down forming a liquid pool. During droplets splashing, some of the small daughter droplets may also float with the wind stream while others will only dive back. In addition, transfer from liquid to vapour state through evaporation will take place during these steps. The different fractions of released liquid could be classified into the following five main types as follows:

Fraction No(1): Vapour generated from falling droplets

Although some vapours maybe generated during liquid jet breakup and droplets splashing, evaporation of free-falling droplets is most probably the main source of fuel vapour generation during the whole process. This fraction of vapours is generated inside the release region and transfers to the remaining cloud volume by both wind motion and Brownian motion.

Fraction No(2): Aerosol droplets generated before impinging

This is the fraction of aerosol droplets generated during liquid jet breakup and falling droplets disintegration. This fraction might be very small except when the liquid is released with very high velocity (usually above 20 m/s). The expectation would be a case in which the ambient air mixture is fully saturated with fuel vapours, when this fraction of aerosol droplets is likely to vaporize quickly.

Fraction No (3): Non-aerosol/Non-splashing droplets

This is the fraction of non-aerosol droplets generated during liquid jet breakup and falling droplets disintegration. In addition, they do not have sufficient kinetic energy to undergo splashing when reaching the ground. These kinds of droplets are most likely to spread on the ground rather than splash forming a liquid pool.

Fraction No (4): Floating Aerosol droplets generated from splashing

The relatively large falling droplets usually undergo splashing when hitting the ground. Some of the resulting daughter droplets could be classified as aerosols ($d \leq 100\mu m$). According to the results presented in previous chapters, the percentage of these aerosols might be relatively large.

Most of these aerosols will probably fall down into the liquid pool. On the other hand, some of them will float and transfer by wind motion. These floating droplets can be assumed to be 2% of total liquid release mass (Atkinson and Coldrick, 2012a). According to the results presented in the previous chapters, aerosol size droplets might be about 50% of released liquid mass. Hence, it will be estimated as 4% of the aerosol mass generated during the splashing process. Similar to the behaviour of aerosols in Fraction No.2, this fraction of droplets will also evaporate as soon as it gets into the unsaturated area and, the only case to account this fraction as liquid droplets is achieved when the whole vapour cloud becomes fully saturated.

Fraction No (5): Non-floating droplets generated from splashing

This fraction contains most of the daughter droplets resulting from splashing. This will include 96% of aerosol size droplets and also all the non-aerosol droplets. The total mass of fractions accounted for in fraction number 3 and 5 are the source. Figure (5.7) simplifies the understanding of the different fractions resulting from the released liquid jet. Each fraction might incorporate in the two-phase cloud or participated in liquid pool formation.

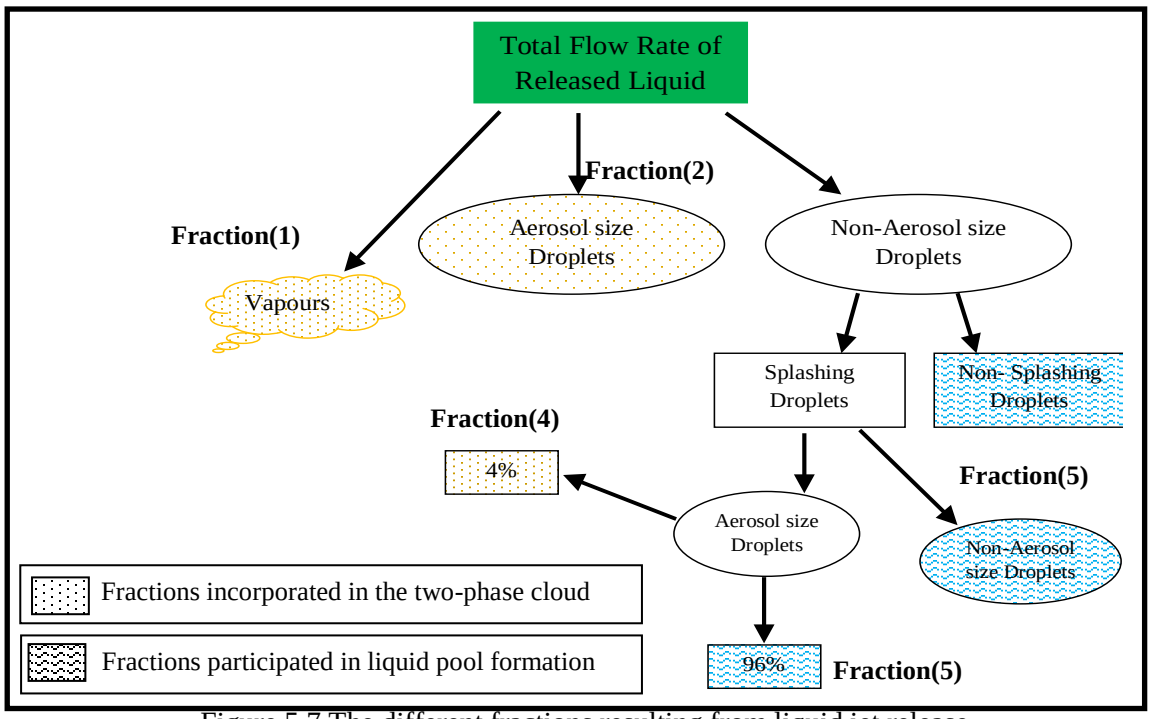

Figure 5.7 The different fractions resulting from liquid jet release

Chapter 6: Validation and Verification of the Numerical Package

6.1 Introduction

The work in this chapter aims to confirm the good performance of the implemented numerical package program to perform the intended functions and to fulfil the requirements. In addition, it is important to determine the degree of compatibility and harmony of the calculated results compared to the experimental measurements and CFD modelling results under the same conditions. One of the most important experimental and modelling research programs in this field was launched by the HSE in 2007. The program was described as a "first step towards developing a mathematical model to predict the size of flammable vapour clouds from overfilling releases" (Atkinson and Gant, 2012b). From this point of view, the numerical calculation package will be used throughout this chapter to solve a typical previously performed experiment and CFD modelling.

6.2 The HSE Experimental and CFD Modelling Programs

In 2007, the Health and Safety Executive (HSE) in the UK started an aspirant research program concerning the generation of flammable vapour of volatile liquids during accidental overfilling of large storage tanks. In fact, this work was motivated by the large disaster that took place at Buncefield oil depot in 2005. A series of reports have been published expressing the results of a large group of free-cascade field experiments. Moreover, the results obtained from the experiments were used to adjust the input parameters of CFD models. The CFD software package CFX 12.1 was used to model and simulate the scenario of typical free-cascade liquid release and vapour generation at different release conditions and then to examine the importance of different parameters on the vapour generation process.

The HSE research team performed two groups of large-scale cascade field experiments. The first group contains 14 experiments using the liquid hexane as a test fuel. Liquid flow rates between 7 and 21 kgs^{-1}were studied at different temperatures (Atkinson and Coldrick, 2012a). The experiments were well instrumented with different types of thermocouples to measure the liquid and vapour temperatures at different points around the cascade. The heat and mass transfer data were used to estimate the

amount of evaporation using thermodynamic calculations and to validate CFD models. In Tests 12 to 14, further measuring thermocouples were installed at different elevations. This developed instrumentation helped to achieve a better understanding of the whole evaporation process. Furthermore, photographs and videos were taken to understand the droplet size spectrum generated from the cascade. Under different release conditions, the major liquid mass was found in droplets of around 2 mm in diameter, and a range of larger and smaller size droplets. The evaporation process was found along the cascade. Around 70% of vaporisation took place above the ground. This value reached nearly 90% within the impact zone. In the second group, further seven experiments were performed using different types of liquids (Atkinson and Coldrick, 2012b). Additional measuring instrumentations were used in this group of experiments. The relative humidity was measured at the beginning of each test, and the vapour concentration was measured during each test using the activated charcoal sample tubes. In addition, thermal images and infrared images were captured during various experiments.

The other part of the HSE work includes 14 CFD models (Atkinson and Gant, 2012b). The models were used to study the effect of different parameters on the vaporisation process during overfilling release incidents. It was found that the vaporisation rate is strongly dependent on liquid droplet size, spray width and the distribution of the spray around the tank.

6.3 Comparison with Field Experiments

In order to compare with field experiment results, the experimental conditions have been identified and used as inputs for the numerical calculations. All experiments were performed at stable ambient conditions with nearly no wind motion. The liquid hexane was freely released from 10m above the ground and along a 1.5m discharge length. Liquid and vapour temperature were measured at different distances and heights around the cascade in three tests. The HSE reports expressed a thermodynamic calculation for the hexane/air mixture at equilibrium condition for Experiment 14 (group No.1) and for Tests 1, 5 and 6 (group No.2). The vaporisation efficiency during liquid release was estimated by comparing the enthalpy change due to evaporation at different measuring points with the enthalpy at equilibrium conditions. Figure 6.1 and Table 6.1summarisethe measured and calculated parameters for Experiments14, 1, 5 and 6. The measurements express three different points at the top of the cascade, down the cascade (splashing area) and at the end of the spray (away from the cascade).

Figure 6.1 Measuring point for experiment No. 14

Table 6.1 Summary of the measured and calculated parameters for experiment No (14)/group.1 and experiments (1, 5 and 6) / group.2

Property	Exp 14/G1			Exp 1/G2			Exp 5/G2			Exp 6/G2		
	A	B	C	A	B	C	A	B	C	A	B	C
Liquid temp (^{o}C)	3.3	-3.8	-10	13.6	1.6	-	9	-2	-	15.7	2.8	-
Vapour temp (^{o}C)	3	-5	-5	12.7	1.4	-1.5	-1	-1.5	-3.5	10.4	1.5	4
Vapour Saturation (%)	0	95	60	0	95	70	0	99	70	0	99	65
Vaporization rate (g/s)	0	900	1054	0	1540	1801	0	971	1092	0	1264	1395
Fraction vaporized (%)	0	6	7	0	10.4	12	0	7.59	8.54	0	10.7	11.8
Vapour concentration (% v/v)	0	4.4	2.7	0	4.9	3.6	0	3.7	2.8	0	4.7	3

Measured value

6.3.1 Selection of Numerical Calculation Inputs

The numerical calculation inputs were selected to be identical to those measured in the real experiments. The only exception is the assumption of liquid and ambient temperatures. Because the numerical package does not account for temperature changes due to heat transfer, these two parameters were assumed to be an average between the initial and final measured temperatures. In Experiment 14, for example, the initial liquid hexane temperature was 3.3 °C and reached -3.8 °C at the end of the cascade. Thus, the liquid temperature was assumed to be0°C as the average temperature during the release time. Similarly, the average ambient temperature was assumed to be-1 °C as an average between 3 and -5 °C. According to Table 6.1, the ratio between vapour saturation inside and outside the cascade was nearly 1.5 times for Experiment14/Group1 and Experiment6/Group2. For the two other experiments, this ratio was closer to 1.25. The release problems were solved using the multi-point mode calculations. Table 6.2 expresses the calculations used to estimate the approximate number of releasing points for each experiment. The initial conditions for each experiment and the corresponding numerical calculations are summarised in Table 6.3.

Table 6.2 Calculations used to estimate the number of release points for each experiment

Exp No	T_{ini} (^oC)	ρ_{Liq} at T_{ini} (kg/ m^3)	Mass flow rate (kg / s)	Volume flow rate (m^3 / s)	Discharge thickness (mm)	Jet diameter (mm)	Jet cross-section area (m^2)	Approximate No of release points
14/G1	3.3	675.3	15	22.2 x 10^{-3}	14.8	15	1.77 x 10^{-4}	126
1/G2	13.6	666.3	15	22.5 x 10^{-3}	15	15	1.77 x 10^{-4}	128
5/G2	9	670.4	12.8	19.1 x 10^{-3}	12.7	13	1.33 x 10^{-4}	144
6/G2	15.7	664.4	11.8	17.8 x 10^{-3}	11.8	12	1.13 x 10^{-4}	136

Table 6.3Initial conditions for experiments and corresponding numerical calculations

Condition	exp14	N. C	Exp 1	N. C	Exp 5	N. C	Exp 6	N. C
Mass flow rate (kg/s)	15	15	15	15	12.8	12.8	11.8	11.8
Volume flow rate (L/s)	22.21	22.21	22.51	22.51	19.1	19.1	17.76	17.76
Number of releasing point	-	126	-	128	-	108	-	101
Entrained air (kg/s)	6.6	6.6	6.6	6.6	6.35	6.35	6.3	6.3
Initial liquid temperature (°C)	3.3	0	13.6	7.5	9	3.5	15.7	9
Final liquid temperature (°C) (End of cascade)	-3.8		1.6		-2		2.8	
initial air temperature (°C)	3	-1	12.7	5.5	-1	-2	10.4	7
air temperature (°C)	-5		-1.5		-3.5		4	
Relative Humidity (%)	50	50	55	55	90	90	87	87
Release Height (m)	10	10	10	10	10	10	10	10
Initial release velocity (m/s)	1	1	1	1	1	1	1	1

6.3.2 Comparison of Vaporisation Results

The results of numerical calculations showed that a jet first wind-induced breakup took place at nearly 92cm below the exit point. After a short distance, the largest mass fraction of liquid droplets was around 2mm in diameter. Figure 6.2 shows the droplet mass distribution at 1 m below the jet breakup point. This regime is typically found in all numerical results and it is quite harmonious with the high-speed images captured in experiments.

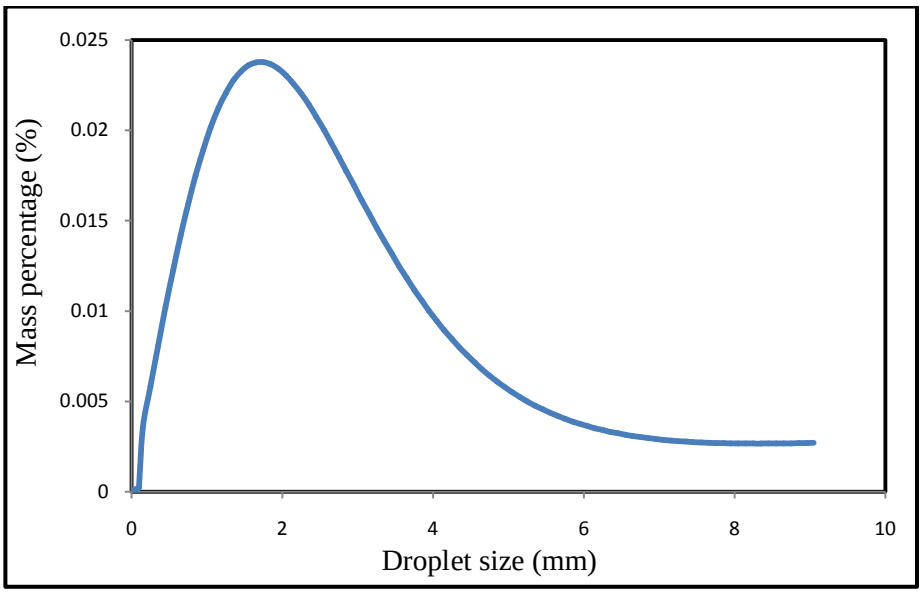

Figure 6.2 Droplet size distribution after 1 m from jet breakup point

The numerical calculation results were compared to the experimental results. A summary of both results is expressed in Table 6.4. The findings of this comparison are summarised as follows:

a- The average rate of vaporisation at the end of cascade was between 80.1% and 83.3% compared to experimental results, and the best filling was found in Experiment 6/Group 2. These results could be accepted when taking into consideration the ignored mechanisms such as the droplet–droplet collisions and the effect of heat transfer on evaporation efficiency.

b- The results of evaporation amount outside the cascade region are less compatible with the experimental results. The best fit was expressed in Experiment 5/Group 2 with a ratio of 91.7%. The other ratios varied between 46.4% and 142%. This variation might exist due to the program's assumption that a fixed value of 4% of splashed aerosol droplets could float with the air stream. In fact, this value is strongly dependent on the dispersion mechanism, which is not considered in

numerical calculations. In general, this variation has a slight effect because the evaporation outside the cascade is around 1 to 1.6% of the total mass released.

c- The total liquid vaporised by the end of spray region was between 75.6% and 90.9% of the experimental results. Figures 6.3 and 6.4 illustrate the rate of vaporisation and the accumulative vaporised mass in 75 seconds estimated from numerical calculations and experimental tests.

Table 6.4 Comparison between experimental results and numerical calculation results

	Average Vaporization rate (g/s)	Fraction vaporized (%)	Vapour concentration (% v/v)	Vapour saturation (%)	Average Vaporization rate (g/s)	Fraction vaporized (%)	Vapour concentration (% v/v)	Vapour saturation (%)	Total Vaporization rate (g/s)	Total Fraction vaporized (%)
	At the end of cascade				Outside cascade				At the end of spray	
Exp 14/GR2 Result	900	6	4.4	95	154	1.03	2.7	60	1054	7.03
Numerical Result	739	4.93	5.4	99.6	220	1.46	3.6	66.4	959	6.39
$\frac{\text{Numerical Result}}{\text{Exp Result}}$ x100	82.2%		122%	105%	142%		133%	110%	90.9%	
Exp 1/GR1 Result	1560	10.4	4.9	95	241	1.6	3.6	70	1801	12
Numerical Result	1250	8.3	6.2	99	112	0.75	4.9	79	1362	9.05
$\frac{\text{Numerical Result}}{\text{Exp Result}}$ x100	80.1%		126%	104%	46.5%		136%	113%	75.6%	
Exp 5 /GR2 Result	971	7.59	3.7	99	121	0.95	2.8	70	1092	8.54
Numerical Result	801	6.26	5.4	99	111	0.87	4.3	79	912	7.1
$\frac{\text{Numerical Result}}{\text{Exp Result}}$ x100	82.5%		145%	100%	91.7%		154%	113%	83.5%	
Exp 6 /GR2 Result	1264	10.7	4.7	99	131	1.1	3	65	1395	11.8
Numerical Result	1053	8.9	5.7	99	89	0.75	3.8	66	1142	9.65
$\frac{\text{Numerical Result}}{\text{Exp Result}}$ x100	83.3%		121%	100%	68.2%		127%	102%	81.8%	

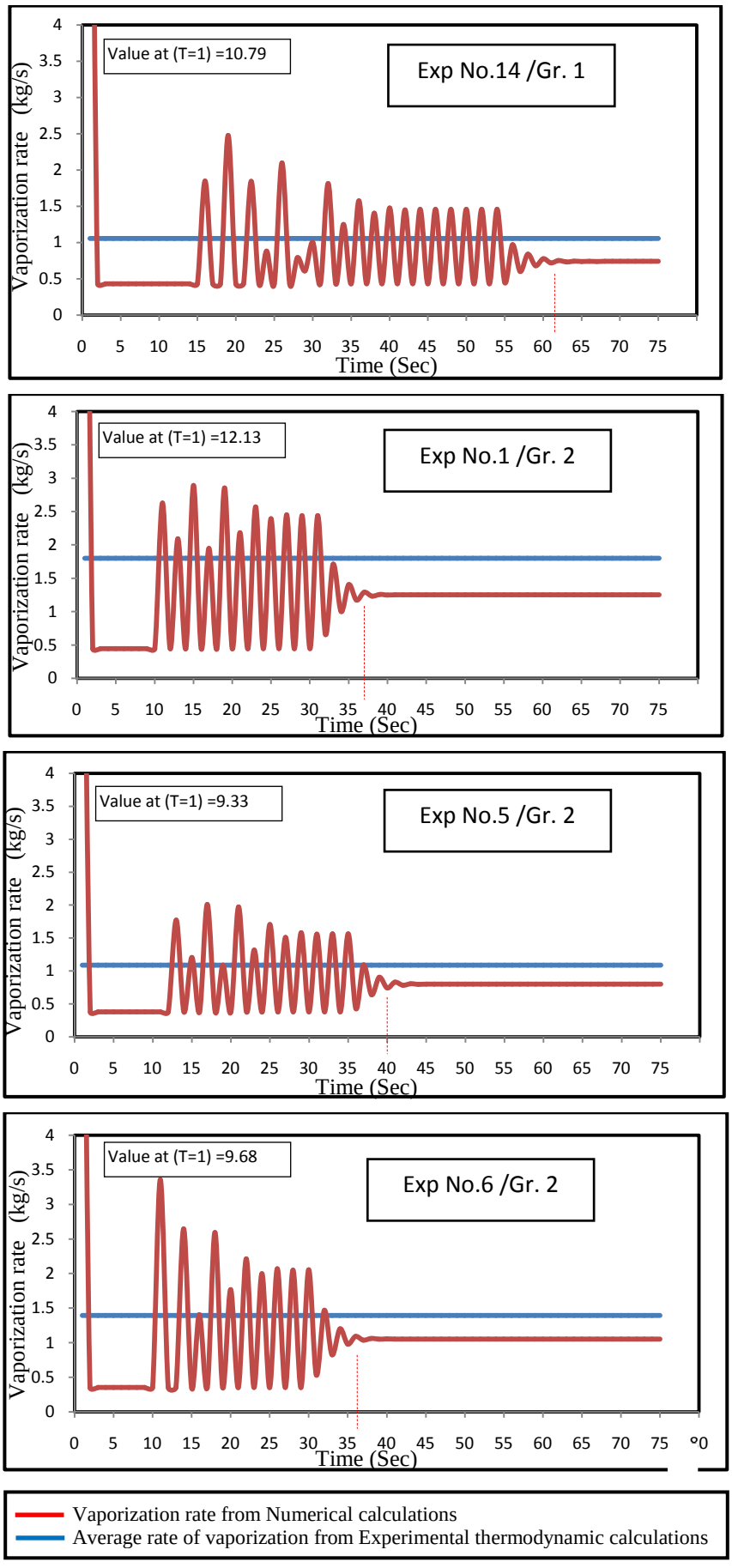

Figure 6.3 Comparison between calculated vaporization and the average rate of vaporization estimated from experimental thermodynamic calculations

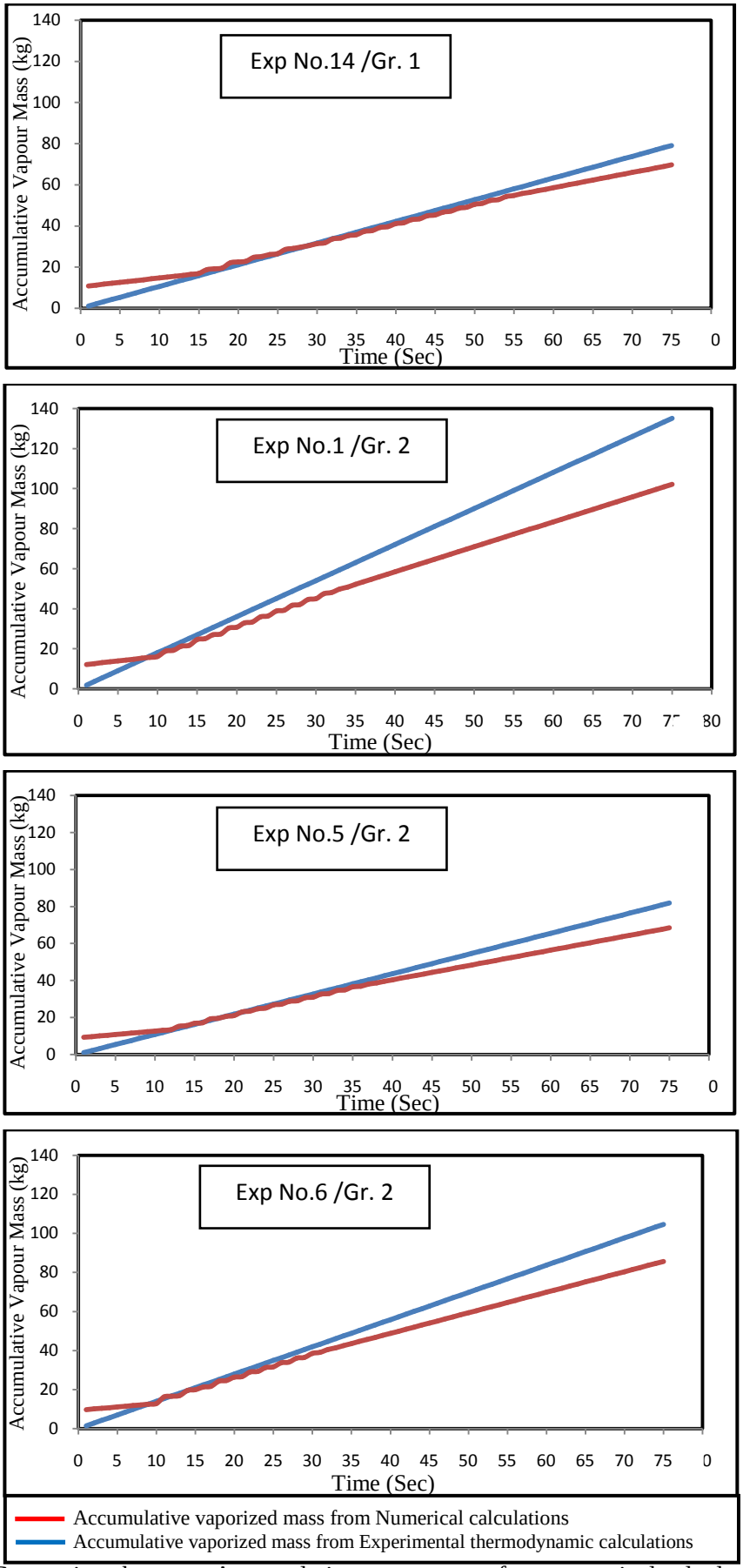

Figure 6.4 Comparison between Accumulative vapour mass from numerical calculations and from experimental thermodynamic calculations

d- The ratio between calculated vapour volume concentrations inside and outside the cascade is nearly similar to the ratio estimated from experimental results. On the other hand, the calculated values of vapour volume concentrations are higher than measured values. This finding is completely understood because the values are measured at lower temperatures and consequently the saturation vapour pressure is lower.

e- The calculated vapour saturation values inside and outside the cascade are very close to the values estimated from the experimental thermodynamic calculations.

f- The results obtained from both the experiments and the numerical calculations expressed the enhancement of vaporised fraction due to splashing mechanism. The impingement of liquid droplets down the cascade increased the amount of vapour with nearly 27% to 40%. Figure 6.5 displays the vapour increasing ratio for each experiment caused by the splashing process.

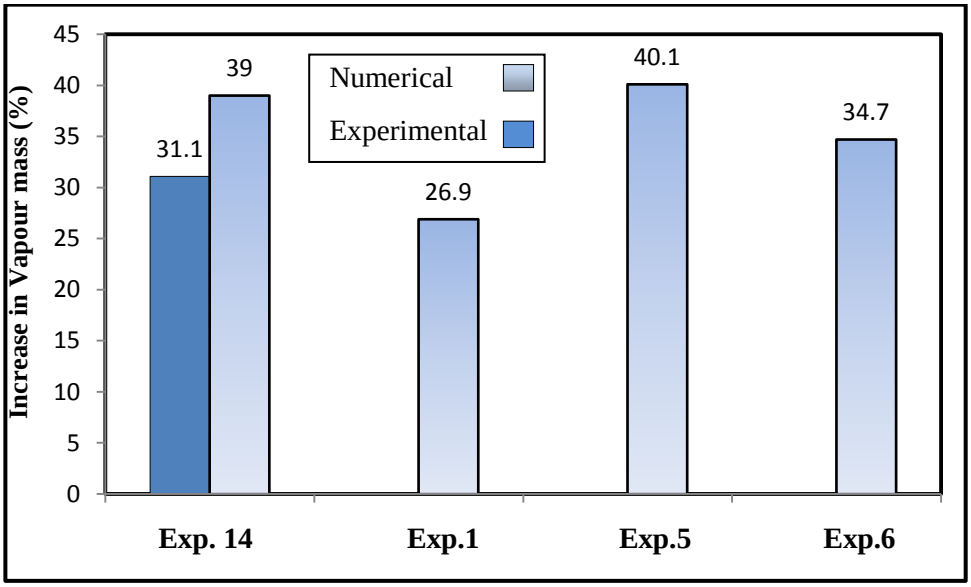

Figure 6.5Increase in vapour mass due to the mechanism of droplet splashing

g- The results also expressed the impact of aerosol formation on vaporisation efficiency. The formation of aerosols allows vaporisation outside the cascade region. This process occurs when the vapour saturation inside cascade region becomes very high. Figure 6.6 shows the enhancement of vaporisation due to the formation of aerosols.

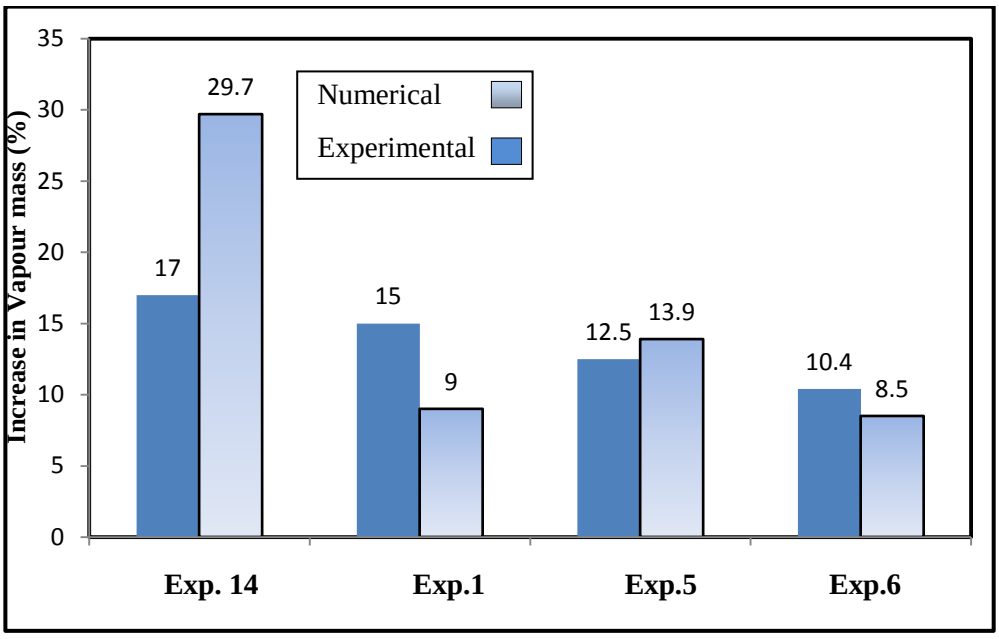

Figure 6.6Increase in vapour mass due to the formation of aerosols

6.4 Comparisons with CFD Modelling

In this section, the numerical calculation results will be compared with the CFD modelling. The HSE research team performed a group of 14 computational fluid dynamic models after the modelling assumptions had been validated with experimental work (Atkinson and Gant, 2012b). The modelling cases were divided into five groups to study the effect of five different factors on vaporisation efficiency during overfilling releases. Figure 6.7 summarises the CFD model program.

Different bund shape/location and tank		Case 1	Case 2 Far	Case 3 Sloping	Case 4 Adjace
Different spray width	Case 5	Case 6 (4.5m)	Case 7 (5.5m)	Case 8 (8m)	
Different droplet sizes		Case 6 (δ=2.2	Case 9 (δ=1.1	Case 10 (δ=3.3	Case 11 (δ=2.2mm)
Different release angles		Case 6 (120^o)	Case 12 (8x15^o)	Case 13 (360^o)	
Obstacle outside the bund		Case 6 (No	Case 14 (obstacl		

Figure 6.7The CFD modelling program performed by the HSE

All cases simulate the overfilling of liquid hexane with 1ms^{-1} initial release velocity from the top of a 15m high rounded tank with a diameter of 25m. The liquid releases at 15 °C and the ambient air is dry, stagnant at a temperature of 0 °C. The release takes place along 120° of the tank circumference except for cases 12 and 13. Finally, the droplet distribution is fixed at a characteristic diameter of2.2mm and an index of 1.5, except cases 9 and 10. The modelling cases included the change in bund, spray width, release angle, droplet size distribution and the existence of an obstacle outside the bund. In fact, all these factors (except droplet size) directly affect the dispersion mechanism rather than the breakup mechanism. Indirectly, breakup and vaporisation mechanisms are dependent on dispersion because the dispersion behaviour controls the vapour concentration inside the cascade region. When dispersion becomes faster, a large amount of air penetrates the cascade. This means better dilution and a lower vapour concentration around the falling droplets. This consequently increases the rate of vaporisation and the final cloud volume in most cases. In the next section, the vaporisation rate will be estimated using the numerical package calculations. Variables between different cases will be the vapour cloud volume and the ratio between vapour concentration inside and outside the cascade region. The cases of Group 1 will not be considered because the effect of bund shape/distance had a minor effect on vaporisation efficiency.

6.4.1 Selection of Numerical Calculation Inputs

The numerical calculation inputs were identical to those used for the CFD modelling, as shown in Table 6.4. Liquid temperature and ambient temperature were set as an average between the initial and final temperatures of the CFD simulation. The value of entrained air inside the cascade was estimated relative to the volume of the vapour cloud resulting from CFD modelling.

The ratio between the vapour concentration inside and outside the cascade region was estimated from the vapour fraction contours of the CFD modelling. Figure 6.8 expresses some examples of such contours for different modelling cases.

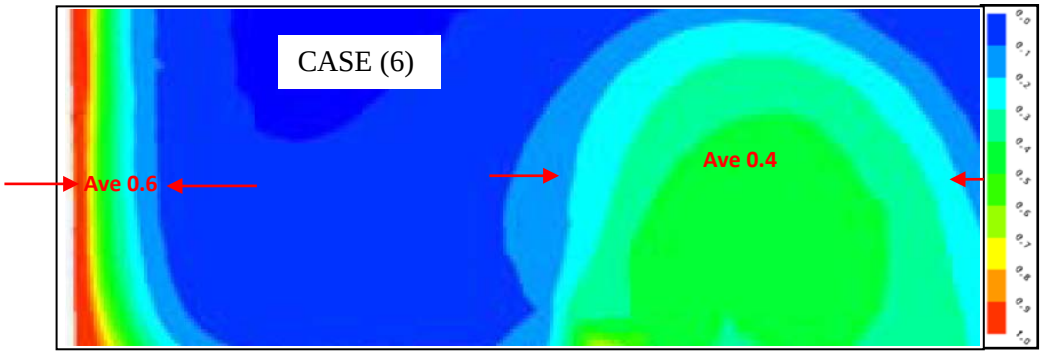

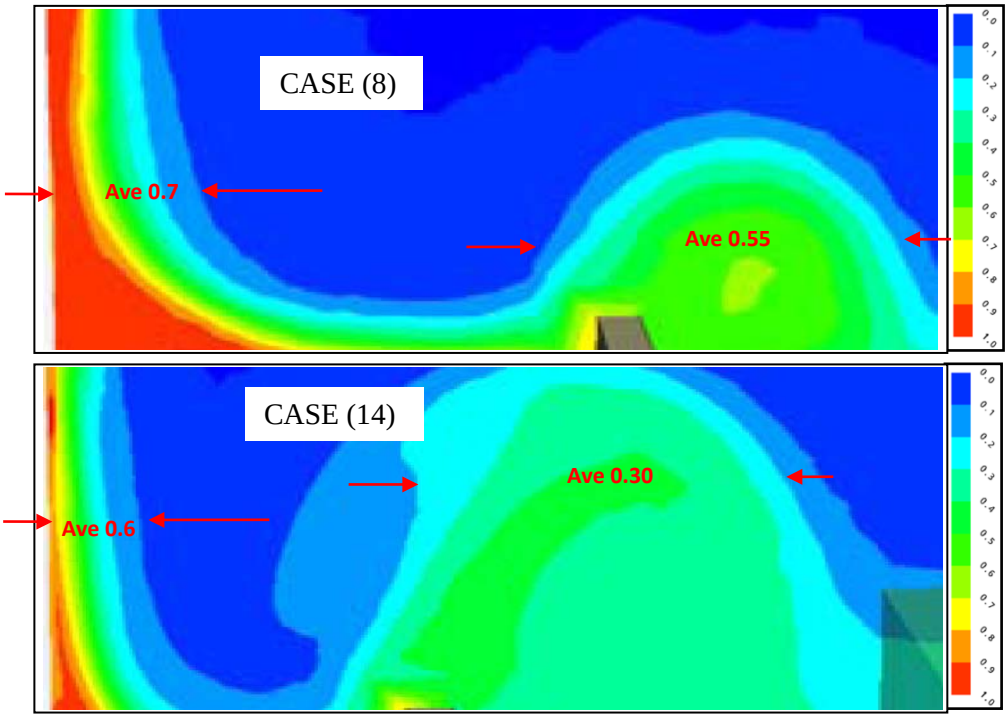

Figure 6.8 Contours of the ratio between vapour volume fraction and volume fraction at saturation condition for cases 6, 8 and 14

The release problem was solved using the multi-point release mode calculations and the number of jets is estimated as follows:

a) In CFD modelling:

Release velocity =1 ms^{-1} / Liquid mass flow rate = 105 $kgsec^{-1}$ Then,

-Release length = 0.333 ×Tank perimeter = 0.333 ×π ×d = 26.18 m

-Volumetric flow rate = mass flow rate / Liquid density at 15 °C = 105/0.665= 158 L/s

-Discharge cross-section = flow rate / velocity = 0.158 (m^3s^{-1}) /1 (m) = 0.158 m^2

-Discharge height = cross-section / discharge length = 0. 158 / 26.18 ≈ 7 mm

b) For the numerical calculations:

-Jet diameter is assumed = 7mm

-Jet cross-section = $\pi r^2 = \pi \times (0.0035)^2 = 3.85 \times 10^{-5}$ m^2

-Volumetric flow rate = mass flow rate / Liquid density at 2.5 °C = 105/676 = 0.155 m^3s^{-1}

-Number of jets = 0.155 / 0.000177 ≈ 4035 jets

Table 6.5 Initial condition for the CFD model and numerical calculations

Condition		CFD modelling	Numerical Calculations
Hexane supply rate (kg/s)		105	105
Release time (s)		60	60
Hexane supply temperature		15	2.5 (°C) (Average
Hexane Final temperature (°C)		-10	
Ambient temperature (°C)		0	-1 (Average
Final Ambient temperature		-2	
Relative Humidity (%)		0	0
Hexane Vapour saturation before release (%)		0	0
Release Height (m)		15	15
Initial release velocity (m/s)		1	1
Vapour cloud volume after 60 sec (m^3)			
	Case5	8250	8250 (1.5 times)
	Case 6	8700	8700 (1.5 times)
	Case 7	9000	9000 (1.5 times)
	Case 8	9000	9000 (1.25 times)
	Case 9	9900	9900 (1.5 times)
	Case 10	7000	7000 (1.5 times)
	Case 11	8850	8800 (1.5 times)
	Case 12	7000	7000 (1.25 times)
	Case 13	7600	7500 (uniform)
	Case 14	11800	11800 (double)

6.4.2 Comparison of Vaporisation Results

The results of the numerical calculations showed that a jet first wind-induced breakup took place at nearly 34cm below the exit point. The total proportion of vaporised hexane during 60 seconds for each case was compared with the corresponding estimated value from CFD modelling. Figures6.9, 6.10, 6.11 and 6.12 illustrate the comparison between both results of numerical and CFD calculations for each group separately. Figure 6.13 express the ratio between both results for each case.

The comparison between the vaporised fractions resulting from CFD and numerical calculations showed a good convergence. No numerical results are more than ±11% of the CFD results. Both methods, numerical and CFD, did not model the droplet–droplet collision. The CFD modelling did not consider the droplet breakup mechanisms, unlike the numerical calculations. On the other hand, some deviation could happen because the numerical package does not deal with energy transfer and dynamic dispersion. In general, the numerical results showed a good response to the change in temperature and the amount of air entrained in the cascade.

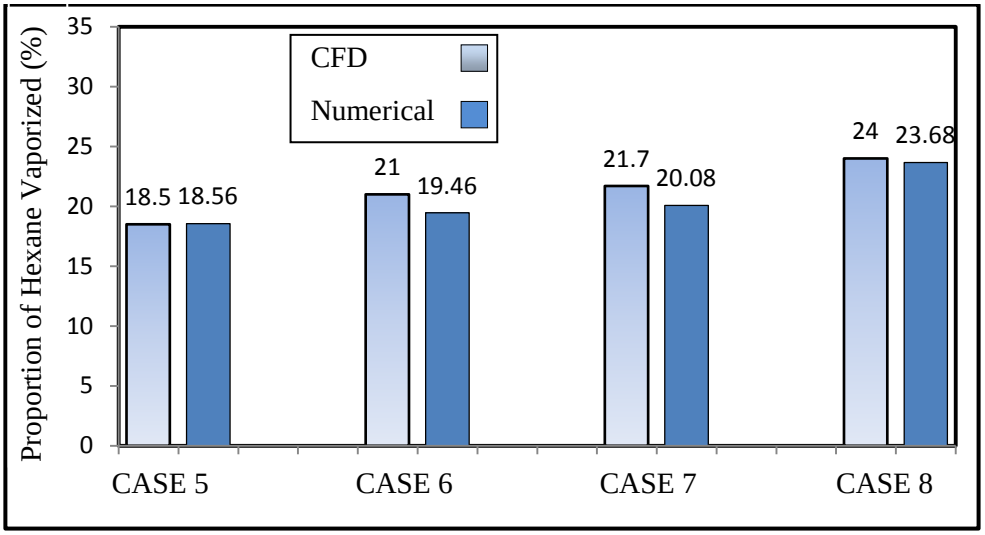

Figure 6.9 Proportion of vaporized Hexane after 60 sec for group (2) cases

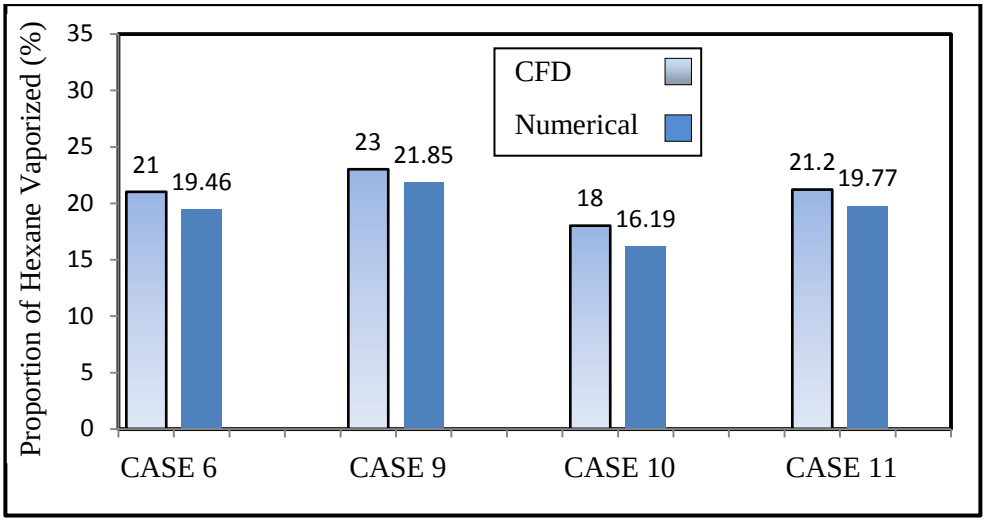

Figure 6.10 Proportion of vaporized Hexane after 60 sec for group (3) cases

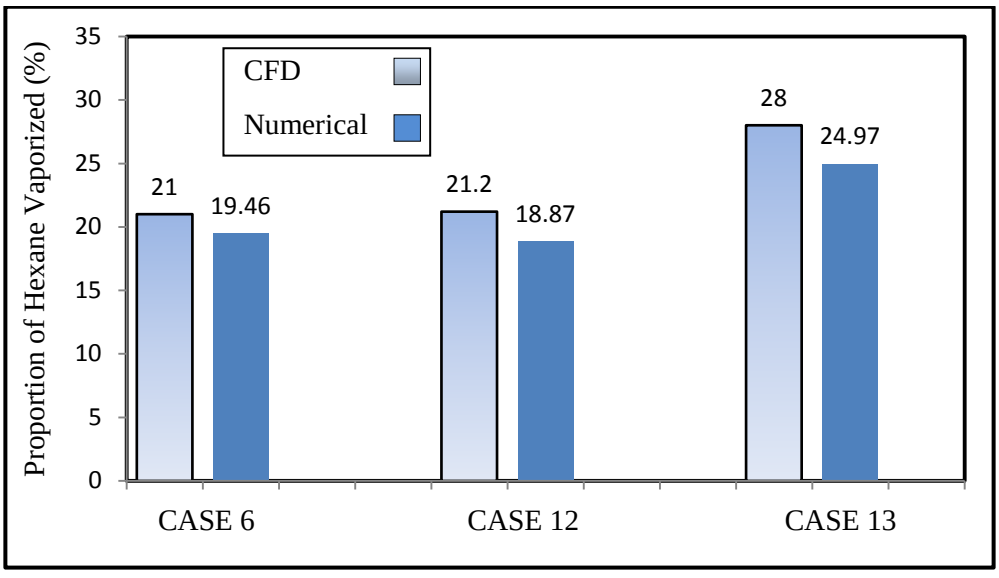

Figure 6.11 Proportion of vaporized Hexane after 60 sec for group (4) cases

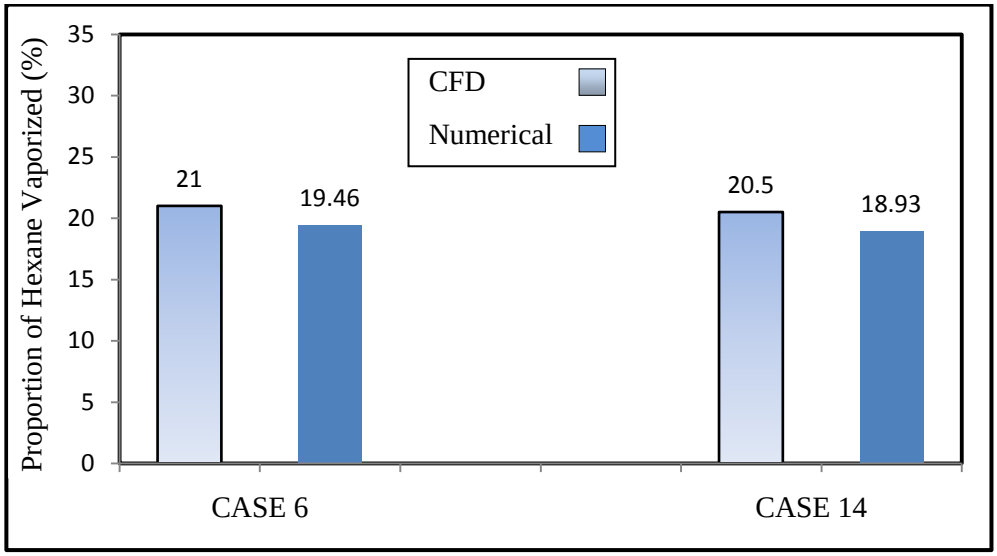

Figure 6.12 Proportion of vaporized Hexane after 60 sec for group (5) cases

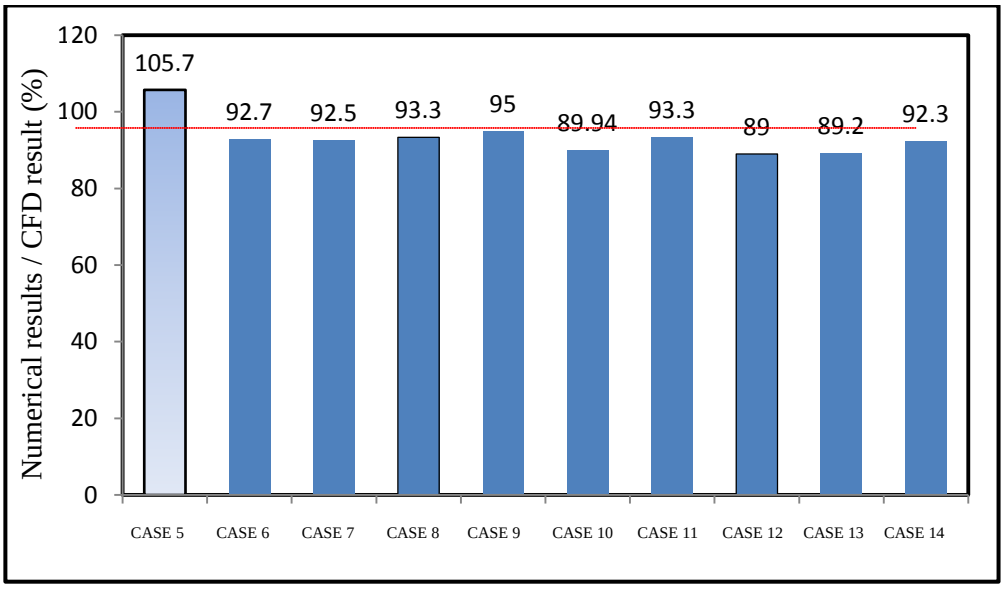

Figure 6.13 The ratio between numerical results and CFD results

Summary

- The implemented numerical package was successfully manipulated to an estimate of the amount of vaporised liquid during liquid overfilling release.
- The numerical program was capable to perform its intended function while utilizing different variables.
- The achieved results displayed a good convergence as well as compatibility with the experimental and CFD modelling results. Moreover, the utilised numerical package showed a great flexibility and sensitivity upon operating different variables.

- The numerical package results concerning four different experiments revealed an agreement with the experimental thermodynamic calculation results of about (75% - 90%).
- The proportion of vaporised liquid estimated by the numerical package showed a maximum deviation of about (±11%) in comparison to the value obtained from CFD simulations.
- The numerical package advocated the great role of the splashing mechanism in enhancing the vaporisation process by (27% - 40%). Moreover, the formation of aerosols increased the amount of vapour by (9% - 30%).

Chapter 7: Case Study on the Vapour Cloud Formation in Buncefield Oil Depot Incident

7.1 Introduction

This chapter presents a case study on the Buncefield Oil Storage Depot incident, which occurred in December 2005. An accidental overfilling of winter patch gasoline took place for nearly 40 minutes, forming an unexpectedly large size of vapour cloud. The resulting explosion was described as the biggest explosion to have happened in Europe since the Second World War (Ottemoller and Evers, 2008). Since that date, a significant change in the way of understanding the formation of vapour clouds from overfilling of volatile liquids became noticeable. The assessment and explanation of what had happened at Buncefield became a point of interest for many researchers in this field. The chapter provides numerical calculations for estimating vapour generation during liquid release using the implemented package. In addition, a survey of the most important investigations and study findings on Buncefield is presented.

7.2 Review of the Incident Investigation

7.2.1 Incident Description

Buncefield depot is a large tank farm located 3 miles from the town centre of Hemel Hempstead, Hertfordshire. This depot was the fifth largest of 108 oil storage sites across the UK. At 6:01 am on Sunday 11 December 2005, a series of explosions started on this site, and concluded by destroying large facilities, injuring many people and spreading pollution over a wide area (Newton, 2008).

According to the third progress report of the Buncefield Incident Investigation Board, the story started a few hours before, when Tank 912 in bund A at the HOSL West site started to receive a flow of about 550 $m^3hour^{-1}$of winter blend unleaded motor gasoline. This type of petrol usually contains approximately 10% butane. At 5:20am, the tank would have been completely full. The automatic system used for closing the valves after filling did not operate. Therefore, fuel cascading started and continued for 41 minutes. For the last 7 minutes, fuel flow rate increased reaching $890m^3hour^{-1}$(Powell, 2006b, c).During that period, up to 300 tons of petrol probably escaped, forming a huge fuel-rich fuel–air cloud. Investigators expected that 10 % of this amount turned to vapour. Manifestations of the vapour cloud formation, showing the thickening

and spreading, were clearly observed by eyewitnesses and CCTV cameras starting from 5:30am in the form of a white mist (Newton, 2008). Such mist is most probably formed of water or ice droplets rather than being petrol droplets (Gant and Atkinson, 2011). The formation of such petrol droplet size is not expected either through vapour condensation or droplet breakup (Coldrick, Atkinson and Gant, 2011; Coldrick, Gant, Atkinson and Dakin, 2011). At 5:46am, the vapour cloud thickness reached about 2 m deep over an area of about 80,000m^2 (Powell, 2006b; Ottemoller and Evers, 2008).The site area covered by the cloud before the explosion was approximately 120,000 m^2 with an average depth of about 2 m; the total cloud volume above the lower explosion limit was about 240,000 m^3 (Burgan *et al*., 2009).Climatic conditions at the time were calm, cold, stable and humid. The relative humidity was recorded as 99%, the temperature was between –1.7 and 1°C and the wind speed was approximately 3ms^{-1} (Powell, 2006a).

7.2.2 What is Unexplained in the Buncefield Incident

The excessive strength and demolition effect due to the high overpressure in the Buncefield incident was unexpected. The mechanism of such violent explosions in open places is not fully understood. Likewise, the way of formation of such cloud sizes due to the conventional pool evaporation mechanism is also inconsequential. According to Annex Number 4 of the Buncefield investigation report (Newton, 2008), there were three essential incomprehensible points that need to be explored in this story, and these points are reviewed as follows:

1- Open flammable cloud explosions

In the past, the ignition of any flammable gas/air mixture in an open space was referred to by the expression “unconfined vapour cloud explosion”. In this type of explosion, free expansion of gaseous products is possible. Therefore, no significant overpressure is expected. However, various investigations on offshore vapour cloud incidents have shown that overpressure could be generated. This overpressure was explained due to turbulence development when obstacles such as pipelines are found. The degree of obstruction would control the increasing of the gas mixture burning rate. For this reason, the word *unconfined* is now replaced with *open* to emphasise that for most incidents some degree of confinement exists. The explosion that happened in Buncefield was typically one of these cases where obstacles like petrol tanks and trees were found around the release area.

2- Formation of vapour clouds

As discussed in the literature review, fuel vapour could be generated from pool evaporation, liquid flashing and liquid droplet evaporation during free fall. The formation of vapour from a stable flammable liquid pool, such as petroleum fuels, under normal ambient conditions is expected to be slow and rarely considered to be a significant source for vapour cloud formation. On the other hand, liquid flashing conditions did not exist in the case of Buncefield, where petrol was stored under normal pressure and the temperature was far below the boiling point.

3- Ignition and burning of vapour clouds

According to the mechanism of formation of such a cloud from liquid pool evaporation as experienced in the Buncefield incident, a small amount of vapour is expected to be delivered and the minimum mixing could be considered. In this case, the active part of the cloud within the flammability limits was expected to be small. The remaining part of the cloud was expected to burn as a 'diffusion flame' rather than explosion. From previous experiences, repercussions from incidents like Buncefield were thought to be of just a large pool fire after the tank failure.

In general, all ambiguous points in the Buncefield investigation are leading to one question. How could the spillage of stable fuel liquid under stable ambient conditions lead to the formation of such a large fuel/air cloud? To answer this question, other mechanisms of vapour generation than evaporation from pool should be investigated.

7.2.3 Formation of a Two-Phase Cloud

Fuel clouds formed by liquid fuel releases, in most cases, should be considered as two-phase clouds. This means the fuel could exist in a cloud in both the gaseous phase (vapour) and the liquid phase (aerosol droplets). In Buncefield, the investigation team believed that petrol had flown through eight triangular breathing holes at the top of the tank. Each hole had an area of 0.07 m^2 (Powell, 2006b).The fuel was first collected in Bund A, where evaporation had started to take place (Newton, 2008). The evaporation from the liquid pool was not the only mechanism for cloud generation. As fuel cascaded over the top of the tank deflector plate, part of the liquid flow was expected to cascade freely away from the tank wall. This scenario is very similar to jet releases where liquid is subjected to disintegration and small liquid droplets are formed. The remaining flow, which was directed back to the wall, would have been subjected to another fragmentation mechanism when impacting the tank wind girder. Liquid splashing at that moment would either have either formed some droplets according to impact energy, or been redirected to form another free cascading flow. At the end, the falling liquid

droplets would have been subjected to another impinging when reaching the ground (Powell, 2006b, c). Figure 7.1 illustrates the liquid flow during tank overfilling.

The investigators have concluded that this cascading scenario was likely to have three main results (Powell, 2006b):

1- Efficient generation of small liquid fuel droplets through liquid free-falling disintegration and droplets splashing.
2- Evaporation of lighter chemical components, such as butanes, pentanes and hexanes, leading to ambient air cooling by 7–8 °C below the zero and water vapour freezing, forming an ice mist.
3- Vigorous mixing of heavy fuel vapours with air, forming a fuel/air cloud.

The massive release of gasoline in addition to the tank structure would form a flammable two-phase cloud (Sharma *et al*, 2013).Some results indicate that such clouds cause more powerful explosions than corresponding vapour-only clouds (Burgan *et al.*, 2009). The presence of aerosol or mist droplets could significantly enhance the flame speed, but not enough to explain the overpressure that resulted in Buncefield (Ballal and Lefebvre, 1981).

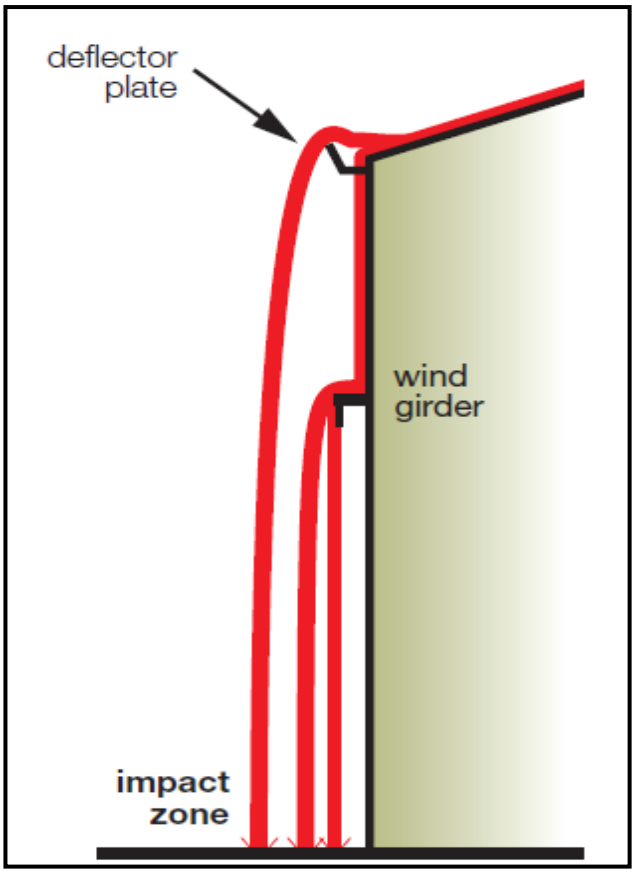

Figure 7.1 Liquid flow during tank overfilling

7.3 Estimating the Fuel Amount Involved in the Explosion

There is a believe that the Buncefield explosion overpressure exceeding 2000 mbar over the vapour cloud area (Burgan *et al.*, 2009; Atkinson and Cusco, 2011). According to qualitative assessment of the damage resulting from the Buncefield explosion, the incident investigators achieved a certain belief that the open area of the Northgate and Fuji car parks was subjected to the highest overpressure. They assumed that an overpressure of 700–1000 mbar led to extensive damage to adjacent buildings in this area (Hailwood, Gawlowski, Schalau and Schonbucher, 2009). Another overpressure of about 7–10 mbar was estimated due to the breakage of some windows in local homes and premises at 2 km away. Although these conclusions were based on published tables, the estimated overpressure magnitude in an uncongested area like the Northgate and Fuji car parks was far exceeding the predictions (Powell, 2006b).The next sections present different methods for estimating the amount of fuel vapour in the Buncefield explosion.

7.3.1 Seismic and Acoustic Measurement of the Buncefield Explosion

The seismic waves that resulted from Buncefield explosion were detected at many seismic stations around the UK and in the Netherlands. In addition, the acoustic waves were recorded by infrasound stations in the Netherlands. An average value of 2.2 ML for the local magnitude was estimated for the Buncefield explosion from 22 seismic station measurements (Ottemoller and Evers, 2008). In general, there is no simple relation to estimate the yield of an explosion from the seismic wave magnitude (Khalturin, Rautian and Richards, 1998). According to previous measurements for explosions with a known yield, this magnitude could be measured for an explosion yield varying between 3 and 250 tons. In addition, the same value was recorded for 2–10 tons of buried explosions. This large spread was explained due to the large coupling variation (Ottemoller and Evers, 2008).

The explosion magnitude was also estimated from theinfrasound records. A yield equivalent to 21.6 (±5) tons of TNT was suggested due to the stratospheric refracted acoustic wave's records. This value is equivalent to 19.5 tons of vapour cloud mass (Ottemoller and Evers, 2008).Estimation of the yield of explosion using different stratospheric arrivals was presented by Ceranna, Le Pichon, Green and Mialle (2009). The average estimate was 51 tons as a mean value for all arrival waves. The variation

between estimate yields using acoustic wave measurements is more acceptable than seismic wave measurements.

7.3.2 Estimating Vapour Mass Using TNT-Equivalent Method

The TNT-equivalent method is a simple well-known approach to estimate the equivalent mass of TNT from a known amount of combustion energy (Crowl, 2003).Although fuel–air explosions and standard TNT explosions are not identical (Formby and Wharton, 1996), this method is based on the similarity between explosions of gas and those of traditional high explosives (Lea and Ledin, 2002).

To apply this method to the Buncefield explosion, a certain damage effect at a certain distance from the explosion centre should be identified. One of the observed damage effects was the severe damage to the Fuji and Northgate buildings. According to the final report from the Buncefield investigation board (Powell, 2006b), this damage was caused by 1,000 mbar overpressure. On the other hand, this amount of damage could result from nearly 689 mbar overpressure (Appendix C1). In addition, the distance between these buildings and the explosion centre is not well defined because they were already placed inside the cloud coverage area. The other damage effect was window breakage in local homes and premises at a distance of 2 km from the explosion centre.

The amount of fuel involved in the Buncefield could be estimated from the TNT-equivalent method as follows (Casal, 2008):

1) According to the damage observed in the far field:

A) Estimating overpressure:

- According to Appendix (C1), typical pressure for glass breakage = 0.0103 bar.

B) Estimating scaled distance:

- The scaled distance (Z) could be estimated from the empirical blast chartsas follows:

For $\Delta P = 0.0103$bar

The corresponding Z value $\approx 83 m/kg^{0.333}$

C) Calculating the Mass of TNT:

The equivalent mass of TNT (W_{TNT}) could be estimated from Equation7.1 as follows:

$$Z = \frac{R}{W_{TNT}^{1/3}} \qquad \text{eq 7.1}$$

If Z = 83 and R (distance from explosion centre) = 2000m

Then,

$$W_{TNT} = \left(\frac{2000}{83}\right)^3 = 13991 \text{ kg} \qquad \text{eq 7.2}$$

D) Calculating the equivalent mass of fuel vapour:

The equivalent fuel vapour mass could be estimated from Equation 7.3 as follows:

$$W_{TNT} = \eta \frac{m_{gas} \Delta H_C}{\Delta H_{TNT}} \qquad \text{eq 7.3}$$

W_{TNT} is the equivalent mass of TNT (kg), η is the empirical explosion efficiency (dimensionless), m_{gas} is the mass of flammable gas or vapour (kg), ΔH_c is the heat of combustion of the flammable gas ($kJkg^{-1}$) and ΔH_{TNT} is the energy of explosion of TNT with a typical value of 4602 $kJkg^{-1}$.

The explosion efficiency (η) is likely influenced by the fuel reactivity and the degree of confinement. Although different values between 1 and 10% were suggested before, the value of 3% is the most acceptable for vapour cloud explosions (Casal, 2008).

Then,

$$\therefore M = \frac{\Delta H_{TNT} W_{TNT}}{\eta \Delta H_C} = \frac{4602 \times 13991}{0.03 \times 46000} = 46656 \text{ kg} \approx 46.5 \text{ tons} \qquad \text{eq 7.4}$$

2) According to the damage observed in the near field:

A) Estimating overpressure:

- According to Appendix (C1), the typical pressure for the destruction of buildings = 0.689 bar.

B) Estimating scaled distance:

For ΔP= 0.689 bar, the corresponding Z value $\approx 4 m/kg^{0.333}$

C) Calculating the Mass of TNT:

If Z = 4 and R (distance from explosion centre) = 100m

Then,

$$W_{TNT} = \left(\frac{100}{4}\right)^3 = 15625 \text{ kg}$$

D) Calculating the equivalent mass of fuel vapour:

$$\therefore M = \frac{\Delta H_{TNT} W_{TNT}}{\eta \Delta H_C} = \frac{4602 \times 15625}{0.03 \times 46000} = 52106 \text{ kg} \approx 52 \text{ tons} \qquad \text{eq 7.5}$$

According to these calculations, the equivalent mass of fuel vapours in the Buncefield explosion could be around 46–50 tons. This amount is nearly 16% of the total released fuel.

7.3.3 Estimating Vapour Mass Generation from the Liquid Pool

The gasoline fuel that escaped in the Buncefield incident was stored under ambient pressure and temperature (Newton, 2008). The release was understood to be directly from overfilling of tank 912 in bund A. The stream was not forced by any pressure and the fuel spill from the top of the tank to the ground was free falling due to gravity.

According to this information, it is not expected that the escaped gasoline would have any vapour fraction resulting from flashing. Fuel vapours in this case could be generated though liquid pool evaporation and falling liquid droplet evaporation (Powell, 2006b). In this section, the amount of vapour generated directly from the liquid pool that was formed around tank 912 inside Bund A will be estimated. The rate of evaporation will be estimated using Equation 2.2as follows:

1- Wind speed (u_w) was nearly 3 ms^{-1}(Powell, 2006a).
2- The length of the pool side parallel to the wind could be estimated graphically relative to the diameter of tank 912 = 25 m (Hailwood, Gawlowski, Schalau and Schonbucher, 2009). Figure 7.2 expresses the layout of Bund A with proportional dimensions to the Buncefield area in Google maps. The poolside was graphically estimated as 124m.Thismeasure is the maximum length of the pool side perpendicular to the wind direction including distances obstructed by petrol tanks.
3- Although liquid gasoline's molecular weight is about 100–110 $gmol^{-1}$ (Riazi, 2005), the molecular weight of gasoline vapours is different according to the different rate of evaporation for different gasoline components. The vapour's molecular weight could be estimated as 62$gmol^{-1}$(EPA, 1995), which is suitable for winter patch gasoline with RVP = 13.5 pa. Tg is the value that will be used in Equation 2.2 instead of liquid molecular weight ($M_{liq)}$ (Maremonti, Russo, Salzano and Tufano, 1999).
4- Atmospheric pressure (P_o) =1.0132 $\times 10^5$Pa = 1 bar
5- The ideal gas constant (R) =8.314 $\times$ 10^3 J $kmo1^{-1}$ K^{-1}
6- The average ambient temperature was estimated to be around 0°C, and the initial petrol temperature when released was 14–15 °C (Atkinson and Gant, 2012a, b).CFD modelling performed by Atkinson and Gant (2012b) to simulate the Buncefield scenario using liquid hexane instead of gasoline proved that most of the released droplets reached the bund floor with temperatures of around -10°C. For simplification and as a worst-case scenario, the liquid pool temperature (T) will be estimated as 0 °C = 273K.

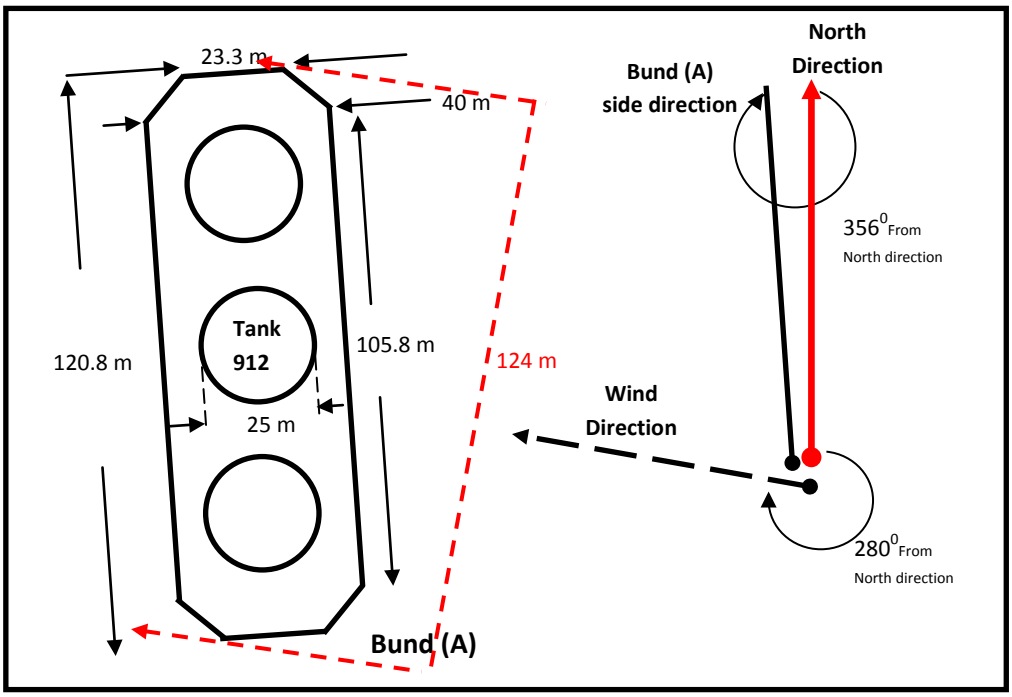

Figure 7.2The layout of Bund (A) with scaled dimensions from Google maps

7- The liquid vapour pressure (P_{liq}) at 0 °C for the winter gasoline patch could be estimated graphically from the motor gasoline ASTM distillation curve (EPA, 1995), assuming the Reid vapour pressure value for such winter gasoline composition to be13.5 psi. True vapour pressure for these conditions was estimated at4.2 psi = 0.286 bar = 28948 Pa (HESS, 2007).

8- P_{amb} (vapour partial pressure) is an average value between the initial condition (P_{amb}=0) and the final saturated condition (P_{amb} =28948 Pa).

Then:

$$G_{pool} = 0.0021 \times (3)^{0.78} \times (124)^{-0.11} \frac{62 \times 1.0132 \times 10^5}{8.314 \times 10^3 \times 273} \ln\left(1 + \frac{28948 - 14474}{1.0132 \times 10^5 - 28948}\right)$$

$$G_{pool} = 0.00147 \ \text{kg m}^{-2}\text{s}^{-1}$$

The total pool area could be estimated from Figure7.2 as follows:

$$\text{Pool area} = \text{Total area inside BundA} - \text{Area of Tanks}$$

$$\text{Pool area} = 4715 - 3 \times \left(3.14 \times \left(12.5^2\right)\right) = 3242.4 \text{m}^2$$

$$\therefore \text{Total Evaporation rate from Pool area} = 3242.4 \times 0.00147 = 4.76 \text{ kg s}^{-1}$$

Total escaping time (5:20 to 6:01 am) = 41 min = 2460 s

$$\therefore \text{Total Evaporation from Liquid Pool} = 11.62076 \times 2460 = 11709 \text{ kg} \approx 11.7 \text{ tons}$$

According to the previous calculations, the total vapour mass from the liquid pool couldreach11.7tons. This amount is nearly 3.9% of the total mass released from tank 912.

The HSE estimated the maximum rate of evaporation in Buncefield using the GASP model and pure hexane instead of gasoline (Atkinson and Gant, 2012b). The rate of vaporisation was nearly 4 kgs^{-1} at 5 ms^{-1} wind velocity, and this result is reasonable with the above calculation result. However, this result was estimated due to the worst-case conditions and this amount is probably over estimated for the following reasons:

1- A wind speed of 3 ms^{-1} was assumed according to Meteorological Office records at 13 km away from the Buncefield depot (Powell, 2006a). This speed might be reduced if we take into account the obstruction of petrol tanks, buildings and the tree line.
2- The pool side length of 124 m is the overall distance facing the wind, but the three 25-m diameter petrol tanks may protect some pool areas from wind exposure.
3- Evaporation from the total bund area is not expected during the first few minutes until the area becomes fully covered with liquid.
4- The temperature was assumed to be 0 °C, which is typical of ambient temperature at the time the release started. In fact, both the vapour cloud temperature and the liquid temperature were decreased gradually, because of fuel evaporation, reaching about -8.5 °C at low fuel release ($550m^3h^{-1}$) and about -7.2 °C at high fuel release ($890m^3h^{-1}$)(Atkinson and Gant, 2012a).The rate of vaporisation should decrease at lower temperatures.
5- The true saturated vapour pressure of 28948 Pa was assumed as suitable for winter batch gasoline with a 13.5 Reid vapour pressure. However, this might not be completely true. Gasoline is a mixture of different boiling point components and, when it evaporates, the lighter components will be lost first. Gradually, the vapour pressure will decrease and consequently the evaporation rate will be decreased (Okamoto *et al.,* 2009). Experiments on these correlations have found that the gasoline vapour pressure could dramatically decrease from 95 kPa to 5 kPa at 40 °C after 70% of the liquid is lost by evaporation and from 34 KPa to 2 kPa at 10 °C when the same mass fraction is lost. In addition, the rate of decrease was found to be inversely proportional to pool depth (Okamoto *et al.,* 2009). According to these results, the gasoline vapour pressure in the Buncefield

explosion is expected to be in a lower range than standard pressure for ideal winter gasoline.

7.3.4 Estimating the Mass of Vapour from Cloud Composition

The most likely composition of the winter batch gasoline released in the Buncefield explosion is 9.6% (w/w_o) of n-butane (as a surrogate for all C4), 17.2% of n-pentane (as a surrogate for all C5), 16% of n-hexane (as a surrogate for all C6) and 57.2% n-decane (as a surrogate for all low-volatility hydrocarbons)(Atkinson *et al.,* 2008). Due to the different volatilities of gasoline components, the more volatile components are likely to evaporate in earlier. The low volatile components remain, forming different droplet compositions (Burger *et al.,* 2003). The weight percent of hydrocarbons in the Buncefield vapour cloud was estimated at nearly 14.16% (Atkinson *et al*., 2008). The three main components forming this ratio are n-butane with 6%, n-pentane with 6.1% and n-hexane for the other 2.06%. Accordingly, the composition of the residual liquid would subsequently change. The percentage of high volatility components will reduce to 2.4% and 11.5% for n-butane and n-pentane, respectively. The percentage of low volatility components will increase, reaching 16.3% and69.6% for n-hexane and n-decane, respectively (Atkinson and Gant, 2012a).

According to the suggested composition, the total mass of fuel vapour mass in Buncefield cloud could be estimated as follows:

Each kg of vapour cloud contains 60 g of n-butane, 61 g of n-pentane, 20.6 g of n-hexane and 858.3 g of air (relative humidity = 99%) at 0 °C.

The density of humid air at 0 °C= 1.290 kgm^{-3}

The density of dry air at 0 °C = 1.2929 $kg\ m^{-3}$

$$\text{The density of n-butane vapour at } 0^{o}\text{C} = \frac{\text{MW}_{\text{butane}}}{\text{MW}_{\text{dryair}}} = \frac{58.12}{28.97} = 2.59\ \text{kg m}^{-3}$$

$$\text{The density of n-pentane vapour at } 0^{o}\text{C} = \frac{\text{MW}_{\text{pentane}}}{\text{MW}_{\text{dryair}}} = \frac{72.15}{28.97} = 3.22\ \text{kg m}^{-3}$$

$$\text{The density of n-hexane vapour at } 0^{o}\text{C} = \frac{\text{MW}_{\text{hexane}}}{\text{MW}_{\text{dryair}}} = \frac{86.17}{28.97} = 3.85\ \text{kg m}^{-3}$$

Then, the volume of each component is calculated separately:

$$\text{The volume of } 60\text{ g n - butane vapour at } 0^{o}\text{C} = \frac{W_{butane}}{\rho_{butane}} = \frac{60}{2.59} = 23.13 \text{ L}$$

$$\text{The volume of } 61\text{ g n - pentane vapour at } 0^{o}\text{C} = \frac{W_{pentane}}{\rho_{pentane}} = \frac{61}{3.22} = 18.94 \text{ L}$$

$$\text{The volume of } 20.6\text{ g n - hexane vapour at } 0^{o}\text{C} = \frac{W_{hexane}}{\rho_{hexane}} = \frac{20.6}{3.85} = 5.36 \text{ L}$$

$$\text{The volume of } 858.3\text{ g humid air at } 0^{o}\text{C} = \frac{W_{humidair}}{\rho_{humidair}} = \frac{858.3}{1.2902} = 665.25 \text{ L}$$

$$\therefore \text{Total volume of } 1\text{ kg gas mixture at } 0^{o}\text{C} = 712.68 \text{ Litre}$$

$$\therefore \text{Vapour cloud density at } 0^{o}\text{C} = \frac{1000}{712.68} = 1.403 \text{ gm/L}$$

Vapour cloud volume = 200,000 m^3 will weigh nearly 280632 kg

Vapour cloud mass = 200,000 × 1.403 = 280.5 tons

$$\therefore \text{Hydrocarbon vapour mass} = 280632 * 0.142 \approx 40 \text{ tons}$$

This value gives a clear indication that evaporation from the pool might not be the main source of vapour generation in the Buncefield explosion and similar fuel release incidents. The other expected source might be liquid droplet evaporation.

The important question that needs to be asked is whether this mixture is located within the flammability limits or not? To answer this question, the flammability limits should be calculated for the hydrocarbon mixture in air. Then, the volume percentage of hydrocarbons will be compared with those limits as follows:

$$\text{LFL of vapour mixture} = \left(\sum_{i=1}^{n} \frac{y_i}{LFL_i} \right)^{-1} \qquad \text{eq 7.3}$$

$$\therefore \text{LFL} = \left(\frac{0.48774}{1.8} + \frac{0.39933}{1.4} + \frac{0.11293}{1.2} \right)^{-1} = 1.5$$

$$\text{UFL of vapour mixture} = \left(\sum_{i=1}^{n} \frac{y_i}{UFL_i} \right)^{-1} \qquad \text{eq 7.4}$$

$$\text{UFL} = \left(\frac{0.48774}{8.4} + \frac{0.39933}{8.3} + \frac{0.11293}{7.7} \right)^{-1} = 8.3$$

$$\text{Molecular weight of vapour mixture} = \sum_{i=1}^{n} \left(y_i \times Mw_i \right) \qquad \text{eq7.5}$$

$$= \left(58.1 \times 0.48774\right) + \left(72.15 \times 0.39933\right) + \left(86.17 \times 0.11293\right) = 66.88 \text{gm/mol}$$

The specification of fuel vapour mixture in Buncefield is presented in Table 7.1.

Table 7.1 Specification of gas mixture components

	Mass (gm)	Volume (L)	Volume % in cloud	Mw (gm/mole)	No of moles (mole)	Mole fraction (%)	FL (v %)	
							LFL	UFL
n-	60	23.1	3.25	58.1	1.03	0.48	1.	8.
n-	61	18.9	2.66	72.15	0.84	0.39	1.	8.
n-	20.	5.36	0.75	86.17	0.23	0.11	1.	7.
Mixt	**14**	**47.4**	**6.66**	**66.88**	**2.11**	**1**	**1.**	**8.**

The results in Table 7.1 prove that the proposed vapour cloud composition is located inside the flammability range. Atkinson and Gant (2012a) suggested that the vapour concentration within bund A and the adjacent area was above stoichiometric at the time of the Buncefield explosion.

7.4 Estimating the Vapour Generation in Buncefield Using the Implemented Numerical Package

In this section, the numerical calculation code is applied to the Buncefield case of overfilling release to estimate the amount of vapour generation. To simplify the problem, n-hexane will be used to simulate the gasoline behaviour. Atkinson and Gant (2012a) illustrated and described some features about the Buncefield release scenario as follows:

1- Liquid release took place from the top of the tank at nearly 15 m above the ground.
2- Nearly 30% of the tank wall surface above the wall girder was wetted during liquid release. This ratio may have slightly increased to 33% during the last 7 minutes.
3- A few meters below the wind girder, liquid droplets and spray formed from each vent release spread over an area of 4.5m^2 and covered a perimeter of about 6m.
4- The vapour cloud volume was nearly 200,000 m^3 spread over an area of about 100,000 m^2 with an average thickness of 2 m.
5- The vapour cloud mass concentration was about 13.7% with a final temperature of about -8.5 °C.

7.4.1 Selection of Numerical Calculation Inputs

The inputs used for the numerical calculations are identical to those measured in Buncefield. As previously performed in Chapter 6, the liquid and ambient temperatures will be assumed as an average between the initial and final temperatures estimated for Buncefield incident (4°C for the liquid as an average between 15 and -8°C, -4°C for ambient temperature as an average between 0 and -8°C). The relative humidity is 99% and the falling distance is nearly 15m. The vapour cloud volume is estimated using the VCA method, which is improved by the HSE (Atkinson and Gant, 2012b), and also according to the cloud volume estimated in the Buncefield investigations. The liquid flow rate is estimated as an average value during the release time. The release problem is solved using multi-point mode calculations. Detailed calculations for estimating the number of release points are expressed in the following steps:

1- Estimating the liquid flow rate:

Liquid volume escaped at $550 m^3 h^{-1}$ = $550 m^3 hr^{-1} \times 34 min/60\ min hr^{-1}$ = $311.7\ m^3$

Liquid volume escaped at $890 m^3 h^{-1}$ = $890 m^3 hr^{-1} \times 7 min/60 min hr^{-1}$ = $103.8\ m^3$

Total escaped liquid volume = 311.7 + 103.8 = $415.5\ m^3$

Total escaped liquid volume = 415.5 x 0.678 = 281.7 tons

Average volume flow rate during 41 minutes = 415.5 / 2460 = 168.9 L/s

Average mass flow rate during 41 minutes = 169 x 0.678 ≈ 115 kg/s

2- Estimating the vapour cloud volume:

a- Vapour cloud volume by VCA method(Atkinson and Gant, 2012b):

The rate of air entrained could be estimated using the following empirical formula:

$$M_{air} = 90\left(\frac{D}{25}\right)^{0.75}\left(\frac{H}{10}\right)^{0.45}\left(\frac{F}{115}\right)^{0.25} \qquad \text{eq 7.6}$$

Where D is tank diameter (m), H is tank height (m) and F is the liquid release rate (kgs^{-1}).

$$M_{air} = 90\left(\frac{25}{25}\right)^{0.75}\left(\frac{15}{10}\right)^{0.45}\left(\frac{115}{115}\right)^{0.25} \approx 108\ kg/s$$

Rate of air volume entrained =108 /1.31 = 82.44 Ls^{-1}

Total vapour cloud volume = 82.44×2460 ≈ 202,800 m^3

b- Vapour cloud volume from the Buncefield investigation ≈ 200,000m^3

Both results are similar and the vapour cloud volume will be proposed = 200,000m^3

3- Estimating the number of release points

Release velocity =1 ms^{-1}, as proved in the HSE's experiments (Atkinson and Coldrick, 2012a, b).

-Release length = 0.333 ×Tank perimeter = 0.3× π ×D = 23.56 m

-Volumetric flow rate = 169 L/s =0.169 m^3s^{-1}

-Discharge cross-section = flow rate / velocity = 0.169 /1 = 0.169 m^2

-Jet diameter is assumed = 8mm

-Jet cross-section = $\pi r^2 = \pi \times (0.004)^2 = 5.03\times 10^{-5} m^2$

-Number of jets = 0.169 / 0.0000503 ≈ 3362 jets (releasing points)

4- Estimating the vapour concentration ratio

According to the experimental and CFD simulation results (discussed in Chapter 6), the ratio between the vapour concentration inside and outside cascade region was usually between 1.25 and 1.5. The overfilling release in Buncefield is very similar to the CFD Case No. 12, where the liquid is flowing through eight triangular breathing holes at the top of the tank. The result of Case 12 indicated that the vapour concentration inside the cascade was nearly 1.25 times the concentration outside the cascade. Hence, this value is proposed for the Buncefield numerical calculations.

7.4.2 Results and Discussion

The results of the Buncefield case numerical calculations are summarised and discussed through the following points.

1- The total mass vaporised during 41 minutes was nearly 31.8 tons. This value is nearly 11.24% of the total released liquid mass. In addition to the probably mass vaporised from the liquid pool of nearly 11.7 tons, the vapour mass of the vapour cloud becomes nearly 43.5 tons. The estimation corresponds with the values estimated using the TNT method and the vapour cloud concentration, and is not far from the value estimated by the Buncefield investigation team. Figure 7.3 compares the different values of the total vapour mass estimated for the Buncefield incident.

2- The vapour fraction generated inside the cascade region is nearly 89.7% of the total vapour mass. The remaining fraction was generated outside the cascade due to evaporation of airborne aerosol droplets. The fluctuation of vapour concentration inside the cascade region allows some aerosol droplets to remain and reach to outside the cascade region.

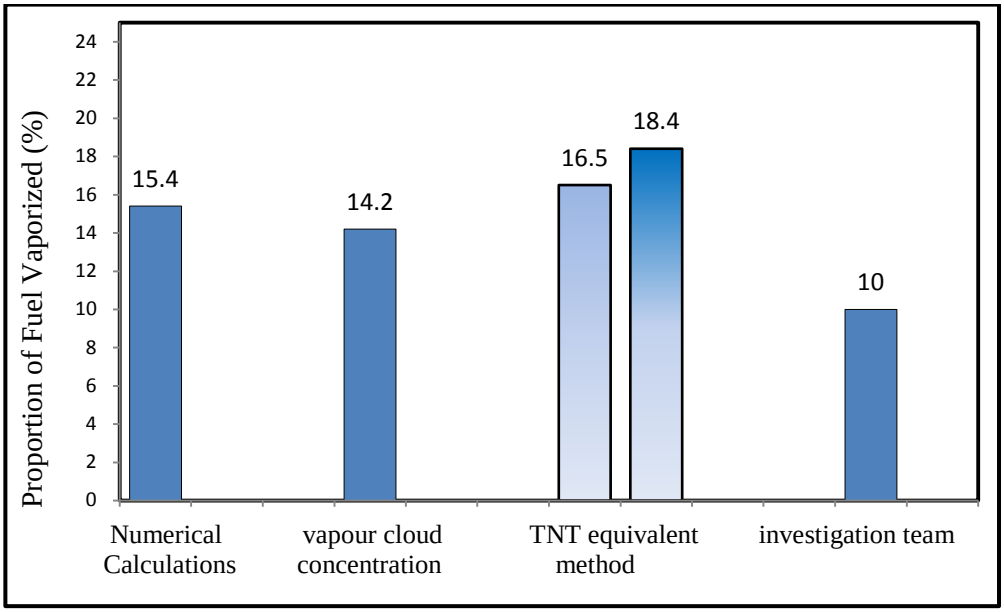

Figure 7.3 Mass percentage of fuel vaporized in Buncefield estimated by different methods

3- The vapour amount generated from falling liquid droplets is nearly 80.47% of the total vapour mass. The remaining fraction is the contribution of the splashing process that takes place down the cascade. This means that the mechanism of droplet splashing enhanced the vaporisation process by nearly 25%. This result confirms the belief of the significant role of the droplet splashing mechanism during overfilling release incidents. Figure 7.4 expresses the accumulative generation of vapour mass due to the evaporation of falling droplets and splashed droplets.

4- The vapour volume concentration was nearly 3.8% (v/v) across the cloud. This value is above the stoichiometric ratio for n-hexane vapour at the proposed temperature (2.2%), and this means that the cloud was flammable during the release time. Figure 7.5 expresses the vapour volume concentration with respect to flammability limits.

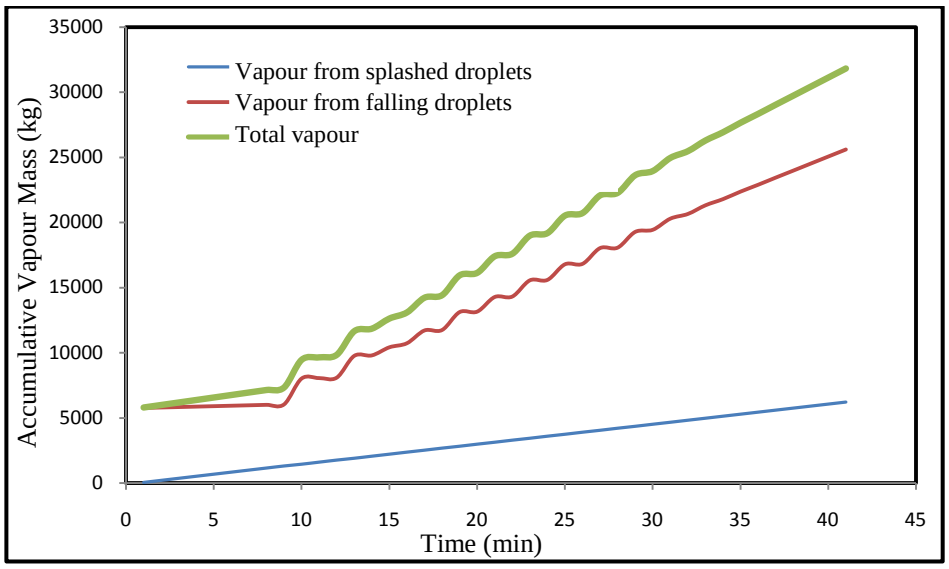

Figure 7.4 Accumulative generation of vapour mass during release time

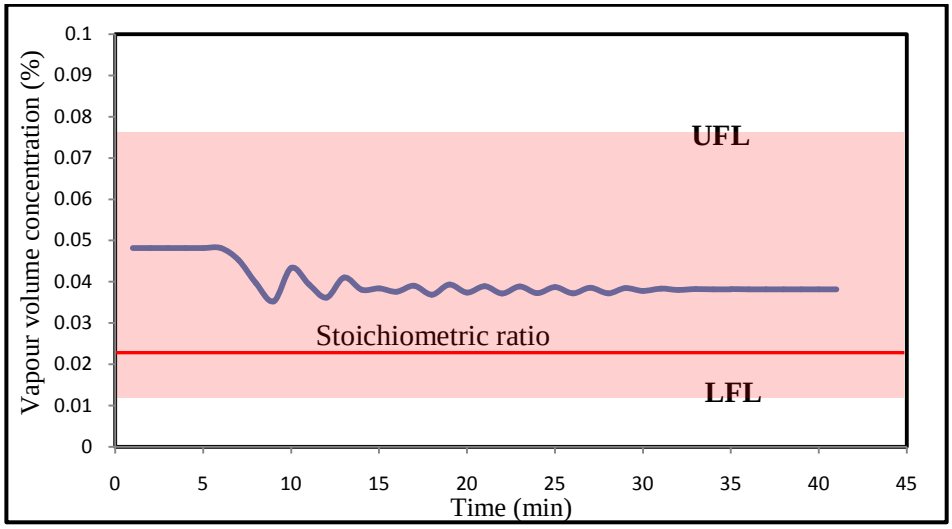

Figure 7.5Accumulative generation of vapour mass during release time

7.5 Conclusions

- The vaporisation process during the overfilling liquid release in Buncefield was represented using the implemented numerical calculation package.
- The total vaporised amount from liquid cascade was nearly 11.24% of the total releases mass, compared to around 4.16% emitted from the liquid pool.
- The estimated result for the proportion of vaporised liquid was comparable with the results estimated by different methods.
- The obtained results had ascertained the significant role of droplet splashing during overfilling release incidents. This assumption was based on the correlation of splashing with a 25% increase in the vaporisation efficiency.
- The formation of aerosols enhanced the vaporisation process by nearly 11%.

Chapter 8: The Effect of Release Conditions on Droplet Size Distribution and Vapour Generation

8.1 Introduction

As discussed in the literature review, many parameters govern the mechanism of liquid jet disintegration. The breakup length and particle size distribution resulting from the primary stage of jet breakup are dependent on many factors. The influence of such factors can be extended to affect the breakup of liquid droplets during the free-falling stage and impinging stage. In general, these factors could be classified into three main categories: the release conditions, the properties of released liquid and the ambient media conditions. Liquid release velocity and discharge orifice diameter could be classified as the release conditions. This category can also include the height of release orifice from the ground or impinging surface. Increasing height gives more allowance for changes happening to falling droplets. The second category is the properties of released liquid itself. Liquid viscosity, density, surface tension, vapour pressure and molecular weight are included in this category. The third category incorporates the properties of ambient media. This includes the ambient gas viscosity, density and temperature. Temperature has an expanded effect of controlling the physical properties of released liquid and gas media.

This study concerns both the quantity of liquid aerosol droplets formation, and the amount of fuel vapour generated during the droplets free fall. The fuel aerosol droplets and vapours release into and disperse in the dry or humid ambient air would form hazardous fuel vapour cloud.

In this chapter, the factors belong to the first category are analysed in details. The effect of these factors is mainly based on the mechanism of jet breakup and secondary breakup of liquid droplets. These two processes are presented together as the primary stage of the model. The effect of formed droplet distribution during primary stage is extended through droplet distribution developments during droplets free falling, and finally the impinging of these droplets at the end of free -falling.

8.2 The effect of Release Orifice Diameter

8.2.1 The effect of Orifice Diameter on Primary Stage

The release orifice diameter is an important parameter affecting the behaviour and quality of liquid breakup when released. To study the effect of changing orifice diameter on the mechanism of liquid jet breakup, the mathematical model had been applied for an Ethanol liquid fuel releasing at velocity of 10 m/s from different orifice diameters ranging from 1 to 20 mm. The ambient air was assumed to be fully saturated with ethanol and water vapours at 20^{o}C to avoid any change in droplets volume caused by evaporation. The release height was assumed to be 5 meters above the ground.

Figures (8.1) and (8.2) show the droplet size distribution resulting after primary disintegration of released liquid jet and after the secondary disintegration of the liquid drops. Table (8.1) summarizes the most important parameters of the primary stage.

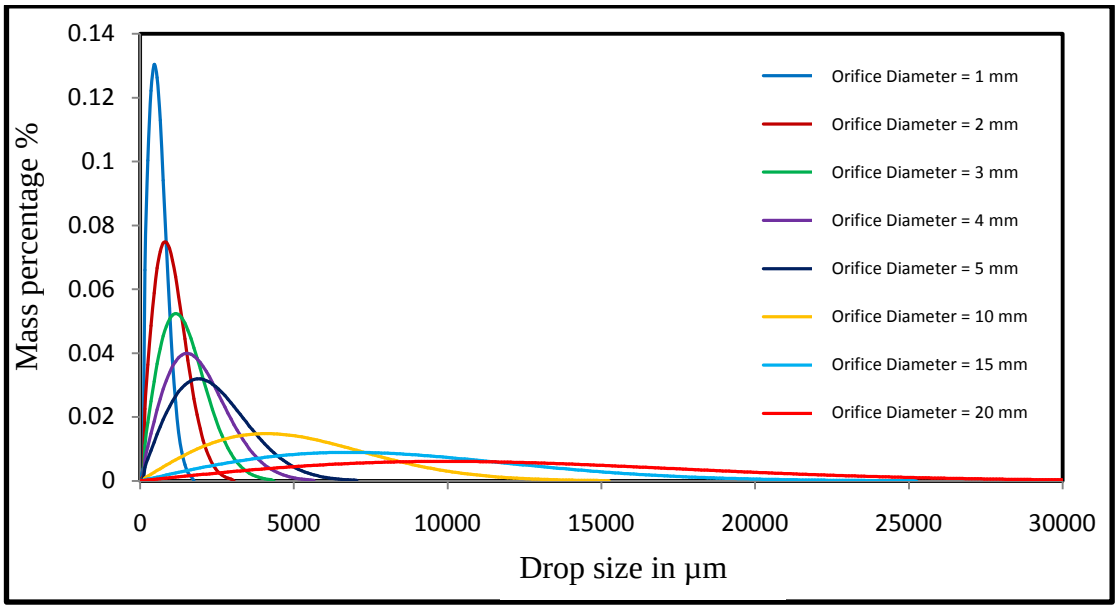

Figure 8.1 Droplet size distribution after jet primary breakup of Ethanol liquid fuel at the nozzle diameter varying from 1mm to 20 mm

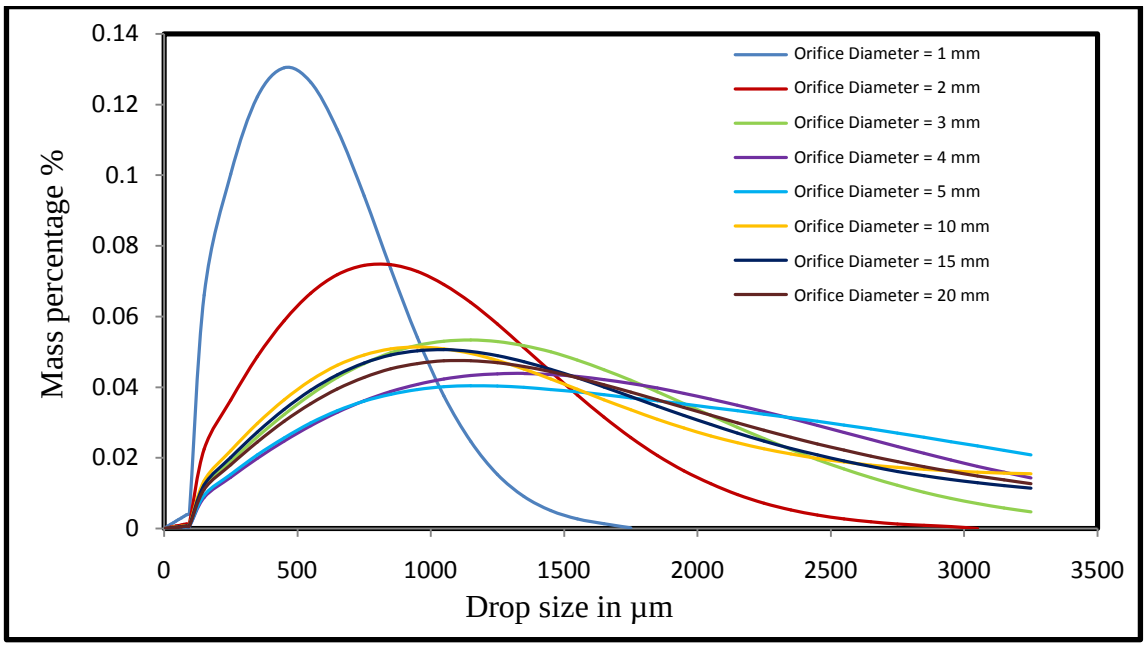

Figure 8.2Droplet size distribution after secondary drops breakup of Ethanol liquid fuel at the nozzle diameter varying from 1mm to 20mm.

Table 8.1 Parameters of the primary stage of 10 m/s ethanol release from an orifice diameter varying from 1mm to 20mm and saturated conditions at 20^{o}C

Orifice diameter (mm)	Volumetric flow rate (L/s)	Breakup regime	Breakup length (m)	$D_{0.999}$ (µm) after jet breakup	$D_{0.999}$ / D_{Or}	$D_{0.999}$ (µm) after drop breakup	Fraction of aerosol size droplets after jet breakup	Fraction of aerosol size droplets after drop breakup
1	0.0078	F.W.I	0.11	1720	1.72	1720	0.0231	0.0231
2	0.0315	F.W.I	0.29	3050	1.53	3050	0.0076	0.0076
3	0.0707	S.W.I	0.50	4300	1.43	3250	0.0037	0.0039
4	0.1257	S.W.I	0.72	5646	1.41	3250	0.0022	0.0030
5	0.1964	S.W.I	0.97	7059	1.41	3250	0.0014	0.0032
10	0.7854	ATOM	0	15232	1.52	3250	0.0003	0.0046
15	1.7671	ATOM	0	25235	1.68	3250	0.0001	0.0042
20	3.1416	ATOM	0	36960	1.85	3250	0.00005	0.0037

F.W.I.....first wind breakup regime S.W.I.....second wind breakup regime ATOM.....atomization regime

During the primary breakup of the liquid jet, the mean and max size of droplets generated from the primary breakup of liquid jet increases by increasing the release orifice diameter. The ratio of the maximum droplet diameter to orifice diameter size

($D_{0.999}/d_{or}$) has a minimum value at orifice diameter between 4mm and 5 mm. This could be explained from the used empirical equation, as the value of orifice diameter appears to be three times in the equation. Different powers and positions of diameter value in the equation had resulted in this minimum value,

$$D_{0.999} = d_{or}\, We_{Liq}^{-0.333}\left(23.5 + 0.000395\, Re_{Liq}\right)$$

We_{Liq}: $\rho_{Liq}\, U_L^{\,2}\, \frac{d_o}{\sigma}$; Re_{Liq}: $\rho_{Liq}\, U_L\, \frac{d_o}{\mu_L}$

During the secondary breakup of liquid droplets, all the droplets formed in the primary breakup step with a diameter above the critical diameter which determined by the liquid release velocity would instantaneously disintegrate. In this case where the release velocity is 10 m/s release velocity, the critical droplet diameter equals 3250µm which would be the maximum droplet size. Therefore, the percentage of small droplets will increase as a result of larger droplets disintegration. As shown in Figure 8.2, the new distribution curves for the release orifices with diameter greater than 3 mm seem approaching each other. The total percentage of liquid aerosol droplets (0 – 100µm) had been calculated from the droplets size distribution in each case and shown in Table 8.1. Although the total percentage of aerosol droplets is relatively small, the increasing of orifice diameter had led to dramatic decrease in percentage of aerosol droplets. After the secondary disintegration of larger droplets, the aerosol percentage had been increased for orifice with a diameter greater than 4mm. A comparison of effect of increasing release orifice diameter on the percentage of aerosol droplets at the end of primary and secondary breakup is presented in Fig 8.3.

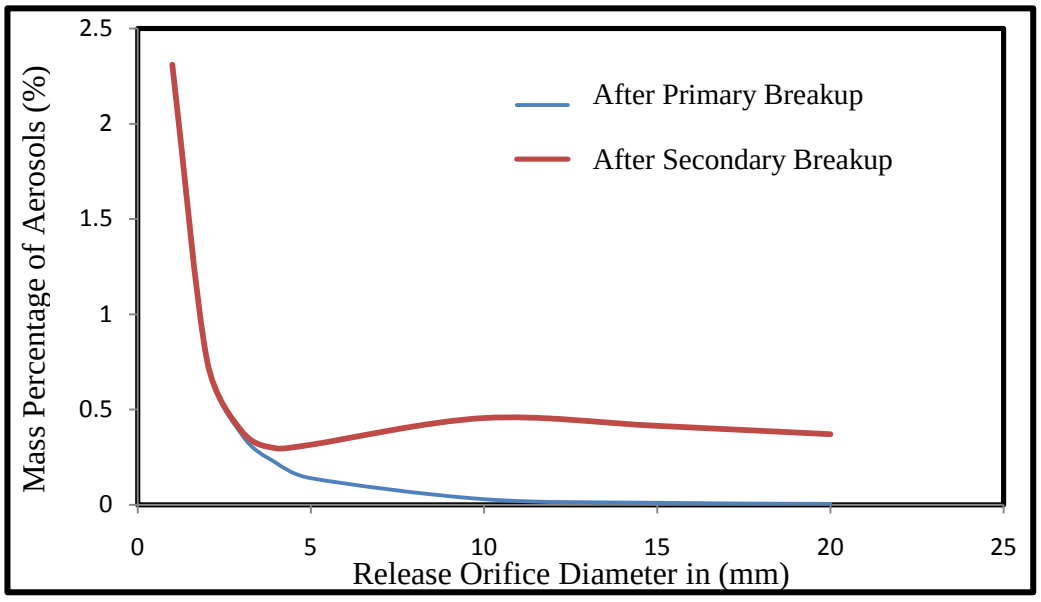

Figure 8.3 Effect of increasing release orifice diameter on the percentage of aerosols after primary breakup and secondary breakup at 10 m/s release velocity

The breakup length is also increased with increasing orifice diameter as shown in Table (8.1). This was true when the breakup regime was classified as first or second wind induced breakup. When the jet breakup gets fully atomized, the breakup length gets very small and was assumed to be zero. Increasing the breakup length result in less for droplets disintegration during free fall and lowers the height of aerosol existence.

To examine the effect of orifice diameter at lower release velocities, the model has been applied at 5m/s release velocity; the other conditions are remained unchanged. Table (8.2) shows the primary stage disintegration parameters for the modified release velocity. Compared to the results at 10 m/s, it could be found that the breakup length had generally increased. The breakup regime didn't reach the full atomization at any orifice diameter from 1 to 20 mm, and the distance of breakup has reached about 3.88 m at the maximum orifice diameter (20mm). The minimum value of $D_{0.999}/d_{or}$ still exists but was shifted to a higher orifice diameter of about 10 mm. After the secondary droplets disintegration, the maximum droplets sizes increase to a value of 13500μm. After secondary droplets disintegration, the percentage of aerosol droplets started to increase when orifice diameter is greater than 10mm. Figure (8.4) shows the relationship between aerosol mass percentage and orifice diameter at 5m/s liquid release velocity.

Table 8.2 parameters of the primary stage for 5 m/s ethanol release from 1-20 mm orifice diameter and saturated conditions at 20°C

Orifice diameter (mm)	Volumetric flow rate (L/s)	Breakup regime	Breakup length (m)	D_{max} (μm) after jet breakup	D_{max} / $D_{Orifice}$	D_{max} (μm) after drop breakup	Fraction of aerosol size droplets after jet breakup	Fraction of aerosol size droplets after drop breakup
1	0.0039	F.W.I	0.075	2592	2.59	2550	0.0102	0.0102
2	0.0157	F.W.I	0.186	4333	2.17	4350	0.0036	0.0036
3	0.0353	F.W.I	0.318	5965	1.99	5950	0.0019	0.0019
4	0.0628	F.W.I	0.464	7574	1.89	7550	0.0012	0.0012
5	0.0981	F.W.I	0.623	9191	1.84	9150	0.0008	0.0008
10	0.3926	S.W.I	1.557	17785	1.78	13150	0.0002	0.0002
15	0.8835	S.W.I	2.658	27491	1.83	13150	0.0000	0.0002
20	1.5707	S.W.I	3.886	38374	1.92	13150	0.0000	0.0004

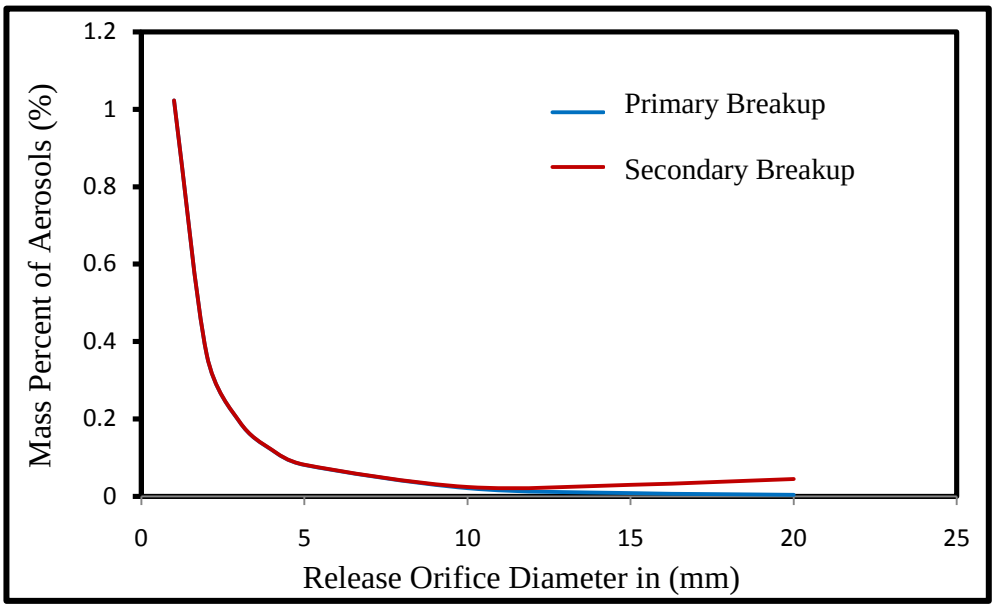

Figure 8.4 The effect of increasing release orifice diameter on the percentage of aerosols after the primary breakup and the secondary breakup at 5 m/s release velocity

8.2.2 Effect on droplets disintegration during free fall.

During free-falling, liquid droplets will be potentially exposed to mass and velocity changes. The extent of these changes is dependent on the size distribution resulted from the primary stage.

As discussed before, changes in droplets mass during free falling may takes place through evaporation or droplets disintegration. The amount of vapour generated from each droplet depends on the droplet size and velocity. Therefore, the total amount of vapour generated from a certain liquid flow rate depends on the droplets size distribution. On the other hand, the presence of large falling droplets increase the number of droplets to disintegrate during free fall.

The results of mathematical model at the lower release velocity (5 m/s) are used to discuss this behaviour. The lower release velocity allows the presence of some large droplets in the free-falling stage. Consequently, further probability for droplets disintegration may takes place during this stage.

As discussed in section 8.2.1, the droplets size distribution resulting from the primary stage always has an upper limit. This upper limit could be described as the maximum stable diameter at the proposed liquid release velocity. During droplets free falling, some of these droplets may lose their stability during acceleration process.

In general, liquid droplets disintegration may take place during free falling if likely breakable droplets exist at the beginning of free-falling stage. The likely breakable

droplets could be the droplets which have a critical velocity, V_{crit}, lower than their terminal settling velocity at the proposed conditions. Other droplets which have the critical velocity higher than the terminal one are not likely to disintegrate during free falling. Figure (8.5) plots the critical velocity and the terminal settling velocity against the droplet diameter. The droplet size of 4250 µm is found to be the minimum likely droplet size for breakup during free falling.

According to maximum droplets size after primary stage, which had been presented in table 8.2, droplets formed from all orifice diameters except the 1mm diameter are potentially undergoing disintegration during free fall. Figure 8.6 shows the percentage of aerosol droplets at each meter of falling distance.

The percentage of aerosol during free-falling stage remained almost constant for orifice diameters smaller than 4mm. yet orifice diameters greater than 5mm, Constant percentage of aerosol increases with falling distance. For orifice diameters greater than 10mm, the aerosol formed during free-falling increases sharply. For example, at 4 meters falling distance the amount of liquid aerosol droplets generated from 10 mm orifice diameter is 8 times higher than the aerosol formed in the primary stage.

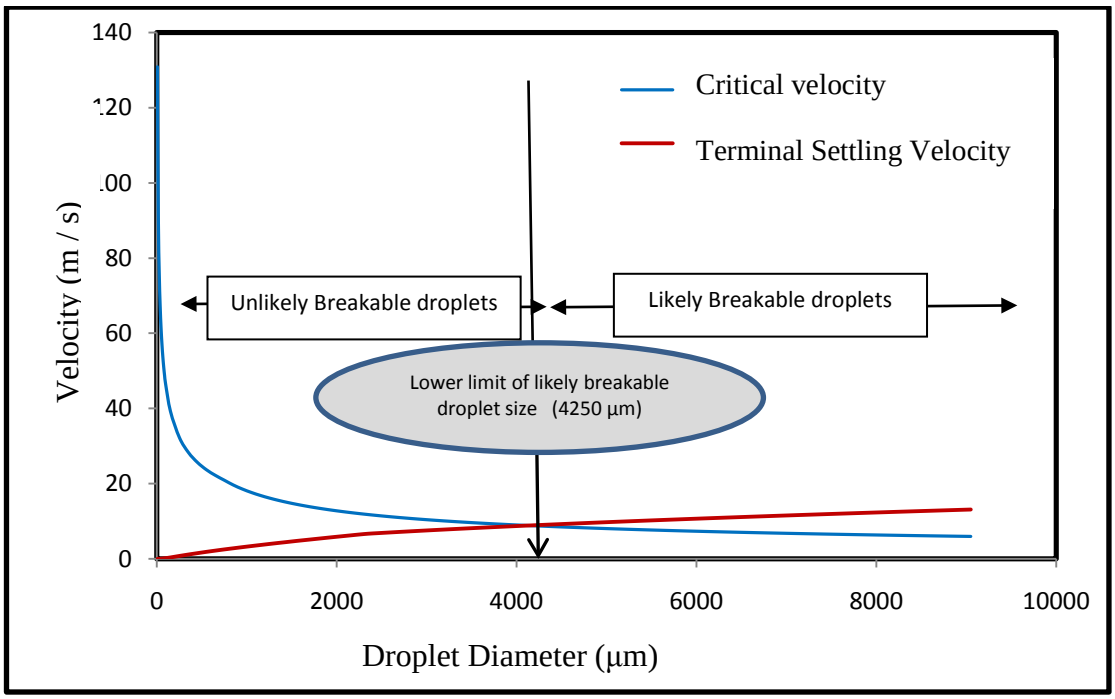

Figure 8.5 Critical and terminal velocity for Ethanol droplets at 20°C and saturated media of fuel and water vapours

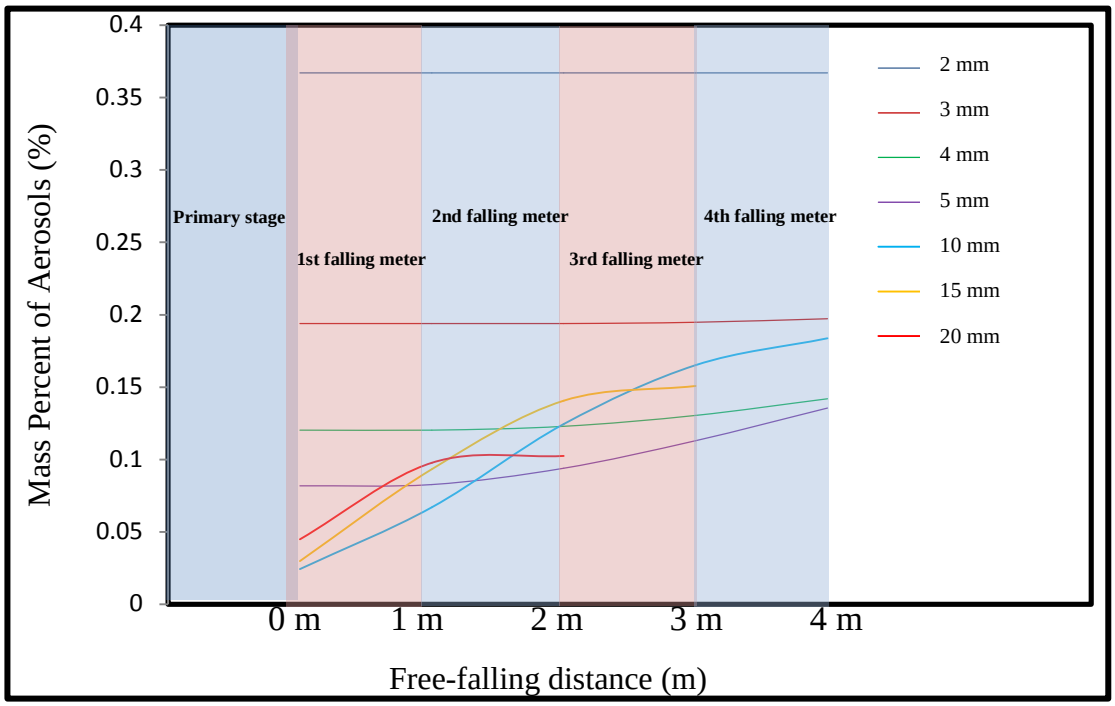

Figure 8.6 Development of aerosol quantity during free fall for each orifice diameter

The difference between free-falling distances is due to the difference between breakup lengths at the different orifice diameters. This means, as the breakup length increases, the remaining distance for the droplets free-falling decreases.

8.2.3 Effect on Splashing process

At the end of free-falling stage, a certain droplets distribution will reach the ground. Larger falling droplets reaching the ground are most likely expected to splash, where aerosol and relatively smaller droplets are expected to just spread on the surface. According to this fact, the estimated amount of aerosol droplets after impingement does not contain the falling aerosol droplets which have very small impact energy and absolutely expected to spread rather than splash. Droplets of high impact energy are nominated for splashing. Splash parameters results showed that 650µm is the minimum droplet size to splash (K >58). Figure 8.7 shows the relationship between release orifice diameter and the maximum aerosol percentage after splash.

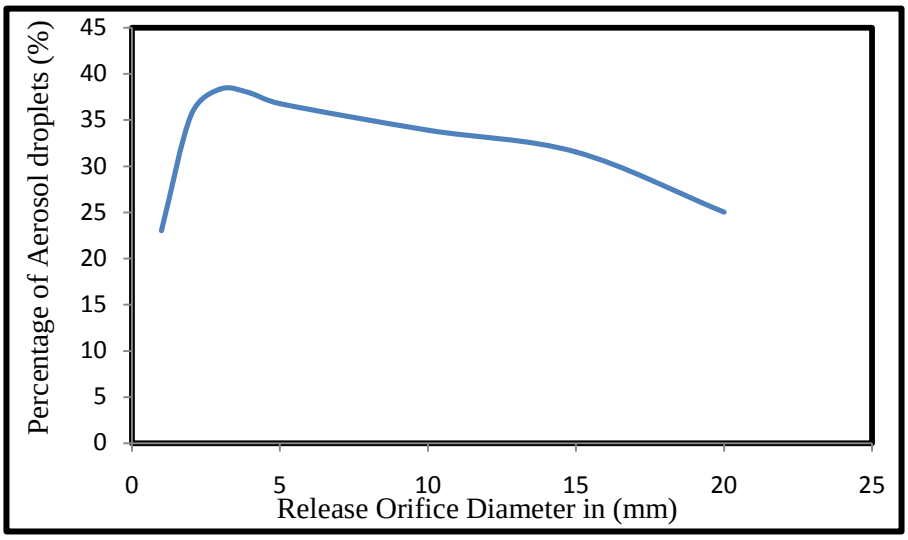

Figure 8.7 Relation between release orifice diameter and percentage of aerosol droplets generated after splashing

Figure 8.7 show that aerosol percentage has a maximum value at nearly 3 mm orifice diameter. The amount of fine droplets might be generated form splashing of larger droplets is dependent on both impinging droplet size and velocity. In general, smaller impinging droplet size tends to give smaller droplets average size after splash. Likewise, faster impinging droplets are likely to generate smaller splash droplets than slower ones. Figures (8.8) and (8.9) express an example on the effect of mother droplet velocity and diameter on median diameter of daughter droplets. The slope of decrease for the daughter mean diameter is higher between 1 to 3 m/s impinging velocity, and then decreased after velocity of 3 m/s. whereas the relation between mother droplet diameter and daughter droplet mean diameter is nearly straight.

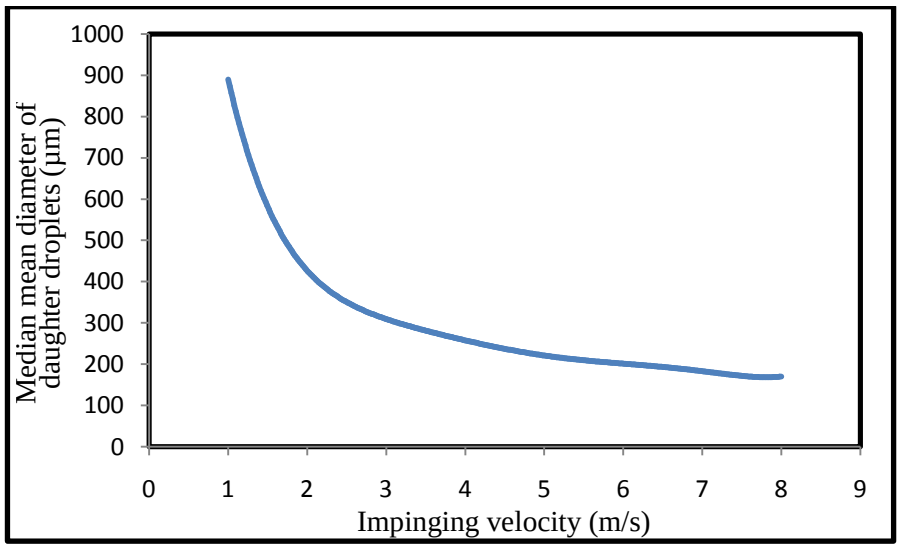

Figure 8.8 Effect of 4050 µm mother droplet velocity on the median diameter of daughter droplets

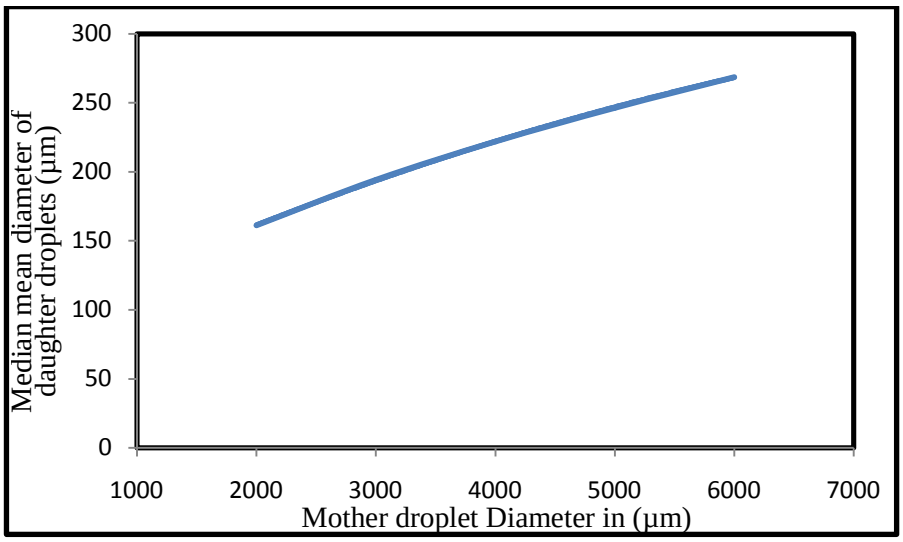

Figure 8.9Effect of 5 m/s splashed mother droplet diameter on the median diameter of daughter droplets

Figures 8.10 express the droplet size distribution just before impinging for the different nozzle diameter cases. The droplet size distribution before impingement is very important parameter. In general, the average droplets diameter generated from smaller nozzle diameter is expected to be smaller. As discusses above, larger droplets may disintegrate during free falling to reach minimum diameter value of (4250µm). As a result of this scenario, droplets size distribution resulting from small orifice diameters will remain with no changes during free falling with small mean diameter value. Large droplets generated from larger orifice diameters will disappear step by step during free falling and thus distribution gets closer and closer but never gets closer with small orifices which are already below the critical value of 4250µm.

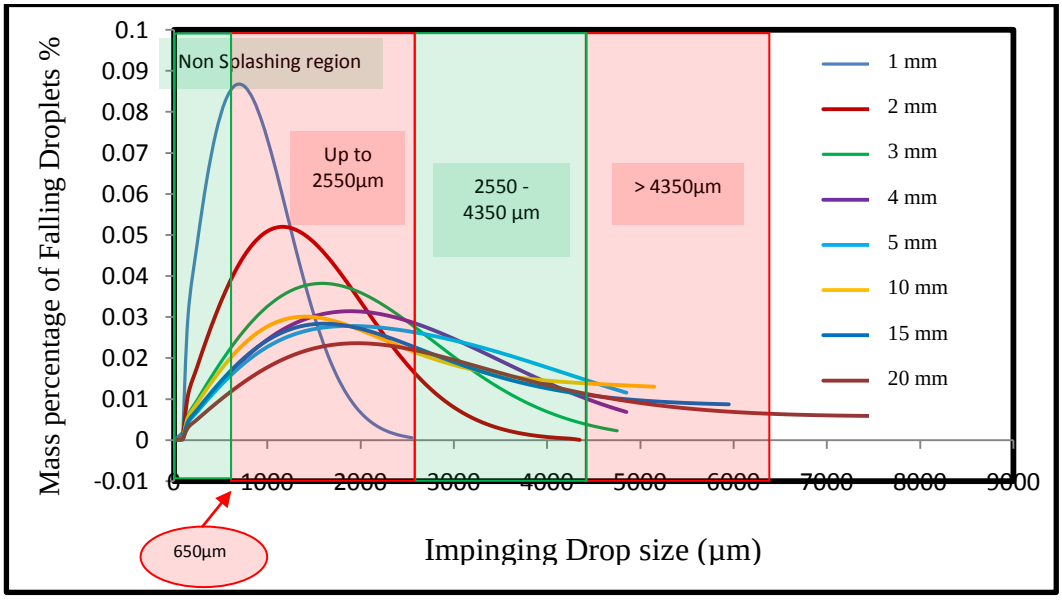

Figure 8.10 Droplets size distribution just before impinging at different nozzle diameters ranging from (1-20 mm)

To explain the relation between release orifice diameter and percentage of aerosol droplets generated after splashing in fig (8.7), droplets sizes will be classified into four different regions, as shown in fig. (8.10):

1- The first region: droplets diameters up to 550µm, which are fairly small and not expected to disintegrate when impinged.

2- The second region: droplets diameters from 650 - 2550µm, which is the smallest splashing droplets and the largest droplets size generated from 1 mm nozzle diameter. This region of mother droplets is expected to generate the largest fraction of aerosol droplets.

3- The third region: droplets diameters from 2650 - 4350µm, which is the non-fragmented medium splashing droplets and the largest droplets size generated from 2 mm nozzle diameter. This region of mother droplets is also expected to generate good fraction of aerosol droplets.

4- The fourth region: droplets diameters larger than 4350µm, which are expected to generate relatively very small fraction of aerosol droplets when splashed.

The cumulative droplet size percentage for each region at the different nozzle diameters are plotted in Figure 8.11. The first region values show that 30% of droplets falling from 1 mm nozzle will not splash. This value will decrease to about 12% at 2mm nozzle, then at 3.5mm it will reduce to 6.9% for the rest of nozzles. This might be the first explanation for why the percentage of aerosol splash increases while nozzle diameter increases to 3mm as the percentage of splashing droplets increases. When nozzle diameter increases again, the percentage of region (2) droplets starts to decrease substituted with larger droplets from region (3) and also region (4) which are scarcer in the production of aerosol droplets. This could explain the decrease of aerosol percentage from about 38% at nozzle diameter of 3mm to about 25% at nozzle diameter of 20mm.

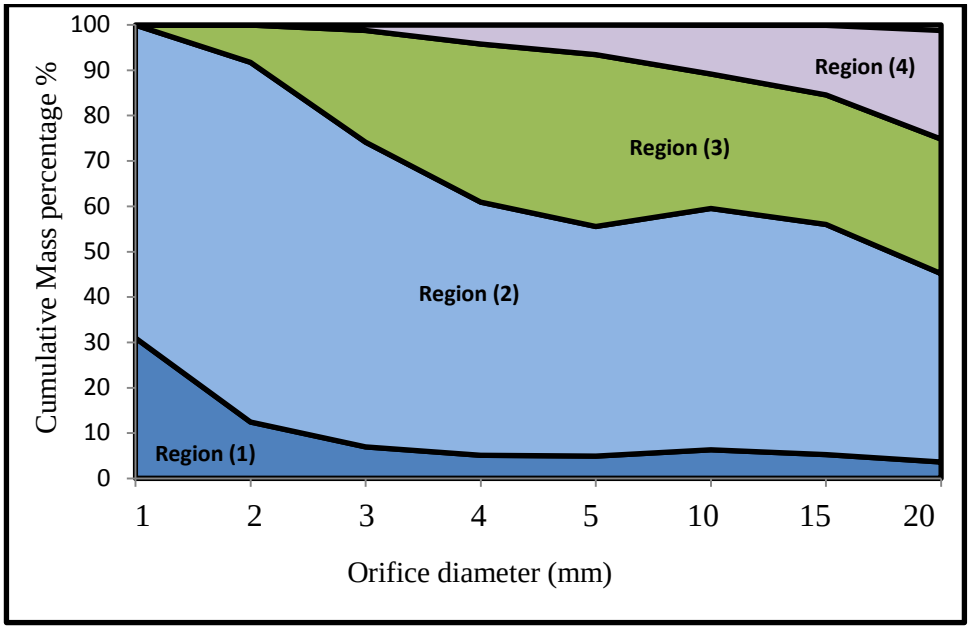

Figure 8.11 Cumulative percentage of impinging droplets regions generated from different orifice diameter

8.2.4 The Effect on Vapour Generation

Figure (8.12) expresses the effect of changing orifice diameter on the amount of vapour generation from both the falling liquid droplets and the aerosols generated from splashing process. It is clear that the amount of vaporised liquid was sharply decreased when the orifice diameter increased from 1mm to 3mm. The decrease has continued but with a lower rate when the orifice diameter increased from 3mm to 20mm.

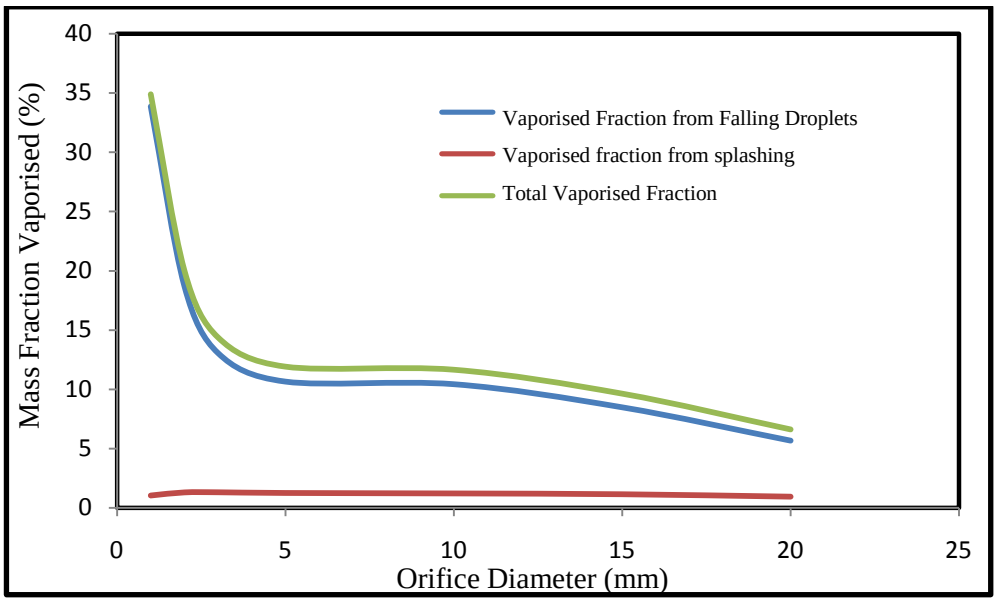

Figure 8.12 The effect of orifice diameter on evaporation

8.3 The effect of Release Velocity

Changes in velocity of droplets after formation is mainly dependent on the initial jet release velocity. At relatively high release velocities, it could be found that a wide range of formed droplets will undergo deceleration after primary stage. This happened because release velocity is already above the terminal settling velocity of many droplet sizes. On the other hand, if release velocity is relatively low, the existence of liquid droplets which tents to accelerate is much higher. A wide range of falling liquid droplets will accelerate to approach their terminal settling velocity.

8.3.1 Release velocity on primary and secondary breakup

Release velocity is a dominating factor which affects the mechanism of liquid jet disintegration. All the disintegration factors of liquid jet and formed droplets are directly dependant on velocity. Therefore, it will subsequently play role in determining the jet disintegration regime, breakup length and size range of formed droplets. Table (8.3) summarizes the parameters of primary stage for 8 different release velocities ranging from 1-30m/s. The other release and ambient conditions are summarized as liquid ethanol releases from 20mm nozzle diameter, 20^{o}C liquid and ambient temperature, and fully saturated air with Ethanol vapour and water vapour. Fig (8.13) presents the droplet size distribution after the primary breakup of liquid jet. Figure (8.14) presents the droplet size distribution after secondary droplets breakup at release velocity ranging from 1 to 10m/s, and Figure (8.15) presents the droplet size distribution after secondary droplets breakup at release velocity ranging from 10 to 30m/s.

Table 8.3 Parameters of the primary stage of ethanol releasing at 1-30 m/s from 20mm orifice diameter and saturated conditions at 20^{o}C

Release Velocity (m/s)	Volumetric flow rate (L/s)	Breakup regime	Breakup length (m)	D_{max} (µm) after jet breakup	D_{max} / $D_{Orifice}$	D_{max} (µm) after drop breakup	Aerosol Fraction after primary breakup	Aerosol Fraction after secondary breakup
1	0.314	F.W.I	1.39	64722	3.24	64750	1.65×10^{-5}	1.65×10^{-5}
2	0.628	F.W.I	2.16	48254	2.41	48250	2.97×10^{-5}	2.97×10^{-5}
3	0.942	F.W.I	2.80	42531	2.13	36550	3.82×10^{-5}	3.95×10^{-5}
4	1.256	S.W.I	3.37	39819	1.99	20550	4.36×10^{-5}	1.27×10^{-4}
5	1.571	S.W.I	3.88	38374	1.92	13150	4.69×10^{-5}	4.48×10^{-4}
10	3.142	ATOM	0	36960	1.85	3250	5.06×10^{-5}	3.71×10^{-3}
15	4.712	ATOM	0	37965	1.90	1450	4.79×10^{-5}	1.42×10^{-2}
20	6.283	ATOM	0	39397	1.96	750	4.45×10^{-5}	4.15×10^{-2}
25	7.854	ATOM	0	40896	2.04	450	4.13×10^{-5}	8.91×10^{-2}
30	9.425	ATOM	0	42366	2.12	250	3.85×10^{-5}	1.91×10^{-2}

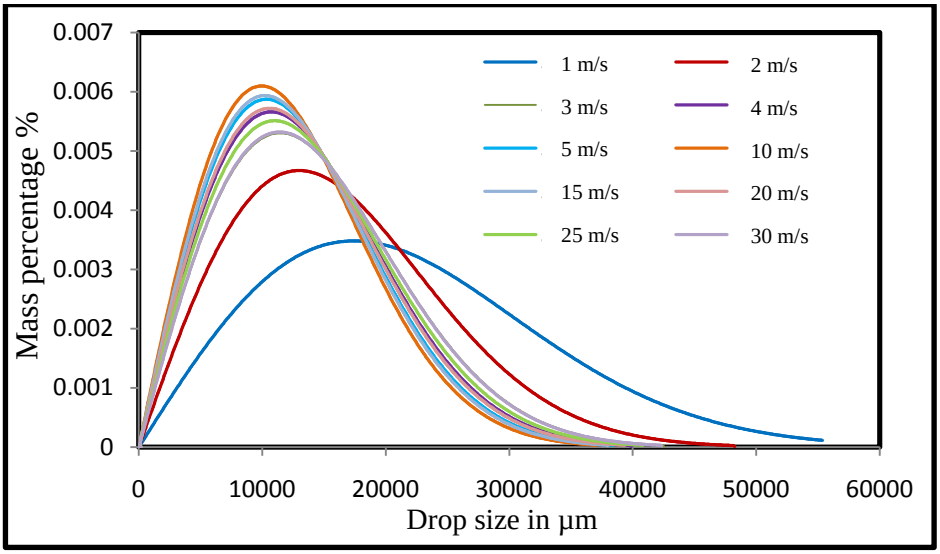

Figure 8.13 Droplet size distribution after jet primary breakup of Ethanol liquid fuel at release velocity = 1-30 m/s

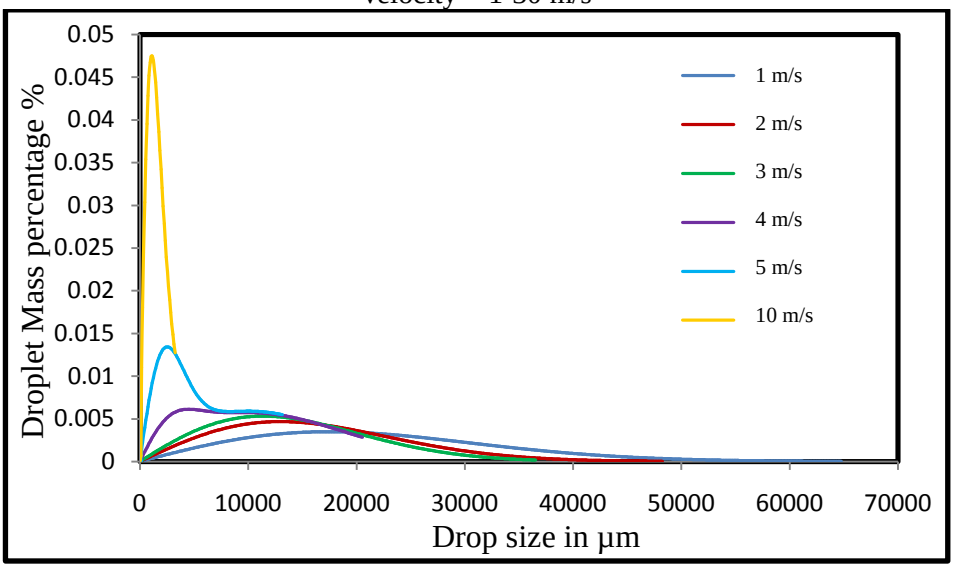

Figure 8.14 Droplet size distribution after secondary breakup of Ethanol liquid fuel at release velocity = 1-10 m/s

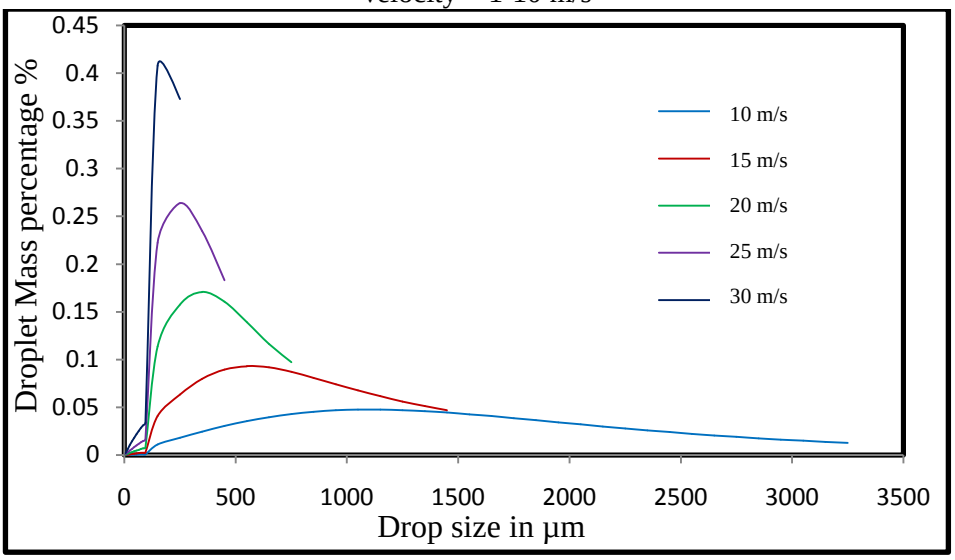

Figure 8.15Droplet size distribution after secondary breakup of Ethanol liquid fuel at release velocity = 10-30 m/s

An overview of the results of table 8.3 shows that the values of maximum droplet diameter after primary disintegration have a minimum value at release velocity of 10m/s. The value of maximum droplet diameter decreased by 43% (from 64722µm to 36960µm) when release velocity increased from 1 to 10m/s, then it increased by about 15% (from 36960µm to 42366µm) when the velocity increase from 10 to 30m/s. This could be understood from the balance between Weber and Reynolds number in Equation (5.22). Where both dimensionless numbers increased in Numerator and denominator, a Point coup will be formed giving a minimum peak value. This value is dependent on the value of nozzle diameter. For similar example conditions and nozzle diameter of 50mm, the minimum peak value appeared at 4m/s release velocity. Whereas at 10mm the value appeared at 18m/s. Figure 8.13 shows that the variation in droplet size distribution after primary breakup when release velocity increased from 1 to 30m/s is not too high.

The values of maximum droplets diameter after secondary disintegration are so different and complete inversely proportional with release velocity. This is mainly depends on the critical velocity of liquid droplets. At 20 m/s release velocity, the maximum droplet size is about 750µm at the proposed conditions, 450µm at 25m/s and 250µm at 30 m/s. At these high velocities, most of the droplets will be classified as aerosol droplets. Results of table 8.3 express that more than 19% of the droplets generated from primary stage at 30m/s release velocity are assumed to be an aerosol, about 8.9% at 25m/s and 4.1% at 20m/s. The value of breakup length increases by increasing release velocity until the disintegration regime transfers into Atomization. Fig (8.14) and (8.15) illustrate the changes in droplet size distribution after secondary breakup due to release velocity increase.

8.3.2 Release velocity on free-falling stage

The change in aerosol mass percentage during free fall, Figure 8.16, shows a convergence between the results for velocities before impingement from 1 to 5 m/s. The differences in aerosol quantity appeared after primary stage as an effect of different release velocities started to disappear from the first falling meter as a consequence of falling disintegration. At higher velocities (starting from 10 m/s), no development during free falling occurs because all the falling droplets are small enough to retain their size along the falling path. In general, the percentage of aerosol droplets at low velocities is found to be around 0.1%, which is insignificant as a source of aerosol but it may still able to accumulate if ambient conditions is suitable for that. The aerosol

percentage generated at release velocities from 10 m/s and above becomes significant and maybe a good source of airborne aerosol. Another look for the relatively high velocity cases shows that no developments in aerosol percentage during free fall. That can be explained by the fact that all the generated droplets are small enough and not expected to disintegrate during acceleration.

Based on the data mentioned, there is a critical droplet diameter for each release conditions and release liquid. This diameter is the lower limit of likely breakable falling droplets. If release velocity is higher than critical velocity of the critical droplet diameter, no development is expected for the falling droplet unless by evaporation.

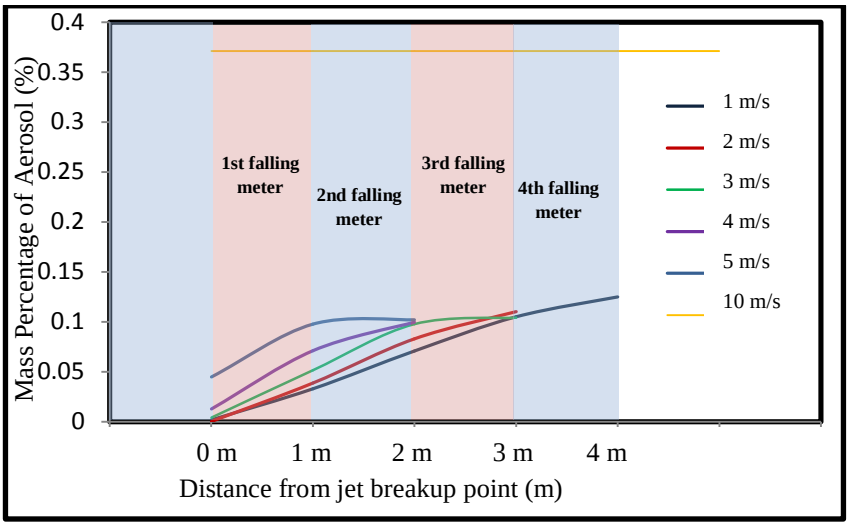

Figure 8.16Development of aerosol quantity during free fall for each release velocity

8.3.3 Release velocity on impingement

Figure (8.17) demonstrates the percentage of aerosol droplets generated after splashing at the different release velocities. The relation between aerosol percentage and release velocity is clear to be non-linear. In details, aerosol percentage decreased by increasing release velocity from 1 to 4 m/s. the behaviour after that changed to increasing until velocity reached 10 m/s. after that, it started to decrease again and finally to percentage at all for the velocities starting from 25 m/s and above.

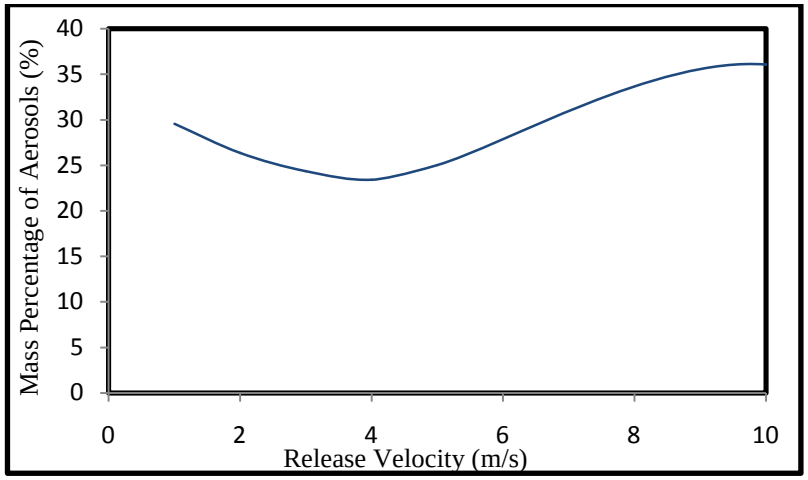

Figure 8.17Relation between release velocity and percentage of aerosol droplets generated after splashing

To investigate the irregular behaviour of aerosol generation after splash, quantitative classification for falling droplets just before impinging is performed in figure (8.19) and falling velocity comparison curve is implemented in figure (8.20). Falling droplets will be classified into four classes:

1- The first region: droplets diameters up to 550µm, which are fairly small and not expected to disintegrate when impinged.

2- The second region: droplets diameters from 650 to 1450 µm, which is the smallest splashing droplets region and the largest droplets size impinged at release velocity of 15 m/s. This region of mother droplets is expected to generate the largest fraction of aerosol droplets.

3- The third region: droplets diameters from 1550 to 3250 µm, which is the largest droplets size impinged at release velocity of 10 m/s. This region of mother droplets is also expected to generate good fraction of aerosol droplets.

4- The fourth region: droplets diameters larger than 3250 µm, which are expected to generate relatively the smallest fraction of aerosol droplets when splashed.

The analysis of data reveal that during increasing release velocity from 1 to 4 m/s, limited decrease for the percentage of region (1), (2) and (3) droplets occurs. In contrast, region (4) shows a slight increase of droplets percentage instead of the expected decrease. Furthermore, Figure 8.19 shows a bit velocity decrease from the same impinging droplets size when release velocity increases. This happened because the falling distance in decreased (Table 8.3). These changes result as the little decrease in percentage of aerosol after splashing. When velocity increased from 4 to 10 m/s, the fine droplets percentage of region (1) becomes relatively higher and reaches about 12%

instead of being around 4%. On the other hand, a palpable percentage increment occurs from 15% to 40% for region (2) t and from 38% to 46% for region (3) which is also a good source for aerosol droplets. In addition, an obvious droplets velocity increase takes place for region (3) droplets. These clear changes will lead to obvious increase in aerosol percentage from 23% to 36%. Above the velocity of 10 m/s, the percentage of non-splashing droplets will dramatically increase. The value of region (1) droplets percentage will reach 38% at 15 m/s, 78.3% at 20 m/s and about 100% for 25 and 30 m/s. this will absolutely scale down the percentage of aerosol droplets generated after splash.

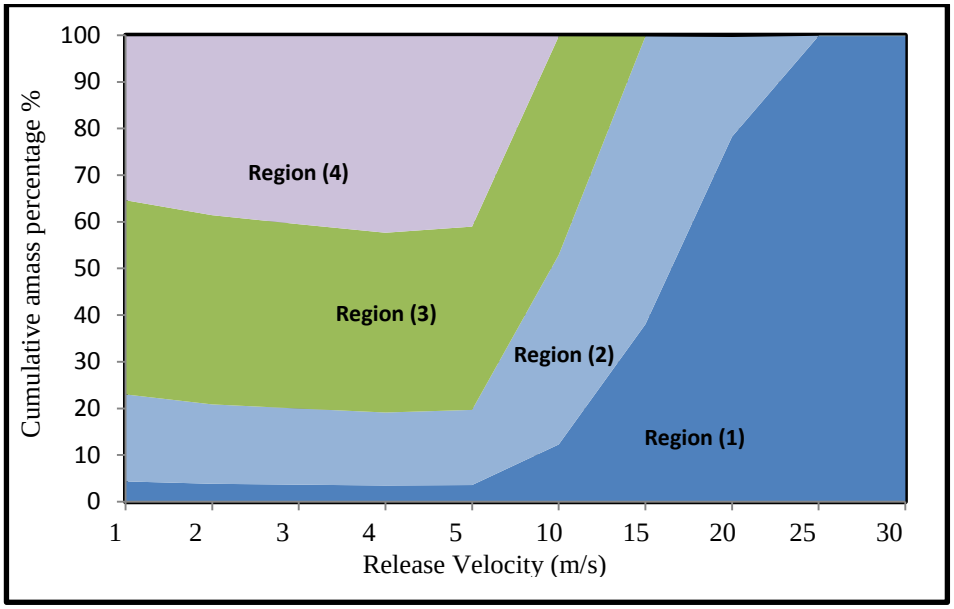

Figure 8.18 Cumulative percentage of impinging droplets regions generated from different release velocities

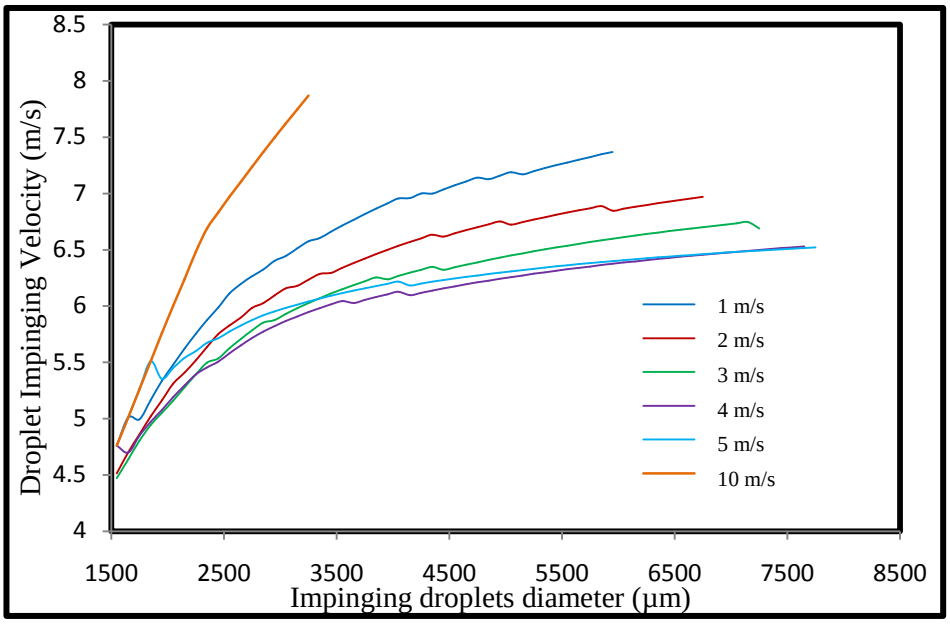

Figure 8.19Impinging velocities for the droplet sizes larger than 1500 µm at different release velocities from (1-10 m/s)

8.3.4 The effect of Release velocity on Vapour Generation

Figure (8.20) expresses the relation between release velocity and the amount of vaporised liquid from both the falling liquid droplets and the aerosol droplets formed in splashing process. It is clear that the liquid vaporised fraction decreased when the velocity increased from 1m/s to 6 m/s. Then, it started to increase afterwards when velocity increased from 6m/s to 20 m/s.

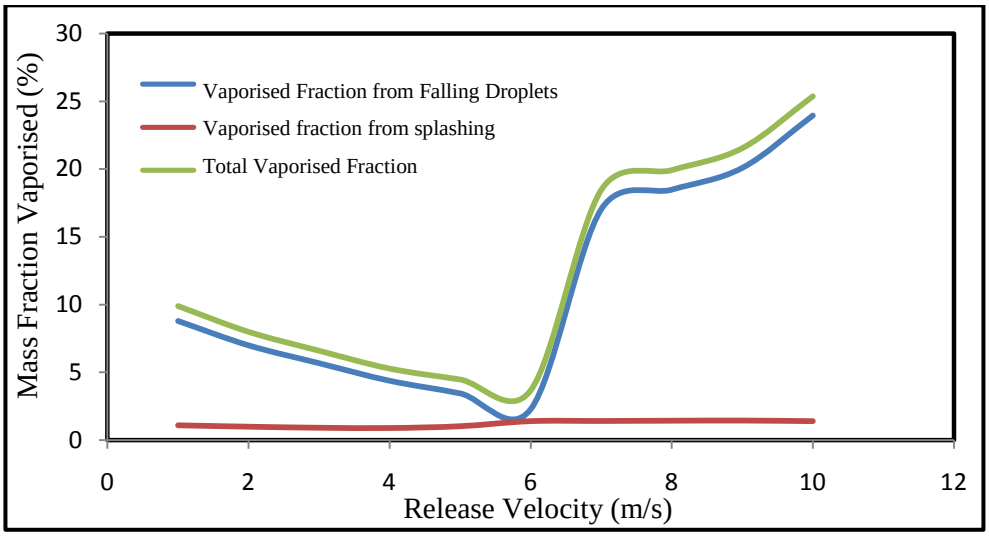

Figure 8.20 The effect of Release Velocity on the Fraction of Vaporised Liquid

8.4 The Effect of Release Height

Release height is the distance at which falling droplets mass and velocity changes take place. Based on the definition, increasing release height is expected to allow more opportunity for more changes. These changes could be summarized as follows:

1- Droplets acceleration or deceleration to reach their terminal settling velocity, unless release velocity is very close to droplet settling velocity.

2- Droplets disintegration when they reach critical velocity, this disintegration can be applied to the most likely breakable droplets which are characterised by critical velocity lower than terminal velocity.

3- Droplets evaporation.

8.4.1 Effect of height on free-falling

The changes that occurred in droplet velocities and droplet sizes (due to disintegration) during free-falling stage are highly dependent on the initial droplet velocities which are already gained after the primary stage. It is necessary to consider

how the size of the developed droplet distribution at 8 meters of free falling may be affected when it is compared at four different release velocities ranging from 2 m/s to 8 m/s (Figures (8.19) to (8.22)). The analysis of this comparison will determine the degree of the changes that could develop throughout the falling distance. Additionally, it will emphasis the role of initial velocity at this stage.

The results show that, as release velocity decreases, the particle size distribution development during free-falling becomes more and more significant. At the highest velocity of 8 m/s, distribution throughout the falling distance seems to be identical, therefore development supposed to be negligible. At 2 m/s release velocity, the upper limit of droplet sizes after primary stage was reaching about 48 mm diameter, then suddenly dropped to about 14 mm after the first falling meter. While droplets falling continued, more and more droplets started to accept velocity by acceleration and more disintegration took place. The upper droplet diameter was about 8.45 mm at the end of second falling meter, 6.45mm at third and gradually reached 4.45 mm at the end of eight falling meter. Falling droplets became stable at the end of ninth meter and the upper size was 4150 µm, which is the upper size of unlikely breakable droplets under the proposed conditions. In addition, falling droplets larger than 3.75 mm did not reach their terminal velocity even after 10 meters of free-falling. At higher release velocity of 4 m/s, initial value of upper droplets diameter after primary stage was reduced to 20.55 mm. This means, some of the droplet sizes which were disintegrated during falling at the lower velocity is now absent. All droplets became stable at the ninth meter of falling, but the amount of disintegration was less. Most of the droplets reached their terminal settling velocity by the end of eight meter. At 8 m/s release velocity, the results were completely different. Droplets resulted for primary stage was bounded by 5.15 mm diameter size. The remaining likely breakable droplets were completely disintegrated by the end of second falling meter, and all the falling droplets reached their terminal settling velocity by the end of third falling meter.

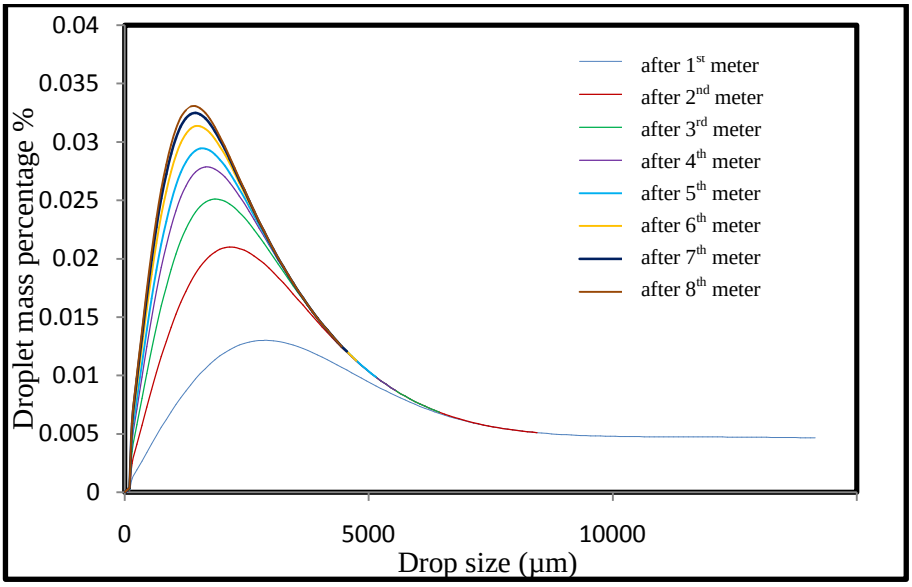

Figure 8.21 Droplet size distribution during 8 meters free falling for Ethanol liquid fuel releasing from 20 mm orifice at release velocity of 2 m/s

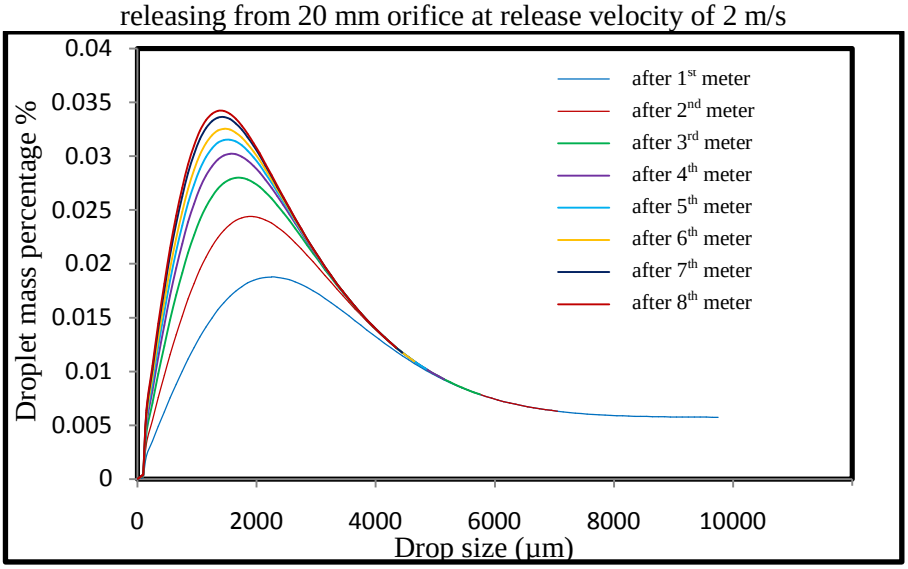

Figure 8.22 Droplet size distribution at 8 meters free falling for Ethanol liquid fuel releasing from 20 mm orifice at release velocity of 4 m/s

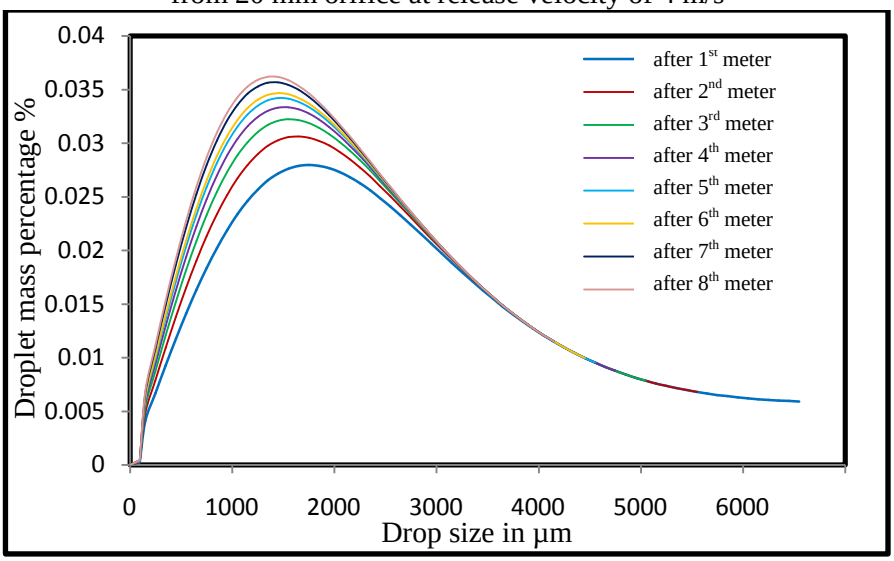

Figure 8.23 Droplet size distribution at 8 meters free falling for Ethanol liquid fuel releasing from 20 mm orifice at release velocity of 6 m/s

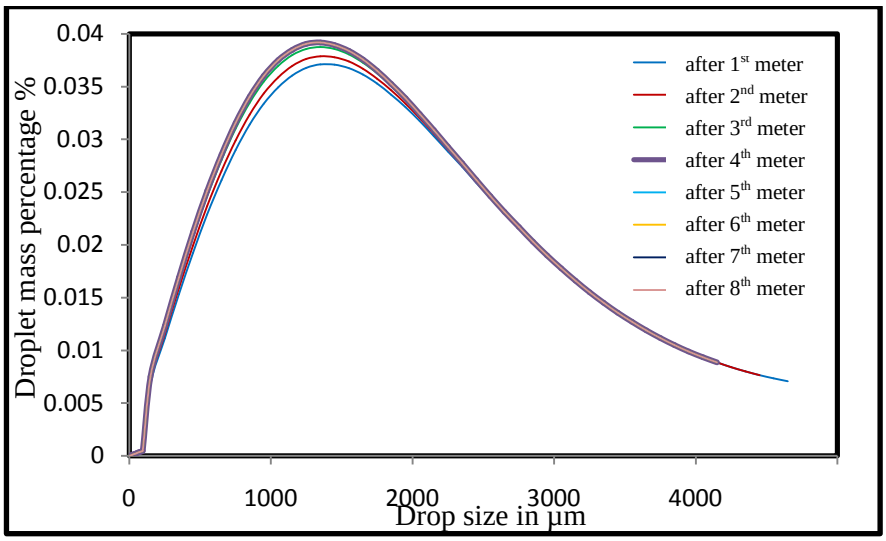

Figure 8.24 Droplet size distribution at 8 meters free falling for Ethanol liquid fuel releasing from 20 mm orifice at release velocity of 8 m/s

Figure 8.23 expresses the development of aerosol droplet percentage during free falling at different release velocities. The comparison shows that falling distance allows some increase in aerosol percentage according to larger droplets disintegration. At thelower release velocities, this increase is tangible compared to that at the higher velocities. At the end, aerosol droplets percentage becomes very close regardless of differences in release velocity. This means, aerosol generation during free fall at the lower release velocities may compensate the shortage in percentage after primary stage.

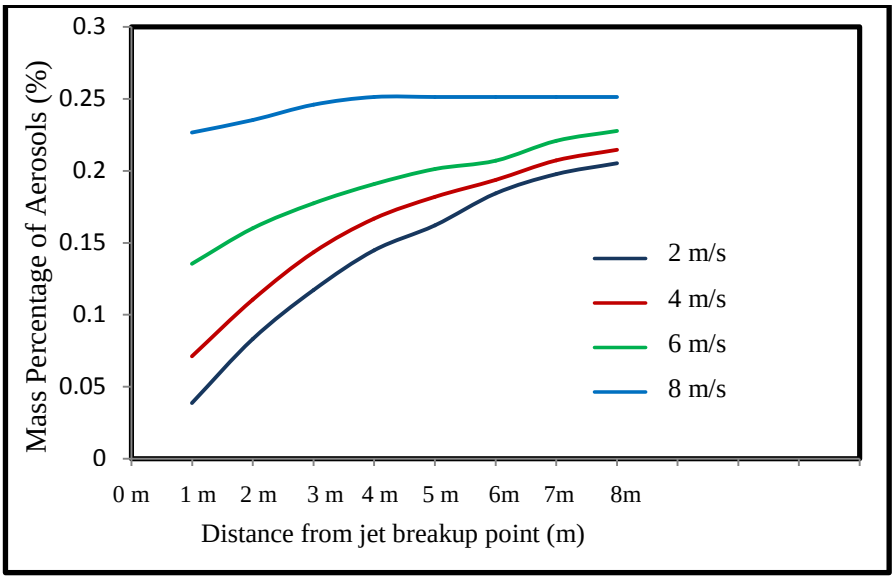

Figure 8.25 Development of aerosol quantity during 8 meters free falling at 2, 4, 6 and 8 m/s release velocities

8.4.2 Effect of height on impingement

Regarding the aerosol generation after impingement, Figure (8.25) expresses the effect of falling distance on the quality of aerosol formation after splash. At low release velocities (2 and 4 m/s), if droplets impingement takes place after a short distance from formation, the amount of splashed aerosol droplets will be very small because the droplets impact energy are still small. If the splash takes place after a distance of falling, a certain development in aerosol quantity arises according to droplets velocity enhancement. At the higher release velocity (6 m/s), the behaviour of aerosol generation after splash is different. Some of the droplets released at velocity higher than terminal velocity. Hence, it will undergo deceleration during free fall. Some other larger droplets will accelerate while their terminal velocity is relatively high. In this case, if impingement takes place directly after formation, aerosol generation will be a bit higher because of the high velocity of small droplets. After a distance, splashing will generate slightly smaller amount of aerosol according to small droplets deceleration. While droplets continue falling, larger droplets acceleration will take place. And this will increase the percentage of aerosol droplets generation. At 8 m/s velocity, the behaviour is absolutely clearer. At the beginning, all droplets velocity will be high even small ones. If splashing happened at that time, a large percentage of aerosol generation will be expected. Thereafter, most of the droplets (about 92%) will undergo deceleration within a short distance. hence, aerosol generation after splash will be reduced.

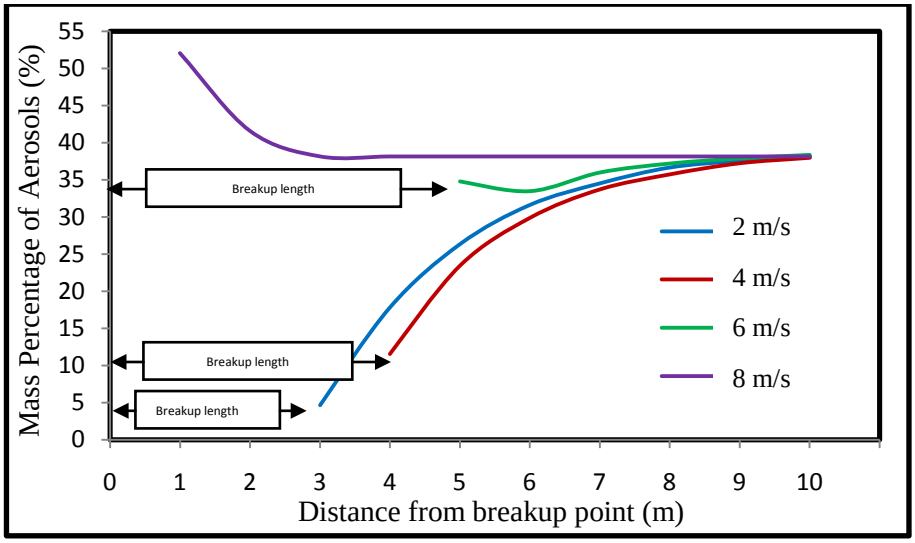

Figure 8.26 Effect of release height and percentage of aerosol droplets generated after splashing

8.4.3 The Effect of Release Height of Vapour Generation

Figure (8.27) plots the realtion between the falling distance and the amount of vaporised liquid during the free-fall of liquid droplets and vaporisation or splashed droplets. It is clear that the vaporised fraction of liquid is directly proportional with the release height.

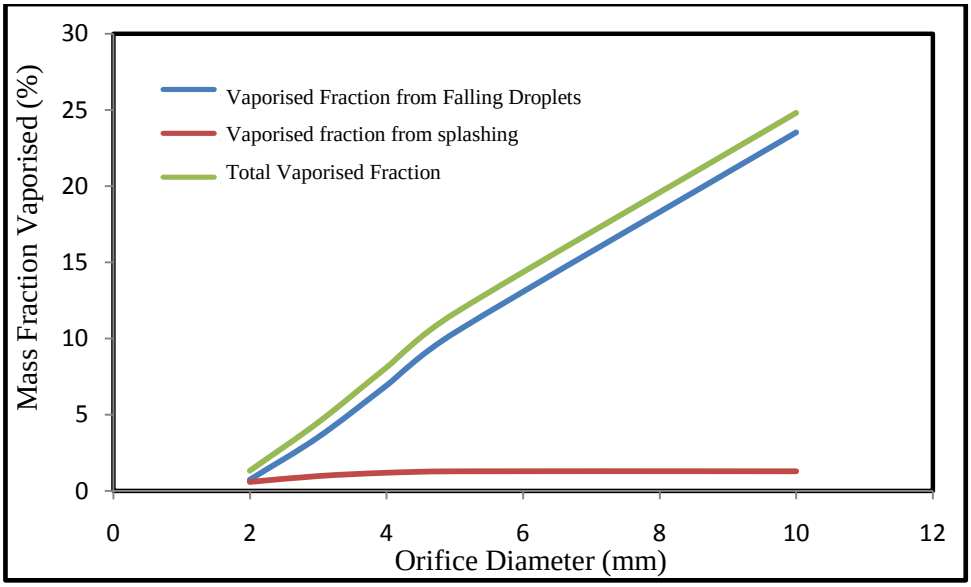

Figure 8.27 The effect of Falling Height of Vaporised Fraction

8.5 Summary

1- Effect of release orifice diameter:

- The maximum drop size generated from liquid jet disintegration is directly proportional to the orifice diameter. While the ratio the maximum diameter and orifice diameter ($D_{0.999}/d_{or}$) has a minimum value at an orifice diameter of about 4-5mm.
- At the end of primary stage, the resulting droplets have an upper diameter which depends on release velocity rather than orifice diameter.
- Increasing the orifice diameter decreases the percentage of aerosol droplet generated after the primary stage. However, the fraction of aerosol droplets generated during the primary stage and the free-fall stage were usually less than 0.02%.

- The mass percentage of the aerosols resulted from splashing is not linearly related with the orifice diameter. The peak value was obtained at 3mm orifice diameter.
- The amount of vaporised liquid was found to be inversely proportional to the orifice diameter. A sharp decrease was noted when orifice diameter increased from 1mm to 3mm. This decrease became less severe when the orifice diameter increased from 3mm to 20mm.

2- The effect of liquid release velocity on the liquid release process:

- The release velocity had a remarkable effect on the breakup mechanism of liquids droplets especially at velocity higher than 6 m/s. However, increasing the release velocity caused a decrease in the maximum droplet size after the primary stage.
- Changing the release velocity had a limited effect on the fraction of aerosols generated from droplets impinging.
- The total amount of vaporised liquid was decreased when the velocity increased from 1m/s to 6m/s and started to increase afterward.

3- The effect of falling height on the liquid release process:

- Increasing the release height gave a higher opportunity for the droplets to accelerate approaching their terminal velocities.
- Increasing the falling height increased the probability of droplet disintegration during free-fall. This is more likely to take place at low release velocity.
- The amount of aerosol generated from splashing increased upon increasing the falling height. This observation attributed to increasing the velocity of the falling droplets.

Chapter 9: The Effect of Liquid Properties on Droplet Size Distribution and Vapour Generation

9.1 Introduction

In this chapter, the physical properties of released liquid will be discussed in details. These properties will include viscosity, surface tension, density, molecular weight and saturated vapour pressure. It's clearly expected that these properties will have an influential effect on the mechanism and output characteristics of liquid disintegration during all promising stages of liquid release. In order to focus the discussion on each property separately, the discussed parameters was hypothetically varied. Table (9.1) express the hypothetical fuel liquids. In this study, ethanol fuel liquid will be the reference liquid to compare with. Therefore, all hypothetical fuel liquids have the same properties of ethanol except one property which is different.

Table 9.1 Properties of hypothetical fuel liquids

Liquid proposed name	hypothetical parameters	Property Value at 298.15K	Property Value for ***Ethanol*** at 298.15K	Deviation from ***Ethanol***
Composition A	Density of Water	1.00 (g/cm3)	0.7870 (g/cm3)	+ 27%
Composition B	Density of N-Hexane	0.6560 (g/cm3)		- 16.6%
Composition C	Molecular Weight of Water	18.02 (gm/mol)	46.069 (gm/mol)	- 60.9%
Composition D	Molecular Weight of Benzene	78.11 (gm/mol)		+ 69.6%
Composition E	Viscosity of Toluene	0.5269 (mPa.s)	1.0941 (mPa.s)	- 47.8%
Composition F	Viscosity of N-Hexane	0.1618 (mPa.s)		- 85.2%
Composition G	Surface Tension of Water	72.71 (dynes/cm)	21.99 (dynes/cm)	+330.7%
Composition H	Surface Tension of N-Pentane	15.47 (dynes/cm)		- 29.6%
Composition I	Saturated Vapour Pressure of N-Hexane	20433.4828 (Pa)	7989.5823 (Pa)	+ 255.7%
Composition J	Saturated Vapour Pressure of N-Pentane	69237.7596 (Pa)		+866.7%

9.2 The Effect of Liquid Viscosity

Liquid viscosity is one of the important physical properties affecting the behaviour during liquid release, and liquid droplets free-falling and impingement. On the other hand, liquid vapour viscosity, like the other properties of the liquid, controls the properties of continuous phase. In this section, two hypothetical liquids are proposed in order to investigate the effect of changing liquid viscosity on the overall mechanism of liquid disintegration during accidental release. Composition (F), composition (E) and the reference liquid (Ethanol) represent the low, medium and high liquid viscosity respectively. Table (9.2) expresses the primary stage breakup properties for the three different release liquids. As can be seen in this table, composition (F), composition (E) and Ethanol (the reference liquid) represent low, medium and high liquid viscosity respectively. Calculations had been performed at 20 mm orifice diameter, 6 m/s release velocity, saturated continuous phase of humidity and fuel liquid vapour and finally temperature of 20^{o}C.

Table 9.2 Primary stage breakup properties at different liquid viscosities

Release Liquid Type	Liquid viscosity (Pa.s)	Liquid Vapour Viscosity (Pa.s)	Air viscosity (Pa.s)	Breakup regime	Breakup length (m)	D_{max} (μm) after jet breakup	D_{max} / $D_{Orifice}$	D_{max} (μm) after drop breakup	Fraction of aerosol size droplets after jet breakup	Fraction of aerosol size droplets after drop breakup
COMP F	0.00031	$6.34x10^{-06}$	$1.71x10^{-05}$	SWI	4.37	98093	4.90	9150	$7.18x10^{-05}$	0.0026
COMP E	0.00058	$6.86x10^{-06}$	$1.72x10^{-05}$			60070	3.00		$1.91x10^{-05}$	0.0018
Ethanol	0.00118	$3.7x10^{-05}$	$1.93x10^{-05}$			37576	1.88		$4.89x10^{-05}$	0.00094

Based on data of primary breakup of liquid column, it is clear that increasing liquid viscosity decreased the value of maximum droplet diameter by increasing the value of liquid Reynolds number. On the other hand, the Weber number of continuous phase does not depend on viscosity. Because of that, no change occurred for breakup regime or breakup length. Figure (9.1) shows the droplet size distribution after primary jet breakup for the three different liquids viscosity. It revealed that the highest viscosity value (Ethanol) has the lowest MMD, D_{max} values, and hence the narrowest droplets distribution range. Furthermore, it can be noticed that the droplets distribution had

completely changed when the initially formed droplets start to interact with the continuous phase where the secondary droplets breakup takes place.

In Figure (9.2), liquids ranking according to droplets sizes and distribution width demonstrated in opposite trend for the three liquids with ethanol has the widest droplet range. Calculations of both terminal settling velocity and critical velocity of disintegration for all droplet sizes shows a very small variation for small droplets and no changes at all for large droplets. This is due to the value of both velocities does not depend on liquid or gas viscosities, except through the value of Drag coefficient value which is assumed to be constant at Newton's region. The value of critical velocity started to be constant regardless viscosity value at 750µm diameter. Whereas for terminal velocity the value was 2350µm. The only factor supposed to control the mechanism in this case is the value of daughter droplets Sauter mean diameter. This value is directly proportional with liquid viscosity value. Figure (9.3) illustrates the effect of changing liquid viscosity on Sauter mean diameter of daughter droplets. It was shown that SMD/D_{mother} increases with the increasing of liquid viscosity, and slope of the relation is higher at lower velocity. Therefore, at lower viscosity liquids, droplets resulting for disintegration are generally smaller, and this explains why the distribution reflects after secondary droplet breakup.

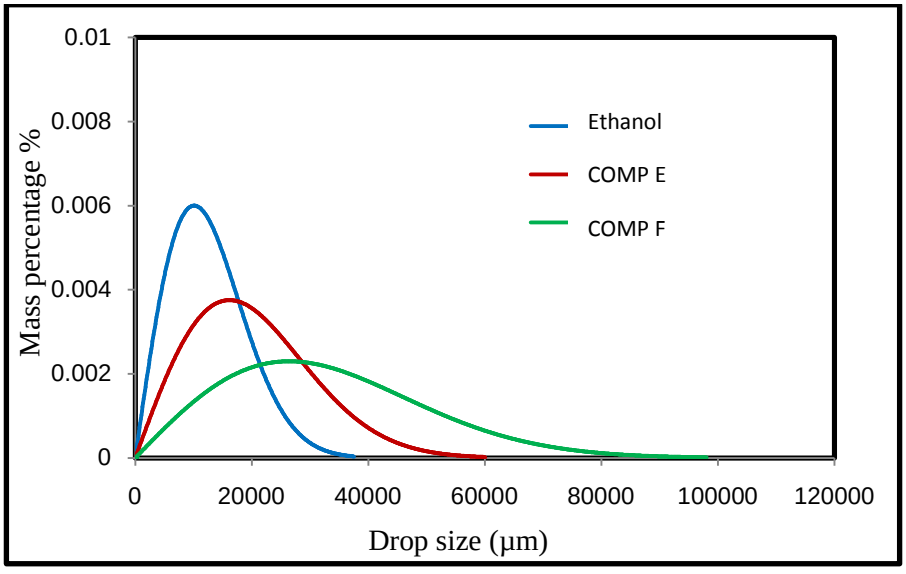

Figure 9.1 Droplet size distribution after primary jet breakup for liquids with different viscosities

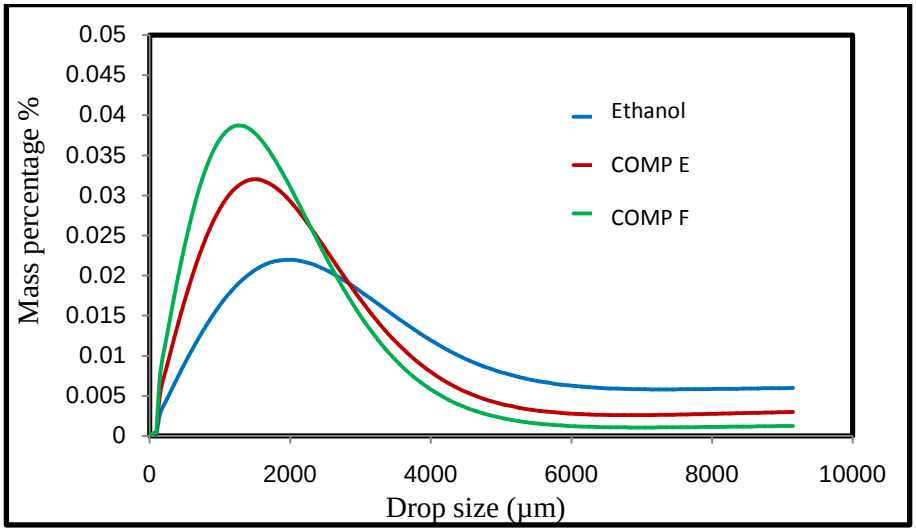

Figure 9.2 Droplet size distribution after secondary drops breakup for liquids with different viscosities

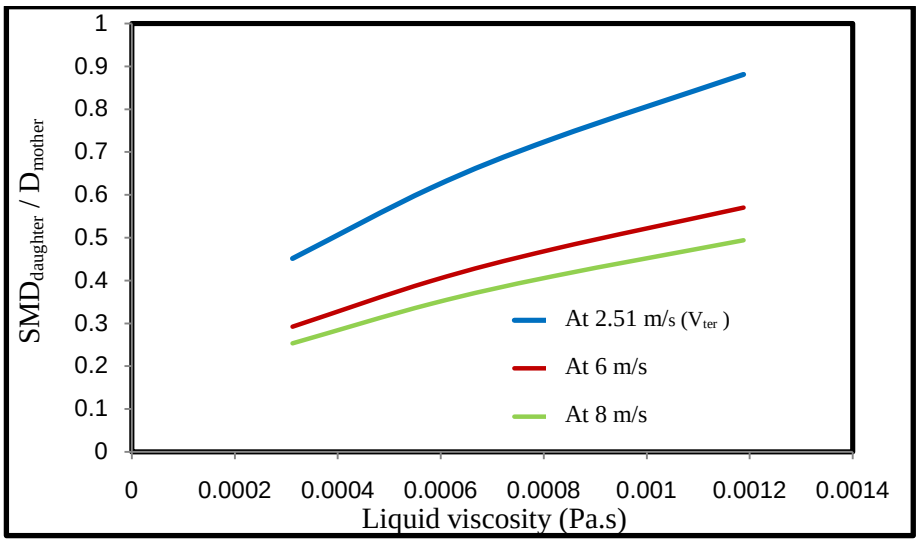

Figure 9.3 The effect of changing liquid viscosity on Sauter mean diameter of daughter droplets for 750µm mother droplet at different relative velocities

After the primary stage, the droplets size distribution during droplets falling does not show any remarkable development. The differences in continuous phase viscosity values didn't make any marked difference in droplet distribution. This is also true for the aerosol percentage during falling distance. Figure (9.4) expresses the development of aerosol percentage at different stages.

At the final stage, the higher liquid viscosity droplets, which have the higher average size falling droplets, certainly are expected to generate the lower amount of aerosol after impinging. But the differences appeared is this stage is more than expected. Although the ratio between median mean diameter of lowest and highest viscosity liquid are about 3:4, the ratio between aerosol percentages generated in both cases has raised up to more

than double value. The existing difference between liquid viscosities magnifies the effect at this stage. The value of mean daughter droplet sizes after splash is directly dependant on Reynolds number, which is inversely proportional with liquid viscosity value. Therefore, higher viscosity liquid again is candidate to generate larger droplets during impingement.

$$d_{mean\ ,after\ \ splash} = 4.23\, d_o \left(\sqrt{9 + \frac{2We_L(We_L+12)}{Re_L}} + 3\right)(We_L + 12)^{-1}$$

$$Re_L = \rho_L U_L \frac{d_o}{\mu_L}$$

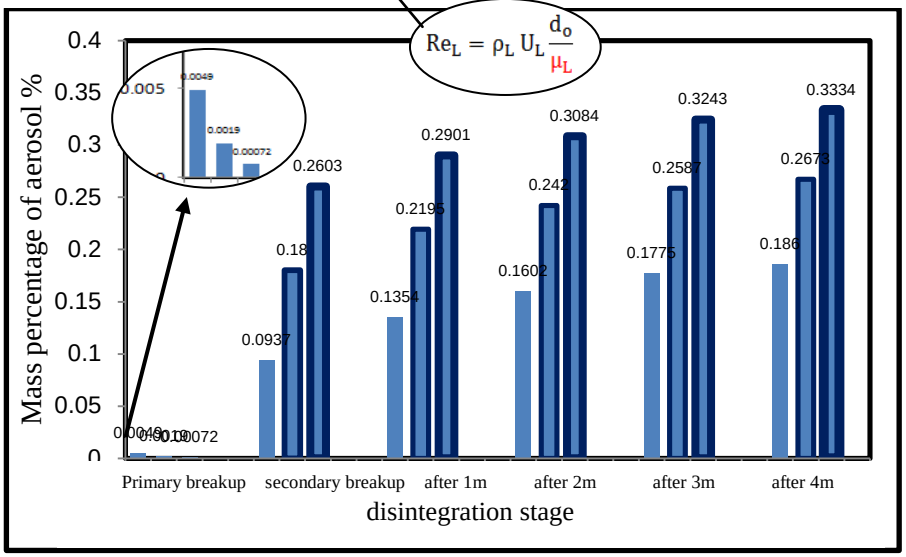

Figure 9.4 Development of aerosol percentage at different stages for different liquid viscosities

Figure (9.5) shows the effect of liquid viscosity on the amount of vaporised fraction, and it is found that increasing liquid viscosity decreases the amount of vaporised fraction in both free-falling stage and impinging stage.

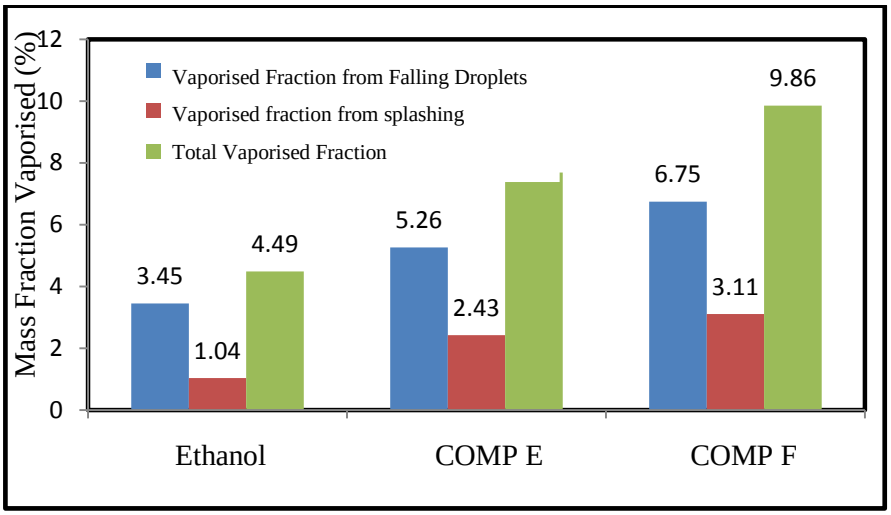

Figure 9.5 The Effect of Liquid Viscosity on the amount of vaporised Liquid

9.3 Effect of Liquid Surface Tension

The second important physical property under scope is the liquid surface tension. To study this property, two hypothetical liquids are proposed in order to investigate the effect of changing liquid surface tension on the mechanism of liquid disintegration during accidental release. Composition (H), the reference liquid (Ethanol) and composition (G) represent the low, medium and high liquid viscosity respectively. Table (9.3) expresses primary stage breakup properties for the three different release liquids. Calculations had been performed at 20 mm orifice diameter, 6 m/s release velocity, saturated continuous phase of humidity and fuel liquid vapour and finally temperature of 20^{o}C.

At the primary breakup of liquid jet, increasing liquid surface tension increased the value of maximum droplet diameter through decreasing the value of liquid Weber number. Weber number of continuous phase also decreased by increasing liquid surface tension, hence breakup regime had transferred from atomization to second wind breakup and finally first wind breakup. Figure (9.5) shows the particle size distribution after primary jet breakup for the three different liquids surface tension. The highest surface tension value (Comp G) has the highest MMD, D_{max} values, and hence the widest droplets distribution range.

Table 9.3 Primary stage breakup properties at different liquid surface tension.

Release Liquid	Liquid surface tension (N/m)	Breakup regime	Breakup length (m)	D_{max} (μm) after jet breakup	D_{max} / $D_{Orifice}$	D_{max} (μm) after drop breakup	Fraction of aerosol size droplets after jet breakup	Fraction of aerosol size droplets after drop breakup
COMP H	0.0160	atom	0	33612	1.68	6550	6.1×10^{-5}	1.3×10^{-3}
Ethanol	0.0224	SWI	4.37	37576	1.88	9150	4.9×10^{-5}	9.4×10^{-4}
COMP G	0.0738	FWI	2.98	55886	2.79	30150	2.2×10^{-5}	9.5×10^{-5}

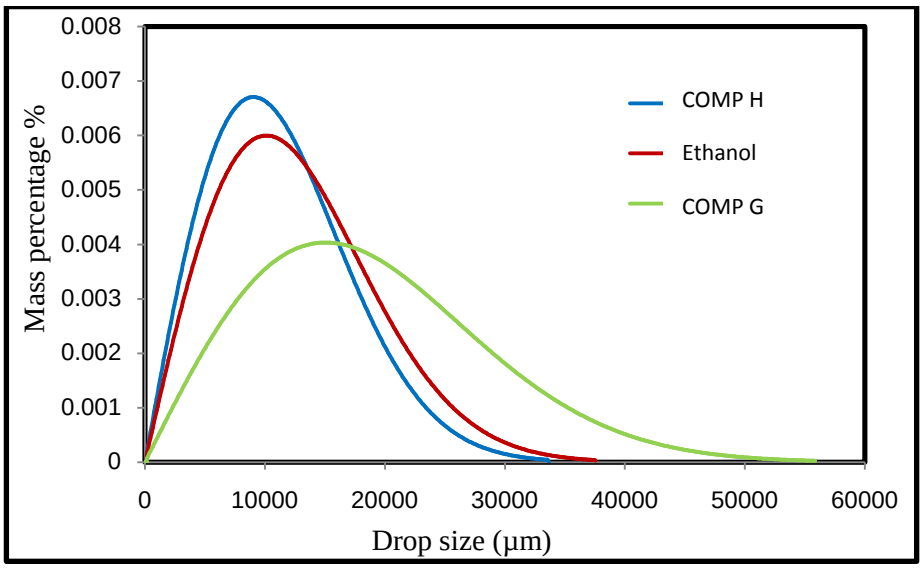

Figure 9.6 Droplet size distribution after primary jet breakup for liquids with different surface tension

At the secondary breakup step, although the liquid surface tension does not affect the mean diameter of daughter droplets, tolerances between the droplet size distributions become wider (shown in fig (9.6)). The reason for this behaviour is the effect of surface tension on the value of droplets critical velocity. Figure (9.7) shows the values of critical velocity of different droplets sizes ranging from 5µm to 5050µm for different liquids. It was found that critical velocity of falling droplet is directly proportional to the value of liquid surface tension. This increase in critical velocity reduces the limits of secondary disintegrated droplets and therefore minimizes the change in droplet size distribution after secondary droplets breakup.

During droplets falling, the effect of high critical velocity will keep limiting disintegration of falling droplets. Droplets breakup will take place in all cases, but the droplet distribution at high surface tension will remain wider, and the maximum droplets size will remain higher.

As shown in Figure (9.8), the development of aerosol droplets Percentage during release and falling progress remain in similar. Hence, the higher liquid surface tension generates the lower percentage of fine droplets at all stages.

In contrast, at the impingement stage, the higher droplet size distribution range generates the lower percentage of fine droplets when splashed. Although the surface tension is a part of mean daughter droplet size equation, the effect of surface tension on Weber number is very small. Weber number appears on that equation in Numerator and denominator with the same power, therefore repeal each other's effect.

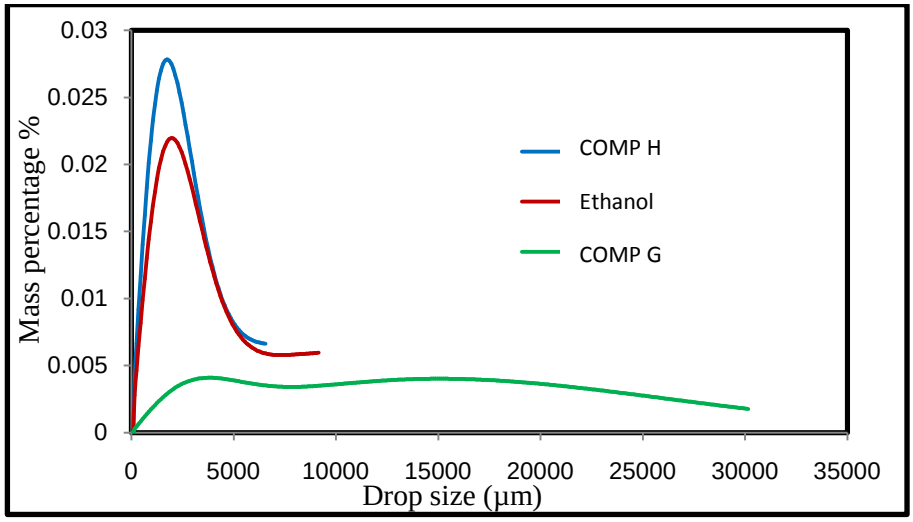

Figure 9.7 Droplet size distribution after secondary drops breakup for liquids with different surface tension

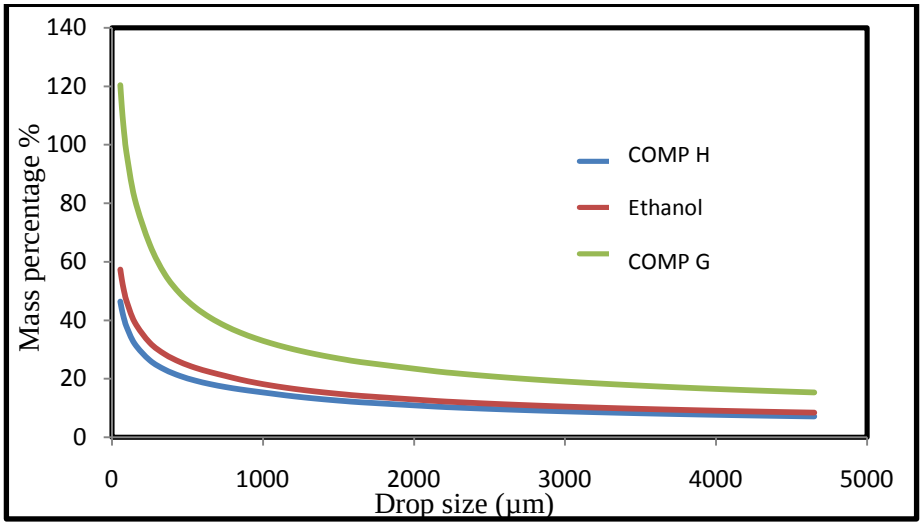

Figure 9.8 Droplet Critical Velocity for different liquids with different surface tension

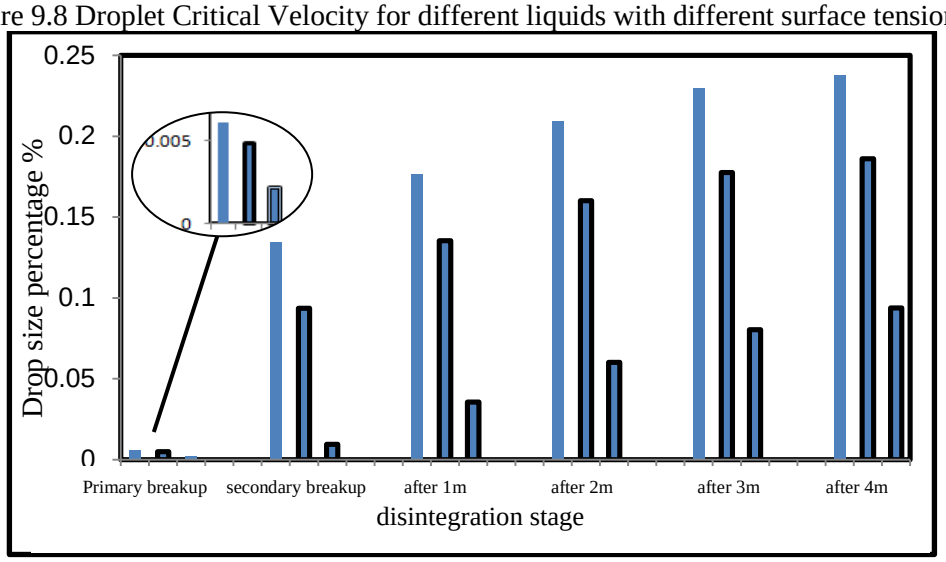

Figure 9.9 Development of aerosol percentage at different stages for different liquid surface tension

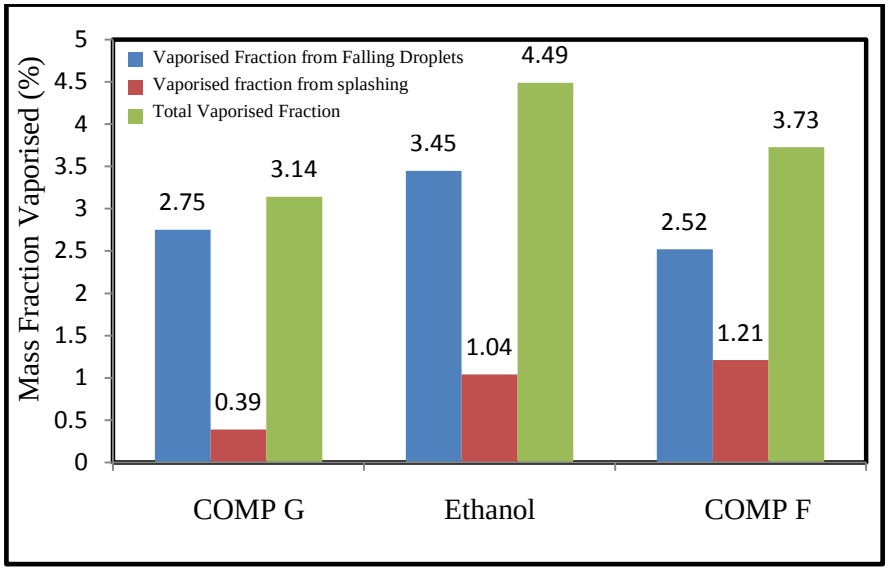

Figure 9.10 The Effect of liquid Surface Tension on Vaporised Fraction

Figure (9.10) shows that the liquid viscosity has a minor effect on the total amount of vaporised liquid during both the free-falling stage and the impinging stage.

9.4 Effect of Liquid Density

The third important physical property is the liquid density. To study this property, another two hypothetical liquids are proposed to investigate the effect of changing liquid density on the mechanism of liquid disintegration during accidental release. Composition (B), the reference liquid (Ethanol) and composition (A) represent the low, medium and high liquid density respectively. Table (9.5) expresses the primary stage breakup properties for the three different release liquids. Calculations had been performed at 20 mm orifice diameter, 6 m/s release velocity, saturated continuous phase of humidity and fuel liquid vapour and finally temperature of 20^{o}C.

At the primary breakup of liquid column, determining the breakup regime is dependent on the continuous phase density rather than liquid density, therefore the liquid density has no effect at all on the breakup regime. On the other hand, a small increase occurred to both the breakup length and the maximum droplets diameter after liquid disintegration. Increasing liquid density by 54% lead to 15% increase in breakup length and only 11% for increase in maximum diameter. Figure (9.8) shows that different liquid densities have limited effect on droplets distribution after primary breakup of liquid column.

Table 9.4 Primary stage breakup properties at different liquid densities

Release Liquid	Liquid density (kg/m^3)	Breakup regime	Breakup length (m)	D_{max} (µm) after jet breakup	D_{max} / $D_{Orifice}$	D_{max} (µm) after drop breakup	Fraction of aerosol size droplets after jet breakup	Fraction of aerosol size droplets after drop breakup	Air density (kg/m^3)
COMP B	660.6	SWI	4.12	36124	1.81	9150	$5.29x10^{-05}$	$8.53 x10^{-04}$	1.23
Ethanol	791.5		4.37	37576	1.88		$4.89x10^{-05}$	$9. 37x10^{-04}$	
COMP A	1015		4.73	40200	2.01		$4.27x10^{-05}$	$1.07x10^{-05}$	

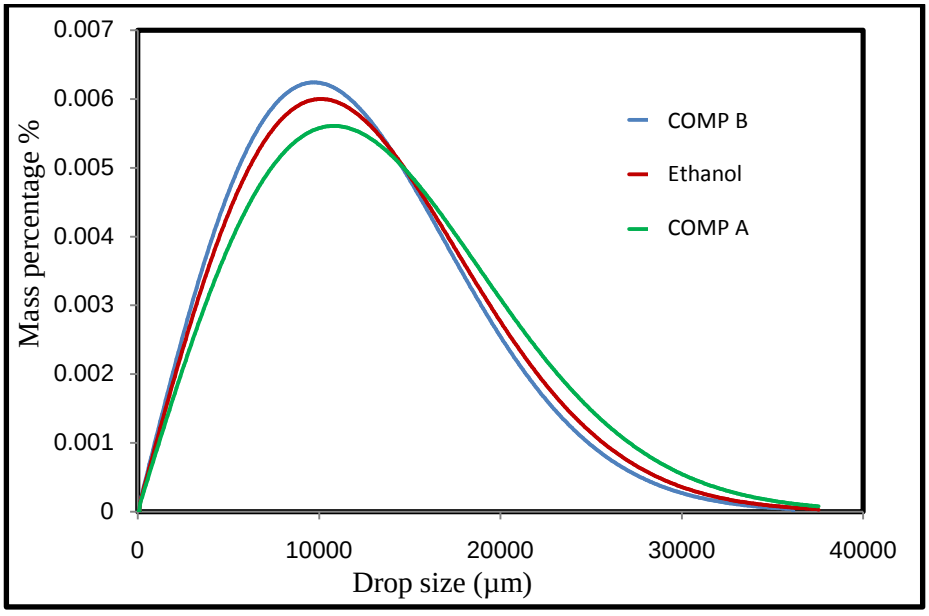

Figure 9.11 Droplet size distribution after primary jet breakup for liquids with different densities

During the secondary breakup of liquid droplets, increasing liquid density decreases the value of mean daughter droplets diameter, and therefore increases the quantity of smaller droplets rather than larger ones. The maximum droplets diameter is not dependent on liquid density. Figure (9.9) expresses droplets size distribution after secondary breakup of liquid droplets.

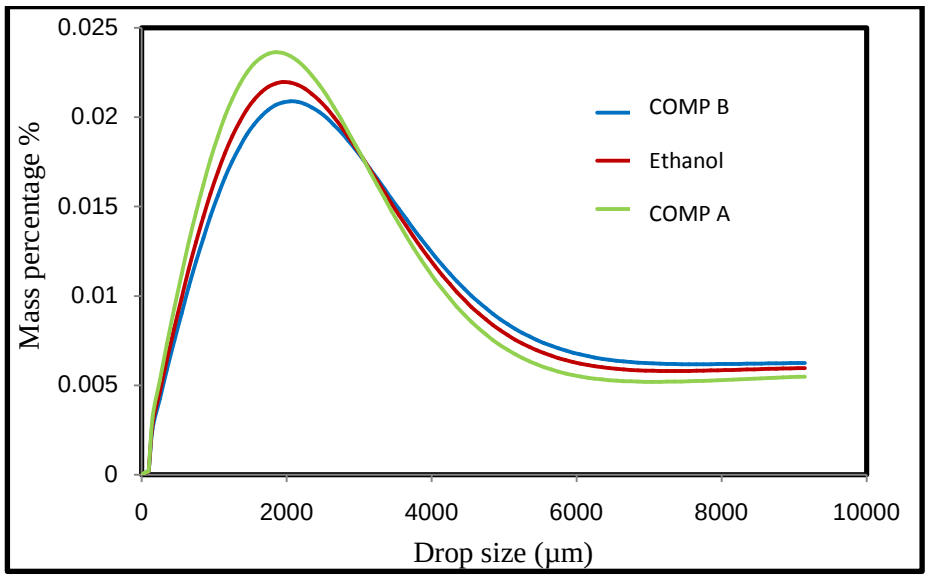

Figure 9.12 Droplet size distribution after secondary drops breakup for liquids with different densities

It can be clearly determined that the liquid density is an important factor to determine the terminal settling velocity during droplets falling. That can be proven by the fact that an increase of the liquid density will increase the terminal settling velocity of droplets which allows the falling droplets to reach higher velocities. This increase could lead to more droplets to disintegrate. Although higher density liquid will earn more amounts of small droplets, the differences in droplets size distribution will remain limited during droplets falling. Development of aerosol percentage during droplets falling in (Fig (9.10) confirms this fact as the differences in aerosol quantity seems to be small.

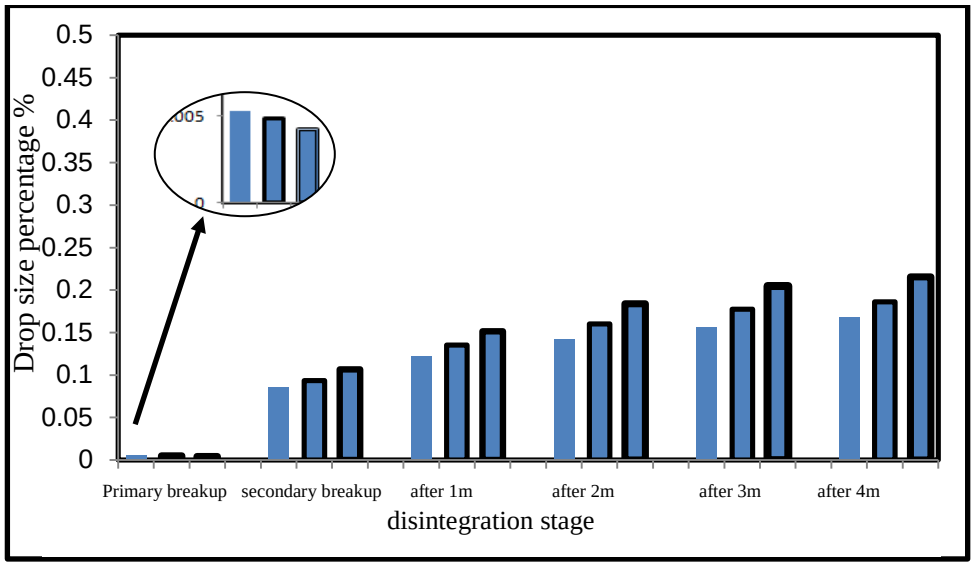

Figure 9.13 Development of aerosol percentage at different stages for different liquid densities

Different behaviour appears on impingement stage, the amount of aerosol generated from higher liquid density was significantly higher. The percentage for Comp A (the highest density) was 59.87% compared to 21.09% for Comp A (the lowest density). The reason is the differences in droplet velocities before impingement which have been raised as a consequence of different terminal settling velocities.

Figure (9.14) expresses the effect of liquid density on vapour generation. It is clear from the figure that increasing liquid density decreases the total amount of the vaporised liquid during free-falling stage and impinging stage.

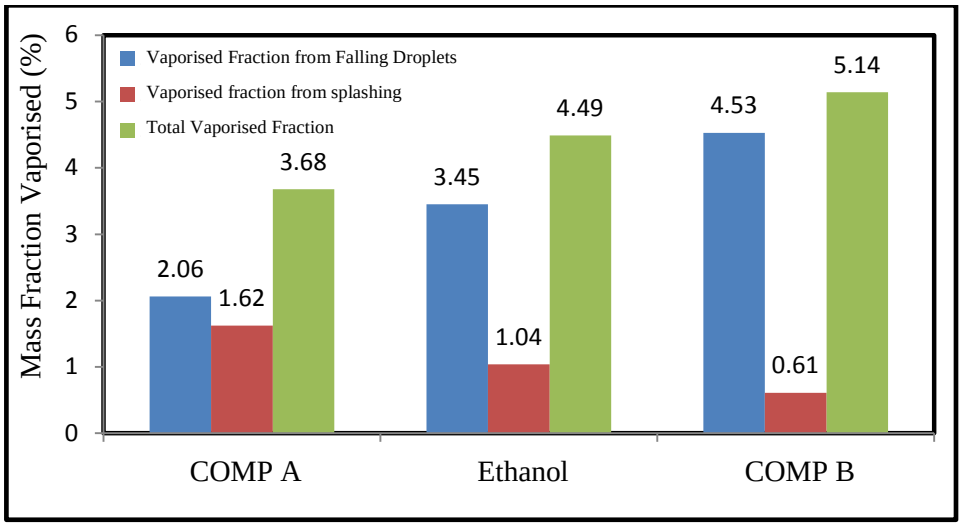

Figure 9.14 The effect of Liquid Density on Evaporation

9.5 Effect of Liquid Molecular Weight

In order to study this property, another two hypothetical liquids are proposed to investigate the effect of liquid molecular weight on the mechanism of liquid disintegration. Compositions (C) and (D) are proposed as lower and higher densities than reference liquid (Ethanol) respectively. Table (9.5) expresses primary stage breakup properties for the three different release liquids. Calculations had been performed at 20 mm orifice diameter, 6 m/s release velocity, saturated continuous phase of humidity and fuel liquid vapour and finally temperature of 20^{o}C.

When higher molecular weight liquid is released, the most influential point supposed to be affected is the continuous phase density. Although changing molecular weight will not cause any change in mole fraction of fuel vapour, overall density and also viscosity of continuous phase are expected to change. Continuous phase density will be increased because the partial density of fuel vapour will increase. While viscosity of gases mixture depends directly on molecular weight of gas components.

Table 9.5 Primary stage breakup properties at different liquid molecular weight

Release Liquid	Molecular Weight (gm/mol)	Breakup regime	Breakup length (m)	D_{max} (µm) after jet breakup	D_{max} / $D_{Orifice}$	D_{max} (µm) after drop breakup	Fraction of aerosol size droplets after jet breakup	Fraction of aerosol size droplets after drop breakup
COMP C	18.02	SWI	4.37	37576	1.88	9650	$4.89x10^{-05}$	0.000852
Ethanol	46.069	SWI	4.37			9150		0.000937
COMP D	78.11	atom	0			8550		0.001046

Release Liquid	Liquid density (kg/m^3)	Partial density of dry air (kg/m^3)	Partial density of fuel vapour (kg/m^3)	Air density (kg/m^3)	Air viscosity (Pa.s)
COMP C	791.5876	1.106773	0.043618	1.167695	$1.89x10^{-05}$
Ethanol			0.111512	1.235589	$1.93x10^{-05}$
COMP D			0.189069	1.313145	$1.97x10^{-05}$

Properties of air show that density is increased by about 12.5% when liquid molecular weight increased from 18.02 to 78.11 gm/mol. The partial density of fuel vapour increased from 4.3% to 18.9%. On the other hand, the change in air viscosity was only about 4%. For those reasons, the higher liquid molecular weight turned the breakup regime to fully atomization according to increasing air Weber number, where maximum droplet size after primary breakup did not been affected.

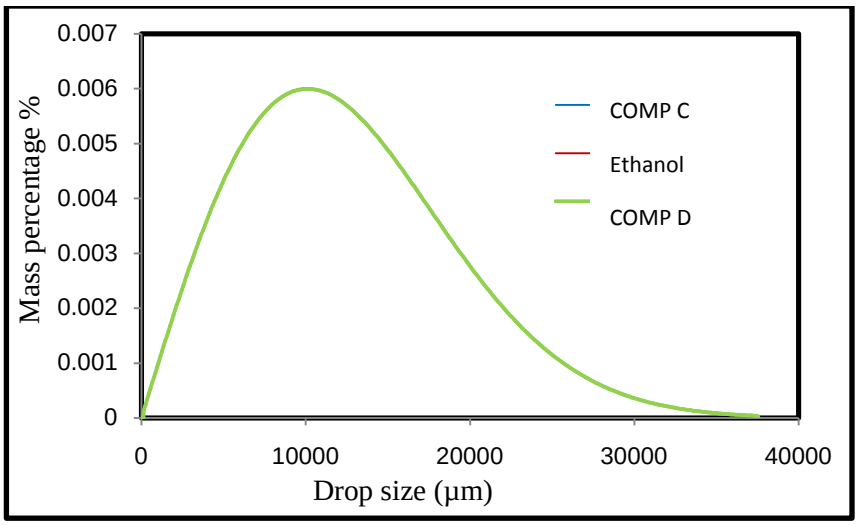

Figure 9.15 Droplet size distribution after primary jet breakup for liquids with different molecular weights

At next step, the role of different molecular weight becomes more effective. The molecular weight does not only affect the vapour density but also has an effect on droplet velocity. Increasing liquid molecular weight will decrease both critical and terminal settling velocity. For secondary breakup of generated droplets, decreasing critical velocity will give higher opportunity for more droplets to disintegrate. This will generate more amounts of fine droplets. On the other hand, air density is inversely proportional with daughter droplets mean value. In the current example, air density increased by 12.5% when liquid molecular weight increased by 433%. This increase should decrease the value of SMD by about 2.8% and subsequently increase the percentage of very small daughter droplets which we called "aerosols". Figure (8.12) shows minor differences in particle distribution at different molecular weights. Table (8.7) expresses the differences appeared in secondary breakup regarding the aerosol percentage and maximum value of droplets diameter.

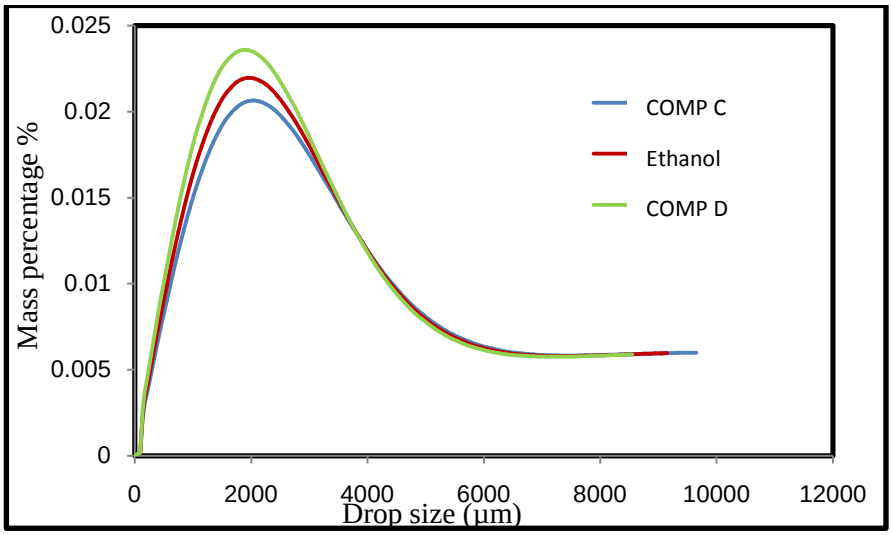

Figure 9.16 Droplet size distribution after secondary drops breakup for liquids with different molecular weights

During droplets falling, disintegration of larger droplets will take place step by step according to droplets acceleration. But in general, disintegration of droplets belong to high molecular weight liquid will be proceeded by step. Distribution curve shape will get no change, and percentage of aerosol droplets will increase gradually with no disparity between different liquids.

When falling droplets reach impingement stage, it was found that liquid molecular weight nearly has no effect on the percentage of aerosol generated during this stage. Droplets with higher molecular weight have a bit lower terminal settling velocity. Hence, it will have a relatively lower impact velocity. And this could be a reason for these droplets to generate smaller amount of aerosol droplets during impinging.

In general, the effect of changing liquid molecular weight seems to be very limited on the quality of liquid disintegration during all stages of accidental liquid release. Figure (9.17) shows the inversely proportional relation between the liquid molecular weight and the amount of vaporised liquid.

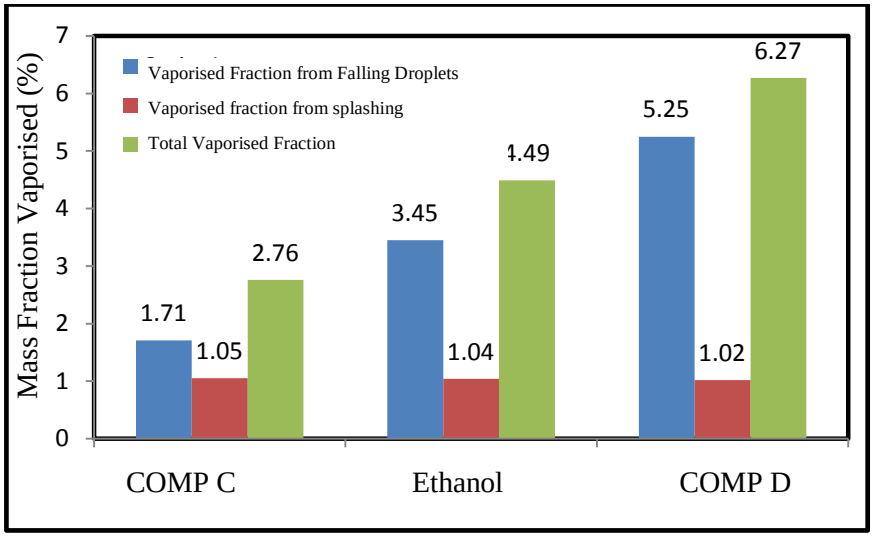

Figure 9.17 The Effect of Liquid Molecular Weight on evaporation

9.6 Effect of Liquid saturation Vapour Pressure

The effect of increasing liquid vapour pressure is very similar to that for liquid molecular weight. In both cases, the result will be in form of increasing air density and viscosity, but this happen in different way. When increasing liquid molecular weight, the same amount of fuel vapour, i.e. the mole fraction, will be heavier. Increasing partial density of that vapour will directly increase the total density of air mixture. In the case of increasing vapour saturated pressure, the mole fraction of fuel vapour inside air mixture, i.e. air content of fuel vapour, will increase. And because this vapour is heavier than air, the total density and viscosity in this case will be increased.

In order to study the effect of changing saturated vapour pressure on the mechanism of liquid disintegration separately, two hypothetical liquids were proposed. Compositions (I) and (J) are both with higher value of saturated vapour pressure. Each liquid is about three time higher pressure value than the lower one. Table (9.8) expresses the primary stage breakup properties for the three different release liquids. Calculations had been performed at 20 mm orifice diameter, 6 m/s release velocity, saturated continuous phase of humidity and fuel liquid vapour and finally temperature of 20^{o}C.

Table 9.6 Primary stage breakup properties at different saturated vapour pressure

Release Liquid	Saturated Vapour Pressure (Pa) at 298.15K	Breakup regime	Breakup length (m)	D_{max} (μm) after jet breakup	D_{max} / $D_{Orifice}$	D_{max} (μm) after drop breakup	Fraction of aerosol size droplets after jet breakup	Fraction of aerosol size droplets after drop breakup
Ethanol	7989.5	SWI	4.37	37576		9150	4.89×10^{-05}	9.37×10^{-04}
COMP I	20433.8	atom	0			8550	4.89×10^{-05}	0.001044
COMP J	69237.8	atom	0			7050	4.89×10^{-05}	0.001394

Release Liquid	Partial density of dry air (kg/m^3)	Partial density of fuel vapour (kg/m^3)	Mole Fraction of Fuel Vapour	Air density (kg/m^3)	Air viscosity (Pa.s)
Ethanol	1.106773	0.111512	0.05819618	1.235589	1.93×10^{-05}
COMP I	0.983492	0.307596	0.1605291	1.308392	2.17×10^{-05}
COMP J	0.499576	1.077289	0.5622188	1.594169	2.97E-05

From previous results, it could be found that increasing saturated vapour pressure of about 8.7 times caused about 10 times increasing in mole fraction of fuel vapour, about 29% increase in total air density and about 53% increase in total air viscosity.

The effect during primary breakup of liquid column is similar to that for molecular weight. Increasing air density will spontaneously increase air Weber number, and therefore change breakup regime toward fully atomization. No change happened to droplet size distribution in this part of the mechanism.

The effect starts to be more obvious in the step of secondary breakup of liquid drops in which droplets will start to interact with continuous phase. When air properties were changed according to changing fuel vapour content, both terminal and critical velocity changes take place. In current example the differences in saturated pressure and also air density cause droplets size distribution disparity by the end of primary stage. Differences in maximum droplet size have reached 30% and nearly 48.8% increase in aerosol percentage has been gained. Figure (9.13) describes the size distribution developments happened in this step compared to symmetric distribution in the first step.

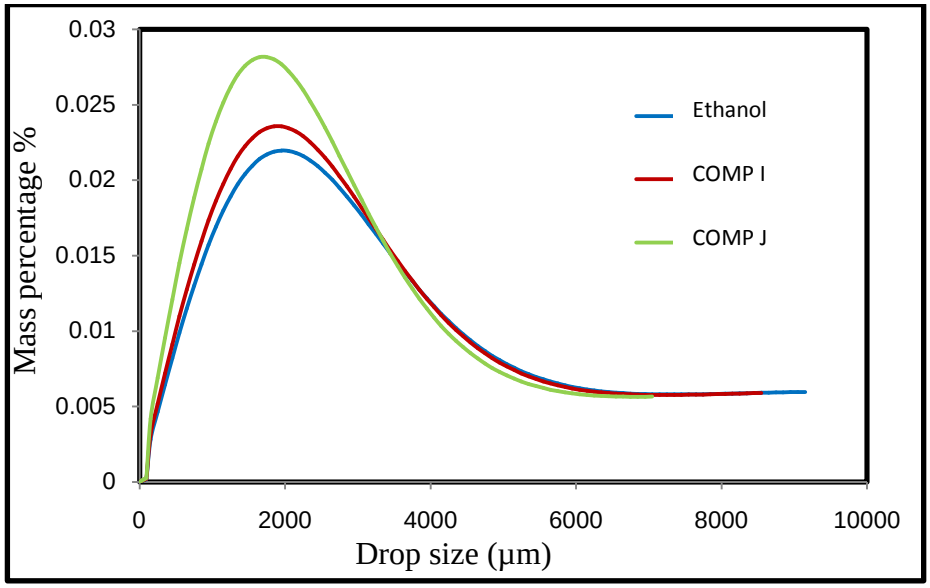

Figure 9.18 Droplet size distribution after secondary drops breakup for liquids with different saturated vapour pressure

This variation will continue during droplets falling, and development of liquid aerosol droplets percentage will take place with the same ratios. Similar to have happened in case of changing molecular weight. Average diameter of daughter droplets produced from droplets disintegration will be smaller, and decreasing the value of terminal and settling velocity will decrease the diameter value of likely breakable droplets.

When the falling droplets impact the surface, the higher air density liquid is supposed to produce lower amount of aerosol droplets. In this example, the variation in air density is much greater. Hence, the variation in aerosol percentage has appeared clearly.

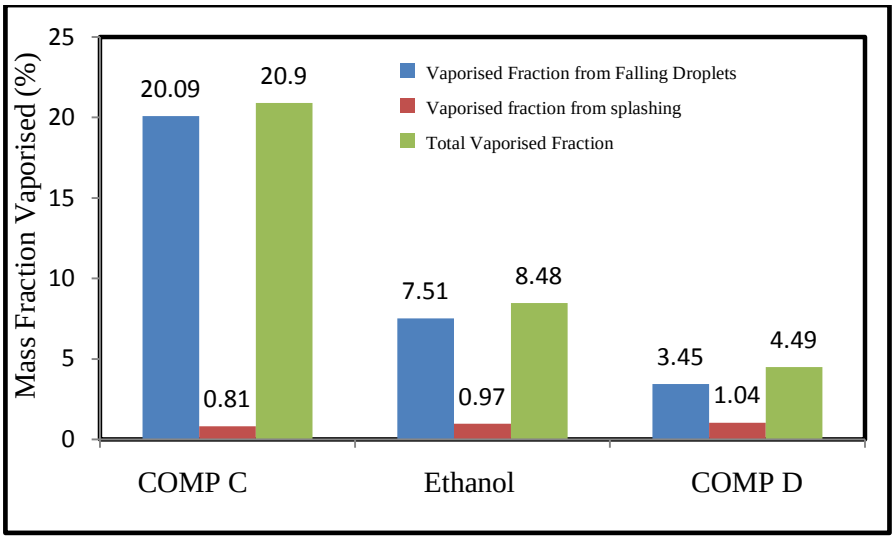

Figure 9.19 The Effect of Saturation Vapour Pressure on Vaporisation

Summary of Conclusions

1- The effect of liquid viscosity on the liquid release process:

- Increasing the liquid viscosity increased the diameters of liquid droplets at the end of primary stage and during droplets falling. It is also provides larger amount of aerosols through falling distance.
- The amount of aerosol droplets produced after droplets impingement is larger for the lower viscosity released liquid.
- Increasing viscosity had generally increased the amount of generated vapours.

2- The effect of liquid surface tension on the liquid release process:

- Increasing the liquid surface tension increases the value liquid droplets and dramatically decreases the percentage of aerosol droplets during both primary stage and falling stage.
- Increasing the liquid surface tension decreases the amount of aerosol droplets generated after impingement and it had a minor effect of vaporization efficiency.

3- The effect of liquid dnsity on the liquid release process:

- Increasing liquid density has a minor effect on the mechanism and quality of aerosol formation during liquid release. On the other hand, it sharply increases the amount of aerosol droplets generated from droplets splashing.
- Increasing the liquid density had decreased the total amount of generated vapours.

4- The effect of liquid molecular weight on the liquid release process:

- Increasing liquid molecular weight could affect the mechanism of liquid disintegration through increasing density and viscosity of continuous phase. But in general, the effect will still limit throughout the mechanism.
- Increasing the molecular weight had decreased the total amount of generated vapours.

5- The effect of liquid saturated vapour pressure weight on the liquid release process:

- Increasing saturated vapour pressure has a similar effect of increasing air density and viscosity.
- The differences in saturated vapour pressure values could lead to more remarkable effects in aerosol percentage, especially during droplets impingement. In addition, it caused a large increase in vapour amount.

Chapter 10: The Effect of Ambient Conditions on Droplet Size Distribution and Vapour Generation

10.1 Introduction

In this chapter, the effect of ambient properties on the liquid breakup mechanisms is examined. These properties include the temperature, the relative humidity and the fuel vapour saturation. Each one of these properties has effect on both the density and viscosity of ambient media. Subsequently, this might change the breakup characteristics of liquid jet and liquid droplets. The temperature also controls the liquid physical properties, which subsequently affect the mechanism of liquid breakup. In addition, the ambient temperature and vapour saturation are the key factors in controlling the evaporation mechanisms of falling liquid droplets.

10.2 The Effect of Temperature

In this section, the effect of the ambient temperature on the liquid breakup characteristics is studied in details. Firstly, the effect of temperature on physical properties of both released liquid and ambient media is discussed. Then, the effect of changing such properties on droplet breakup and droplet size distribution is analysed. The final part on this section reviews the effect of Temperature and Saturation Vapour Pressure on Approaching Flammability.

10.2.1 The Effect of Temperature on Physical Properties

The physical properties of gases and liquids are temperature dependant except the molecular weight. These properties play an important role in controlling the different mechanisms of liquid breakup. The effect of the temperature on the physical property depends on liquid type and temperature range. The temperature investigated here is from -20 to +50^{o}C for N-pentane. The upper temperature limit is 30^{o}C because the liquid boiling point is 36^{o}C. The overall effect of temperature change on breakup mechanisms is a combination of the effect of different properties.

10.2.1.1 Temperature Effect on Liquid Density

In general, the liquid density decreases with increasing of the liquid temperature. Figure (10.1) illustrates the change of liquid density with respect to temperature for the

five different liquid fuels. The relationship between the density and the temperature appeared to be linear.

When temperature was increased from -20 to +30oC, the density decrease is 7.26% for N-Pentane. 6.25% for N-hexane, 6.25% for the N-Hexane and 5.2% for the three other liquids. Therefore, the different between highest and lowest change rate was about 40%. In general, effect of temperature on liquid density is seems to be limited and impact of this change on breakup mechanism is not expected to be noticeable.

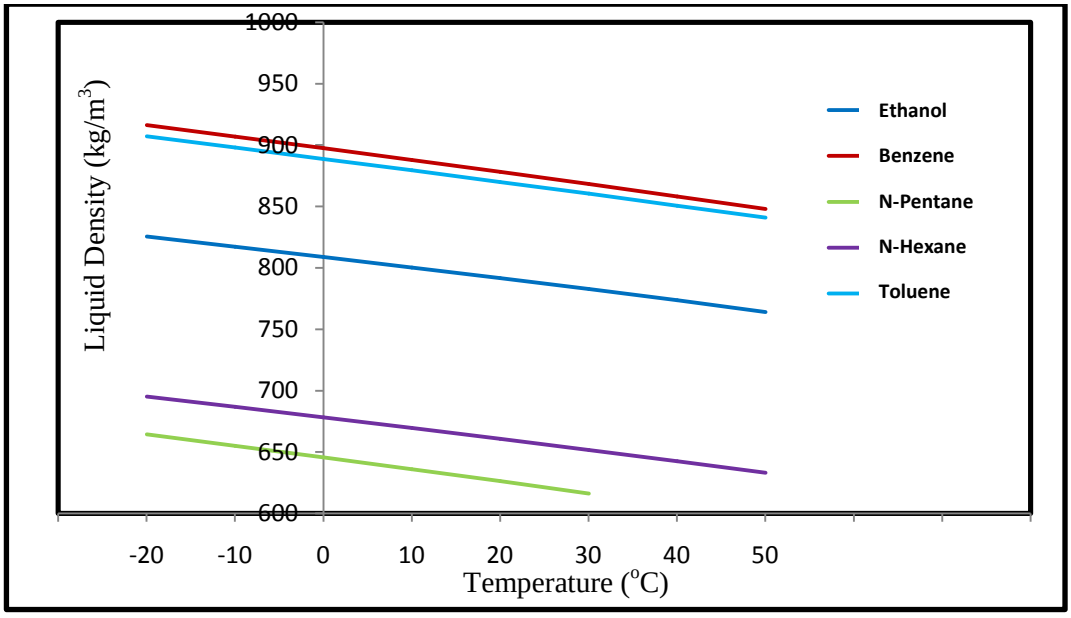

Figure 10.1 Liquid Density change with temperature for different types of fuel liquids

10.2.1.2 The effect of temperature on liquid viscosity

Figure (10.2) shows the liquid viscosity varying against the temperature. In general, the viscosity of all liquids decreased with increasing of temperature. The change in viscosity for Ethanol is 65.3% when temperature raised from -20 to +30^{o}C, 54.6%, for Benzene, 52.1% for Toluene, 40.4% for N-Hexane and finally 34.8% for N-Pentane. At 50^{o}C, viscosity decrease reached 75.7% for the Ethanol, in comparison with 48% at 10^{o}C. There is no linear relationship between viscosity and temperature. Therefore it is expected that the effect of temperature on the liquid viscosity would be more noticeable during the process of liquid breakup.

10.2.1.3 The effect of temperature on liquid surface tension

Figure (10.3) presents liquid surface tension against temperature. It seems that liquid surface tension behaves in similar way as liquid density. There is linear relationship between the surface tension and the temperature. The percentage of decrease is

something intermediate between the decrease of liquid density and liquid viscosity. For the five examples of liquid fuels, liquid surface tension decreased by 15.5 to 27.1% when temperature is raised from -20 to +30°C. Benzene fuel liquid expresses the lowest percentage of decrease by 15.5%, and N-Pentane shows the highest percentage of decrease for all the five liquid examples by 27.1% and nearly 75% higher than Benzene. The role of this effect is expected to be moderate on liquid breakup mechanisms.

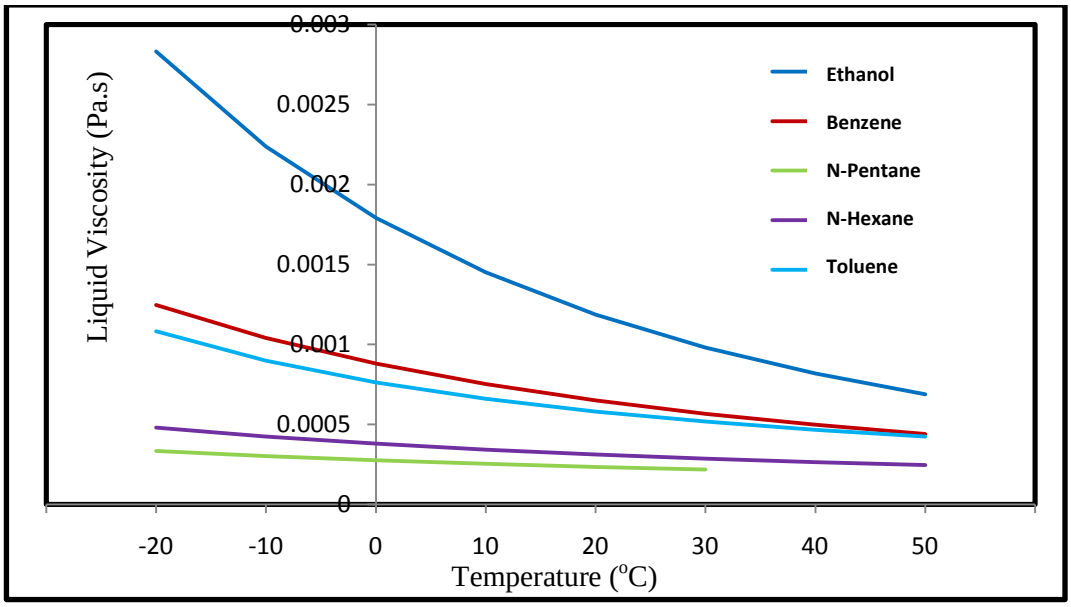

Figure 10.2 Liquid Viscosity change with temperature for different types of fuel liquids

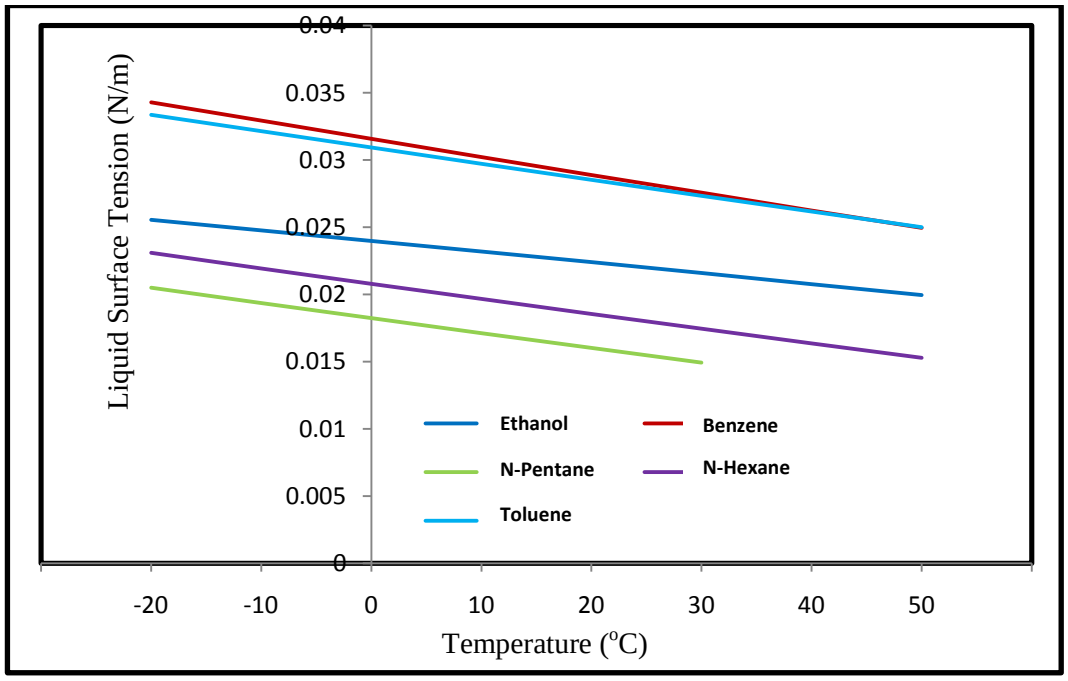

Figure 10.3 Liquid surface tension change with temperature for different types of fuel liquids

10.2.1.4 The effect of temperature on Gas Mixture density

The effect of temperature on the gas mixture density could be studied in two aspects. The first aspect could be observed from the general law of ideal gases, where temperature is directly proportional to the volume occupied by the same gas mass at constant pressure. Hence, the gas density is also inversely proportional to the ambient temperature. Therefore, the gas mixture density is also inversely proportional to ambient temperature. According to the ideal gas laws, the gas or vapour density would decrease by about 22% when the temperature is raised from -20 to +50^{o}C.

The second aspect is the effect of the air mixture saturation vapour pressure of both water vapour and fuel vapours in air. The density of the water vapour is smaller than density of the dry air. On the other hand, the density of liquid fuels vapours are heavier than air because their molecular weight are larger than air. Therefore, increasing the ambient temperature of the mixtures may have different effects on water vapour and fuel vapour, vapour pressures of water and fuels. Figure (10.4) shows the influence of temperature on saturated vapour pressure of water and different fuel liquids.

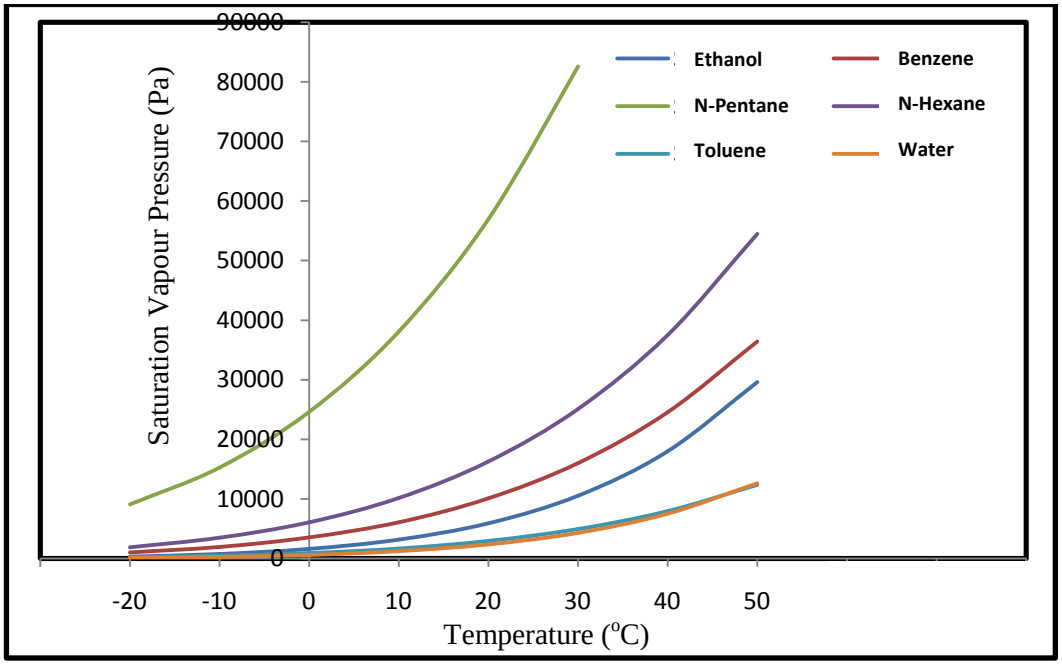

Figure 10.4 The influence of temperature on saturation vapour pressure of fuels and water

The analysis of Fig 10.4 can be concluded as the following:

1- The saturation temperature is strongly influenced by the ambient temperature. The temperature influence is also dependent on the fuel type.

2- The saturation pressure of N-Pentane has the highest value. Water and Toluene have the lowest saturation pressure saturation pressure.

3- In general, the saturation temperature increases with the increasing of temperature.

Figure (9.5) shows the density of the vapour phase against the ambient temperature calculated for different liquids release from the 20mm diameter orifice at velocity of 6m/s.

The results of density calculations, expressed by the above figure, show that for all types of liquids, density of gas mixture decreases with increasing temperature. After a certain temperature value, the density of air goes in the opposite direction and starts to increase. This temperature value varies from liquid to another, and density at this temperature might be the lowest possible density for this conditions. Liquids with higher vapour pressures are seemed to have lower temperature values at which density changes behaviour.

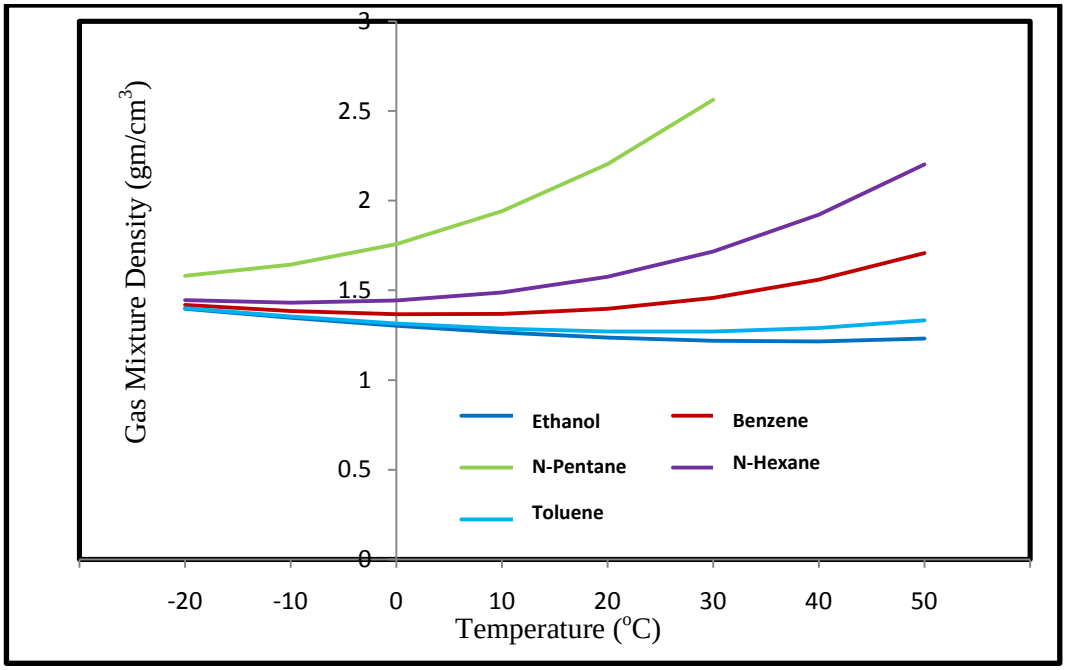

Figure 10.5 The effect of temperature on the density of gas mixtures containing different types of fuel vapours

For N-Pentane liquid (with Mw=72.15 gm/mol and saturated vapour pressure = 9074 Pa at -20°C), this value didn't appear during the proposed temperature region and seems to be lower than -20°C. In case of N-Hexane (with Mw=86.17 gm/mol and saturated vapour pressure = 1869 Pa at -20°C), the lowest density value appeared at temperature of about -10°C. This relatively low temperature proves that, the effect of increasing density through increasing the fraction of high molecular mass hexane vapour will lead the impact on density quickly at this temperature. Therefore, this value gets high in case of Benzene (with Mw=78.11 gm/mol and saturated vapour pressure = 995 Pa at -20°C) of about 0°C. Toluene and Ethanol expressed the highest temperature values of about 30

and 40^{o}C respectively. And although Ethanol liquid has a higher vapour pressure value, air mixed with Toluene vapour changed its behaviour at lower temperature. This could express the role of vapour molecular weight, where Toluene Mw is 92.14 gm/mol compared to 46.07 gm/mol for the Ethanol. Hence, the heavier weight of Toluene vapour have migrated the effect of fraction increase to nearly the double and the final effect on density increasing was more impassive.

10.2.1.5 The effect of temperature on gas mixture viscosity

As discussed in the previous section, increasing temperature allows larger amount of water and fuel vapours in air. Viscosity of gas mixture depends on mole fraction, molecular weight and viscosity of each gas. When temperature increases, mole fraction of vapours increases in favour of dry air mole fraction. In fact, gas molecular weight is not effective in this case because it increases in both numerator and denominator. Then, the only factor affects viscosity of gas mixture is the viscosity of vapours which replace the dry air molecules. In addition, the effect of temperature on each gas viscosity. Figure (10.6) shows the viscosity of different fuel vapours and water vapour compared to dry air viscosity at different temperatures. According to data expressed by this figure, the only vapour which has viscosity higher than dry air is the Ethanol vapour. All other vapours viscosities are smaller than dry air viscosity, and water vapour is the least of all. All gases viscosities increased by increasing temperature from -20 to +50^{o}C with ratio varying from 21% (for dry air) to 50% (for water vapour). According to these facts, effect of increasing temperature on gas mixture viscosity will depend on both the decreasing effect caused by dry air replacement and the general effect of increasing gases viscosities by temperature. Figure (10.7) expresses the effect of temperature increase of gas mixture viscosity for different released fuel liquids.

The results of gas mixture calculations, expressed by Fig (10.7), show that:

- For mixture containing Ethanol vapour, gas viscosity increased continuously by increasing temperature. This increase in completely understood under the effect of both gases viscosity increase by temperature and replacement of dry air by the higher viscosity ethanol vapour.
- For mixture containing Toluene, Benzene and N-Hexane vapours, the gas mixture viscosity increased until reaching a maximum value (20, 10 and -10^{o}C

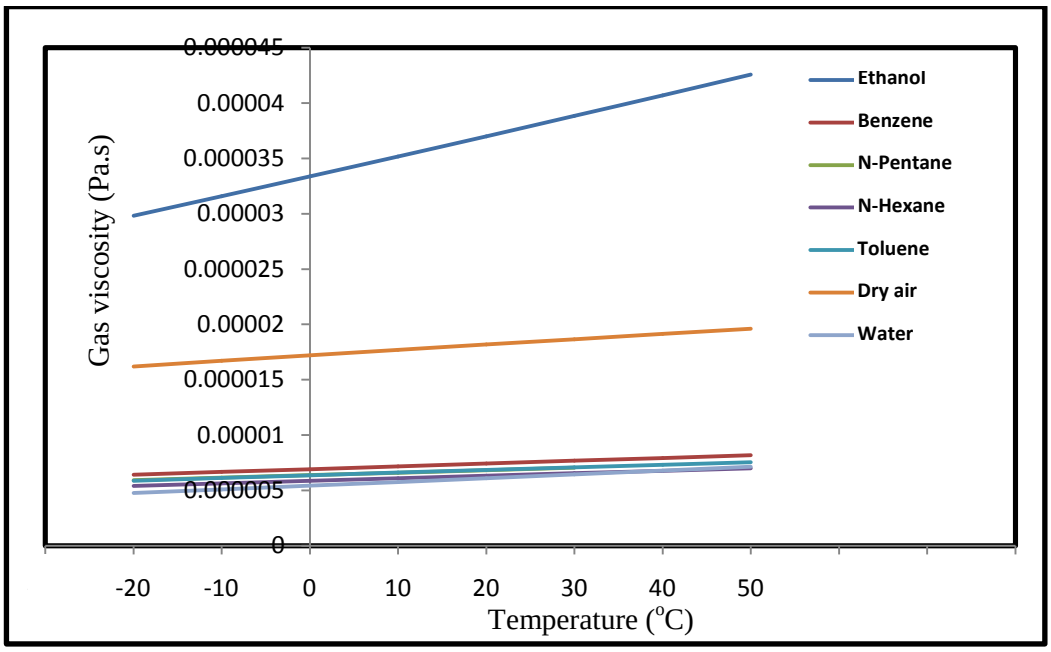

Figure 10.6 The influences of temperature on the viscosity of dry air, water vapour and fuel vapours

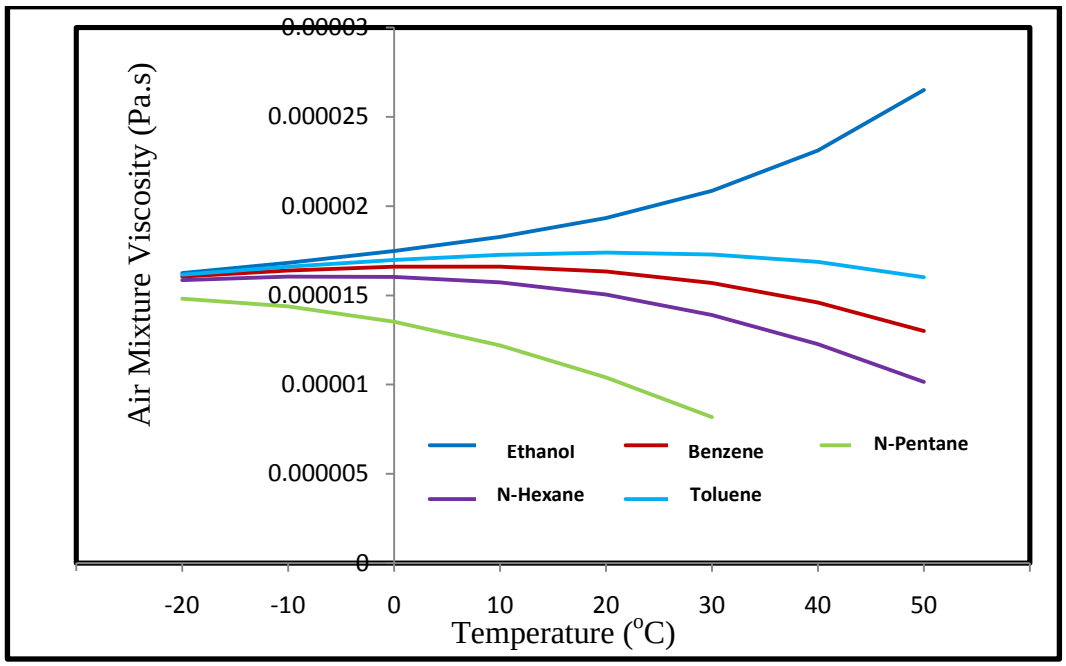

Figure 10.7 The effect of temperature on the viscosity of gas mixtures containing different types of fuel vapours

respectively), and then it started to decrease. This behaviour could be explained according to the leading effect of viscosity increase by temperature at low temperature, where the fraction of vapours is still very small. And after a certain temperature, the effect of vapour replacement will take the lead.

- For mixture containing N- Pentane vapour, increasing period didn't appear and viscosity decrease took place from the beginning. The proposed maximum

viscosity value in this case is seems to be lower than -20°C. This might be understood according to the largely noticed value of Pentane vapour pressure.

10.2.2 Effect of temperature on primary breakup of liquid jet

The direct effect of temperature change on physical properties of both released liquid and gas mixture will influence on the mechanisms and outcomes during different stages of liquid breakup. During the first step, which is primary breakup of liquid jet after release, breakup regime, breakup length and droplets distribution could be influenced by temperature changes.

One of the most important parameters at this stage is the Weber's number of air mixture, which controls the liquid jet breakup regime. For laminar release flow, breakup length is dependent on both liquid Weber and Ohnesorge numbers. Similarly, the upper limit of droplets distribution is dependent on Weber and Reynolds numbers. Figure (10.8) shows the impact of temperature change on those parameters.

In figure (10.8/A), it is shown that increasing temperature led to general increasing in air Weber's number. This increase is small for ethanol and toluene, but more significant for the other three liquids.

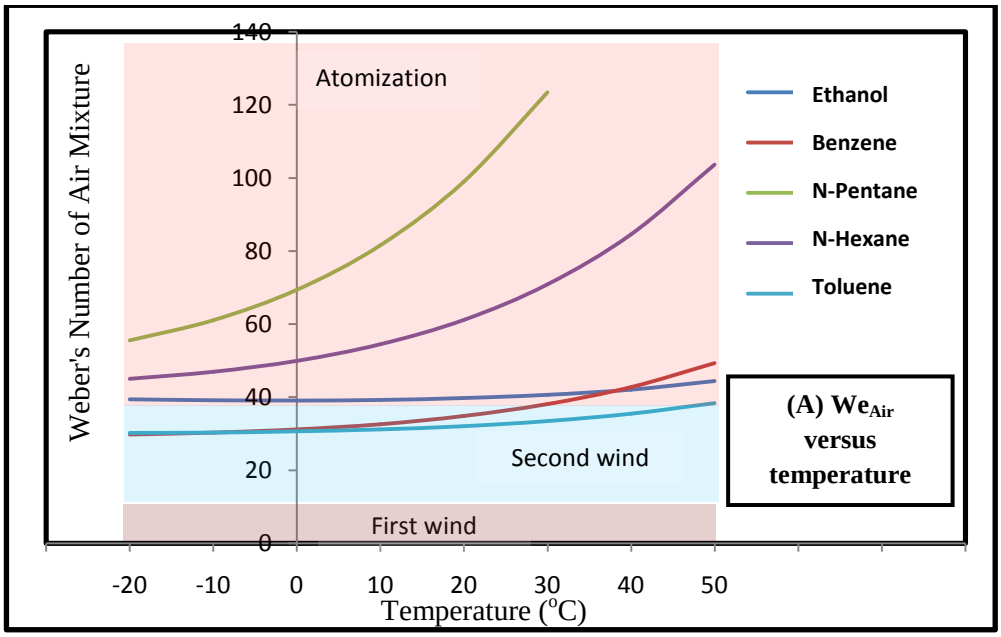

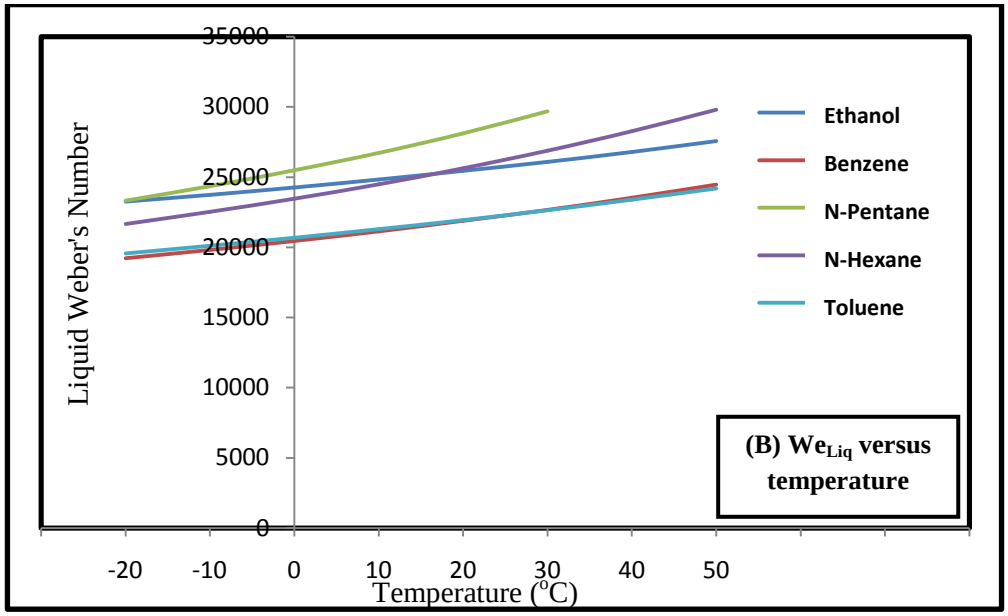

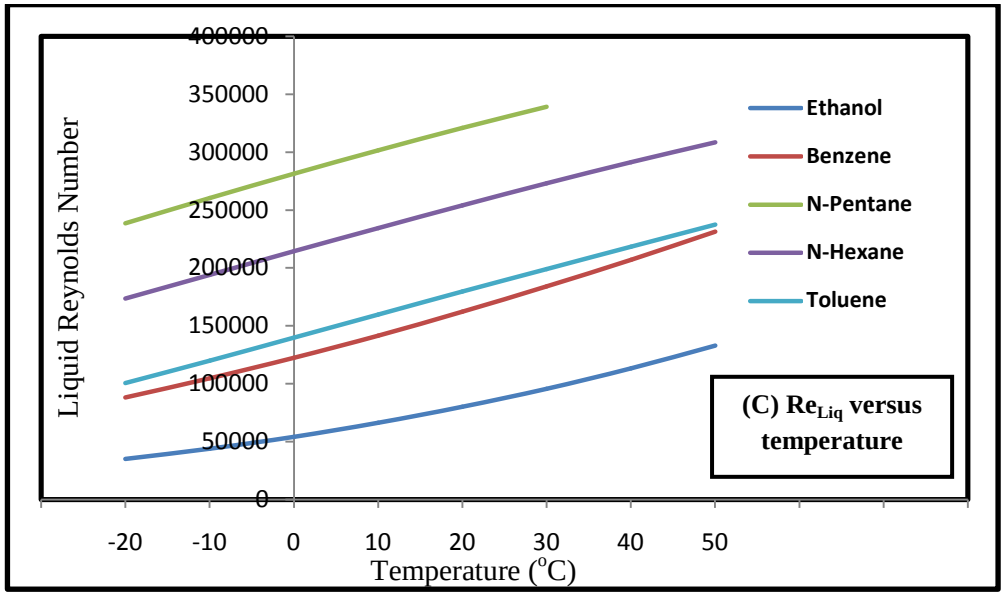

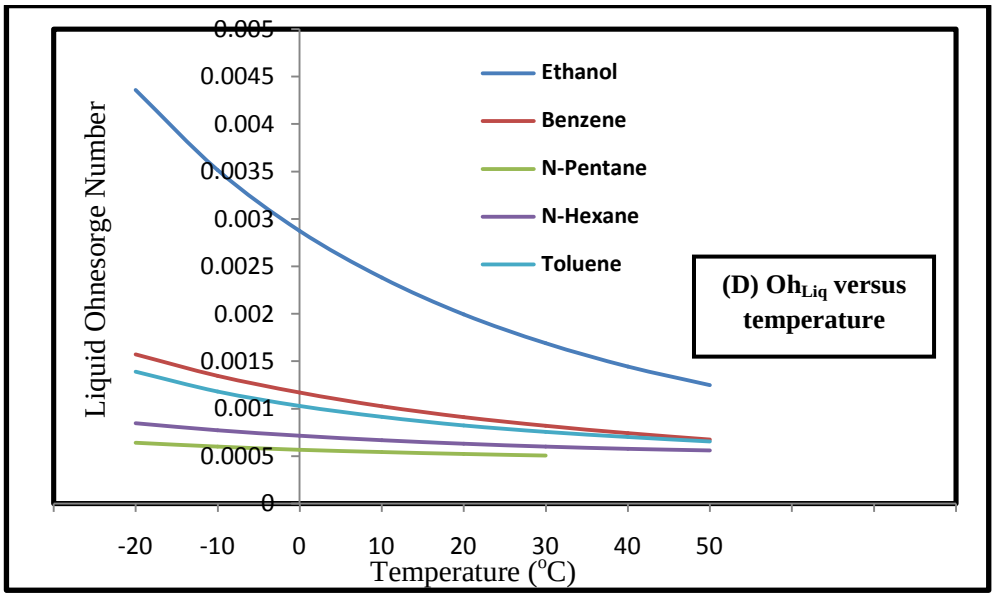

Figure 10.8 Effect of temperature change on different dimensionless numbers

As shown in Figure (10.8/B), Liquid Weber's number is also increased when the ambient temperature increases. The liquids Reynolds numbers have also increased with the ambient temperature as shown in Figure (10.8/C). The Ohnesorge number value decreases in Figure (10.8/D) with ambient temperature. In general, this decrease will not be effective in breakup length where the value of Ohnesorge number is very small.

After jet breakup, the maximum droplets diameter is dependent on both Weber and Reynolds numbers of the released liquid. Weber's number in this case has a limited effect on droplet size values. The value of Reynolds number is more influential and it's directly proportional with the maximum diameter value. The maximum droplet size after jet breakup is expected to increase when temperature increases. Figure (10.9) presents the maximum droplet diameter against the ambient temperature for the fuel liquids. The increasing in the maximum droplet size also indicates a wider range of droplet size distribution, and however results smaller fraction of aerosol droplet sizes.

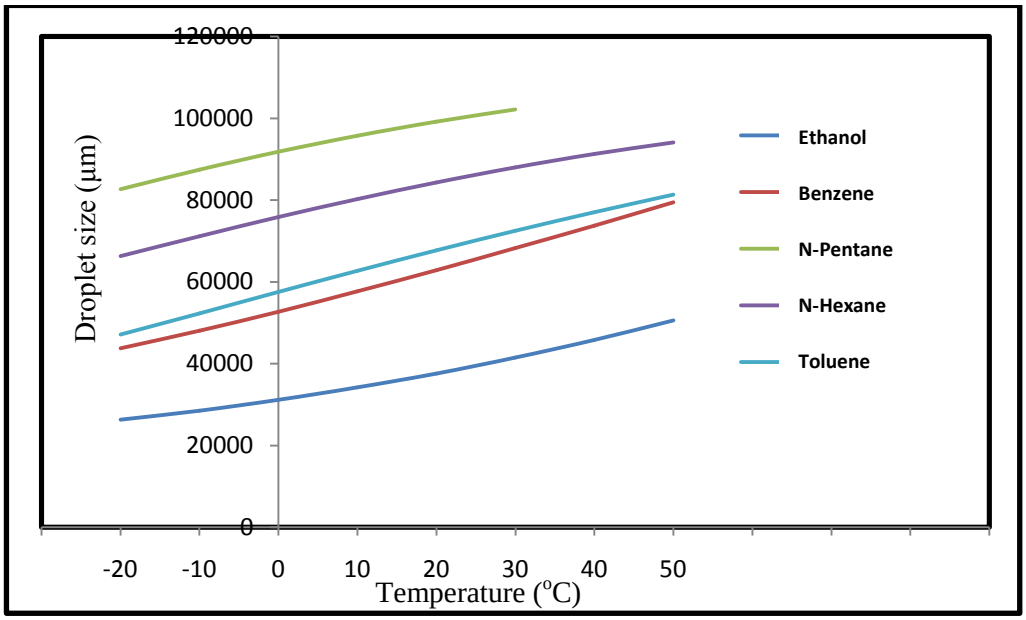

Figure 10.9 Effect of temperature on maximum droplets size after primary jet breakup

Figure (10.10) presents the droplet size distribution and percentage of aerosol droplets formed after primary jet breakup for liquid Ethanol release. With respect to temperature change, this kind of behaviour also seems for all other liquids. Increase in maximum droplets size indicates more droplets would be available to undergo secondary instantaneous disintegration during the primary stage of liquid release. This is because larger droplets have a higher possibility of achieving velocity above critical velocity at the moment of formation. This means, secondary breakup of liquid droplets during primary stage is expected to be higher at higher temperatures. This further disintegration will increase the population of smaller particles and push the value of mean diameter to

be smaller. And therefore, percentage of aerosol droplets is expected to be higher at higher temperatures. Figure (10.11) presents the droplet size distribution and percentage of aerosol droplets at the end of primary stage of the liquid release.

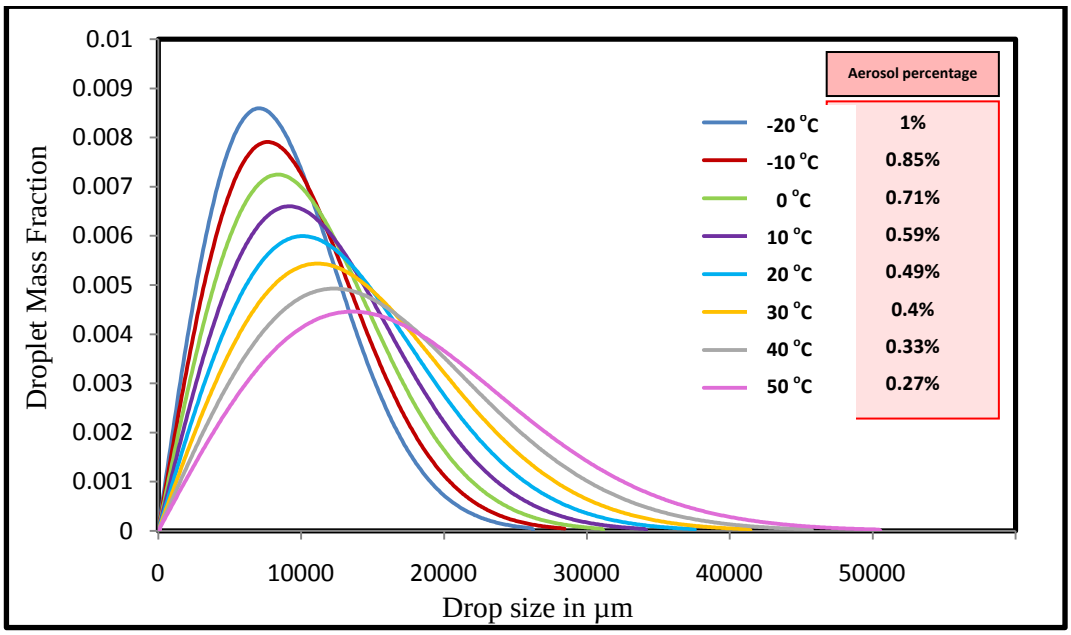

Figure 10.10 Droplet size distribution after jet primary breakup at different temperatures ranging from -20 to +50°C for liquid ethanol releasing at saturated conditions from 20 mm orifice diameter and release velocity of 6 m/s

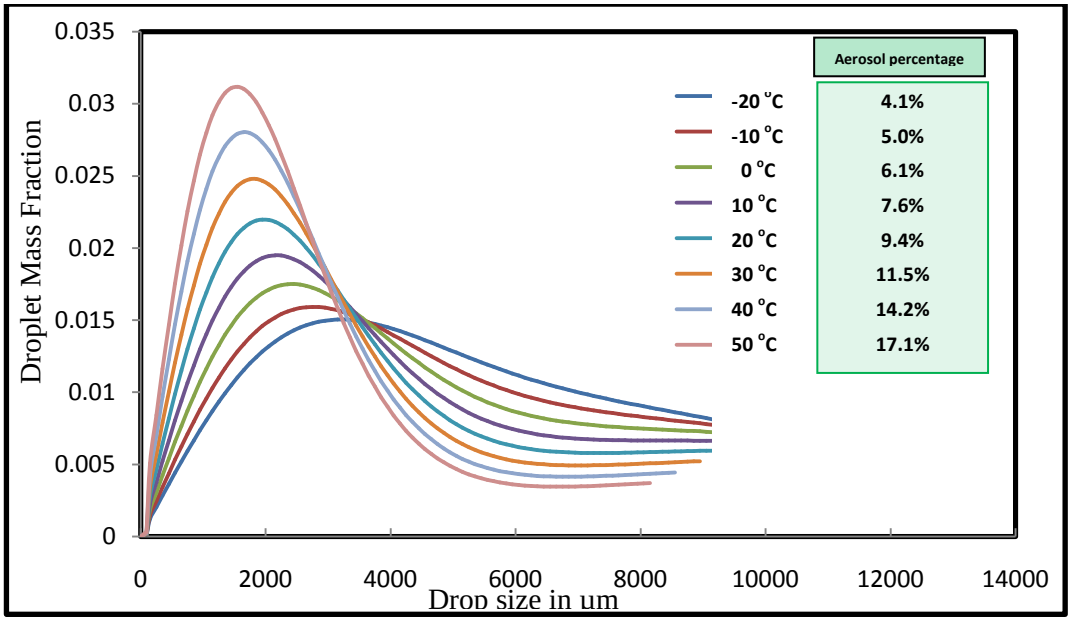

Figure 10.11 Droplet size distribution after secondary breakup of liquid droplets at different temperatures ranging from -20 to +50°C for liquid ethanol releasing at saturated conditions from 20 mm orifice diameter and release velocity of 6 m/s

10.2.3 Effect of temperature on falling liquid droplets.

The most important parameters during droplets falling are the terminal settling velocity and the critical velocity of disintegration. These two parameters control the behaviour of droplets during falling in air. Terminal and critical velocities can be used to determine whether the droplet accelerate or decelerate, disintegrate or keep stable and finally may control the mean diameter of disintegrated daughter droplets. The temperature effect on liquids and gases physical properties is extended to change these important parameters.

10.2.3.1 Effect on terminal settling velocity

As discussed before, the terminal velocity for droplets moving in Stokes region is dependent by liquid density, gas density and gas viscosity, which all are dependent on temperature. In addition, the slip correction factor is also dependent on mean free bath of air, which is also temperature dependent. The effect of air density could be negligible because it's too small compared to liquid density. Where the current liquids densities decrease by 5.2 -7.26% when temperature is raised from -20 -50^{o}C, and this may cause some decrease in droplets settling velocities. Air viscosity, which varies from liquid to another, could have the upper hand in controlling velocity changes. For liquid like ethanol, air viscosity increases by 63% when temperature increases from -20 -50^{o}C, and this push the settling velocity down. In other case when Pentane is used, air viscosity increase by about 44% during the same region of temperature. The mean free path of air is inversely proportional with temperature. Its value increases by 36.4%, from by 0.055 to 0.075μm, when temperature increases from -20 to 50^{o}C, and this will lead to some increase for the equation correction factor. Anyway the effect of temperature on slip correction factor is very limited and at best the change is less than 1% which could be not taken into account. Figures (10.12) and (10.13) show the terminal velocity of falling droplets for Ethanol and N-Pentane release, respectively. Air viscosity seems to be the most controlling factors for settling velocity behaviour. Hence, while air viscosity in case of release ethanol increased by 63%, settling velocity of various droplet sizes decreased by nearly 43%. With the same principle when N-Pentane released, settling velocity increased by nearly 68% according to 44% decrease in air viscosity.

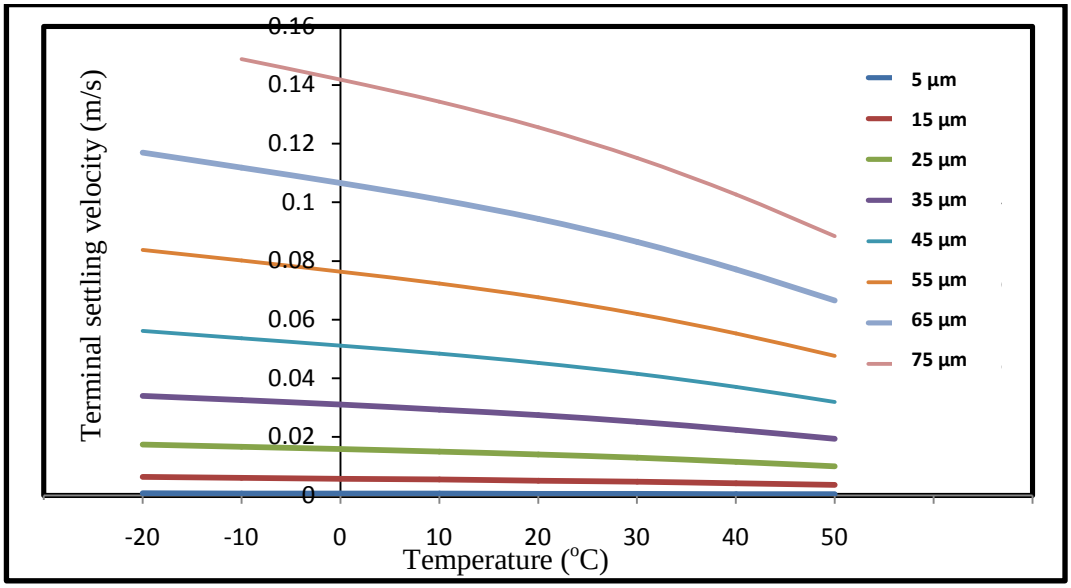

Figure 10.12 Relation between temperature and terminal settling velocity of falling droplets through ambient air saturated with humidity and ethanol vapour

For larger droplets moving under Newton's or intermediate conditions, dependency of settling velocity could be changed. In this case, droplets terminal settling velocity will depend on density of liquid, density of air and drag coefficient of air. During intermediate region, drag is dependent on Reynolds number of air which is affected by air density and viscosity. According to these effects, terminal settling velocity expresses dissimilar behaviours according to released liquid type at different temperatures. When the released liquid is ethanol, terminal velocity will continue decreasing with temperature increase for droplets up to 1950 µm (intermediate region).

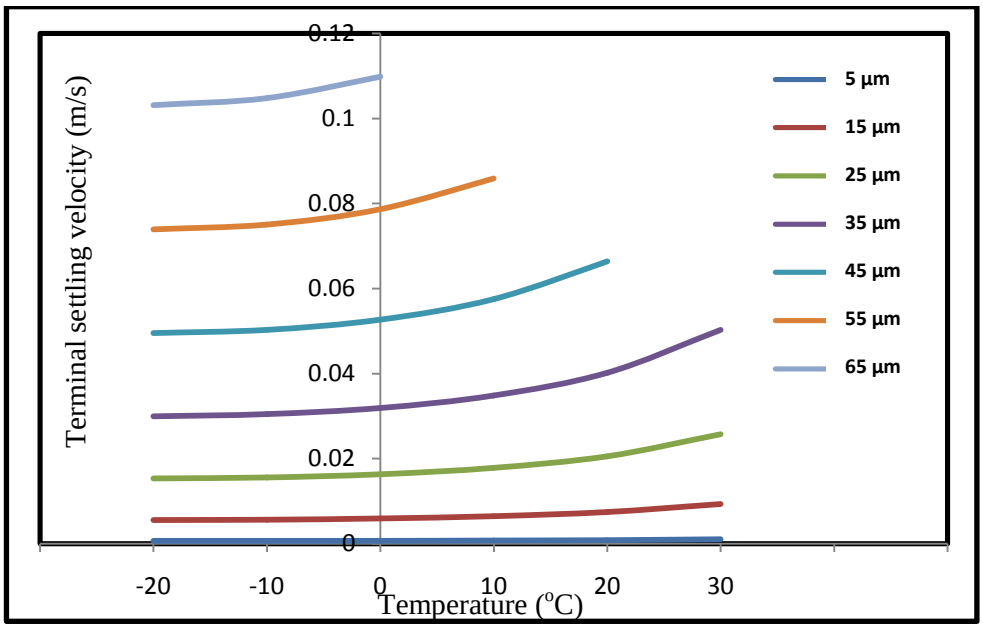

Figure 10.13 Relation between temperature and terminal settling velocity of falling droplets through ambient air saturated with humidity and N-Pentane vapour

This means the decrease effect of liquid density and increasing effect of drag coefficient have exceeded the decreasing effect of air density. Droplets larger than 1950 μm will behave differently; the value of settling velocity will increase until temperature reaches 30^{o}C and then starts to decrease. This behaviour is according to end of drag coefficient effect which becomes constant. In general, the effect of temperature on terminal settling velocity in these two regions is limited and decreases by increasing droplet size.

10.2.3.2 Effect on droplets critical velocity of disintegration

All droplet sizes critical velocities are directly proportional with liquid surface tension and air viscosity. On the other hand, inversely proportional with air density to the power two, i.e. highly affected by air density. As discussed before, liquid surface tension is inversely proportional to temperature for all released liquids. Air viscosity behaves similarly except when ethanol is the released liquid. The density of Air mixed with benzene, pentane and hexane increases when temperature increases, and also toluene at low temperature. On the contrary, when the existing vapour is ethanol or toluene at temperature above 30^{o}C, density will decrease when temperature increases. The estimated values of critical velocities at different temperatures for different released liquids expressed similar behaviour. For all droplet sizes, critical velocity decreased when temperature increased. The difference was just in the rate of this decrease. Ethanol droplet for examples expressed a decrease rates larger than 25% for fine aerosol droplets, around 20% for other aerosol droplets, 15% average decrease for smaller than 1 mm non-aerosol droplets and less than 10% decrease rate for droplets larger than 1 mm. Pentane liquid expresses velocity decrease of about 18% for aerosol droplets and nearly 33% decrease for non-aerosol droplets.

10.2.3.3 Effect on droplets falling time and velocity

The behaviour of falling droplets during release is pretty complicated. It’s dependent on many factors and all of these factors are in different ways affected by temperature changes. As discussed above, settling and critical velocities of various droplet sizes for different fuel liquids are proposed to decrease when temperature increases. Exceptional from this behaviour is the pentane aerosol droplets which terminal velocity increases. Therefore, target velocity to be reached by smaller droplet will be farther, and for large droplets will be closer. This is not only the point of view, whereas droplets falling velocity is dependent on the rate of acceleration or deceleration of these droplets during

falling. The controlling factor of velocity change is the drag force, which is in many ways temperature dependent. To understand this behaviour, detailed comparison study has been performed. The finding of this study could be presented in Table (10.1).

Table 10.1 The behaviour of droplets motion during free-falling due to temperature increase

	Aerosol droplets	Decelerating non-aerosol droplets	Accelerating droplets
Ethanol	Decelerating time is negligible. Terminal velocity decreases hence falling time increases.	Deceleration rate increases when temperature increased. Time and distance of deceleration decreased. Falling time increases.	Acceleration rate is maximum at temperature between 20-30^{o}C. Falling time still increases and becomes negligible for droplets larger than 2550μm.
N-Pentane	Decelerating time is negligible. Terminal velocity increases hence falling time decreases.	Deceleration rate increases when temperature increased. Time and distance of deceleration decreased. Falling time increases.	Acceleration rate decreases when temperature increased. Falling time increases and becomes negligible for droplets larger than 650μm.
Toluene	Decelerating time is negligible. Terminal velocity decreases hence falling time increases.	Deceleration rate is lowest at 40^{o}C. Falling time increases.	Acceleration rate is maximum at 20^{o}C. Falling time is negligible

10.2.3.4 Effect on particle distribution of daughter droplets

According to the above discussion, it's clear that increasing temperature will generally lead to decrease both settling and critical velocities. Therefore, it's expected that more droplets will be subjected to disintegration after jet breakup and during droplets falling, and maximum size of falling droplets will get smaller. This further disintegration will produce larger amount of aerosol droplets in air. In addition, average diameter of generated daughter droplets will be affected by temperature change. Sauter mean diameter of probably disintegrated droplet is inversely proportional to both liquid and air densities, and directly proportional to air viscosity. Figure (10.14) presents the effect of temperature change on the ratio between Sauter diameter of daughter droplets and initial diameter of mother droplet. According to the results, it's easy to say that increasing temperature decreases saunter mean diameter of generated daughter droplets.

The highest decrease rate of 69.7% was expressed by ethanol, where the lowest rate expressed by Pentane was 16.1%. This behaviour supports generation of larger amount of aerosol droplets.

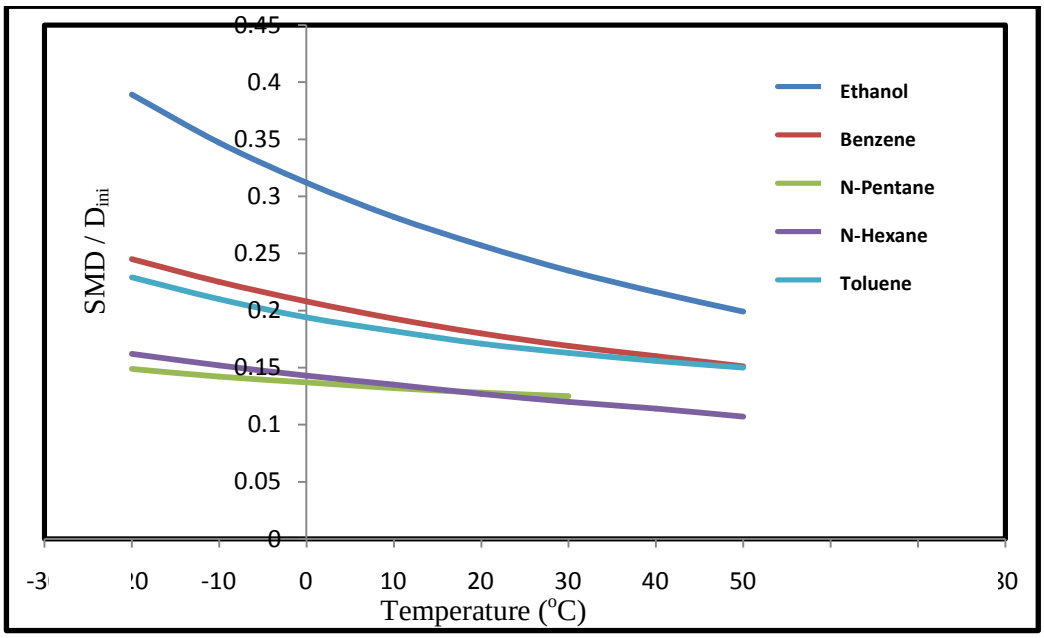

Figure 10.14 Temperature effect on sauter mean diameter of daughter droplets generating from 2950μm of different fuel drops

The discussion clearly shows that ambient temperature is a very important factor which could increase the amount of generated aerosol. In current example, most of the temperature effect through increasing aerosol fraction appeared during the first step of droplets disintegration and directly after jet breakup before the end of release primary stage. This happened because release velocity is relatively close to the lower limit of likely breakable droplets velocity. Hence, most of the likely breakable droplets are expected to undergo disintegration during primary stage. Figure (10.15) presents the effect of temperature change on percentage of aerosol generated from N-Pentane fuel release.

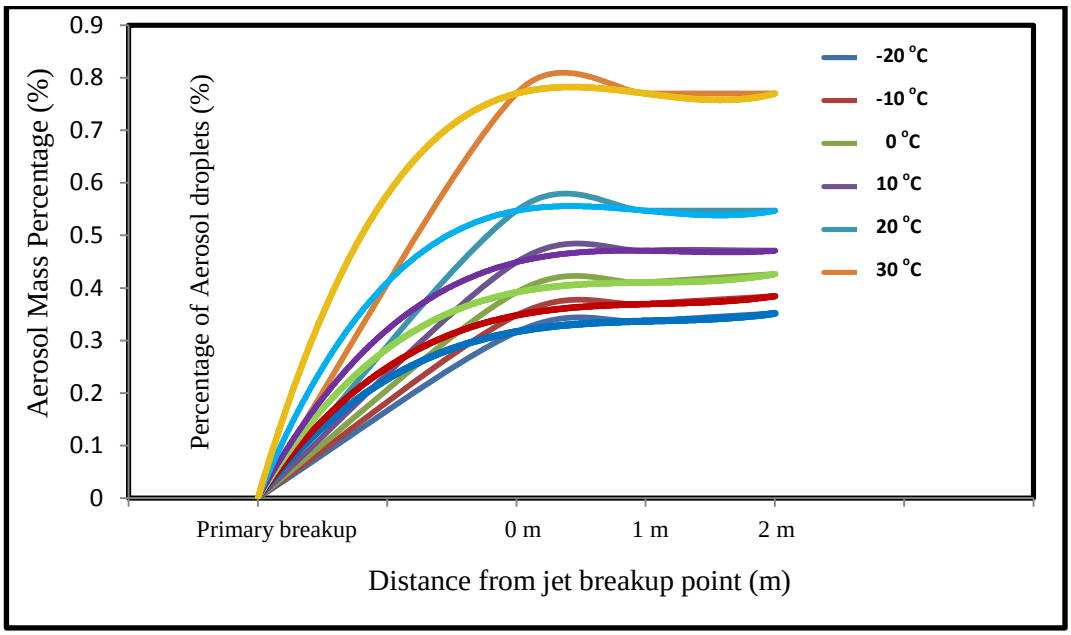

Figure 10.15 Development of aerosol percentage generated from liquid Pentane releasing from 20 mm orifice at saturated conditions and velocity of 6 m/s at different temperatures

10.2.4Effect of temperature on liquid droplets impingement

The effect of temperature on splashing of impinged droplets could appear in two different ways. First way is the effect on spread-splash transition of impinged droplets. Splashing parameter (K) depends on Weber and Reynolds numbers of falling droplets. The second way is the effect on mean diameter and size distribution of daughter droplets which also depends on Weber and Reynolds numbers. In addition, size distribution of falling droplets, which are likely to splash, is a dominant factor in controlling sizes of resulting droplets after splash.

Temperature effect on droplets spread-splash transition.

Both Weber and Reynolds number of liquid droplets increase with temperature increasing. On the other hand, temperature effect on terminal velocity of liquid droplets may limit this increase because terminal velocity is inversely proportional with temperature. Therefore, behaviour of splash parameter according to temperature change is expected to be a competition between these two opposite effects. Parameter of ethanol droplets for example expressed a steady increasing during temperature increase. This increase had allowed droplets of 650µm after 20^{o}C to transfer from spreading to splashing region. Hence, it will support generation of fine droplets after splash while this droplet size was forming about 2.4% of total droplets population at 20^{o}C and it has reached about 3.3% at 50^{o}C. A same behaviour had been achieved for 550µm and 2.5%

toluene droplets after 50^{o}C. No change has been achieved for the droplets of the three other liquids in this study. But we have to keep in mind that droplet size distribution interval is 100µm. if the interval is narrower, a change may be achieved.

10.2.4.1 Temperature effect on mean diameter of daughter droplets

According to the empirical equation for estimating mean diameter of daughter droplets, diameter is dependent on Weber number, Reynolds number and mother droplet size. As discussed before, behaviour of these numbers is a competition between physical properties changes which push to increase, and the effect of terminal velocity which pulls to decrease. This challenge in not similar for all type of liquids. Weber number of Ethanol liquid droplets upon impingement has a maximum value at temperature near 10^{o}C, where Reynolds number is always increase during temperature increase. Toluene droplets are not similar which have Weber and Reynolds numbers always increasing. for pentane droplets its away from this behaviour, Weber number increases with temperature for droplets up to 1050µm, have a maximum value for droplets between 1150-1850µm at temperature between -10 - 20^{o}C and then starts to decrease with temperature increase for larger droplets. On the other hand, Reynolds number increases with temperature for droplets up to 1250µm and for larger droplets it's always have a maximum value at temperature between 10 - 20^{o}C.

The other important factor is the mother droplets sizes. Increasing temperature as mentioned above may push some droplets to splash rather than spreading, and this could enhance the fraction of aerosol daughter droplets. In addition, particle size distribution of splashed mother droplets is shifted for smaller values at higher temperature, and this also will produce larger fractions of aerosol droplets. Figure (10.16) presents the droplets size distribution of mother droplets just before impingement for ethanol and toluene liquids as examples.

According to all discussed factors affecting the droplets size distribution, it's not easy to expect the impact of temperature change on the population of aerosol droplets after splash. The factors are too many and each fuel liquid has its own scenario. Figure (10.17) presents the impact variation of temperature change on the fraction of aerosol droplets generated after splash for different examples of fuel liquids. It's clear from the figure that all liquid fuels except n-pentane have expressed increasing in aerosol fraction after splash when temperature increased. This increase has varied from just 3% for n-hexane, 60 and 84% for benzene and toluene and reaching nearly 11 times increase for the case of ethanol. N-pentane expressed 13% decrease when temperature is raised to

30°C. In general, all liquid fuels expressed more than 50% fraction of aerosol droplets at high temperature after splash.

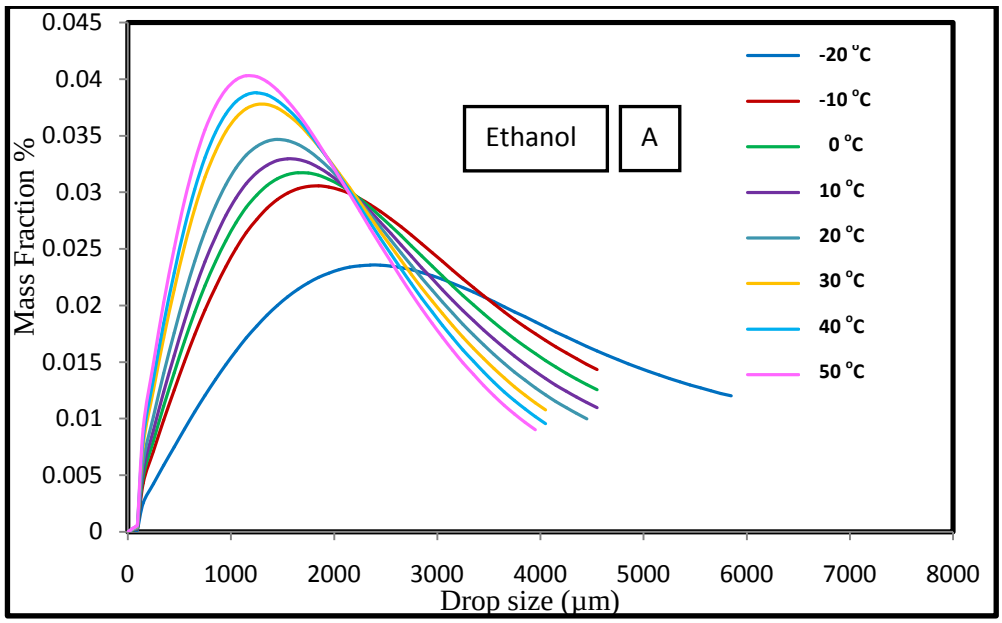

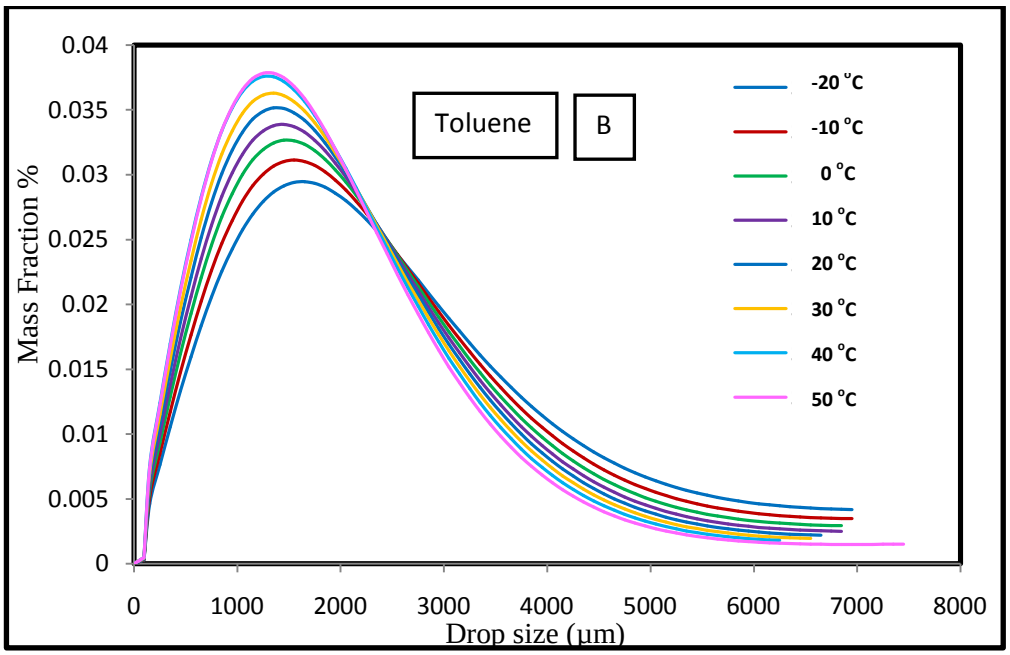

Figure 10.16 Droplets size distribution of mother droplets just before impingement for ethanol (A) and toluene (B) liquid droplets at temperature range from -20°C to +50°C

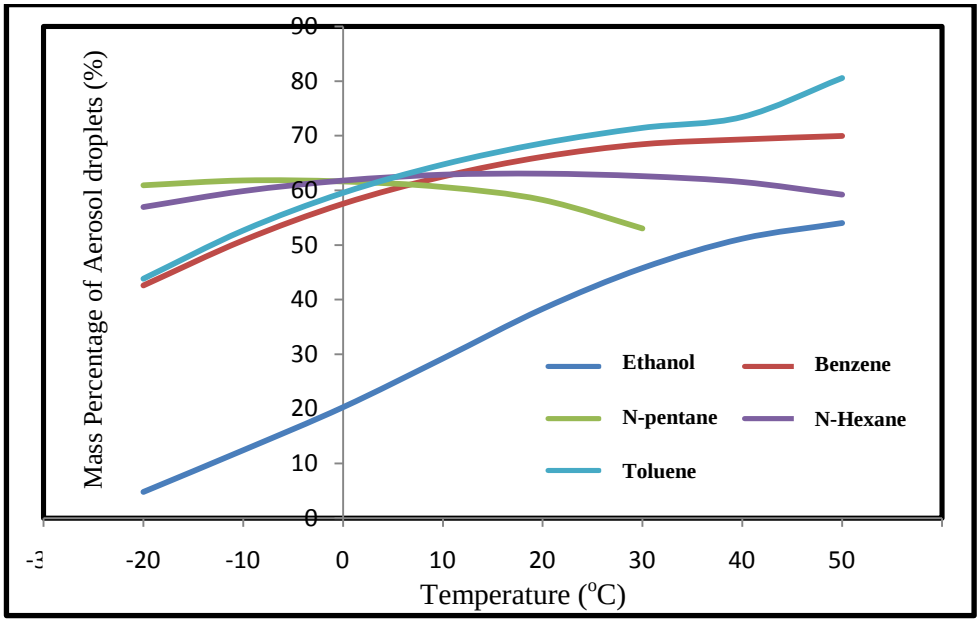

Figure 10.17 Effect of temperature change (from -20°C to +50°C) on percentage of aerosol droplets generated after splashing from different fuel liquids

10.2.5 Effect of Temperature and Saturation Vapour Pressure on Approaching Flammability

The saturated vapour pressure is a specific property for each liquid fuel. It gives an idea about the maximum volume fraction which could be occupied by the fuel vapours inside the air mixture volume. This property is directly proportional to liquid temperature, i.e., fuel vapour may occupy a larger volume percentage at higher temperatures.

For example, the saturated vapour pressure of N-hexane at 0°C is nearly 0.05993 bars. This means, at normal ambient pressure of 1 bar and temperature of 0°C, N-Hexane vapours cannot occupy more than 5.993% of the total air mixture volume. According to the high molecular weight of hexane, this ratio is equal to 15.971% of the total air mixture mass.

During accidental fuel releases, and when fuel vapour starts to become a component of air mixture, volume and mass fractions of fuel vapours start to increase gradually. Then, step by step, the air mixture containing fuel vapour becomes more and more saturated. During this scenario, a certain critical time may appear on the surface when the vapour volume fraction exists in between the flammability limits. Which means the fuel-air mixture is ready to burn or maybe explode.

It's very important at this time to assess the hazard potential of any accidental release depending on liquid fuel type and existing temperature. Table (10.2) expresses the

relation between vapour saturation level and both the mass and volume fractions of N-hexane vapour at 0^{o}C.

Table 10.2 Relation between fuel vapour saturation level, gas mixture density, vapour volume fraction and vapour mass fraction for N-Hexane vapour at 0^{o}C

Fuel Vapour Saturation (%)	Vapour Cloud Density (kg/m^3)	Volume Percentage of Hexane Fuel Vapour (%)	Mass Percentage of Hexane Fuel Vapour (%)
0	1.290	0	0
10	1.305	0.599	1.766
20	1.321	1.199	3.490
30	1.336	1.798	5.175
40	1.351	2.397	6.822
50	1.367	2.997	8.432
60	1.382	3.596	10.007
70	1.397	4.195	11.547
80	1.413	4.795	13.053
90	1.428	5.394	14.528
100	1.443	5.993	15.971

The N-hexane has a flammability limits between 1.2% and 7.7 v/v$_o$ (Appendix. A1), and a stoichiometric ratio of about 2.2% v/v$_o$ (Atkinson and Gant, 2012a). The data shown in table (10.1) proves that hexane vapour may reach the lower flammability limit at a vapour saturation level between 20% and 30%, but will never reach the upper flammability limit at this temperature. The gas mixture could be around the stoichiometric ratio at a saturation level between 30% and 40%.This means, the N-hexane vapour during release becomes very dangerous starting from a saturation level of nearly 20% till reaching the fully saturation level.

This behaviour could change at different temperatures; the flammability limits maybe achieved at different saturation levels. Furthermore, the whole story may become change from this when another liquid fuel is used. Figure (10.18) expresses the values of the maximum vapour volume fraction for five different liquid fuels at different temperatures ranging from -20 to +50^{o}C.

Benzene, for example, has a lower flammability limit of nearly 1.4%. According to the value of benzene's saturated vapour pressure, this volume fraction could not be reached below-14.7^{o}C. Hence, a benzene air mixture is safe and not flammable at temperatures below this point. Above this temperature, the cloud will be flammable between two limits of saturation as expressed in Fig (10.19). In addition, while the temperature increases, the distance between those limits will get narrower; this means less chance of being flammable. At 50^{o}C, a benzene vapour cloud is only flammable if the vapour saturation is between 3.9% and 19.7%.This means continuing evaporation

will give a high possibility of being rich and hence not flammable. The best temperature region for supporting benzene /air mixture flammability might be between 0 - 25°C.

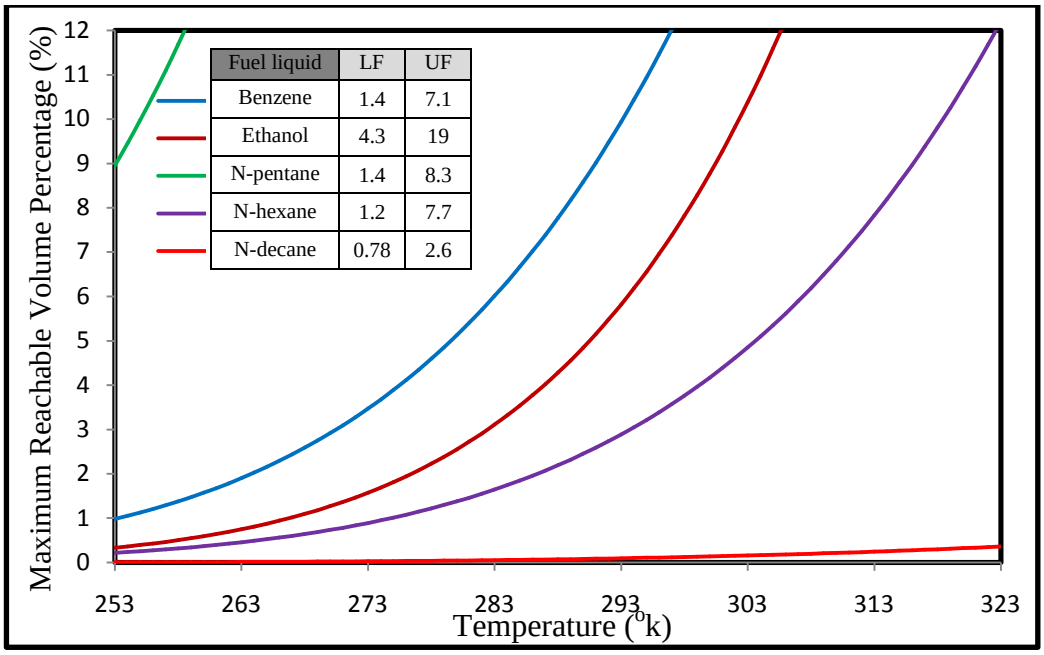

Figure 10.18 Maximum Reachable vapour volume fraction for five different fuel liquids at different temperatures ranging from253 to 323°K (-20 to +50°C)

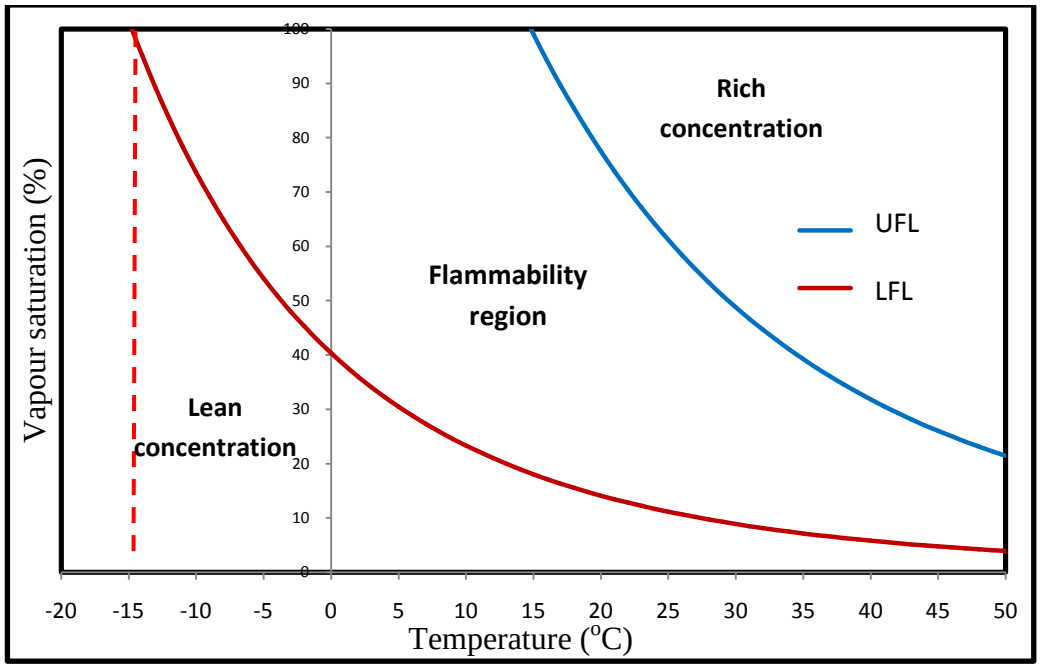

Figure 10.19 Relation between vapour saturation level and flammability limits for Benzene vapour at different temperatures ranging from -20 to +50°C

This behaviour is different for other liquid fuels such as ethanol. The relation between vapour saturation and flammability at different temperatures (Fig. (10.20)) shows that an ethanol vapour cloud cannot be flammable below15.1°C. Above this temperature, the vapour saturation level becomes more supportive for flammability during temperature increase.

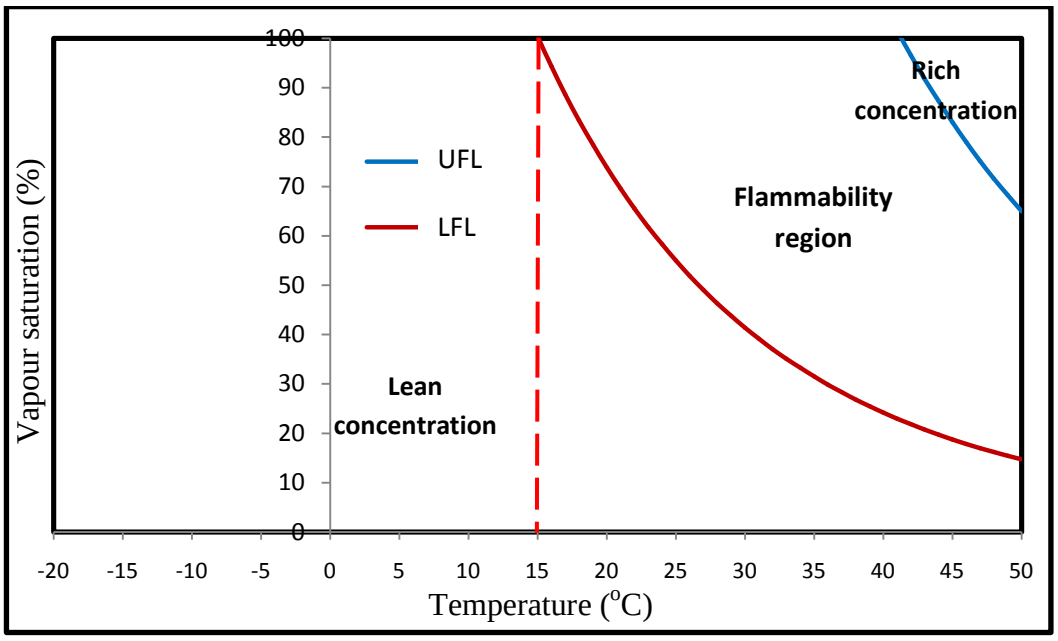

Figure 10.20 Relation between vapour saturation level and flammability limits for Ethanol vapour at different temperatures ranging from -20 to +50°C

The relation between the vapour saturation level and flammability limits for N-Pentane, expressed in Figure (10.21), is completely different. The N-pentane fuel is characterized by relatively high saturated vapour pressure values. The relation expressed by Figure (10.20) shows that all temperatures ranging between -20 and +50°C could support pentane flammability. The chance of its being flammable starts to decrease at higher temperatures because the vapour concentration becomes very rich.

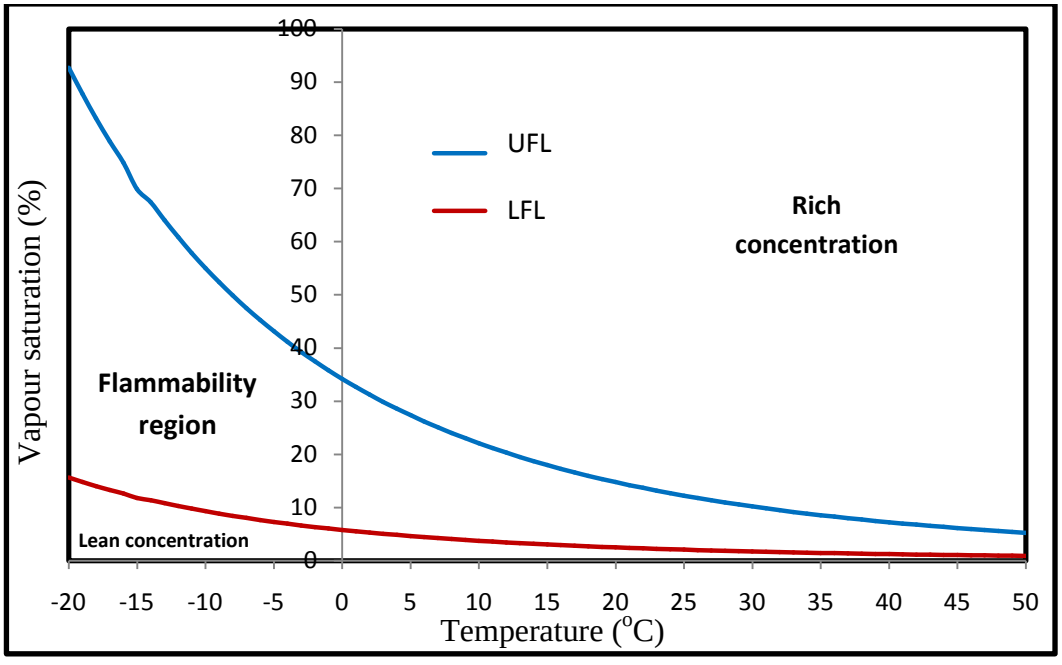

Figure 10.21 Relation between vapour saturation level and flammability limits for N-pentane vapour at different temperatures ranging from -20 to +50°C

According to the results expressed by figures from (10.18) to (10.20), the relation between the vapour saturation level and the flammability limits could appear in different ways depending on released liquid type. In general, flammable materials which are characterized by high values of saturated vapour pressure are expected to support flammability better at lower temperatures. On the contrary, liquids characterized with lower saturated vapour pressure values could have a better chance to form flammable clouds at higher temperatures.

10.3 Effect of Humidity

The expected effect of humidity change on the mechanisms of liquid breakup is through its impact on air density and viscosity. And it's logical to believe that the effect of humidity maybe more influential when fuel vapours are absent or of low concentrations. And it's also likely to believe that this impact could be more effective when temperature is higher, therefore amount of vapour content in air will be larger. To investigate and assess the size of the role played by humidity, air properties had been compared at different humidity conditions and different temperatures. Figures (10.22) and (10.23) express the variation in air density and viscosity for six different examples. Results obtained from these examples could be expressed as following:

1-Regarding air density change:

- Depending on ethanol vapour saturated conditions, changing relative humidity from 0 to 100% caused a density change of 0.09% at -10^{o}C, 0.84% at 20^{o}C and 4% at 50^{o}C.
- Substituting ethanol with toluene which is twice the molecular weight gave a density change of 3.7% at 50^{o}C.
- Depending on 50% ethanol vapour saturation, changing relative humidity from 0 to 100% caused a density change of 0.86% at 20^{o}C and 4.3% at 50^{o}C.

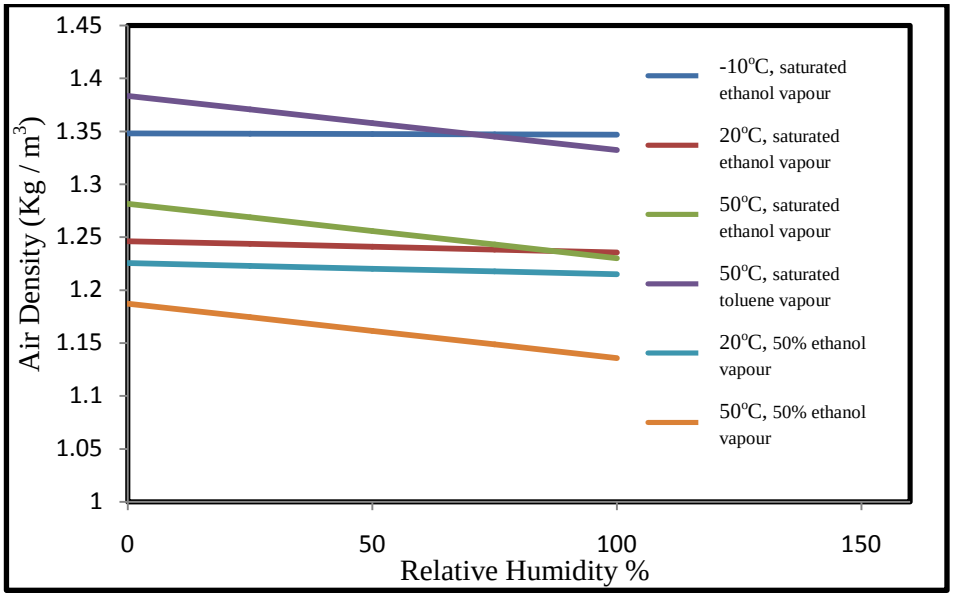

Figure 10.22 The impact of relative humidity changes on density of air mixture

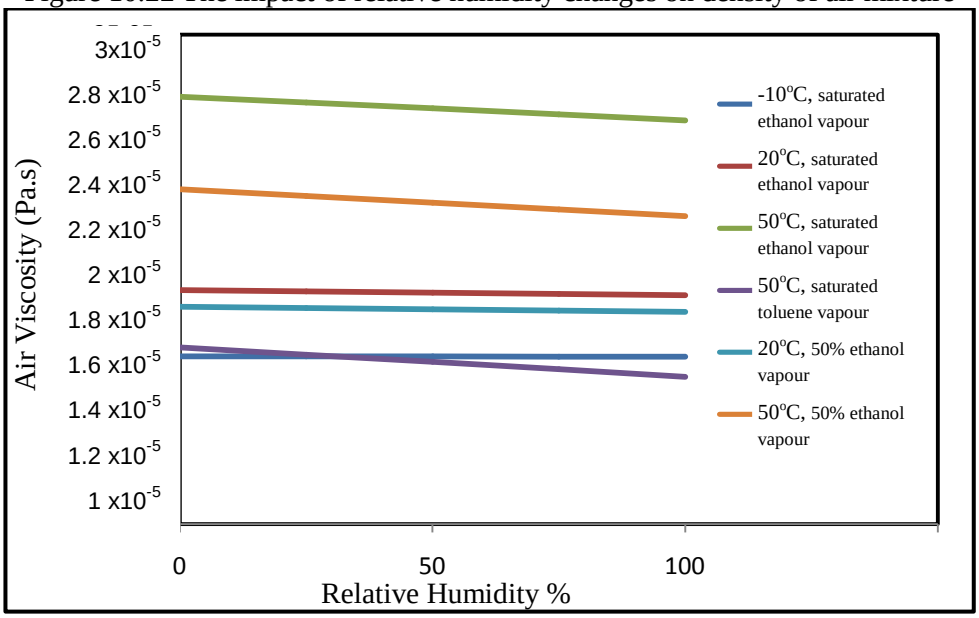

Figure 10.23The impact of relative humidity changes on viscosity of air mixture

2-Regarding air viscosity change:

- Depending on ethanol vapour saturated conditions, changing relative humidity from 0 to 100% caused a viscosity change of 0.14% at -10°C, 1.1% at 20°C and 3.5% at 50°C.
- Substituting ethanol with toluene gave a density change of 7% at 50°C.
- Depending on 50% ethanol vapour saturation, changing relative humidity from 0 to 100% caused a density change of 1.1% at 20°C and 4.6% at 50°C.

The above results shows that effect of relative humidity on physical properties of air mixture is generally limited even at high temperatures and using a high molecular weight fuel liquid. To discuss the impact of these changes on the mechanism of liquid

breakup, example of toluene fuel at 50^{o}C will be chosen as it seems to express the largest impact on physical properties of air mixture.

Whereas no changes in liquid properties in this case, the influence of air physical properties does not extend to all parts of liquid breakup mechanism. Density of air plays a role in determining the primary breakup regime of liquid jet, determining terminal and critical droplets velocities and estimating daughter droplets sauter mean diameter for disintegrated droplets. Air viscosity effect is limited by determination of droplets terminal velocities. Variation of different parameters is discussed in Table (10.3) depending on minimum and maximum values of relative humidity (0,100%), 50^{o}C and liquid toluene as the released liquid fuel.

Table 10.3 Effect of relative humidity on different parameters of liquid toluene breakup mechanism at 6 m/s release from 20mm orifice diameter, at 50^{o}C and saturated fuel vapour

Humidity (%)	Air density (kg/m^3)	Air viscosity (Pa.s)	We_A	Breakup regime	Breakup length (m)	D_{max} (µm) after jet breakup	D_{max} (µm) after drop breakup
0%	1.383	1.72E-05	39.82	SWI	4.298	81329	9050
100%	1.332	1.6E-05	38.34	SWI	4.298	81329	9450
	Percentage of aerosol droplets after jet breakup	Percentage of aerosol droplets after drop breakup	Percentage of aerosol droplets after 1st meter	Percentage of aerosol droplets after 2nd meter	Percentage of aerosol droplets after 3rd meter	Percentage of splashed droplets of falling droplets	Percentage of aerosol droplets from splash
0%	0.001%	0.234%	0.266%	0.284%	0.299%	89.1%	73.3%
100%	0.001%	0.226%	0.258%	0.278%	0.292%	92.2%	75.4%

Calculation results in Table (10.3) expressed that increasing relative humidity from 0 to 100% has decreased air density of about 3.7% and air viscosity of nearly 7%. These changes have decreased the air Weber number by 3.7%. No updates occurred for breakup regime, breakup length, aerosol droplets fraction or maximum droplet size after primary breakup. Droplets critical velocity of disintegration has increased of about 1.9%, where terminal settling velocities have been increased by 5-7% for aerosol droplets, about 3% for non-aerosol droplets up to 1950µm and about 1.9% for larger droplets. The impact of this increase was larger size of maximum droplet diameter after secondary breakup. Hence, smaller amount of aerosols generated of nearly 2-3%. The

percentage of splashed droplets was 89.1% of total falling droplets when humidity is absent, and increased to 92.2% when water vapour is fully saturated. And finally, nearly 2.9% increase in aerosol droplets generated after splash. Therefore, it could be seen that variation of relative humidity in best cases is found but still limited.

10.4 Effect of Fuel Vapour Saturation

Fuel vapour saturation is one of the most dominating factors during liquid jet breakup procedure. Not only because it's one of the most important factors controlling air properties, but also because it's the most influential factors on droplet evaporation during free-falling. Although evaporation is not a part of liquid breakup mechanism, both of them are working in parallel and strongly attached with each other. Droplets evaporation modifies droplets size distribution and ambient conditions continuously during falling, leading to major changes in breakup scenario. On the other hand, behaviour of droplets disintegration and resulting droplets size distribution control droplets evaporation rate.

When accidental fuel release starts, fuel vapour saturation at the beginning is assumed to be nil inside release area. With the passage of time, vapour concentration will be built up and could reach saturated condition. Degree of vapour saturation inside this area is dependent on the ration between vapour generation rate and dilution rate, and this could be a part of the dispersion mechanism.

During this part of the study, there are two basic directions to investigate. First direction is the effect of fuel vapour concentration on properties of air mixture, which may influence different parameters during breakup mechanism. And the second direction is the relation between vapour concentration and rate of droplets evaporation. It is worth mentioning that evaporation rate is also dependent on ambient temperature.

10.4.1 Effect on physical properties of air mixture

Earlier in this chapter, the effect of increasing fuel vapour content through temperature increase on air density and viscosity was discussed in (10.2.1.4) and (10.2.1.5). In this section, the effect of increasing fuel vapour content will be studied at constant temperature. This means no change in gases properties and no change in water vapour content. The only factor affecting now is the specific properties of released liquid vapour when vapour saturation is increased. Gas properties, which had been discussed before, show that all fuel vapour densities are larger that dry air. Hence, increasing fuel vapour saturation should increase air mixture density. On the contrary,

all fuel vapours expressed in this study have viscosity lower than dry air except for ethanol vapour. Therefore, increasing vapour saturation is supposed to decrease air mixture viscosity. Figures (10.24) to (10.27) present the variation of air density and viscosity when vapour saturation is varying from 0 to 100% at different condition examples.

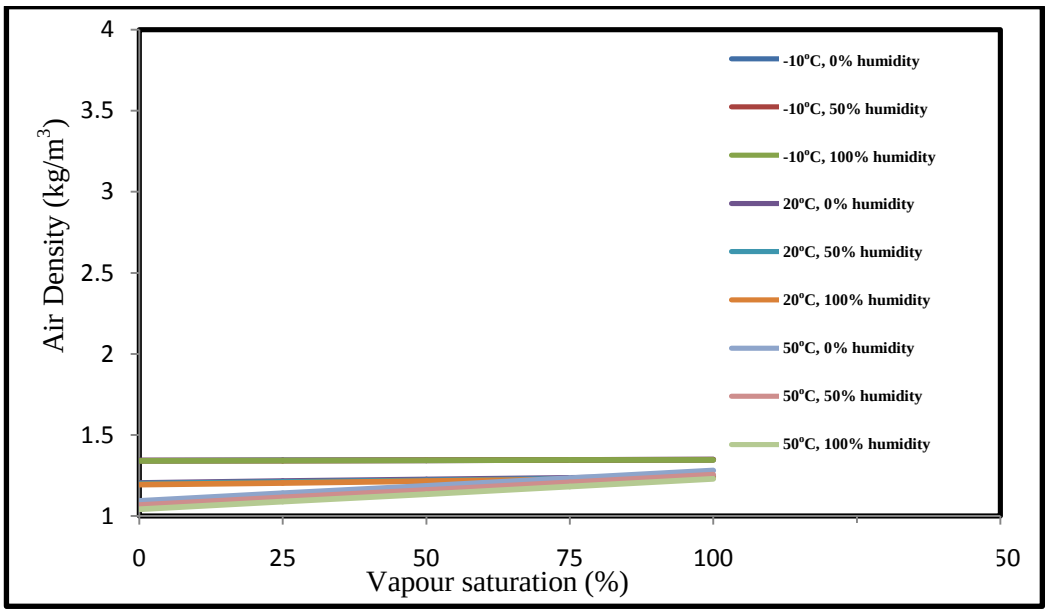

Figure 10.24 Effect of ethanol vapour saturation increase on air mixture density at three different temperatures (-10, 20 and 50°C) and three different relative humidity's (0, 50 and 100%)

Figure (10.24) expresses air mixture density at five increasing values of ethanol vapour saturation at 0,25,50,75 and 100%. The values were estimated at three different temperatures (-10, 20 and 50°C) at three different relative humidity values (0, 50 and 100%). Estimated values, which have been expressed by the figures, show that:

- Typical to what had been discussed before, air mixture density increases when vapour saturation increases according to fraction increase of higher densities fuel vapours.
- Rate of increase with respect to vapour saturation in higher at higher temperatures where fuel vapour mole fraction is larger at higher temperatures. At -10°C, regardless of relative humidity the change in air density was about 0.4% when vapour saturation increased from 0 to 100%. Where at 50°C the change had reached values between 17.3 and 18.1% according to relative humidity value. This increase causes a similar increase for the values of air Weber number, and pushing the jet disintegration toward higher degrees. At low temperatures it's not expected for this amount of change to cause regime transfer from case to another, but this could be probable at high temperatures.
- Increasing relative humidity has slightly decreased the values of air density but didn't make change on density increase rate.

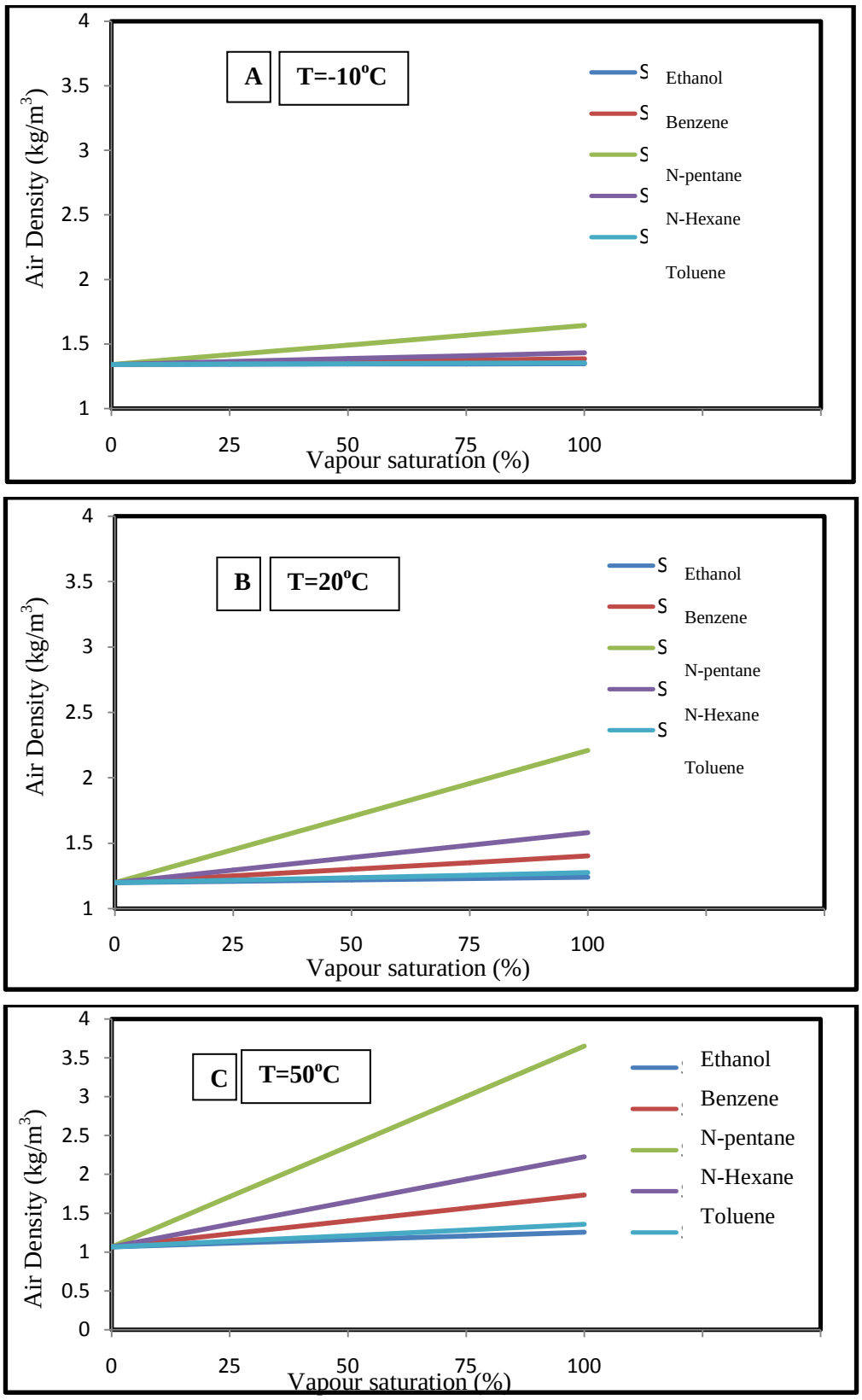

Figure 10.25 Effect of different fuels vapour saturation increase on air mixture density at three different temperatures (-10, 20 and 50°C) and 50 % relative humidity)

In figure (10.25), the effect had been studied for the five different fuel liquids at three different temperatures and relative humidity had been assumed at 50% as an average value. As mentioned before, disparity between air mixture densities for different liquid

fuels is due to differences in molecular weights and saturated vapour pressure values. This disparity is seems to appear more clearly at higher temperature because variation in vapour pressure becomes wider. Hence, increasing temperature expresses the effect the effect of vapour saturation increase obviously.

Figures (10.26) and (10.27) are the same studies but for viscosity discussion. The same conclusions for air density had been drawn for viscosity. Figure (10.26) expresses the role of temperature to declare the effect of vapour saturation on air viscosity. Viscosity increase was about 0.8% at -10^{o}C regardless humidity value. At 50^{o}C, this value had reached 40 to 44.3% according to humidity value. The role of humidity is seemed to be negligible at the lowest temperatures and about 10% of the value at the highest one. Figure (10.28) had confirmed the role of temperature in representing the effect of vapour saturation on air mixture viscosity.

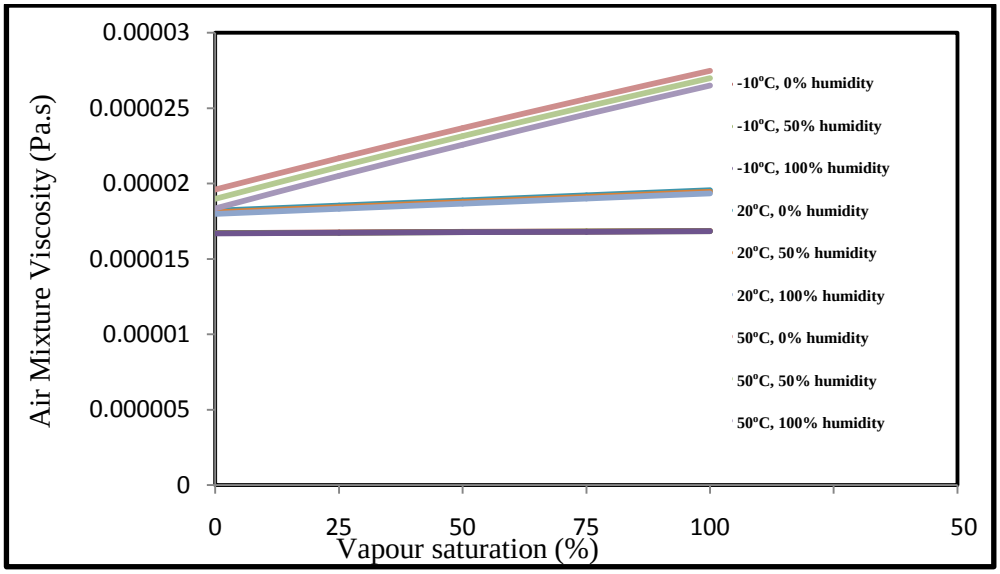

Figure 10.26 Effect of ethanol vapour saturation increase on air mixture viscosity at three different temperatures (-10, 20 and 50^{o}C) and three different relative humidity's (0, 50 and 100%)

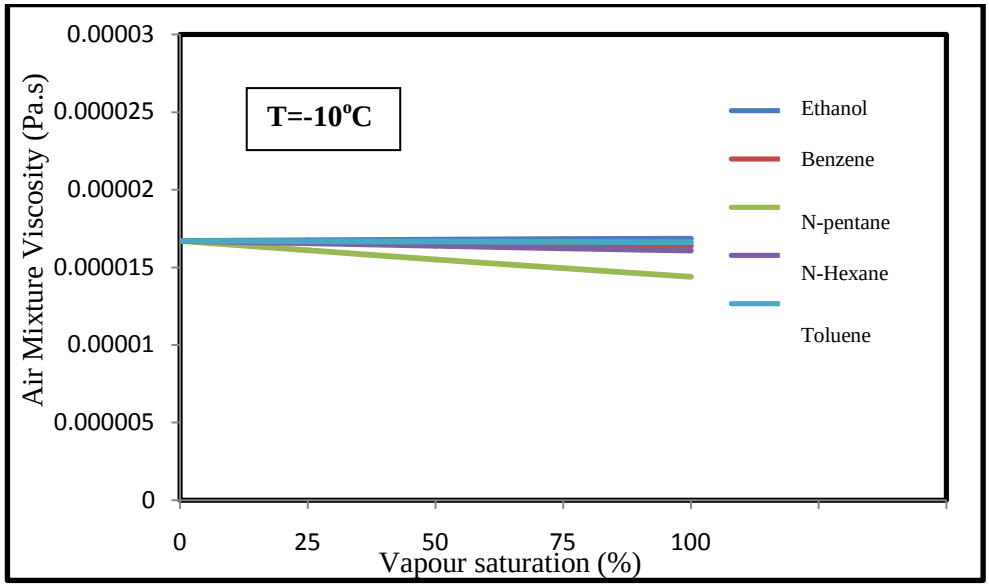

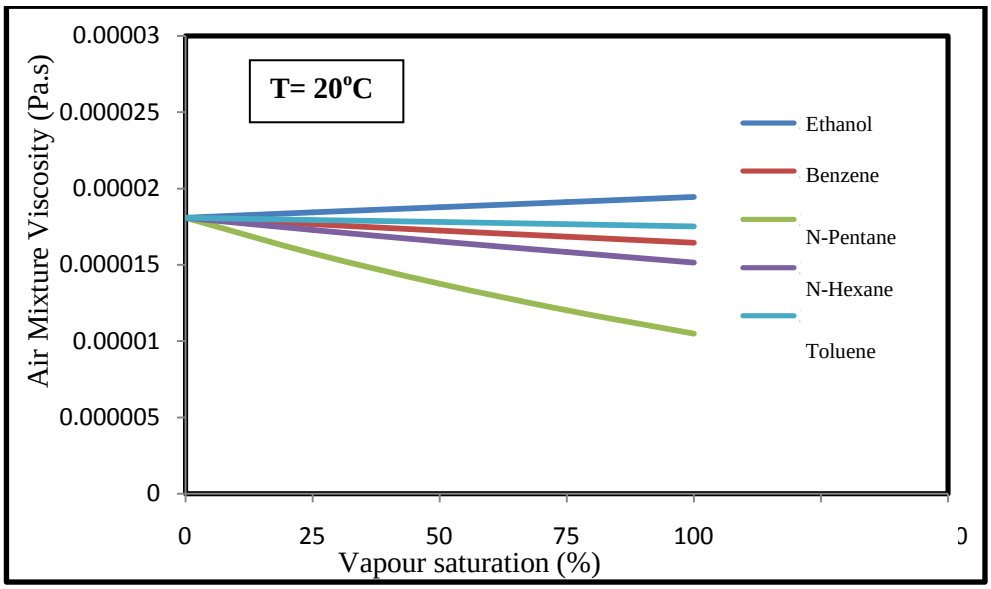

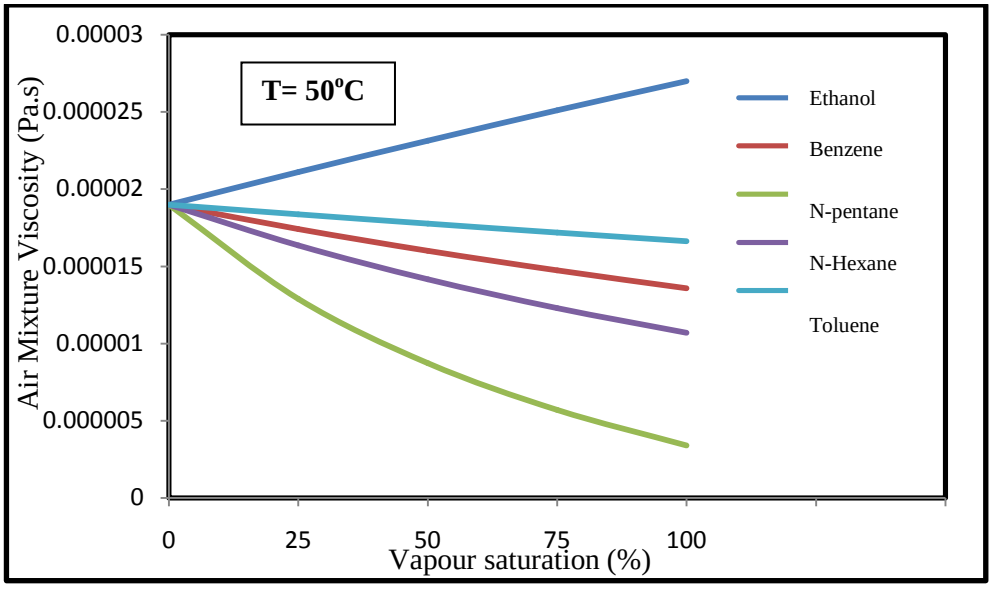

Figure 10.27 Effect of different fuels vapour saturation increase on air mixture viscosity at three different temperatures (-10, 20 and 50°C) and 50 % relative humidity)

10.4.2 Effect on Droplets Evaporation Rate

During studying the liquid breakup mechanisms in accidental fuel releases, a small region around release point is usually under scope where most of the action takes place inside. In most cases, this region has conical shape. Jet breakup and droplets disintegration take place inside this region, and droplets during falling are also a good source of fuel vapours. Consequently at this case, we can admit that this region is a main source of aerosol droplets and fuel vapours. These liquid and vapour species will disperse later in the whole release site.

When release mechanism starts and droplets evaporation starts to take place, vapour saturation will be very low. At this case, evaporation rate will assume to be of highest rate at proposed temperature. This evaporation will build up the vapour saturation and as a result evaporation will get slower. If the region gets saturated with fuel vapour, droplets evaporation could temporarily stopped. During release process, vapour saturation inside this region could be mutable depending on environmental conditions. Although release region could be stable and isolated from outer influences, infiltration of generated aerosols and vapours to outside areas will continue according to wind motion and Brownian motion of different particles. It's logically acceptable that vapour saturation inside release region should be of high values during release process. However, evaporation rate is studied in this chapter at various saturation values.

10.4.2.1 Impact of vapour saturation on generated vapours fraction

Evaporation of droplets is dependent on many factors. One of these factors is the partial pressure of fuel vapour in surrounding air mixture. It is also dependent on ambient temperature, droplet diameter and physical properties of both liquid and gases.
To investigate the relation between fuel vapour saturation and the amount of vapour generated from falling droplets, mass percentage of vapours compared to the total released liquid mass had been estimated at different saturation values of 0, 25, 50, 75 and 100%. Figure (10.29) shows the decrease in mass percentage of generated ethanol fuel vapour with respect to vapour saturation increase at three different temperatures. One of the important clear points regarding these results is the irregular curve slope, where decrease rate seems to be minimal between 25 and 50% saturation values. The maximum rate of decrease appears during first interval (0-25%) and the last interval (75-100%). this behaviour was also typical for other fuel liquids examples. At higher temperatures, variation in vapour saturation values becomes clearer. Figure (10.30)

expresses the variation in vapour mass fraction with respect to vapour saturation for the five different fuel liquids at three different temperatures.

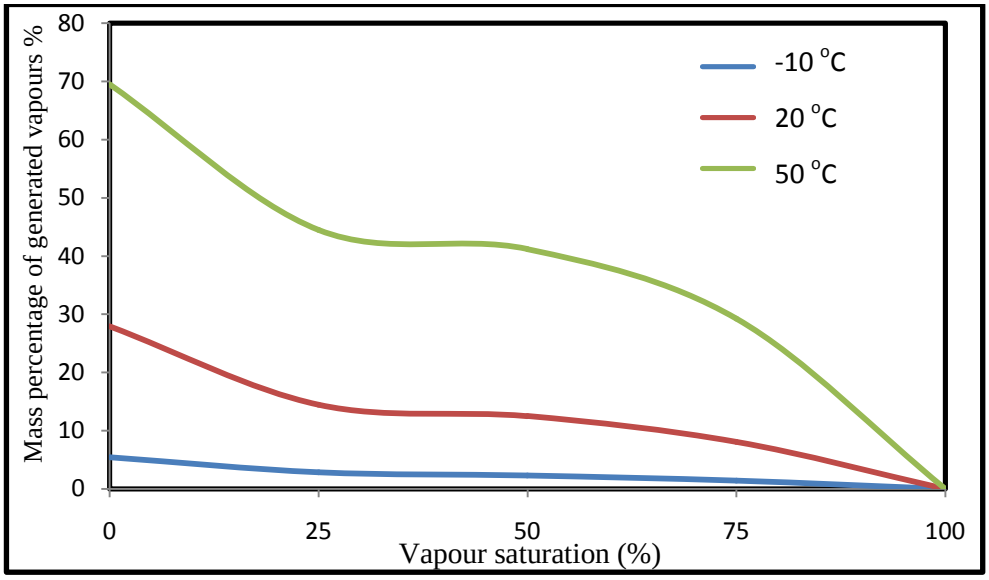

Figure 10.28 Effect of vapour saturation on mass percentage of ethanol vapours generated at three different temperatures

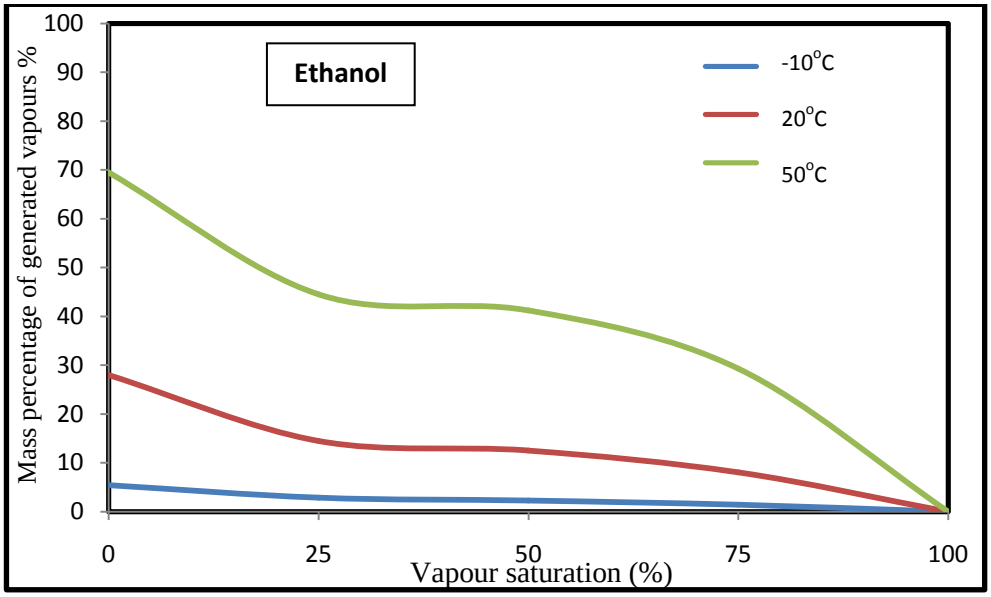

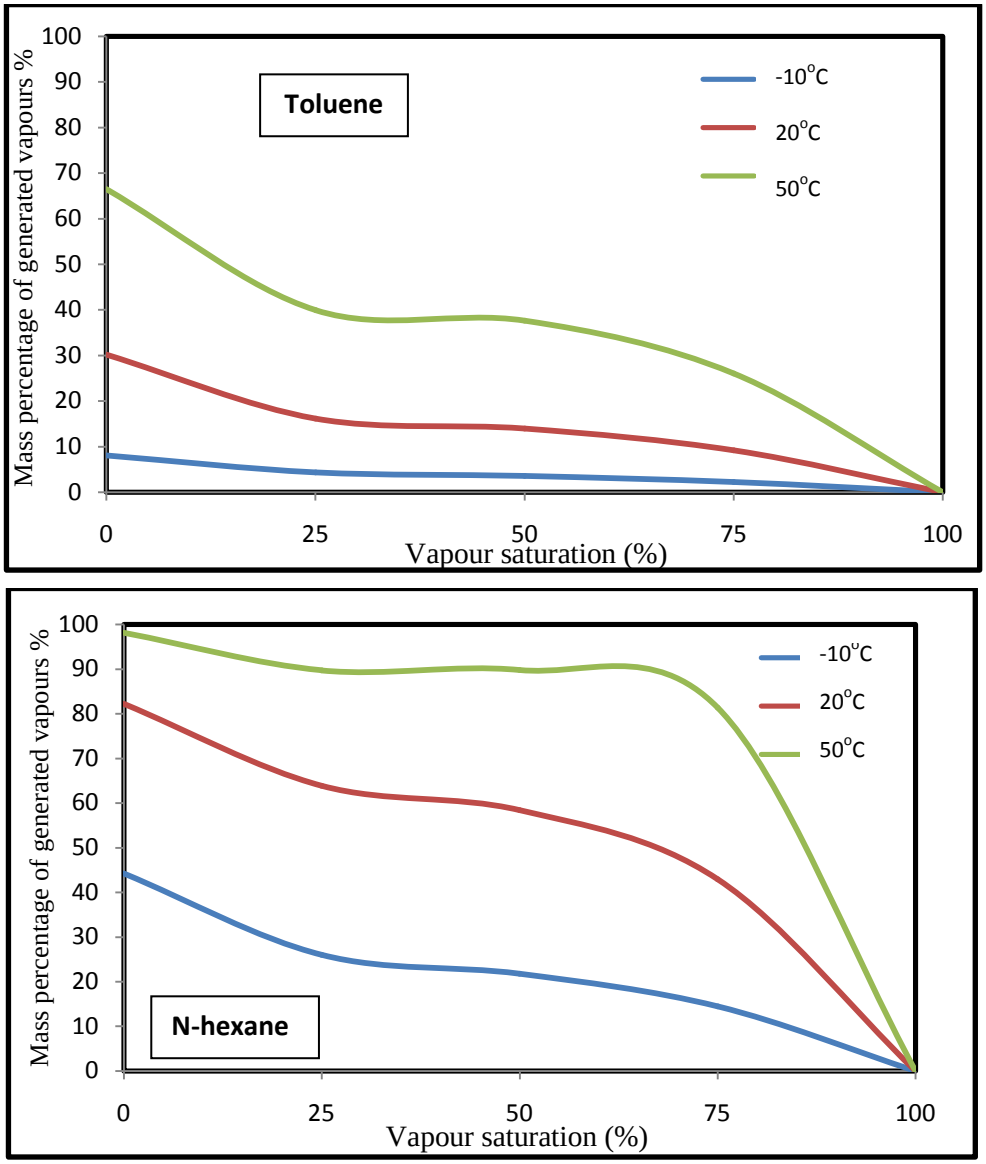

Figure 10.29 Effect of vapour saturation on mass percentage of vapours generated at three different temperatures for different liquid fuels releases

The results expresses by this figure confirms the findings of figure (10.29). In addition, some notes could be written as comment on this comparison as follows:

- The ranking of fuel liquid according to percentage of vapours generated during droplets falling is similar that for saturated vapour pressure of them, except in toluene case where amount of vapours became larger than ethanol. This note shows that the value of liquid saturated vapour pressure is the most effective property in controlling evaporation behaviour during droplets free-falling.
- At relatively high temperatures, amount of vapours generated from liquid droplets seems to be independent on vapour saturation value. Pentane for example gave the maximum amount of vapours independently at 20°C when

vapour saturation varied from 0 to 75%. At 50^{o}C, hexane fuel had shared pentane the same behaviour of independency on saturation value.

- High saturated vapour pressure liquids gave huge fractions of vapours during droplets free-falling, even at low temperatures and high vapour saturation values. Remarkable value of 38.57% of pentane falling droplets mass had evaporated at 75% vapour saturation value and -10^{o}C. This value had risen to 79.2% at the same saturation condition and temperature of just 20^{o}C. Values like that show how much falling droplet could be a source of liquid vapours.

An important question is needed to be asked at this moment about the regularity of vapour generation and relation with falling height. To answer this question, a more detailed investigation is needed to be performed on fractions of vapours generated along the falling distance. Figure (10.30) and (10.31) discuss the relation between vapour fractions generated from falling droplets evaporation and falling distance at different examples with various small and large vapour fractions.

Figure (10.30) discussed 8 examples of relatively small to medium total amount of vapour generation, ranging from 2.29 to 31.47% of the total released fuel mass. While figure (10.31) has turned to another 6 examples of relatively large amount of vapour generation, ranging from 42.94 to 99.8% of total fuel mass. The examples have included various fuels, temperatures and vapour saturation values, and the droplets falling distance was about 5.2 to 5.5m measured from the end point of primary stage. In each example, mass percentage of vapours generated in first meters to fifth meter has been compared to each others.

There are two clear observations should be noticed from the both figures. First, in most examples, first falling meter have the largest percentage of generated vapours and then gradually decreases during the rest of meters. The second observation is that variation between vapour fractions for the five meters is minimum when the total vapour percentage is relatively small, then variation gets larger when total vapour percentage increases. In example (1), when total vapour percentage was 5.41% of released liquid mass, percentage of vapour generated during third meter was just 14.4% larger than lowest percentage which was recorded in meter number two, 33.9% for example (3) when total vapour was 12.5%, 46.1 and 77.5% for examples 6 and 7 when total vapours were 27.95 and 31.47% respectively. In example (9) when total vapour percentage was 69.53%, vapour generated during the first meter was 3.46 times that for meter number 5, 35.67 times in example (12) where total vapour percentage was

98.08% and 3006 times in example (13) when total vapour reached 99.8% of the total liquid mass. The relationship is not fully linear, but in general the percentage of generated vapour could give an impression about the distribution of vapour fractions during the falling distances.

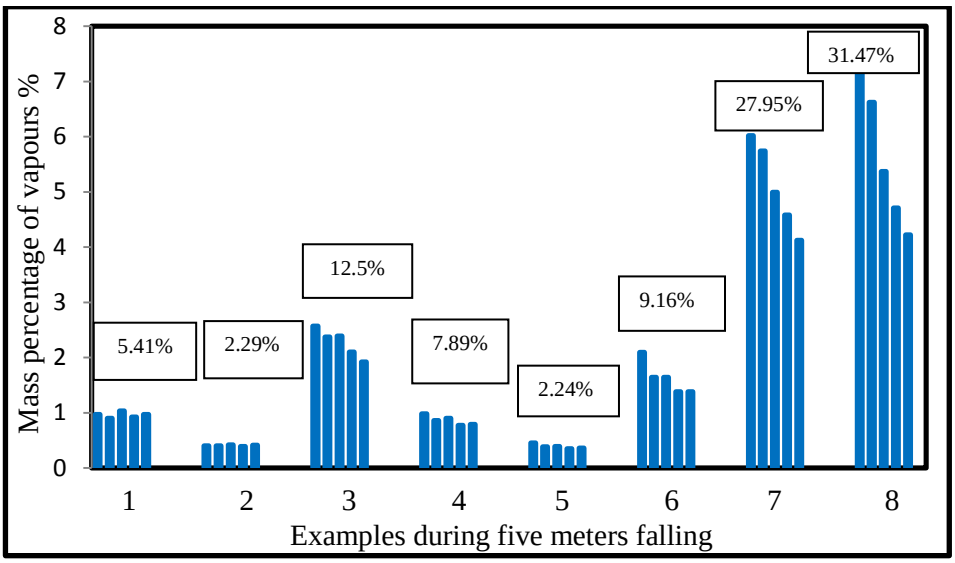

Figure 10.30 Examples for the small vapour fractions generated from falling droplets during the five meters falling after droplets formation

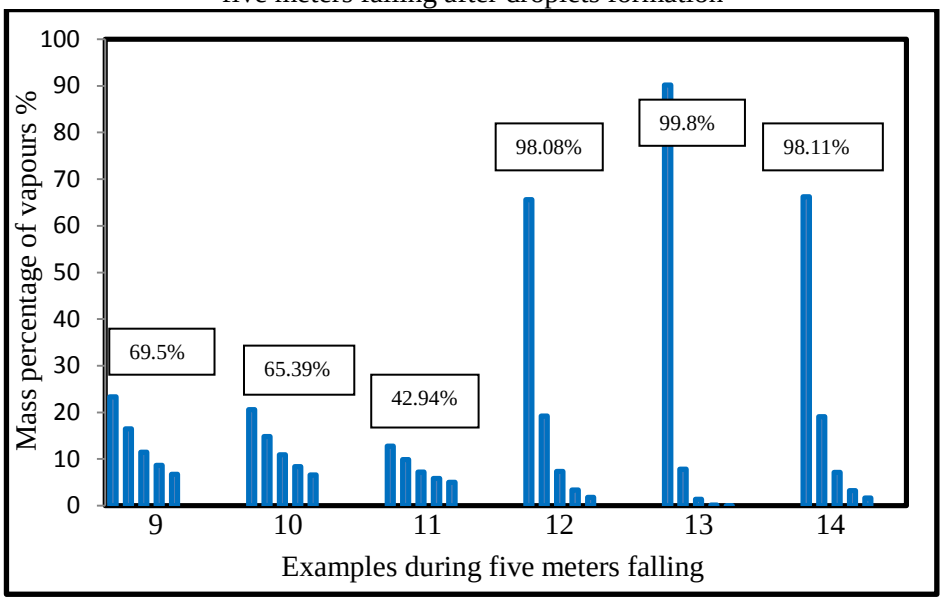

Figure 10.31 Examples for the large vapour fractions generated from falling droplets during the five meters falling after droplets formation

1- Ethanol at -10°C, 0% vapour saturation	**8- Benzene at 20°C, 25% vapour saturation**
2- Ethanol at -10°C, 50% vapour saturation	**9- Ethanol at 50°C, 0% vapour saturation**
3- Ethanol at 20°C, 50% vapour saturation	**10- Benzene at 50°C, 25% vapour saturation**
4- Benzene at -10°C, 75% vapour saturation	**11- Hexane at 50°C, 75% vapour saturation**
5- Toluene at -10°C, 75% vapour saturation	**12- Pentane at 20°C, 0% vapour saturation**
6- Toluene at 20°C, 75% vapour saturation	**13- Pentane at 50°C, 0% vapour saturation**
7- Ethanol at 20°C, 0% vapour saturation	**14- Hexane at 50°C, 0% vapour saturation**

10.4.2.2 The influence of vapour saturation on droplets size distribution

Monitoring of droplets size distribution when air mixture is partially saturated with fuel vapour might be very difficult. During droplets falling, all droplets sizes are subjected to continuous changes in size according to continuous evaporation. Small droplets, such as aerosol droplets, may completely disappear. Size of other larger droplets could get smaller, hence it might distributed is another size region. For this reason, studying the behaviour of aerosol generation under the influence of vapour saturation variation is seems to be not quite so simple. In present model program, falling distance is divided into meters. Hence, monitor shows and prints the current status after each meter. During this meter distance, lots of changes may take place and fluctuation of aerosol percentage could happen. For accurate aerosol monitoring, a general picture of the situation should be taken after a short distance or time period as small as possible. Practically, using the program under this condition could be very difficult. The amount of resulting data will be larger than possibility to analyze. For example, current program describes droplets size distribution in a matrix with 25 columns and 20010 rows to give a complete picture for droplets sizes, fractions, velocities, evaporation...etc. When program is used to solve a problem assuming than falling distance in 10 meters, then program have to fill in complete matrix cells after each falling meter. If the proposed distance is reduced to 1 cm, this means the program will has to fill 1000 matrices during running. If the time is possible, the amount of resulting data will be more than possible.
It was found that the best way to investigate the effect of vapour saturation variation is to estimate the changes in major scenario outcomes. When droplets are formed and during falling stage, part of liquid droplets will continue to fall and reach the ground, while the other part will not continue till the end. This part could be transfer into vapour form or floating aerosol form. Droplets reaching the ground may spread or splash. If spreading takes place, the role of these spreading droplets will come to an end. On the other hand, if splashing takes place, some of the generated daughter droplets maybe drifted again inside the scene. Fine daughter droplets in the range of aerosol or maybe in the range of mist droplets may float after splashing and be a part of the mixed phase cloud. Larger daughter droplets will unlikely to float, and similar to spreading droplets will be out of the scene.

Therefore, for the total mass of released fuel liquid, there were four fractions are need to be looking for as follows:

- Fraction of vapour generated during droplets free-falling.

- Fraction of liquid droplets spreading when impact the surface.
- Fraction of large daughter droplets resulting from splash and directly falls to the ground.
- Fraction of small daughter droplets resulting from splash and could float again and becomes incorporated in mixed phase cloud.

Fractions of generated vapour and small droplets resulting from splash are the two main hazardous fractions which we are look for in assessing vapour clouds generation. Anyway, the remaining liquid fractions are not completely innocent, where they could be a source of vapour through liquid pool formation. Figure (10.33) expresses the variation in the four types of fractions according to vapour saturation changes during ethanol liquid release condition at different temperatures.

Conclusions from figure (10.32) could be expressed as follows:

- At all different temperatures, percentage of generated vapour decreases when vapour saturation increases, while percentage of floating droplets after splash increases. This behaviour had been proved for all other fuel liquids cases. It's logically accepted that when evaporation decreases, small falling droplets will be allowed to maintain their sizes and could reach the ground. And because daughter droplets mean diameter is directly proportional to mother droplet diameter, splashing of larger amount of relatively small droplets will simply generate larger amounts of floatable aerosol droplets.
- Total fractions of both vapours and floating droplets increases when vapour saturation decreases or temperature increases. These fractions could be assumed as risk indicator in accidental fuel releases. These two fractions, in addition to aerosol fraction generated during liquid breakup, could be the main source of mixed cloud formation. Hence, it could be concluded that, the higher the fuel vapour saturation the lower the risk factor. And the higher the temperature the higher the risk factor.

Finally, it becomes clear now that factors of temperature and fuel vapour saturation are paramount factors in controlling the majority of vapour and aerosol generation. Vapour saturation building-up during incidents is dependent on both rate of vapour generation and release surrounding conditions. During the next chapter, proposed examples will be discussed in order to investigate the scenario of vapour saturation building-up and accumulation of vapour and aerosols in incident site.

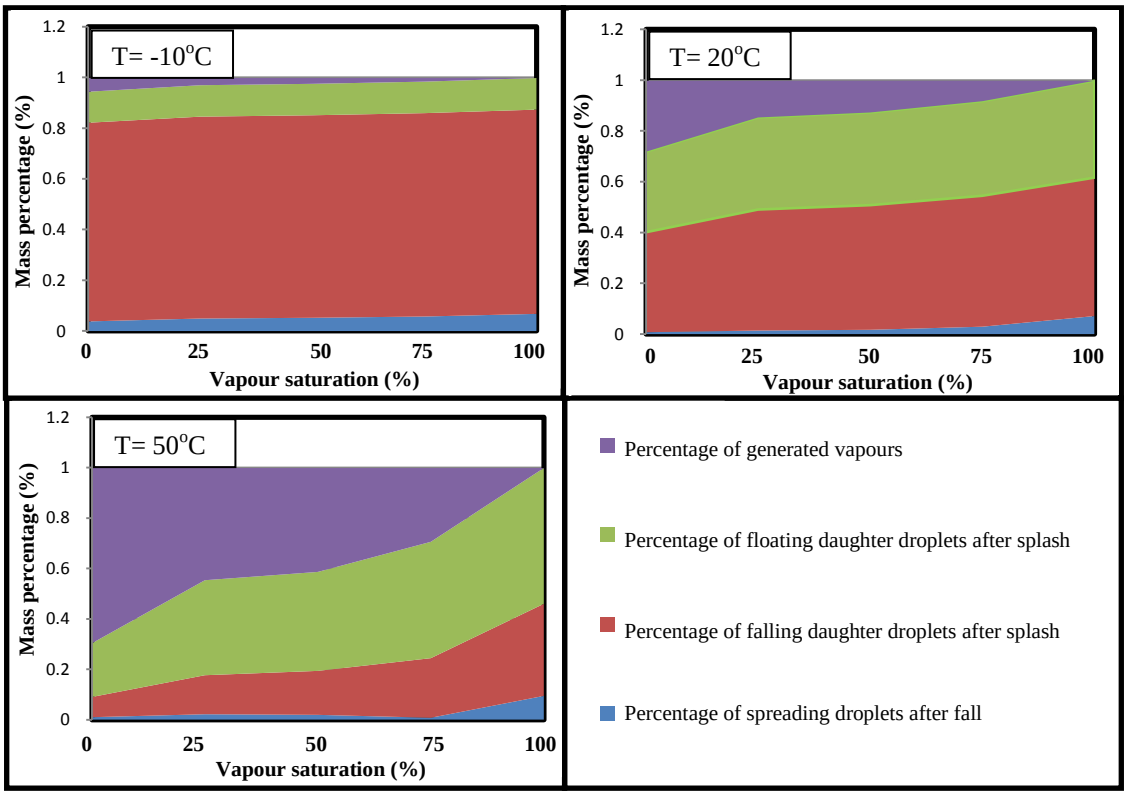

Figure 10.32 Effect of vapour saturation variation on mass percentage of vapours generated, spreading droplets, falling daughter droplets and floating daughter droplets at three different temperatures and ethanol vapour saturation ranging from 0 to 100%

Summary

1- The effect of ambient temperature on the liquid release process:

- Changing the ambient temperature has a direct effect on fuel liquids and air mixture physical properties as follows:
  - Increasing temperature from -20 to +50°C had increased liquid density by 5.2 to 7.26%, liquid viscosity by 34.8 to 65.3% and liquid surface tension by 15.5 to 27.1%.
  - When temperature increases, air mixture density testified a competition between decreasing the density of each component and increasing the percentage of high density fuel vapour. The value of air density seems to have a minimum vale at a certain temperature when increasing effect starts to beat the decreasing effect.
  - Gas mixture viscosity was decreased when temperature increased, except for ethanol example which is the only liquid was having a vapour viscosity higher than dry air.

- Increasing the ambient temperature increases the values of air Weber number, jet breakup length and maximum droplet size after jet breakup.
- In general, increasing temperature decreases both terminal settling velocity and critical velocity of disintegration for the falling liquid droplets. In addition, it decreases sauter mean diameter of daughter droplet after drop disintegration.
- Aerosol droplets generation after secondary breakup and during droplets free-falling increases when temperature increases.

2- The effect of ambient humidity on the liquid release process:

Changing humidity has a small impact on liquid breakup mechanism and also a minom effect on vaporisation effieciency.

3- The effect of ambient fuel vapour saturation on the liquid release process:

- The air mixture density increases when vapour saturation increases according to fraction increase of higher densities fuel vapours, where air mixture viscosity decreases except when the released liquid is ethanol.
- The liquid saturated vapour pressure might be the most effective property in controlling evaporation behaviour during droplets free-falling.
- Increasing vapour saturation decreases the amount of liquid vapours generated during droplet free-falling.
- Vapour generations seems to be homogeneous during falling distance when total percentage of generated vapours is relatively small. At higher mass percentage of vapour, generation rate will gradually decrease.
- Total fractions of both vapours and floating droplets increases when vapour saturation decreases or temperature increases.
- The value of saturation vapour pressure for any liquid fuel at a certain temperature is a limiting factor for maximum volume and for the mass fraction occupied by this fuel in the vapour cloud.
- Fuel liquids with higher saturated vapour pressure values have better chance to form a flammable fuel/air cloud at lower temperatures while the others with lower saturated vapour pressure values have a better chance at higher temperatures.
- Increasing the saturation vapour pressure has a great impact on increasing the amount of vaporised liquid during free-fall and impinging stages.

Chapter 11: Conclusions and Recommendations for Future Work

The presented thesis aimed to design a comprehensive numerical package capable of predicting the expected fraction of vaporised liquid obtained from falling droplets in the course of accidental liquid releases. This study was mainly persuaded by the lack of knowledge regarding the role of liquid breakup and droplet vaporisation in the development of flammable vapour clouds. In order to estimate the vaporised fraction, different liquid breakup mechanisms were studied, and the droplet size distribution was further estimated from the empirical and numerical models.

11.1 Conclusions

The main outcomes of this research may be summarised into:

Conclusions from the comparison with experimental and CFD modelling results:

- The suggested numerical package was capable of estimating the liquid fraction vaporised from falling droplets during the process of liquid release.
- The program ability is finite with the specified limitations. The calculations are valid for liquid jet releasing vertically from plain round orifice in stagnant air. Although collision and coagulation of falling droplets are not expected to take place significantly, minor deviation should be considered due to such mechanisms.
- The results obtained from numerical calculation were comparable and harmonious with both the experimental and CFD simulation results. The estimated vaporised fraction was between 75% and 90% of the fraction obtained from four different experiments. Furthermore, the difference between numerical calculation results and CFD simulation results was less than 11% for nine different cases.
- The sensitivity of numerical calculation results toward the change of temperature and vapour saturation was comparable with the experimental and the CFD results.
- The effect of different droplets splashing mechanism on the vaporised fraction was confirmed by both experimental and numerical calculation. Numerical calculations showed that the formation of fine droplets due to

splashing could increase the vaporised fraction by 27.5 to 40.1% *(the value obtained from Experiment (14) was nearly 31.1%).*

- The formation of aerosols enhanced the vaporisation process due to the evaporation that took place outside the cascade region. The total fraction of vaporised liquid increased by 8.5 to 29.7% (according to the numerical calculation results), and by 10.4 to 17% (according to the results obtained from experiments).

<u>According to the case study on Buncefield explosion:</u>

- The total estimated proportion of vaporized liquid in Buncefield incident was nearly 15.4% of the total liquid released. About 11.24% of this fraction was due to droplet evaporation, and the remaining fraction (4.16%) was thought to be triggered by pool evaporation. These results confirm the significant role of droplet evaporation in the formation of vapour clouds.
- The results were analogous to the results obtained using different estimation methods. The results obtained from TNT equivalency method were 16.5% and 18.4% for far field and near field damages respectively. According to the vapour cloud concentration, which has been studied by the HSE researchers, the amount of vapour contributed might be nearly 14.2% of the total release liquid fuel.
- The numerical calculations conducted on Buncefield incident confirmed the influence of splashing mechanism. The obtained results revealed that the vaporization efficiency was enhanced by nearly 25% due to splashing process. In addition, the formation of aerosols increased the amount of vapour by nearly 11.4%.

<u>Conclusions from the sensitivity study on the effect of the release conditions:</u>

1- The effect of release conditions

➢ The orifice diameter

- The increase in the orifice diameter caused a moderate increase in the average droplet size. Yet, the ratio of the maximum diameter and orifice diameter ($D_{0.999}/d_o$) has a minimum value at an orifice diameter of about 4 -5 mm.
- Increasing the orifice diameter triggered a decrease in the percentage of the aerosol droplet formed due to the liquid breakup. However, this decrease is

negligible and had no significant effect on the process of generation of cloud vapour.

- By the end of the primary stage the maximum value scored for the droplet's diameter was directly dependent on the liquid release velocity.
- The orifice diameter and the quantity of the formed aerosol after droplets impinging showed a non-linear relationship. The peak value was obtained at 3mm orifice diameter.
- It was observed that amount of vapour generation was inversely proportional to the orifice diameter. Furthermore, it was noted that a sharp decline in the vapour generation was obtained upon the increase in the orifice diameter from 1mm to 3mm. This increase in diameter caused the vapour generation to decline from 34.9% to 14.4%, showing a 59% decrease. However, this decrease became less severe when the orifice diameter was increased from 3mm to 20mm. This increase in diameter caused the vapour generation to drop from 14.3% to 6.6%, showing a 54% decrease with increasing the orifice diameter nearly 7 times.

➢ Release velocity

- The release velocity had a remarkable impact on both the droplet size distribution and the amount of the generated vapour.
- The increase in the release velocity prompted a decrease in the maximum average droplet diameter, especially at velocity higher than 6 m/s.
- Changing the release velocity had a limited effect on the fraction of aerosols generated from droplets impinging.
- The total amount of vaporised liquid decreased when the liquid release velocity increased from 1m/s to 6m/s and then it started to increase afterward.

➢ Release height

- Increasing the release height gave a higher opportunity for the droplets to improve and change the velocity of the falling droplets. Furthermore, it provides a better chance for the occurrence of the process of evaporation from the falling droplet.
- Increasing the falling height induced a regular increase in the amount of formed vapour. An increase of 1.3% of the total weight of the flowing liquid was scored when the releasing height was 2 m. This increase t reached 24.8% of the total weight of the flowing liquid when the releasing height was increased up to 10m.

Conclusions from the sensitivity study on the effect of the liquid physical properties:

- Viscosity

  - An increase in the liquid's viscosity produced a slight increase in the average droplet size of the formed liquid.
  - Moreover, the increase in the liquid's viscosity prompted a general increase in the amount of formed vapours. This was observed in both the stage of droplets falling and aerosol formation.

- Surface tension

  - An increase in the liquid's surface tension caused an upsurge in the average droplet's diameter that was formed after the primary stage as well as during the stage of droplets falling.
  - The increase in the liquid's surface tension caused a mild change in the amount vapour produced either during the droplets falling stage or the droplets impinging and aerosol founding stage.

- Density

  - The changes in liquid's density showed a minimal effect on the droplets size distribution.
  - The increase in the liquid's density was accompanied by a decline in the amount of vapour generated from the droplets evaporation during falling. However, an inverse relation was observed during the impinging stage where the amount of vapour generated showed a significant upsurge.

- Molecular weight

  - The molecular weight showed a negligible impact on the droplets size distribution in all stages.
  - However, it showed a significant influence on the amount of generated vapours. The increase in the molecular weight caused a considerable decrease in the amount of vapours generated during evaporation from the falling liquid droplets.

- Saturation vapour pressure

  - The increase in the Saturation vapour pressure caused a drastic rise in the amount of vapours generated during evaporation from the falling liquid droplets.
  - Conversely, its effect was trivial in influencing the droplets size distribution.

Conclusions from the sensitivity study on the effect of the ambient conditions:

- Temperature

- The increase in temperature had variable consequences on both the physical properties of the flowing liquid as well as the ambient properties. When the temperature was increased from(20^0C to 50^0C) this triggered an increase in the density by 5.2%- 7.26%, the viscosity by 34%-56% and the surface tension by 15.5%-27.1%.
- The increase in temperature caused an increase in the density and viscosity of the ambient properties as well.
- The increase in temperature produced a fall in the terminal setting velocity and the critical velocity.
- The increase in temperature prompted an enormous increase in the amount of vapour formed during droplets falling as well as splashing.

- Humidity

- The changes in humidity showed a negligible impact on the droplets size distribution.
- However, the increase in humidity demonstrated a significant increase in the amount of formed vapour.

- Vapour concentration

- The increase in fuel vapour concentration caused an increase in the ambient density and a remarkable decline in the ambient' viscosity “except in case of ethanol”.
- The increase in vapour concentration instigated decline in the amount of gases produced during the falling of droplets.

11.2 Recommendations for future Works

Modelling the accidental liquid release through numerical calculations was a very tough and complex mission. Hence, the implemented numerical package presented in this work has been simplified with different assumptions. Further mechanisms should be introduced to achieve better accuracy. The following points could be recommended for future research:

- Extending the work for multi-component liquids such as petroleum products and commercial liquid fuels. Estimating the vaporized fraction for such liquid needs a detailed study on the preferential evaporation of lighter fractions.
- Introducing other different types of release such as horizontal releases and upward releases.
- Applying the effect of light and moderate wind motion on the formation and dispersion of flammable vapour cloud.
- The program might be powered by incorporating further mechanisms for liquid droplets impinging on deep and shallow layers. In addition, going deeper inside additional factors affecting impingement mechanism such as surface roughness of impinging surface, impact angle and heat transfer during impinging.
- Integrating the mechanism of heat transfer due to the evaporation of falling liquid droplets

References

Abbasi, T. and Abbasi, S.A., 2007. Dust explosions–cases, causes, consequences, and control. Journal of Hazardous Materials, Volume 140, Issues 1–2, Pages 7-44.

AIChE, 1996. Guidelines for use of vapour cloud dispersion models, second edition, centre for chemical process safety of the American institute of chemical engineers, New York.

Allen, M. D. and Raabe, O. G., 1982. Re-evaluation of Millikan's oil drop data for the motion of small particles in air. Journal of Aerosol Science, Volume 13, Issue 6, Pages 537-547.

Allen, M. D. and Raabe, O. G., 1985. Slip correction measurements of spherical solid aerosol particles in an improved Millikan apparatus. Aerosol Science and Technology, Volume 4, Issue 3, pages 269-286.

Alp, E. and Matthias, C. S., 1991. COBRA. A heavy gas/liquid spill and dispersion modelling system. Journal of Loss Prevention in the Process Industries, Volume 4, Issue 3, Pages 139-150.

Ambrose, D., Sprake, C.H.S. and Townsend, R., 1974. Thermodynamic properties of organic oxygen compounds. XXXIII. The Vapour Pressure of Acetone, J. Chem. Thermodyn., 6, 693-700.

Ambrose, D. and Sprake, C.H.S., 1970. Thermodynamic properties of organic oxygen compounds. XXV. Vapor Pressures and Normal Boiling Temperatures of Aliphatic Alcohols, J. Chem. Thermodyn., 2, 631-645.

Arai, M., Shimizu, M. and Hiroyasu, H., 1985. Breakup length and spray angle of high speed jet, in: Proc. of the Third International Conference on Liquid Atomization and Spray Systems (Yule, A. J., and Eisenklam, P., eds.), Institute of Energy, London, UK, pp. 1B/4/1–10.

Aston, J.G. and Messerly, G.H., 1940. The heat capacity and entropy, heats of fusion and vaporization and the vapour pressure of n-butane. J. Am. Chem. Soc., 62, 1917-1923.

Atkinson, G. and Cusco, L., 2011. Buncefield: A violent, episodic vapour cloud explosion. Process Safety and Environmental Protection, Volume 89, Issue 6, Pages 360-370.

Atkinson, G., Gant, S., Painter, D., Shirvill, L. and Ungut, A., 2008. Liquid dispersal and vapour production during overfilling incidents. IChemE Hazards symposium series - University of Manchester, UK.

Atkinson, G.T. and Coldrick, S., 2012a. Vapour cloud formation: Experiments and modelling. RR908 Research Report, Prepared by the Health and Safety Laboratory for the Health and Safety Executive (HSE).

Atkinson, G.T. and Coldrick, S., 2012b. Vapour cloud formation, Phase 2 - Work Package 2. The Fianl Research Report FP/12/18, Prepared by the Health and Safety Laboratory for the Health and Safety Executive (HSE).

Atkinson, G., Coldrick, S., Gant, S. and Cusco, L., 2014. Flammable vapour cloud generation from overfilling tanks: Learning the lessons from Buncefield. Journal of Loss Prevention in the Process Industries, In Press, Available online 21 November 2014.

Atkinson, G.T. and Gant, S.E., 2012a. Buncefield investigation: Liquid flow and vapour production. RR936 Research Report, Prepared by the Health and Safety Laboratory for the Health and Safety Executive (HSE).

Atkinson, G.T. and Gant, S.E., 2012b. Flammable vapour cloud risks from tank overfilling incidents. RR937 Research Report, Prepared by the Health and Safety Laboratory for the Health and Safety Executive (HSE).

Badoux, R.A.J., 1985. Some Experiences of a Consulting Statistician in Industrial Safety and Reliability. Journal of Reliability Engineering, Volume 10, Issue 4, Pages 219-232.

Bai, C. X. and Gosman, A. D., 1995. Development of methodology for spray impingement simulation. SAE paper 950283.

Ballal, D. R. and Lefebvre, A. H., 1981. Flame propagation in heterogeneous mixtures of fuel droplets, fuel vapour and air. 18th International Symposium on Combustion, the Combustion Institute, Pittsburgh, PA, USA, pp 321-328.

Baron, P. A. and Willeke, K., 2001. Aerosol measurement: principles, techniques and applications. Second edition, Library of Congress Cataloging-in-Publication Data, John Wiley and Sons, Inc.

Baron, P. A. and Willeke, K., 2001. Aerosol measurement: principles, techniques and applications. Second edition, Library of Congress Cataloguing-in-Publication Data by John Wiley and Sons.

Barrett, J.C. and Clement, C.F., 1988. Growth rates for liquid drops. Journal of Aerosol Science, Volume 19, Issue 2, Pages 223-242.

Bayvel, L. and Orzechowski, Z., 1993. Liquid atomization - combustion an international series, Taylor & Francis, Washington DC, USA.

Berg, M. and Ulrich, J., 1997. Experimental based detection of the splash limits for the normal and oblique impact of molten metal particles on different surfaces, Journal of Materials Synthesis and Processing. Volume 5, Issue 1, Pages 45–49.

Bigot, J. P., Touil, A., Bonnet, P. and Lacôme J. M., 2005. Rain-out investigation: Initial droplet size measurement. Journal of Loss Prevention in the Process Industries, Volume 18, Issues 4–6, Pages 433-442.

Bjerketvedt D., Bakke J. R. and Wingerden K. V., 1997. Gas explosion handbook. Journal of Hazardous Materials, Volume 52, Issue 1, Pages 1 - 150.

Blackmore, D.R., 1982. Heavy Gas Dispersion Models. Journal of Hazardous Materials, Volume 6, Pages 107-128.

Bowen, P. J. and Cameron, L. R. J., 1999. Hydrocarbon aerosol explosion hazards: A review, Process Safety and Environmental Protection, Volume 77, Issue 1, Pages 22-30.

Bradley, P.L. and Baxter, A., 2002. Fires, explosions and related incidents at work in Great Britain in 1998/1999 and 1999/2000. Journal of Loss Prevention in the Process Industries, Volume 15, Pages 365–372.

Brambilla, S. and Manca, D., 2009. Accidents involving liquids: A step ahead in modelling pool spreading, Journal of Hazardous Materials Volume 161, Issues 2-3, Pages 1265–1280.

Brenn, G., 2011. Droplet collision. From handbook of atomization and sprays-theory and applications, edited by Ashgriz, N., Part I, chapter 7, Pages 157-181, Springer Science and Business Media.

Bricard, P. and Friedel, L., 1998. Two phase jet dispersion. Journal of hazard materials, Volume 59, Issues 2–3, Pages 287-310.

Bricard, P. and Friedel, L., 1998. Two-phase jet dispersion, Journal of Hazardous Materials, Volume 59, Issues 2-3, Pages 287–310.

Brown, R. and York, J. L., 1962. Sprays formed by flashing liquid jets. AIChE Journal, Volume 8, Number 2, Pages 149-153.

Burgan, B. et al, 2009. Buncefield Explosion Mechanism - Phase 1, Volumes 1&2, Prepared by the Steel Construction Institute for the Health and Safety Executive, RR718 Research Report.

Burger, M., Schmehl, R., Prommersberger, Schaefer, P., O., Koch, R. and Wittig, S., 2003. A Droplet evaporation modelling by the distillation curve model: accounting for kerosene fuel and elevated pressures. International Journal of Heat and Mass Transfer, Volume 46, Issue 23, Pages 4403-4412.

Burgoyne, J. H. and Cohen, L., 1954. The effect of drop size on flame propagation in liquid aerosols. Proceedings of the Royal Society of London. Series A, Mathematical and Physical Sciences, Volume 225, Issue 1162, Pages 375-392.

Carruth, G.F. and Kobayashi, R., 1973. Vapour Pressure of Normal Paraffins Ethane Through n-Decane from Their Triple Points to About 10 Mm Hg. Journal of Chemical Engineering Data, Volume 18, Issue 2, Pages115-126.

Casal, J., 2008. Evaluation of the effects and consequences of major accidents in industrial plants. Industrial safety series-volume 8, Elsevier Science Publishers B.V.

Ceranna, L., Le Pichon, A., Green, D. N. and Mialle, P., 2009. The Buncefield explosion: a benchmark for infrasound analysis across Central Europe. Geophys. J. Int., Volume 177, Pages 491–508.

Chang, J. I. and Lin, C.C., 2006. A study of storage tank accidents. Journal of Loss Prevention in the Process Industries, Volume 19, Pages 51–59.

Chigier, N., 1991. The Physics of Atomization, in: Proc. of the Fifth Int. Conf. On Liquid Atomization and Spray Systems (Semerjian, H. G., ed.), ILASSAmericas and NIST, Gaithersburg, MD, USA, pp. 49–64.

Chou, W. H. and Faeth, G. M., 1998. Temporal properties of secondary drop breakup in the bag breakup regime, International Journal of Multiphase Flow, Volume 24, Issue 6, Pages 889–912.

Chou, W. H., Hsiang, L. P. and Faeth, G. M., 1997. Temporal properties of drop breakup in the shear breakup regime, International Journal of Multiphase Flow, Volume 23, Issue 4, Pages 651-669.

Cleary, V., Bowen, P. and Witlox, H., 2007. Flashing liquid jets and two-phase droplet dispersion: I. Experiments for derivation of droplet atomisation correlations. Journal of Hazardous Materials, Volume 142, Issue 3, Pages 786-796.

Clift, R., Grace, J. R. and Weber, M. E., 1978. Bubbles, Drops, and Particles. Academic Press, New York.

Cohen, R. D., 1991. Shattering of liquid drops due to impact, Proceeding: Mathematical and physical sciences, Vol. 435, No. 1895, pp. 483-503.

Coldrick, S., Atkinson, G.T. and Gant, S.E., 2011. Large scale evaporating liquid cascades – an experimental and computational study. Proc. IChemE Hazards XXII Symposium, Liverpool, UK.

Coldrick, S., Gant, S.E., Atkinson, G.T. and Dakin, R., 2011. Factors affecting vapour production in large scale evaporating liquid cascades. Process Safety and Environmental Protection, Volume 89, Issue 6, Pages 371-381.

Cossali G. E., Coghe, A. and Marengo, M., 1997. The impact of a single drop on a wetted solid surface. Experiments in Fluids, Volume 22, Issue 6, Pages 463-472.

Crowl, D.A., 2003. Understanding explosions. Centre for Chemical Process Safety of the American Institute of Chemical Engineers in New York, ISBN 0-8169-0779-X.

Cunningham, E., 1910. On the velocity of steady fall of spherical particles through fluid medium. Proceedings of the Royal Society of London, Series A, Pages 357-365.

Das, T.R., Reed, C.O. Jr. and Eubank, P.T., 1973. PVT Surface and thermodynamic properties of n-Butane. J. Chem. Eng. Data, Volume 18, Issue 3, Page 244-253.

Davies, C. N., 1978. Evaporation of airborne droplets - In Fundamentals of Aerosol Science. Edited by ed. D. T., Pages 135-164, John Wiley & Sons, New York.

De´chelette, A., Babinsky, E. and Sojka, P.E., 2011. Drop size distributions. From handbook of atomization and sprays-theory and applications, edited by Ashgriz, N., Part III, Chapter 23, Pages 479-495, Springer Science and Business Media.

Dykhuizen, R. C., 1994. Review of impact and solidification of molten thermal spray droplets. Journal of Thermal Spray Technology, Volume 3, Number 4, Pages 351-361.

Eckhoff, R. K., 2005. Explosion hazards in the process industry. Gulf Publishing Company, Houston, Texas, USA.

EPA, 1995. Compilation of air pollution emission factors, Volume I: stationary point and area sources, AP-42, Fifth edition, Office of Air Quality Planning and Standards Office of Air and Radiation, U.S. Environmental Protection Agency Research Triangle Park, NC.

Formby, S.A. and Wharton, R.K., 1996. Blast characteristics and TNT equivalence values for some commercial explosives detonated at ground level. Journal of Hazardous Materials, Volume 50, Issues 2–3, Pages 183-198.

Fowler, A. H. K. and Hazeldean J. A., 1998. Fires, explosions and related incidents at work in Great Britain in 1994/95 and 1995/96. Journal of Loss Prevention in the Process Industries, Volume 11, Pages 347–352.

Fowler, A.H.K. and Baxter, A., 2000. Fires, explosions and related incidents at work in Great Britain in 1996/97 and 1997/98. Journal of Loss Prevention in the Process Industries, Volume 13, Pages 547–554.

Friedlander, S. K., 1977. Smoke, dust and haze: fundamentals of aerosol behaviour, John Wiley & Sons.

Fuchs, N. A., 1959. Evaporation and droplet growth in gaseous media. Translated from the Russian by Pratt, J.M., Pergamon Press, London.

Gant, S.E. and Atkinson, G.T., 2011. Dispersion of the vapour cloud in the Buncefield Incident. Process Safety and Environmental Protection, Volume 89, Issue 6, Pages 391-403.

Grant, R. P. and Middleman, S., 1966. Newtonian Jet Stability, AIChE J., Volume 12, Issue 4, Pages 669–678.

Grover, R. O. and Assanis, D. N., 2004. A Comparison of Classical Atomization Models against Current Experimental Measurements within a Zero-Dimensional Framework. ILASS Americas, 17th Annual Conference on Liquid Atomization and Spray Systems, Arlington, VA.

Guildenbecher, D.R., Lo´pez-Rivera, C. and Sojka, P.E., 2011. Droplet Deformation and Breakup, Handbook of Atomization and Sprays - Theory and Applications, edited by Ashgriz, N., Part I, Chapter 6, pp. 145-156, Springer New York Dordrecht Heidelberg, London.

Guildenbecher,D. R., Rivera,C. L. and Sojka, P. E., 2009. Secondary Atomization, Exp. Fluids, Volume 46, Issue 3, Pages 371–402.

Gunn, R. and Kinzer, G. D., 1949. The terminal velocity of fall for water droplets in stagnant air. Journal of Meteorology, Volume 6, Issue 4, Pages 243-248.

Hailwood, M., Gawlowski, M., Schalau, B. and Schonbucher, A., 2009. Conclusions drawn from the buncefield and naples incidents regarding the utilization of consequence models. Chem. Eng. Technology, Volume 32, No. 2, Pages 207–231.

Han, J. and Tryggvason, G., 2001. Secondary breakup of axisymmetric liquid drops. II. Impulsive acceleration, Phys. Fluids, Volume 13, Issue 6, Pages 1554–1565.

Herbert, I., 2010. The UK Buncefield incident – The view from a UK risk assessment engineer. Journal of Loss Prevention in the Process Industries, Volume 23, Issue 6, Pages 913-920.

HESS, 2007. Material safety data sheet of gasoline all grades. MSDS No. 9950.

Hidy, G.M., 1984. Aerosols: an industrial and environmental science. Academic press, INC. London.

Hinds, W. C., 1999. Aerosol technology: properties, behaviour, and measurement of airborne particles. Second Edition, published by John Wiley & Sons.

Hinkle, S. E., 1989. Water drop kinetic energy and momentum measurement considerations. Applied Engineering in Agriculture, Volume 5, No. 3, Pages 386-391.

Hinze, J. O., 1955. Fundamentals of the Hydrodynamic Mechanism of Splitting in Dispersion Processes, AIChE J., Volume 1, Issue 3, Pages 289–295.

Hiroyasu, H., Shimizu, M. and Arai, M., 1982. The breakup of high speed jet in a high pressure gaseous atmosphere, in: Proceedings of the Second International Conference of Liquid Atomization and Spray Systems, ILASS82-Americas and Department of Chemical Engineering, University of Wisconsin-Madison, USA.

Holterman, H.J., 2003. Kinetics and evaporation of water drops in air. IMAG report 12-2003, CIP data royal library, ISPN: 90-5406-234-7. (Leave this one here).

Hsiang, L. P. and Faeth, G. M., 1992. Near-limit drop deformation and secondary breakup. International Journal of Multiphase Flow, Volume 18, Issue 5, Pages 635-652.

Hsiang,L. P. and Faeth, G. M., 1993. Drop Properties after Secondary Breakup, Intl. J. Multi. Flow, Volume 19, Issue 5, Pages 721–735.

Jones, W.S., Tamplin, W.S., 1953. Physical Properties of Ethylene Glycol in Glycols, edited by George O. and Curme, Jr., Chapter 3, Reinhold Publishing Corporation, 330 West Forty-Second Street, New York, U.S.A., 1952, 27-62.

Kay, P., Bowen, P. and Witlox, H., 2010. Sub-cooled and flashing liquid jets and droplet dispersion II. Scaled experiments and derivation of droplet size correlations. Journal of Loss Prevention in the Process Industries, Volume 23, Issue 6, Pages 849-856.

Kennedy, J. B., and Roberts, J., Rain Ingestion in a Gas Turbine Engine, in: Proc. of the Fourth Ann. Conf. ILASS (Simmons, H., Kennedy, J. B., Reitz, R. D., and Zimmer, D., eds.), ILASS-Americas, Hartford, CT, USA, pp. 154–162 (1990).

Khalturin, V.I., Rautian, T.G. and Richards, P.G., 1998. The seismic signal strength of chemical explosions, Bull. seism. Soc. Am., Volume 88, Issue 6, Pages 1511–1524.

Kim, M., Do, K., Choi, B. and Han, Y., 2011. First-order perturbation solutions of liquid pool spreading with vaporization. International Journal of Hydrogen Energy, Volume 36, Issue 4, Pages 3268-3271.

Kinoshita, C. M., Teng, H. and Masutani, S. M., 1994. A study of the instability of liquid jets and comparison with Tomotika's analysis. International Journal of Multiphase Flow, Volume 20, No. 3, Pages 523-533.

Kletz, T., 1999. What went wrong - case histories of process plant disasters. Fourth Edition, published by Gulf Publishing Company, Houston, TX.

Kohlbrand, H. T., 1991. Case history of a deflagration involving an organic solvent/oxygen system below its flash point. Plant/Operations Progress, Volume 10, Issue 1, pages 52–54.

Kondo S., Takizawa, K., Takahashi, A., Tokuhashi, K. and Sekiya, A., 2008. A study on flammability limits of fuel mixtures. Journal of Hazardous Materials, Volume 155, Issue 3, Pages 440–448.

Kondo, S., Takahashi, A., Takizawa, K. and Tokuhashi, K., 2011. On the pressure dependence of flammability limits of CH2=CFCF3, CH2F2 and methane. Fire Safety Journal, Volume 46, Issue 5, Pages 289-293.

Koopman, R. P., Ermak, D. L. and Chan, S. T., 1989. A review of recent field tests and mathematical modelling of atmospheric dispersion of large spills of Denser-than-air gases. Atmospheric Environment (1967), Volume 23, Issue 4, Pages 731-745.

Koshy, A., Mallikarjunan, M. M. and Raghavan, K. V., 1995. Causative factors for vapour cloud explosions determined from past-accident analysis. Journal of Loss Prevention in Process Industries, Volume 8, Issue 6, Pages 355-358. Elsevier Science Ltd.

Kretschmer, C.B., Wiebe, R., 1949. Liquid-vapour equilibrium of ethanol-toluene solutions. J. Am. Chem. Soc., Volume 71, Pages 1793-1797.

Lane, W. R., 1951. Shatter of drops in streams of air. Ind. Eng. Chem., Volume 43, Issue 6, Pages 1312–1317.

Lautkaski, R., 2008. Experimental correlations for the estimation of the rainout of flashing liquid releases. Journal of Loss Prevention in the Process Industries, Volume 21, Issue 5, Pages 506-511.

Lea, C. J. and Ledin H. S., 2002. A review of the state-of-the-art in gas explosion modelling. Fire and Explosion Group, Health and Safety Laboratory, Harpur Hill, Buxton, UK.

Lee, K. W. and Chen, H., 1984. Coagulation rate of polydisperse particles. Aerosol Science and Technology, Volume 3, Issue 3, Pages 327-334.

Lee, K. W., 2002. A methodology for assessing risk from released hydrocarbon in an enclosed area. Journal of Loss Prevention in the Process Industries, Volume 15, pages 11–17.

Lee, K. W., Putnam, A. A., Gieseke, J. A., Golovin, M. N. and Hale, J. A., 1979. Spray nozzle designs for agricultural aviation applications, NASA-CR- 159702.

Lefebvre, A. H., 1989. Atomization and sprays, Hemisphere Publishing Corporation, New York, NY, USA.

Lian, P., Mejia, A. F., Cheng, Z. and Mannan, M. S., 2010. Flammability of heat transfer fluid aerosols produced by electrospray measured by laser diffraction analysis, Journal of Loss Prevention in the Process Industries, Volume 23, Issue 1162, Pages 337-345.

Lin, S. P., 2003. Breakup Of Liquid Sheets And Jets. Cambridge University Press 2003, ISBN-13: 978-0-511-06381-7 eBook (NetLibrary).

Liu, H., 2000. Science and engineering of droplets- fundamentals and applications. Published by Noyes Publications / William Andrew Publishing, LLC Norwich, New York, U.S.A.

Long, Y., Chaumerliac, N., Deguillaume, L., Leriche, M. and Champeau, F., 2010. Effect of mixed-phase cloud on the chemical budget of trace gases: A modeling approach. Atmospheric Research, Volume 97, Issue 4, Pages 540-554.

Madejski, J., 1979. Solidification of droplets on a cold surface. International Journal of Heat and Mass Transfer, Volume 19. Pages 1009-1013.

Makhviladze, G. M., Roberts, J. P. and Yakush, S. E., 1999. Combustion of two-phase hydrocarbon fuel clouds released into the atmosphere. The journal of Combustion and Flame, Volume 118, Issue 4, Pages 583-605.

Maremonti, M., Russo, G. , Salzano, E. and Tufano, V., 1999. Post-accident analysis of vapour cloud explosions in fuel storage areas. Process Safety and Environmental Protection, Volume 77, Issue 6, Pages 360-365.

Maremonti, M., Russo, G., Salzano, E. and Tufano, V., 1999. Post-accident analysis of vapour cloud explosions in fuel storage areas. Institution of Chemical Engineers, Trans IChemE, Volume 77, Part B.

McCarthy, M. J., and Molloy, N. A., Review of stability of liquid jets and the influence of nozzle design. Chem. Eng. J., 7:1–20 (1974) The Chemical Engineering Journal, Volume 7, Issue 1, Pages 1-20.

Melean, Y. and Sigalotti, L. D., 2005. Coalescence of colliding van der Waals liquid drops. International Journal of Heat and Mass Transfer, Volume 48, Issues 19–20, Pages 4041-4061.

Merrington, A. C., and Richardson, E. G., 1947. The Breakup of Liquid Jets, Proceedings of the Physical Society, Volume 59, Number 1, pages 1–13.

Miesse, C. C., 1955.Correlation of experimental data on the disintegration of liquid jets, Ind. Eng. Chem., Volume 47, Issue 9, Pages1690–1701.

Mishra, K. B., Wehrstedt, K. and Krebs, H., 2014. Amuay refinery disaster: The aftermaths and challenges ahead. Fuel Processing Technology, Volume 119, March 2014, Pages 198-203.

Mizutani, Y. And Nakajima, A., 1973a. Combustion of fuel vapour-drop-air systems: Part I - Open burner flames. Combustion and Flame, Volume 20, Issue 3, June Pages 343-350.

Mizutani, Y. And Nakajima, A., 1973b. Combustion of fuel vapour-drop-air systems: Part II—Spherical flames in a vessel. Combustion and Flame, Volume 20, Issue 3, Pages 354-357.

Moen, I.O., 1993. Transition to detonation in fuel-air explosive clouds. Journal of Hazardous Materials, Volume 33, Issue 2, Pages 159-192.

Moita, A.S. and Moreira,A.L.N., 2007. Drop impacts onto cold and heated rigid surfaces: Morphological comparisons, disintegration limits and secondary atomization. International Journal of Heat and Fluid Flow, Volume 28, Pages 735–752.

Mugele, R. A., and Evans, H. D., 1951. Droplet size distributions in sprays. Journal of Industrial and Engineering Chemistry, Volume 43, Issue 6, Pages 1317–1324.

Mundo, C., Sommerfeld, M. and Tropea, C., 1995. Droplet-wall collisions: Experimental studies of the deformation and breakup process. International journal of Multiphase Flow, Volume 21, No. 2, Pages 151 173.

Nevers, N., 1992. Cloud formation with air on vapour or liquid mixing. Journal of Loss Prevention in Process Industries, Volume 5, Issue 4, Pages 205-210.

Newton, L. et al., 2008. The Buncefield Incident 11 December 2005: The final report of the Major Incident Investigation Board. Volume (1), published by Crown.

Ohnesorge, W., 1936. Formation of drops by nozzles and the breakup of liquid jets. Z. Angew. Math. Mech., Volume 16, Pages 355-358.

Okamoto K., Watanabe N., Hagimoto Y., Miwa, K. and Ohtani H., 2009. Changes in evaporation rate and vapor pressure of gasoline with progress of evaporation. Fire Safety Journal, Volume 44, Issue 5, Pages 756-763.

O'Rourke, P. J. and Amsden, A. A., 1987. The Tab Method for Numerical Calculation of Spray Droplet Breakup, SAE Paper 872089:1–10.

Osborn, A.G., Douslin, D.R., 1974. Vapor-pressure relations for 15 hydrocarbons. J. Chem. Eng. Data, Volume 19, Issue 2, Pages 114-117.

Ottemoller, L. and Evers, L.G., 2008. Seismo-acoustic analysis of the Buncefield oil depot explosion in the UK. International Journal of Geophysics, Volume 172, Page 1123–1134.

Park, K. 1994. Development of a non-orthogonal-grid computer code for the optimisation of direct-injection diesel engine combustion chamber shapes. Ph.D. thesis, University of Manchester Institute of Science and Technology, Manchester, UK.

Park, K. and Watkins, A. P., 1996. Comparison of wall spray impaction models with experimental data on drop velocities and sizes, International Journal of Heat and Fluid Flow, Volume 17, Issue 4, Pages 424-438.

Pattison, M. J., Martini, R., Banerjee, S. and Hewitt, G. F., 1998. Modelling of dispersion of two-phase releases: part 1- conservation equations and closure relationships. Process Safety and Environmental Protection, Volume 76, Issue 1, February 1998, Pages 31-40.

Perry, R. H., Green, D. W. and Maloney, J. O., 1997. Perry's chemical engineers' handbook. Seventh Edition, Library Of Congress Cataloging-In-Publication Data.

Petekson, R.J., Grewal, S.S. and EL-Wakil, M. M., 1984. Investigations of liquid flashing and evaporation due to sudden depressurization. International Journal of Heat and Mass Transfer, Volume 27, Issue 2, Pages 301-310.

Petekson, R.J., Grewal, S.S. and EL-Wakil, M. M., 1984. Investigations of Liquid Evaporation Due To Sudden Flashing and Depressurization. International Journal of Heat and mass transfer, Volume 27, Issue 2, Pages 301-310.

Piskunov, V.N., Petrov, A.M. and Golubev, A.I., 2003. Modeling particle formation kinetics in mixed-phase clouds. Journal of Aerosol Science, Volume 34, Issue 11, Pages 1555-1580.

Pitzer, K.S.and Scott, D.W., 1943. The thermodynamics and molecular structure of benzene and its methyl derivatives, J. Am. Chem. Soc., Volume 65, Pages 803-829.

Polymeropoulos, C.E. and Das, S., 1975. The effect of droplet size on the burning velocity of kerosene-air sprays. Combustion and Flame, Volume 25, Pages 247-257.

Powell, T., 2006a. The Buncefield incident 11 December 2005: The Buncefield investigation Progress report. The final report of the Major Incident Investigation Board, Volume 2.

Powell, T., 2006b. The Buncefield incident 11 December 2005: The Buncefield investigation third Progress report. The final report of the Major Incident Investigation Board, Volume 2.

Powell, T., 2006c. The Buncefield incident 11 December 2005: Initial Report to the health and safety commission and the environment agency of the investigation into

the explosions and fires at the Buncefield oil storage and transfer depot, Hemel Hempstead, on 11 December 2005. The final report of the Major Incident Investigation Board, Volume 2.

Puttock, J. S., McFarlane, K., Prothero, A., Rees, F. J., Roberts, P. T., Witlox, H. W. M. and Blewitt, D. N., 1991. Dispersion models and hydrogen fluoride predictions. Journal of Loss Prevention in the Process Industries, Volume 4, Issue 1, Pages 16-28.

Rayleigh, L., 1878. On the instability of jets. Proceeding of the London Mathematical Society, Volume 10, Pages 4 –13.

Razzaghi, M., 1989. Droplet size estimation of two-phase flashing jets. Nuclear Engineering and Design, Volume 114, Issue 1, Pages 115-124.

Reist, P. C., 1984. Introduction to aerosol science. McMillan publishing company, NY.

Reitz, R. D., 1978. Atomization and other breakup regimes of a liquid jet, Ph.D. Thesis, Princeton University, Princeton, NJ, USA.

Reitz, R. D. and Bracco, F. V., 1986. Mechanisms of breakup of round liquid jets. Edited by Cheremisinoff, N. P. The Encyclopaedia of Fluid Mechanics, Gulf Publishing, Houston, TX, USA, Volume 3, Issue 10, Pages 233–249.

Riazi, M. R., 2005. Characterization and properties of petroleum fractions. Library of Congress Cataloging-in-Publication Data, ASTM manual series American Society for Testing and Materials, Philadelphia, USA.

Rosin, P. and Rammler, E. 1933. The laws governing the fineness of powdered coal. Journal of the institute of fuel, Volume 7, Pages 29-36.

Rutland, D.F. and Jameson, G.J., 1970. Theoretical prediction of the sizes of drops formed in the breakup of capillary jets. Chemical Engineering Science, Volume 25, Issue 11, Pages 1689-1698.

Sampson, R. D., Chung, K. K. and Lozowski, E. P., 1996. A Simple Experiment to Measure the Splash Mass Produced by a Free-Falling Buoyant Sphere Impacting a Deep Quiescent Liquid. Journal of Colloid and Interface Science, Volume 181, Issue 2, Pages 673-675.

Sartor, J. D. and Abbott, C. E., 1975. Prediction and measurement of the accelerated motion of water drops in air. Journal of Applied Meteorology, Volume 14, Pages 232-239.

Saury, D., Harmand, S. and Siroux, M., 2005. Flash evaporation from a water pool: Influence of the liquid height and of the depressurization rate. International Journal of Thermal Sciences, Volume 44, Issue 10, Pages 953–965.

Savic, S., 2000. Liquid fuel spray characteristics. Ph.D. thesis, the University of Brighton in collaboration with Ricardo Consulting Engineers, UK.

Scargiali, F., Grisafi, F., Busciglio, A. and Brucato, A., 2011. Modeling and simulation of dense cloud dispersion in urban areas by means of computational fluid dynamics. Journal of Hazardous Materials, Volume 197, Pages 285-293.

Sehmel, G.A., 1984. Deposition and resuspension. in: atmospheric science and power production. Edited by: Randerson, D., Technical Information Center, Office of Scientific and Technical Information, U.S. Department of Energy, Pages 533–583.

Shakeri,S. and Chandra, S., 2002. Splashing of molten tin droplets on a rough steel surface, International Journal of Heat and Mass Transfer, Volume 45, Pages 4561–4575.

Sharma, R.K., Gurjar, B.R., Wate, S.R., Ghuge, S.P. and Agrawal, R., 2013. Assessment of an accidental vapour cloud explosion: Lessons from the Indian Oil Corporation Ltd. accident at Jaipur, India. Journal of Loss Prevention in the Process Industries, Volume 26, Pages 82-90.

Shavit, U. and Chigier, N., 1996. Development and evaluation of a new turbulence generator for atomization research. experiments in Fluids, Volume 20, Issue 4, Pages 291-301.

Simmons, H. C., 1977a. The correlation of drop-size distributions in fuel nozzle sprays part i: the drop-size/volume-fraction distribution, J. Engr. Power, Pages 309–314.

Simmons, H. C., 1977b. The correlation of drop-size distributions in fuel nozzle sprays part ii: the drop-size/number distribution. J. Engr. Power, Pages 315–319.

Slinn, W.G.N., 1984. Precipitation scavenging. in: atmospheric science and power production. Edited by: Randerson, D., Technical Information Center, Office of Scientific and Technical Information, U.S. Department of Energy, pages 466–532.

Spicer, T. O. and Havens J., 1996. Application of dispersion models to flammable cloud analyses. Journal of Hazardous Materials, Volume 49, Issue 2-3, Page 115-124.

Stow, C. D., and Hadfield, M. G., 1981. An experimental investigation of fluid flow resulting from the impact of a water drop with an unyielding dry surface. Proceedings of the Royal Society of London. Series A, Mathematical and Physical Sciences, Volume 373, Issue 1755, Pages 419-441.

Stull, D.R., 1947. Vapor Pressure of Pure Substances Organic Compounds, Ind. Eng. Chem., Volume 39, Pages 517-540.

Tan, W., Liu, X., Liu, L., Liu, Y. and Wang, Z., 2012. Numerical study on the initial expansion of two-phase cloud from an instantaneous release. Journal of Loss Prevention in the Process Industries, Volume 25, Issue 6, Pages 989-992.

Tanasawa, Y., and Toyoda, S., 1955. On the atomization of liquid jet issuing from a cylindrical nozzle. The Technology Reports of the Tohoku University, Japan, No. 19-2, Pages. 135–156.

Taylor, G.I., 1934. The function of emulsion in definable field flow. Proceedings of the Royal Society of London. Series A. Mathematical and Physical Sciences, Volume 146, Pages 501-523.

Van De Sande, E. and Smith J. M., 1976. Jet break-up and air entrainment by low velocity turbulent water jets. Chemical Engineering Science, Volume 31, Issue 3, Pages 219-224.

van Rijn, C.J.M., 2004. Nano and Micro Engineered Membrane Technology. Membrane Science and Technology Series, Volume 10, copyright by Elsevier B.V., ISBN: 0-444-51489-9.

Vincent, J. H., 1995. Aerosol science for industrial hygienists. Elsevier Science Ltd, the Boulevard, Langford Lane, Kidlington, Oxford, U.K.

Wachters, L. H. J. and Westerling, N, A. J., 1966. The heat transfer from a hot wall to impinging water drops in a spheroidal state. Chemical Engineering Science, Volume 21, Pages 1047-1056.

Wang, D. M. 1992. Modelling spray wall impaction and combustion processes of diesel engines. Ph.D. thesis, University of Manchester, Faculty of Technology, Manchester, UK.

Wang, D. M. and Watkins, A. P., 1993. Numerical modelling of diesel wall spray phenomena. Int. J. Heat Fluid Flow, Volume 14, No. 3, Pages 301-312.

Watkins, A. P. and Wang, D. M. 1990. A new model for diesel spray impaction on walls and comparison with experiment. Proc. COMOD1A 90 Int. Symposium on Diagnostics and Modelling of Combustion in L C. Engines, Kyoto, Japan, Pages 243-248.

Weber, C., 1931. Disintegration of liquid jets. Journal of Applied Mathematics and Mechanics, Volume 11, Issue 2, Pages 136–154.

Wiekema, B.J., 1984a. Vapour cloud explosions-an analysis based on accidents-part I. Journal of Hazardous Materials, Elsevier Science Publishers, Amsterdam, Netherlands, Volume 8, Pages 295-311.

Wiekema, B.J., 1984b. Vapour Cloud Explosions-An Analysis Based On Accidents-Part II. Journal of Hazardous Materials, Elsevier Science Publishers, Amsterdam, Netherlands, Volume 8, Pages 313-329.

Willeke, K., 1976. Temperature dependence of particle slip in a gaseous medium. Journal of Aerosol Science, Volume 7, Issue 5, Pages 381-387.

Williamham, C.B., Taylor, W.J., Pignocco, J.M., Rossini, F.D., 1945. Vapor pressures and boiling points of some paraffin, Alkylcyclopentane, Alkylcyclohexane, and Alkylbenzene Hydrocarbons. J. Res. Natl. Bur. Stand. USA, Volume 35, Pages 219-244.

Williams, M. M. R. and Loyalka, S. K., 1991. Aerosol science theory and practice – with special applications to the Nuclear Industry. Pergamon Press plc, Headington Hill Hall, Oxford, UK.

Witlox, H., Harper, M., Bowen, P. and Cleary, V., 2007. Flashing liquid jets and two-phase droplet dispersion: II. Comparison and validation of droplet size and rainout formulations. Journal of Hazardous Materials, Volume 142, Issue 3, Pages 797-809.

Witlox, H., Harper, M., Oke, A., Bowen, P. and Kay, P., 2010. Sub-cooled and flashing liquid jets and droplet dispersion I. Overview and model implementation/validation. Journal of Loss Prevention in the Process Industries, Volume 23, Issue 6, Pages 831-842.

Witlox, W. M. and Bowen, P. J., 2001. Flashing liquid jets and two-phase dispersion: a review. Contract research report No: 403/2002, Health and Safety Executive, UK.

Woodward J. L., 1989. Dispersion modelling of an elevated high momentum release forming aerosols. Journal of Loss Prevention in the Process Industries, Volume 2, Issue 1, Pages 22-32.

Wu, Z. N., 2003. Prediction of the size distribution of secondary ejected droplets by crown splashing of droplets impinging on a solid wall, Probabilistic Engineering Mechanics, Volume 18, Issue 3, Pages 241-249.

Yang, P., Wei, H. L., Baum, B. A., Huang, H.L., Heymsfield, A. J., Hu, Y. X., Gao, B.C. and Turner, D. D., 2003. The spectral signature of mixed-phase clouds composed of non-spherical ice crystals and spherical liquid droplets in the terrestrial window region. Journal of Quantitative Spectroscopy and Radiative Transfer, Volumes 79–80, Pages 1171-1188.

Yaws, C. L., 2008. Thermochemical properties of chemicals and hydrocarbons, William Andrew.

Zebel, G. 1966. Coagulation of aerosols. In Aerosol Science, ed. by Davies, C. N., London: Academic Press, Pages 31-58.

Appendix A

Appendix A1. Physical Properties for different compounds

Liquid	Formula a	Melting Temp(K) a	Boiling Temp (K) a	Molar mass (gm/mol) b	Density At 298.15K (g/cm^3) a	Viscosity At 298.15K (mPa.s) b	Surface tension At 298.15K (dynes/cm) a	Flammability Limits (V%) b	
								LFL	UFL
Water	H_2O	273.15	373.15	18.02	1.000	0.9631	72.71	-	-
Ethanol	C_2H_5OH	159.05	351.44	46.07	0.787	1.0941	21.99	4.3	19
Butane	C_4H_{10}	134.86	272.65	58.1	0.806	0.1579	11.87	1.8	8.4
n-pentane	C_5H_{12}	143.42	309.22	72.15	0.621	0.2249	15.47	1.4	8.3
Benzene	C_6H_6	278.68	353.24	78.11	0.873	0.6051	28.21	1.4	7.1
n-hexane	C_6H_{14}	177.83	341.88	86.17	0.656	0.1618	17.98	1.2	7.7
Toluene	C_7H_8	178.18	383.78	92.1	0.865	0.5269	27.93	1.2	7.1
n-Decane	$C_{10}H_{22}$	243.51	447.30	142.3	0.728	0.8713	23.41	0.78	2.6

a (Yaws, 2008) b (Riazi, 2005)

Appendix A2. Density regression coefficient for different liquids (Yaws, 2008)

Compound	A	B	C	n	T_{min}	T_{max}
Water	0.32500	0.27000	647.13	0.23000	290.00	647.13
Ethanol	0.27600	0.27668	516.25	0.23670	159.05	516.25
Butane	0.30558	0.24463	610.00	0.28571	141.15	610.00
n-pentane	0.23100	0.26874	469.65	0.28215	143.42	469.65
Benzene	0.30170	0.26855	562.16	0.28180	278.68	562.16
n-hexane	0.23300	0.26601	507.43	0.27810	177.84	507.43
Toluene	0.29180	0.26188	591.79	0.29889	178.18	591.79
n-Decane	0.23590	0.25668	618.45	0.28570	243.49	618.45

$$\rho_{Liq}(T) = AB^{-\left(1-\frac{T}{C}\right)^n} \qquad \text{eq. A1}$$

Where ρ_{Liq} is the saturated liquid density at Temperature T (gm / cm^3), A, B, C and n are the regression coefficients for chemical compound and T is the temperature (^oK).

Appendix A3. Coefficients for viscosity of pure vapour compound (Riazi, 2005)

Vapour	A	B	C	D	T_{min}	T_{max}
air	1.4241E-06	5.0390E-01	1.0828E+02	0.0000E+00	80	2000
Water	6.1842E-07	6.7780E-01	8.4722E+02	7.4074E+04	273	1073
Ethanol	1.06E-006	8.0660E-001	5.2700E+02	0.0000E+00	200	1000
n-Butane	2.2982E-07	6.9440E-01	2.2772E+02	-1.450E+04	135	1000
n-pentane	6.3411 E-08	8.4760 E-01	4.1722 E+01	0.0000 E+00	143	1000
Benzene	3.1347E-08	9.6760E-01	7.9000E+00	0.O000E+00	279	1000
n-hexane	1.7505 E-07	7.074 E-01	1.5711 E+02	0.0000E+00	178	1000
Toluene	8.7274 E-07	4.9400 E-01	3.2378 E+02	0.0000E+00	178	1000
n-Decane	2.6408E-08	9.4870E-01	7.1000E+01	0.0000E+00	243	1000

$$\mu_{Vapour}(T) = \frac{1000\, A\, T^{B}}{\left(1 + \frac{C}{T} + \frac{D}{T^{2}}\right)}$$

Where μ_{Vapour} is the Viscosity of vapour at Temperature T (centi poise), A, B, C and D are the viscosity coefficients of pure vapour compound and T is the temperature (^{o}K).

Appendix A4. Coefficients for viscosity of pure liquid compound (Riazi, 2005)

Compound	A	B	C	D	E	T_{min}	T_{max}
Water	-5.284E+01	3.704E+03	5.866E+00	-5.879E-29	1.0E+01	273	646
Ethanol	7.875E+00	7.820E+02	-3.042E+00	0.000E+00	0.0E+00	200	440
n-Butane	-7.247E+00	5.348E+02	-5.747E-01	-4.662E-27	1.0E+01	135	420
n-pentane	-2.038E+01	1.050E+03	1.487E+00	-2.017E-27	1.0E+01	143	465
Benzene	-7.37 E+00	1.038 E+03	-6.181E-01	-1.02 E-28	1.0E+01	279	545
n-hexane	-2.071E+01	1.208E+03	1.499E+00	0.000E+00	0.0E+00	178	343
Toluene	-6.067E+01	3.149E+03	7.482E+00	-5.709E-27	1.0E+01	178	384
n-Decane	-1.647E+01	1.534E+03	7.511E-01	0.000E+00	0.000E+00	243	448

$$\mu_{Liq}(T) = 1000\ \exp\left(A + \frac{B}{T} + C\ln T + D\, T^{E}\right)$$

Where μ_{Liq} is the Viscosity of liquid at Temperature T (centi poise),A, B, C, D and E are the viscosity coefficients of pure liquid compound and T is the temperature (^{o}K).

Appendix A5. Vapour pressure coefficients for liquid compounds (Perry, 1997)

liquid	C1	C2	C3	C4	C5	T_{min}	T_{max}
Water	73.649	-7258.2	-7.3037	4.1653E-06	2	273.16	647.13
Ethanol	74.475	-7164.3	-7.327	3.1340E-06	2	159.05	513.92
n-Butane	66.343	−4363.2	−7.046	9.4509E−06	2	134.86	425.12
n-pentane	78.741	-5420.3	-8.8253	9.6171E-06	2	143.42	469.7
Benzene	83.918	-6517.7	-9.3453	7.1182E-06	2	278.68	562.16
n-hexane	104.65	-6995.5	-12.702	1.2381E-05	2	177.83	507.6
Toluene	80.877	-6902.4	-8.7761	5.8034E-06	2	178.18	591.8
n-Decane	112.73	−9749.6	−13.245	7.1266E−06	2	243.51	617.7

$$P(T) = \exp\left[C_1 + \left(\frac{C_2}{T}\right) + (C_3 \times \ln T) + C_4 \times T^{C_5}\right]$$

Where P(T) is the saturated vapour pressure (Pa), C1, C2, C3, C4 and C5 are the vapour pressure coefficient for pure liquid component and T is the temperature (^{o}K).

Appendix A6. Antoine's coefficients

liquid	A	B	C	T (k)
Water	4.6543 [e]	1435.264 [e]	-64.848 [e]	255.9 – 373 [e]
Ethanol	5.37229 [a]	1670.409 [a]	-40.191 [a]	273 - 351.70 [a]
n-Butane	3.85002 [j]	909.65 [j]	-36.146 [j]	195.11 - 272.81 [j]
	4.35576 [k]	1175.581 [k]	-2.071 [k]	272.66 - 425 [k]
n-pentane	3.9892 [g]	1070.617 [g]	-40.454 [g]	268.8 - 341.37 [g]
Benzene	4.01814 [d]	1203.835 [d]	-53.226 [d]	287.70 - 354.07 [d]
n-hexane	3.45604 [i]	1044.038 [i]	-53.893 [i]	177.70 - 264.93
	4.00266 [d]	1171.53 [d]	-48.784 [d]	286.18 - 342.69 [d]
Toluene	4.14157 [h]	1377.578 [h]	-50.507 [h]	273.0 - 323.0 [h]
n-Decane	0.21021 [i]	440.616 [i]	-156.896 [i]	243.49 - 310.59 [i]

(Kretschmer and Wiebe, 1949)
(Jones and Tamplin, 1952)
(Ambrose, Sprake, et al., 1974)
(Williamham, Taylor, et al., 1945)
(Stull, 1947)
(Ambrose and Sprake, 1970)
(Osborn and Douslin, 1974)
(Pitzer and Scott, 1943)
(Carruth and Kobayashi, 1973)
Aston and Messerly, 1940
Das, Reed, et al., 1973

$$\log(P) = A - \left(\frac{B}{T + C}\right)$$

Where P is the saturated vapour pressure (Bar), A, B and C are the Antoine's coefficients and T is the temperature (^{o}K).

Appendix A7. Surface tension regression coefficient for different liquids (Yaws, 2008)

Compound	A	B	n	T_{min}	T_{max}
Water	134.834	647.13	1.0000	273.16	647.13
Ethanol	43.807	516.25	0.8000	159.05	516.25
n-butane	52.660	425.18	1.2330	134.86	425.18
n-pentane	52.090	469.65	1.2054	143.42	469.65
Benzene	71.950	562.16	1.2389	278.69	562.16
n-hexane	56.081	507.43	1.2843	177.84	507.43
Toluene	66.850	591.79	1.2456	178.18	591.79
n-Decane	55.777	618.45	1.3198	243.51	618.45

$$\sigma(T) = A\,(1 - \frac{T}{B})^{n}$$

σ... Surface tension at Temperature T (dynes / cm)

A, B and n are surface tension regression coefficients for chemical compound

T is the temperature in K

Appendix B

Section B-1: The main sub-command
Part A: Declarations
General declaration:

```
Dim matrix5(1 To 20010, 1 To 126) As Double
```

Private declaration:

```
Dim Dnozzle As Single, Uliquid As Single, Height As Single, Tliquid As Single
Dim Tambient As Single, Humidity As Single
Dim Vconc As Single, flow As Single, liq As Byte
Dim liqdin As Single, liqsur As Double, liqvis As Double, airdin As Single
Dim airvis As Double, LMw As Single
Dim VMw As Single, LMb As Single, LBb As Single, ppf As Single, psatf As Single
Dim ppv As Single, psatv As Single
Dim WeA As Double, WeL As Double, ReL As Double, ReA As Double
Dim Je As Double, OhA As Double, OhL As Double
Dim matrix1(1 To 5, 1 To 1) As Single
Dim matrix2(1 To 13, 1 To 1) As Single
Dim c, breakup, fallH As Single, L As Single, Ddrop As Single, Dmax As Single
Dim MMD As Single, SMD As Single
Dim matrix3(1 To 20010, 1 To 7) As Double
Dim matrix4(1 To 20010, 1 To 25) As Double
Dim distance1 As Single, remaindistance As Single
Dim vapourfraction1 As Double, vapourvolume1 As Double
```

Part B: Checking Inputs Acceptance

```
For i = 1 To 10
If Val(Text1.Text) < 1 Or Val(Text1.Text) > 100 Then
Text1.Text = InputBox("Input pipe diameter value between 1 to 100 mm")
End If
Next i
For i = 1 To 10
If Val(Text2.Text) < 1 Or Val(Text2.Text) > 50 Then
Text2.Text = InputBox("Input liquid velocity value between 1 to 50 m/s")
End If
Next i
For i = 1 To 10
If Val(Text3.Text) < 1 Or Val(Text3.Text) > 25 Then
Text3.Text = InputBox("Input release height value between 1 to 10 m")
End If
Next i
For i = 1 To 10
If Combo1.Text = "" Then
Combo1.Text = InputBox("choose type of liquid WATER, ETHANOL, BENZENE, N-PENTANE, N-HEXANE OR TOLUENE  ")
End If
Next i
For i = 1 To 10
If Val(Text4.Text) < -30 Or Val(Text4.Text) > 50 Then
Text4.Text = InputBox("Input liquid temperature value between -30 and +50 C ")
End If
Next i
For i = 1 To 10
If Val(Text5.Text) < -30 Or Val(Text5.Text) > 50 Then
Text5.Text = InputBox("Input ambient temperature value between -30 and +50 C ")
End If
Next i
For i = 1 To 10
If Val(Text6.Text) < 0 Or Val(Text6.Text) > 100 Then
Text6.Text = InputBox("Input humidity value between 0 to 100% ")
End If
Next i
For i = 1 To 10
If Val(Text7.Text) < 0 Or Val(Text7.Text) > 100 Then
Text7.Text = InputBox("Input fuel vapour saturation value between 0 to 100% ")
End If
Next i
```

Part C: Naming Inputs

```
Dnozzle = Val(Text1.Text) / 1000
Uliquid = Val(Text2.Text)
Height = Val(Text3.Text)
Tliquid = Val(Text4.Text) + 273
Tambient = Val(Text5.Text) + 273
Humidity = Val(Text6.Text) / 100
Vconc = Val(Text7.Text) / 100
flow = 3.14159265538979 * Uliquid * (Dnozzle ^ 2) * 1000 / 4
If Combo1.Text = "WATER" Then
liq = 1
End If
If Combo1.Text = "ETHANOL" Then
liq = 2
End If
If Combo1.Text = "BENZENE" Then
liq = 3
End If
If Combo1.Text = "N-PENTANE" Then
liq = 4
End If
If Combo1.Text = "N-HEXANE" Then
liq = 5
End If
If Combo1.Text = "TOLUENE" Then
liq = 6
End If
Form4.Text1(9).Text = Combo1.Text
```

Part D: Filling Matrix1

```
matrix1(1, 1) = liq
matrix1(2, 1) = Tliquid
matrix1(3, 1) = Tambient
matrix1(4, 1) = Humidity
matrix1(5, 1) = Vconc
```

Part E: Calling For Physical Properties

```
Call phy_properties(matrix1, matrix2)
LMw = matrix2(1, 1)
VMw = matrix2(2, 1)
LMb = matrix2(3, 1)
LBb = matrix2(4, 1)
liqdin = matrix2(5, 1)
liqsur = matrix2(6, 1)
liqvis = matrix2(7, 1)
airdin = matrix2(8, 1)
airvis = matrix2(9, 1)
ppv = matrix2(10, 1)
```

```
psatv = matrix2(11, 1)
ppf = matrix2(12, 1)
psatf = matrix2(13, 1)
Part F: Calculating Dimensionless Factors
WeL = (Uliquid ^ 2) * liqdin * Dnozzle / liqsur
WeA = (Uliquid ^ 2) * airdin * Dnozzle / liqsur
Je = ((Uliquid ^ 2) * airdin * Dnozzle / liqsur) *
((liqdin / airdin) ^ 0.45)
ReL = liqdin * Uliquid * Dnozzle / liqvis
ReA = airdin * Uliquid * Dnozzle / airvis
OhL = (WeL ^ 0.5) / ReL
OhA = (WeA ^ 0.5) / ReA
Form5.Text1(8).Text = WeL
Form5.Text1(9).Text = WeA
Form5.Text1(10).Text = Je
Form5.Text1(11).Text = ReL
Form5.Text1(12).Text = ReA
Form5.Text1(13).Text = OhL
Form5.Text1(14).Text = OhA
Part F: Jet Breakup Regimes
If Je < 0.1 Then
c = "dripping"
Else
If WeA < 0.4 Then
c = "Rayleigh breakup"
End If
If WeA >= 0.4 And WeA < 13 Then
c = "first wind induced"
End If
If WeA >= 13 And WeA < 40 Then
c = "second wind induced"
End If
If WeA >= 40 Then
c = "Atomization"
End If
End If
Part G: Filling Matrix 3
For i = 1 To 10
matrix3(i, 1) = 10 * (i - 1)
matrix3(i, 2) = 10 * i
Next i
For i = 1 To 20000
matrix3(i + 10, 2) = (100 * i) + 100
matrix3(i + 10, 1) = 100 * i
Next i
For i = 1 To 20010
matrix3(i, 3) = (matrix3(i, 2) + matrix3(i, 1)) / 2
Next i
Part H: Dripping or Rayleigh Case
Characteristics
breakup = "Liquid breakup occurs"
If c = "dripping" Or c = "Rayleigh breakup" Then
If c = "dripping" Then
Ddrop = (((6 * Dnozzle * liqsur) / (liqdin * 9.81)) ^
0.333) * 1000000
L = 0
fallH = Height - L
End If
If c = "Rayleigh breakup" Then
Ddrop = 1.88 * Dnozzle * 1000000
If ReA < 2000 Then
L = 19.5 * Dnozzle * (WeL ^ 0.5) * ((1 + (3 *
OhL)) ^ 0.85)
End If
If ReA >= 2000 Then
L = 8.51 * Dnozzle * (WeL ^ 0.32)
End If
fallH = Height - L
If fallH <= 0 Then
breakup = "no breakup"
Ddrop = 0
End If
End If
For i = 1 To 20010
If Ddrop <= matrix3(i, 2) And Ddrop > matrix3(i,
1) Then
matrix3(i, 6) = 1
End If
Next i
End If
Part I: Other Regimes Characteristics
If c = "first wind induced" Or c = "second wind
induced" Or c = "Atomization" Then
If ReL < 2000 Then
L = 19.5 * Dnozzle * (WeL ^ 0.5) * ((1 + (3 *
OhL)) ^ 0.85)
End If
If ReL >= 2000 Then
L = 8.5 * Dnozzle * (WeL ^ 0.32)
End If
If c = "Atomization" Then
L = 0
End If
fallH = Height - L
If fallH <= 0 Then
breakup = "no breakup"
Else
Dmax = Dnozzle * (23.5 + (0.000395 * ReL)) *
1000000 / (WeL ^ 0.333)
End If
MMD = Dmax / 3.1572
SMD = MMD / 1.47551
Part J: Putting Data in Jet Breakup Array for
Other Regimes
If Dmax > 0 Then
For i = 1 To 20010
If Dmax > matrix3(i, 2) Then
matrix3(i, 4) = 1 - Math.Exp(-0.693 * ((matrix3(i,
1) / MMD) ^ 2))
matrix3(i, 5) = 1 - Math.Exp(-0.693 * ((matrix3(i,
2) / MMD) ^ 2))
matrix3(i, 6) = matrix3(i, 5) - matrix3(i, 4)
End If
If Dmax <= matrix3(i, 2) And Dmax > matrix3(i, 1)
Then
matrix3(i, 4) = 1 - Math.Exp(-0.693 * ((matrix3(i,
1) / MMD) ^ 2))
matrix3(i, 5) = 1 - Math.Exp(-0.693 * ((Dmax /
MMD) ^ 2))
matrix3(i, 6) = matrix3(i, 5) - matrix3(i, 4)
End If
Next i
End If
End If
matrix3(1, 7) = Uliquid
matrix3(2, 7) = liqdin
matrix3(3, 7) = liqsur
matrix3(4, 7) = liqvis
matrix3(5, 7) = airdin
matrix3(6, 7) = airvis
matrix3(7, 7) = Tambient
Form5.Text1(0).Text = flow
Form5.Text1(1).Text = c
Form5.Text1(2).Text = breakup
Form5.Text1(3).Text = L
Form5.Text1(4).Text = Ddrop
Form5.Text1(5).Text = SMD
Form5.Text1(6).Text = MMD
```

```
Form5.Text1(7).Text = Dmax
Part K: Recording Primary Disintegration
For i = 1 To 20010
If matrix3(i, 6) > 0 Then
matrix5(i, 1) = matrix3(i, 3)
matrix5(i, 4) = matrix3(i, 6)
End If
Next i
Part L: Secondary Breakup
If fallH > 0 Then
Call secondary_breakup(matrix3, matrix4)
For i = 1 To 20010
If matrix4(i, 3) > 0 Then
matrix5(i, 2) = matrix4(i, 5)
matrix5(i, 3) = matrix4(i, 6)
matrix5(i, 6) = matrix4(i, 10)
matrix5(i, 5) = matrix4(i, 7)
End If
Next i
For i = 1 To 20010
If matrix4(i, 4) > 0 Then
matrix5(i, 7) = matrix4(i, 4)
End If
Next i
For i = 1 To 20010
If matrix4(i, 4) = 0 Then
matrix4(i, 1) = 0
matrix4(i, 2) = 0
matrix4(i, 3) = 0
matrix4(i, 5) = 0
matrix4(i, 6) = 0
matrix4(i, 7) = 0
End If
Next i
matrix4(1, 25) = fallH
matrix4(2, 25) = airdin
matrix4(3, 25) = airvis
matrix4(4, 25) = liqdin
matrix4(5, 25) = liqsur
matrix4(6, 25) = liqvis
matrix4(7, 25) = Tliquid
matrix4(8, 25) = Tambient
matrix4(9, 25) = VMw
matrix4(10, 25) = liq
matrix4(11, 25) = psatv
matrix4(12, 25) = psatf
matrix4(13, 25) = ppv
matrix4(14, 25) = ppf
matrix4(16, 25) = flow
matrix5(1, 126) = fallH
matrix5(2, 126) = airdin
matrix5(3, 126) = airvis
matrix5(4, 126) = liqdin
matrix5(5, 126) = liqsur
matrix5(6, 126) = liqvis
matrix5(7, 126) = Tliquid
matrix5(8, 126) = Tambient
matrix5(9, 126) = VMw
matrix5(10, 126) = liq
matrix5(11, 126) = psatv
matrix5(12, 126) = psatf
matrix5(13, 126) = ppv
matrix5(14, 126) = ppf
matrix5(15, 126) = flow
End If
Part M: Free Falling
Meter 1 Falling
If fallH > 0 Then
If fallH >= 1 Then
distance1 = 1
remaindistance = fallH - 1
Else
distance1 = fallH
remaindistance = 0
End If
matrix4(15, 25) = distance1
Call droplet_falling(matrix4, matrix4)
For v = 1 To 20010
If matrix4(v, 20) > 0 Then
For w = 1 To 20010
If matrix4(v, 20) > matrix4(w, 1) And matrix4(v,
20) <= matrix4(w, 2) Then
matrix4(w, 24) = matrix4(w, 24) + matrix4(v, 23)
End If
Next w
End If
Next v
vapourfraction1 = 0
For e = 1 To 20010
vapourfraction1 = vapourfraction1 + matrix4(e, 22)
Next e
vapourvolume1 = vapourfraction1 * flow
matrix4(17, 25) = vapourfraction1
matrix4(18, 25) = vapourvolume1
For i = 1 To 20010
matrix5(i, 8) = matrix4(i, 9)
matrix5(i, 9) = matrix4(i, 10)
matrix5(i, 10) = matrix4(i, 13)
matrix5(i, 11) = matrix4(i, 14)
matrix5(i, 12) = matrix4(i, 4)
matrix5(i, 13) = matrix4(i, 19)
matrix5(i, 14) = matrix4(i, 20)
matrix5(i, 15) = matrix4(i, 21)
matrix5(i, 16) = matrix4(i, 22)
matrix5(i, 17) = matrix4(i, 23)
matrix5(i, 18) = matrix4(i, 24)
Next i
matrix5(1, 124) = matrix4(17, 25)
matrix5(1, 125) = matrix4(18, 25)
matrix5(11, 124) = distance1
matrix5(11, 125) = remaindistance
End If
End of Meter 1 Falling
Meter 2 Falling
If remaindistance > 0 Then
If remaindistance >= 1 Then
distance1 = 1
remaindistance = remaindistance - 1
Else
distance1 = remaindistance
remaindistance = 0
End If
matrix4(15, 25) = distance1
Call extra_falling(matrix4, matrix4)
For v = 1 To 20010
If matrix4(v, 20) > 0 Then
For w = 1 To 20010
If matrix4(v, 20) > matrix4(w, 1) And matrix4(v,
20) <= matrix4(w, 2) Then
matrix4(w, 24) = matrix4(w, 24) + matrix4(v, 23)
End If
Next w
End If
Next v
vapourfraction1 = 0
For e = 1 To 20010
vapourfraction1 = vapourfraction1 + matrix4(e, 22)
Next e
```

```
vapourvolume1 = vapourfraction1 * flow
matrix4(17, 25) = vapourfraction1
matrix4(18, 25) = vapourvolume1
For i = 1 To 20010
matrix5(i, 19) = matrix4(i, 9)
matrix5(i, 20) = matrix4(i, 10)
matrix5(i, 21) = matrix4(i, 13)
matrix5(i, 22) = matrix4(i, 14)
matrix5(i, 23) = matrix4(i, 4)
matrix5(i, 24) = matrix4(i, 19)
matrix5(i, 25) = matrix4(i, 20)
matrix5(i, 26) = matrix4(i, 21)
matrix5(i, 27) = matrix4(i, 22)
matrix5(i, 28) = matrix4(i, 23)
matrix5(i, 29) = matrix4(i, 24)
Next i
matrix5(2, 124) = matrix4(17, 25)
matrix5(2, 125) = matrix4(18, 25)
matrix5(12, 124) = distance1
matrix5(12, 125) = remaindistance
End If
End of Meter 2 Falling
Meter 3 Falling
If remaindistance > 0 Then
If remaindistance >= 1 Then
distance1 = 1
remaindistance = remaindistance - 1
Else
distance1 = remaindistance
remaindistance = 0
End If
matrix4(15, 25) = distance1
Call extra_falling(matrix4, matrix4)
For v = 1 To 20010
If matrix4(v, 20) > 0 Then
For w = 1 To 20010
If matrix4(v, 20) > matrix4(w, 1) And matrix4(v,
20) <= matrix4(w, 2) Then
matrix4(w, 24) = matrix4(w, 24) + matrix4(v, 23)
End If
Next w
End If
Next v
vapourfraction1 = 0
For e = 1 To 20010
vapourfraction1 = vapourfraction1 + matrix4(e, 22)
Next e
vapourvolume1 = vapourfraction1 * flow
matrix4(17, 25) = vapourfraction1
matrix4(18, 25) = vapourvolume1
For i = 1 To 20010
matrix5(i, 30) = matrix4(i, 9)
matrix5(i, 31) = matrix4(i, 10)
matrix5(i, 32) = matrix4(i, 13)
matrix5(i, 33) = matrix4(i, 14)
matrix5(i, 34) = matrix4(i, 4)
matrix5(i, 35) = matrix4(i, 19)
matrix5(i, 36) = matrix4(i, 20)
matrix5(i, 37) = matrix4(i, 21)
matrix5(i, 38) = matrix4(i, 22)
matrix5(i, 39) = matrix4(i, 23)
matrix5(i, 40) = matrix4(i, 24)
Next i
matrix5(3, 124) = matrix4(17, 25)
matrix5(3, 125) = matrix4(18, 25)
matrix5(13, 124) = distance1
matrix5(13, 125) = remaindistance
End If
End of Meter 3 Falling
Meter 4 Falling
If remaindistance > 0 Then
If remaindistance >= 1 Then
distance1 = 1
remaindistance = remaindistance - 1
Else
distance1 = remaindistance
remaindistance = 0
End If
matrix4(15, 25) = distance1
Call extra_falling(matrix4, matrix4)
For v = 1 To 20010
If matrix4(v, 20) > 0 Then
For w = 1 To 20010
If matrix4(v, 20) > matrix4(w, 1) And matrix4(v,
20) <= matrix4(w, 2) Then
matrix4(w, 24) = matrix4(w, 24) + matrix4(v, 23)
End If
Next w
End If
Next v
vapourfraction1 = 0
For e = 1 To 20010
vapourfraction1 = vapourfraction1 + matrix4(e, 22)
Next e
vapourvolume1 = vapourfraction1 * flow
matrix4(17, 25) = vapourfraction1
matrix4(18, 25) = vapourvolume1
For i = 1 To 20010
matrix5(i, 41) = matrix4(i, 9)
matrix5(i, 42) = matrix4(i, 10)
matrix5(i, 43) = matrix4(i, 13)
matrix5(i, 44) = matrix4(i, 14)
matrix5(i, 45) = matrix4(i, 4)
matrix5(i, 46) = matrix4(i, 19)
matrix5(i, 47) = matrix4(i, 20)
matrix5(i, 48) = matrix4(i, 21)
matrix5(i, 49) = matrix4(i, 22)
matrix5(i, 50) = matrix4(i, 23)
matrix5(i, 51) = matrix4(i, 24)
Next i
matrix5(4, 124) = matrix4(17, 25)
matrix5(4, 125) = matrix4(18, 25)
matrix5(14, 124) = distance1
matrix5(14, 125) = remaindistance
End If
End of meter 4 falling
Meter 5 falling
If remaindistance > 0 Then
If remaindistance >= 1 Then
distance1 = 1
remaindistance = remaindistance - 1
Else
distance1 = remaindistance
remaindistance = 0
End If
matrix4(15, 25) = distance1
Call extra_falling(matrix4, matrix4)
For v = 1 To 20010
If matrix4(v, 20) > 0 Then
For w = 1 To 20010
If matrix4(v, 20) > matrix4(w, 1) And matrix4(v,
20) <= matrix4(w, 2) Then
matrix4(w, 24) = matrix4(w, 24) + matrix4(v, 23)
End If
Next w
End If
Next v
vapourfraction1 = 0
```

```
For e = 1 To 20010
vapourfraction1 = vapourfraction1 + matrix4(e, 22)
Next e
vapourvolume1 = vapourfraction1 * flow
matrix4(17, 25) = vapourfraction1
matrix4(18, 25) = vapourvolume1
For i = 1 To 20010
matrix5(i, 52) = matrix4(i, 9)
matrix5(i, 53) = matrix4(i, 10)
matrix5(i, 54) = matrix4(i, 13)
matrix5(i, 55) = matrix4(i, 14)
matrix5(i, 56) = matrix4(i, 4)
matrix5(i, 57) = matrix4(i, 19)
matrix5(i, 58) = matrix4(i, 20)
matrix5(i, 59) = matrix4(i, 21)
matrix5(i, 60) = matrix4(i, 22)
matrix5(i, 61) = matrix4(i, 23)
matrix5(i, 62) = matrix4(i, 24)
Next i
matrix5(5, 124) = matrix4(17, 25)
matrix5(5, 125) = matrix4(18, 25)
matrix5(15, 124) = distance1
matrix5(15, 125) = remaindistance
End If
End of meter 5 falling
Meter 6 falling
If remaindistance > 0 Then
If remaindistance >= 1 Then
distance1 = 1
remaindistance = remaindistance - 1
Else
distance1 = remaindistance
remaindistance = 0
End If
matrix4(15, 25) = distance1
Call extra_falling(matrix4, matrix4)
For v = 1 To 20010
If matrix4(v, 20) > 0 Then
For w = 1 To 20010
If matrix4(v, 20) > matrix4(w, 1) And matrix4(v,
20) <= matrix4(w, 2) Then
matrix4(w, 24) = matrix4(w, 24) + matrix4(v, 23)
End If
Next w
End If
Next v
vapourfraction1 = 0
For e = 1 To 20010
vapourfraction1 = vapourfraction1 + matrix4(e, 22)
Next e
vapourvolume1 = vapourfraction1 * flow
matrix4(17, 25) = vapourfraction1
matrix4(18, 25) = vapourvolume1
For i = 1 To 20010
matrix5(i, 63) = matrix4(i, 9)
matrix5(i, 64) = matrix4(i, 10)
matrix5(i, 65) = matrix4(i, 13)
matrix5(i, 66) = matrix4(i, 14)
matrix5(i, 67) = matrix4(i, 4)
matrix5(i, 68) = matrix4(i, 19)
matrix5(i, 69) = matrix4(i, 20)
matrix5(i, 70) = matrix4(i, 21)
matrix5(i, 71) = matrix4(i, 22)
matrix5(i, 72) = matrix4(i, 23)
matrix5(i, 73) = matrix4(i, 24)
Next i
matrix5(6, 124) = matrix4(17, 25)
matrix5(6, 125) = matrix4(18, 25)
matrix5(16, 124) = distance1
matrix5(16, 125) = remaindistance
End If
End of meter 6 falling
Meter 7 falling
If remaindistance > 0 Then
If remaindistance >= 1 Then
distance1 = 1
remaindistance = remaindistance - 1
Else
distance1 = remaindistance
remaindistance = 0
End If
matrix4(15, 25) = distance1
Call extra_falling(matrix4, matrix4)
For v = 1 To 20010
If matrix4(v, 20) > 0 Then
For w = 1 To 20010
If matrix4(v, 20) > matrix4(w, 1) And matrix4(v,
20) <= matrix4(w, 2) Then
matrix4(w, 24) = matrix4(w, 24) + matrix4(v, 23)
End If
Next w
End If
Next v
vapourfraction1 = 0
For e = 1 To 20010
vapourfraction1 = vapourfraction1 + matrix4(e, 22)
Next e
vapourvolume1 = vapourfraction1 * flow
matrix4(17, 25) = vapourfraction1
matrix4(18, 25) = vapourvolume1
For i = 1 To 20010
matrix5(i, 74) = matrix4(i, 9)
matrix5(i, 75) = matrix4(i, 10)
matrix5(i, 76) = matrix4(i, 13)
matrix5(i, 77) = matrix4(i, 14)
matrix5(i, 78) = matrix4(i, 4)
matrix5(i, 79) = matrix4(i, 19)
matrix5(i, 80) = matrix4(i, 20)
matrix5(i, 81) = matrix4(i, 21)
matrix5(i, 82) = matrix4(i, 22)
matrix5(i, 83) = matrix4(i, 23)
matrix5(i, 84) = matrix4(i, 24)
Next i
matrix5(7, 124) = matrix4(17, 25)
matrix5(7, 125) = matrix4(18, 25)
matrix5(17, 124) = distance1
matrix5(17, 125) = remaindistance
End If
End of meter 7 falling
Meter 8 falling
If remaindistance > 0 Then
If remaindistance >= 1 Then
distance1 = 1
remaindistance = remaindistance - 1
Else
distance1 = remaindistance
remaindistance = 0
End If
matrix4(15, 25) = distance1
Call extra_falling(matrix4, matrix4)
For v = 1 To 20010
If matrix4(v, 20) > 0 Then
For w = 1 To 20010
If matrix4(v, 20) > matrix4(w, 1) And matrix4(v,
20) <= matrix4(w, 2) Then
matrix4(w, 24) = matrix4(w, 24) + matrix4(v, 23)
End If
Next w
```

```
End If
Next v
vapourfraction1 = 0
For e = 1 To 20010
vapourfraction1 = vapourfraction1 + matrix4(e, 22)
Next e
vapourvolume1 = vapourfraction1 * flow
matrix4(17, 25) = vapourfraction1
matrix4(18, 25) = vapourvolume1
For i = 1 To 20010
matrix5(i, 85) = matrix4(i, 9)
matrix5(i, 86) = matrix4(i, 10)
matrix5(i, 87) = matrix4(i, 13)
matrix5(i, 88) = matrix4(i, 14)
matrix5(i, 89) = matrix4(i, 4)
matrix5(i, 90) = matrix4(i, 19)
matrix5(i, 91) = matrix4(i, 20)
matrix5(i, 92) = matrix4(i, 21)
matrix5(i, 93) = matrix4(i, 22)
matrix5(i, 94) = matrix4(i, 23)
matrix5(i, 95) = matrix4(i, 24)
Next i
matrix5(8, 124) = matrix4(17, 25)
matrix5(8, 125) = matrix4(18, 25)
matrix5(18, 124) = distance1
matrix5(18, 125) = remaindistance
End If
End of meter 8 falling
Meter 9 falling
If remaindistance > 0 Then
If remaindistance >= 1 Then
distance1 = 1
remaindistance = remaindistance - 1
Else
distance1 = remaindistance
remaindistance = 0
End If
matrix4(15, 25) = distance1
Call extra_falling(matrix4, matrix4)
For v = 1 To 20010
If matrix4(v, 20) > 0 Then
For w = 1 To 20010
If matrix4(v, 20) > matrix4(w, 1) And matrix4(v,
20) <= matrix4(w, 2) Then
matrix4(w, 24) = matrix4(w, 24) + matrix4(v, 23)
End If
Next w
End If
Next v
vapourfraction1 = 0
For e = 1 To 20010
vapourfraction1 = vapourfraction1 + matrix4(e, 22)
Next e
vapourvolume1 = vapourfraction1 * flow
matrix4(17, 25) = vapourfraction1
matrix4(18, 25) = vapourvolume1
For i = 1 To 20010
matrix5(i, 96) = matrix4(i, 9)
matrix5(i, 97) = matrix4(i, 10)
matrix5(i, 98) = matrix4(i, 13)
matrix5(i, 99) = matrix4(i, 14)
matrix5(i, 100) = matrix4(i, 4)
matrix5(i, 101) = matrix4(i, 19)
matrix5(i, 102) = matrix4(i, 20)
matrix5(i, 103) = matrix4(i, 21)
matrix5(i, 104) = matrix4(i, 22)
matrix5(i, 105) = matrix4(i, 23)
matrix5(i, 106) = matrix4(i, 24)
Next i
matrix5(9, 124) = matrix4(17, 25)
matrix5(9, 125) = matrix4(18, 25)
matrix5(19, 124) = distance1
matrix5(19, 125) = remaindistance
End If
End of meter 9 falling
Meter 10 falling
If remaindistance > 0 Then
If remaindistance >= 1 Then
distance1 = 1
remaindistance = remaindistance - 1
Else
distance1 = remaindistance
remaindistance = 0
End If
matrix4(15, 25) = distance1
Call extra_falling(matrix4, matrix4)
For v = 1 To 20010
If matrix4(v, 20) > 0 Then
For w = 1 To 20010
If matrix4(v, 20) > matrix4(w, 1) And matrix4(v,
20) <= matrix4(w, 2) Then
matrix4(w, 24) = matrix4(w, 24) + matrix4(v, 23)
End If
Next w
End If
Next v
vapourfraction1 = 0
For e = 1 To 20010
vapourfraction1 = vapourfraction1 + matrix4(e, 22)
Next e
vapourvolume1 = vapourfraction1 * flow
matrix4(17, 25) = vapourfraction1
matrix4(18, 25) = vapourvolume1
For i = 1 To 20010
matrix5(i, 107) = matrix4(i, 9)
matrix5(i, 108) = matrix4(i, 10)
matrix5(i, 109) = matrix4(i, 13)
matrix5(i, 110) = matrix4(i, 14)
matrix5(i, 111) = matrix4(i, 4)
matrix5(i, 112) = matrix4(i, 19)
matrix5(i, 113) = matrix4(i, 20)
matrix5(i, 114) = matrix4(i, 21)
matrix5(i, 115) = matrix4(i, 22)
matrix5(i, 116) = matrix4(i, 23)
matrix5(i, 117) = matrix4(i, 24)
Next i
matrix5(10, 124) = matrix4(17, 25)
matrix5(10, 125) = matrix4(18, 25)
matrix5(20, 124) = distance1
matrix5(20, 125) = remaindistance
End If
End of Meter 10 Falling
Part N: Splashing
If fallH > 0 Then
Call splashing(matrix4, matrix4)
For i = 1 To 20010

matrix5(i, 118) = matrix4(i, 1) * 1000000
matrix5(i, 119) = matrix4(i, 2)
matrix5(i, 120) = matrix4(i, 3)
matrix5(i, 121) = matrix4(i, 4)
matrix5(i, 122) = matrix4(i, 5)
matrix5(i, 123) = matrix4(i, 6)
Next i
End If
MsgBox (" PROCEDURE DONE ")
```

Section B-2: Calling-Command for Physical Properties

Part A: Declarations
Dim Dnozzle As Single, Uliquid As Single, Height As Single, Tliquid As Single
Dim Tambient As Single, Humidity As Single
Dim Vconc As Single, flow As Single, liq As Byte
Dim liqdin As Single, liqsur As Double, liqvis As Double, airdin As Single
Dim airvis As Double, LMw As Single
Dim VMw As Single, LMb As Single, LBb As Single, ppf As Single
Dim psatf As Single, fuelvapourvis As Double, liquidtype As Byte
Dim a1 As Single, b1 As Single, c1 As Single, d1 As Single, a2 As Single
Dim b2 As Single, c2 As Single, a3 As Double, b3 As Single
Dim c3 As Single, d3 As Single, a4 As Single, b4 As Single, c4 As Single
Dim d4 As Double, e4 As Single, A5 As Single, B5 As Single, C5 As Single
Dim ppa As Single, ppv As Single, Ra As Single, Rv As Single, Rf As Single
Dim psatv As Single, molwatervapour As Single, molfuelvapour As Single
Dim dryairvis As Single, watervapourvis As Single, moldryair As Single
Dim moltotal As Single, molfractiona As Single, molfractionv As Single
dim molfractionf As Single
Dim rationair As Single, ratiovapour As Single, rationfuel As Single
Part B: Data Base
Tliquid = matrix3(2, 1)
Tambient = matrix3(3, 1)
Humidity = matrix3(4, 1)
Vconc = matrix3(5, 1)
If matrix3(1, 1) = 1 Then
liquidtype = 1
LMw = 18.02
VMw = 18.02
LMb = 273.15
LBb = 373.15
Density Coefficients
a1 = 0.325
b1 = 0.27
c1 = 647.13
d1 = 0.23
Surface Tension Coefficients
a2 = 134.834
b2 = 647.13
c2 = 1
Fuel Vapour Viscosity Coefficients
a3 = 0.00000061842
b3 = 0.6778
c3 = 847.22
d3 = 74074
Liquid Fuel Viscosity Coefficients
a4 = -52.84
b4 = 3704
c4 = 5.866
d4 = -5.8791E-29
e4 = 10
Antoines Coefficients
A5 = 4.6543
B5 = 1435.264
C5 = -64.848
End If
If matrix3(1, 1) = 2 Then
liquidtype = 1
LMw = 46.069
VMw = 46.069
LMb = 159.05
LBb = 351.44
a1 = 0.276
b1 = 0.27668
c1 = 516.25
d1 = 0.2367
a2 = 43.807
b2 = 516.25
c2 = 0.8
a3 = 0.00000106
b3 = 0.8066
c3 = 527
d3 = 0
a4 = 7.875
b4 = 782
c4 = -3.042
d4 = 0
e4 = 0
A5 = 5.37229
B5 = 1670.409
C5 = -40.191
End If
If matrix3(1, 1) = 3 Then
liquidtype = 1
LMw = 78.11
VMw = 78.11
LMb = 278.68
LBb = 353.24
a1 = 0.3017
b1 = 0.26855
c1 = 562.16
d1 = 0.2818
a2 = 71.95
b2 = 562.16
c2 = 1.2389
a3 = 0.000000031347
b3 = 0.9676
c3 = 7.9
d3 = 0
a4 = -7.37
b4 = 1038
c4 = -0.6181
d4 = -1.02E-28
e4 = 10
A5 = 4.01814
B5 = 1203.835
C5 = -53.226
End If
If matrix3(1, 1) = 4 Then
liquidtype = 1
LMw = 72.15
VMw = 72.15
LMb = 143.42
LBb = 309.22
a1 = 0.231
b1 = 0.26874
c1 = 469.65
d1 = 0.28215
a2 = 52.09
b2 = 469.65
c2 = 1.2054
a3 = 0.000000063411
b3 = 0.8476
c3 = 41.722
d3 = 0
a4 = -20.38
b4 = 1050

```
c4 = 1.487
d4 = -2.017E-27
e4 = 10
A5 = 3.9892
B5 = 1070.617
C5 = -40.454
End If
If matrix3(1, 1) = 5 Then
liquidtype = 1
LMw = 86.17
VMw = 86.17
LMb = 177.83
LBb = 341.88
a1 = 0.233
b1 = 0.26601
c1 = 507.43
d1 = 0.2781
a2 = 56.081
b2 = 507.43
c2 = 1.2843
a3 = 0.00000017505
b3 = 0.7074
c3 = 157.11
d3 = 0
a4 = -20.71
b4 = 1208
c4 = 1.499
d4 = 0
e4 = 0
A5 = 4.00266
B5 = 1171.53
C5 = -48.784
End If
If matrix3(1, 1) = 6 Then
liquidtype = 1
LMw = 92.141
VMw = 92.141
LMb = 178.18
LBb = 383.78
a1 = 0.2918
b1 = 0.26188
c1 = 591.79
d1 = 0.29889
a2 = 66.85
b2 = 591.79
c2 = 1.2456
a3 = 0.00000087274
b3 = 0.494
c3 = 323.78
d3 = 0
a4 = -60.67
b4 = 3149
c4 = 7.482
d4 = -5.709E-27
e4 = 10
A5 = 4.14157
B5 = 1377.578
C5 = -50.507
End If
```

Part C: Calculating Density, Viscosity and Surface Tension

```
If liquidtype = 1 Then
liqdin = (a1 / (b1 ^ ((1 - (Tliquid / c1)) ^ d1))) * 1000
liqsur = (a2 * ((1 - (Tliquid / b2)) ^ c2)) / 1000
liqvis = (1000 * Math.Exp((a4 + (b4 / Tliquid) + (c4 * Math.Log(Tliquid)) + (d4 * (Tliquid ^ e4))))) / 1000
fuelvapourvis = (1000 * a3 * (Tambient ^ b3) / (1 + (c3 / Tambient) + (d3 / (Tambient ^ 2)))) / 1000
End If
```

Part D: Calculating Air Density

```
psatv = (10 ^ (4.6543 - (1435.265 / (Tambient - 64.848)))) * 101325
psatf = (10 ^ (A5 - (B5 / (C5 + Tambient)))) * 101325
ppv = Humidity * psatv
ppf = Vconc * psatf
Ra = 287.058
Rv = 461.495
Rf = 8314.4 / VMw
If matrix3(1, 1) = 1 Then
psatf = 0
ppf = 0
Rf = 0
ppa = 101325 - ppv
airdin = (ppa / (Ra * Tambient)) + (ppv / (Rv * Tambient))
Else
ppa = 101325 - ppv - ppf
airdin = (ppa / (Ra * Tambient)) + (ppv / (Rv * Tambient)) + (ppf / (Rf * Tambient))
Form2.Text12.Text = (ppf / (Rf * Tambient))
End If
Form2.Text13.Text = airdin
Form4.Text1(7).Text = airdin
Form2.Text1.Text = Tambient
Form2.Text2.Text = Ra
Form2.Text3.Text = Rv
Form2.Text4.Text = Rf
Form2.Text5.Text = psatv
Form2.Text6.Text = psatf
Form2.Text7.Text = ppa
Form2.Text8.Text = ppv
Form2.Text9.Text = ppf
Form2.Text10.Text = (ppa / (Ra * Tambient))
Form2.Text11.Text = (ppv / (Rv * Tambient))
If Form2.Text11.Text = "" Then
Form2.Text11.Text = 0
End If
```

Part E: Calculating Air Viscosity

```
dryairvis = (1000 * 0.0000014241 * (Tambient ^ 0.5039) / (1 + (108.28 / Tambient) + (0 / (Tambient ^ 2)))) / 1000
watervapourvis = (1000 * 0.00000061842 * (Tambient ^ 0.6778) / (1 + (847.22 / Tambient) + (74074 / (Tambient ^ 2)))) / 1000
moldryair = ppa / (8.3144 * Tambient)
molwatervapour = ppv / (8.3144 * Tambient)
molfuelvapour = ppf / (8.3144 * Tambient)
moltotal = moldryair + molwatervapour + molfuelvapour
molfractiona = moldryair / moltotal
molfractionv = molwatervapour / moltotal
molfractionf = molfuelvapour / moltotal
rationair = 5.38516
rationvapour = 4.244997
rationfuel = MWv ^ 0.5
If matrix3(1, 1) = 1 Then
fuelvapourvis = 0
airvis = ((molfractiona * rationair * dryairvis) + (molfractionv * rationvapour * watervapourvis)) / ((molfractiona * rationair) + (molfractionv * rationvapour))
Else
airvis = ((molfractiona * rationair * dryairvis) + (molfractionv * rationvapour * watervapourvis) +
```

```
(molfractionf * rationfuel * fuelvapourvis)) /
((molfractiona * rationair) + (molfractionv *
ratiovapour) + (molfractionf * rationfuel))
End If
Form3.Text1.Text = dryairvis
Form3.Text2.Text = watervapourvis
Form3.Text3.Text = fuelvapourvis
Form3.Text4.Text = molfractiona
Form3.Text5.Text = molfractionv
Form3.Text6.Text = molfractionf
Form3.Text7.Text = airvis
Form4.Text1(8).Text = airvis
Form4.Text1(0).Text = LMw
Form4.Text1(1).Text = VMw
Form4.Text1(2).Text = LMb
Form4.Text1(3).Text = LBb
Form4.Text1(4).Text = liqdin
Form4.Text1(5).Text = liqsur
Form4.Text1(6).Text = liqvis
matrix4(1, 1) = LMw
matrix4(2, 1) = VMw
matrix4(3, 1) = LMb
matrix4(4, 1) = LBb
matrix4(5, 1) = liqdin
matrix4(6, 1) = liqsur
matrix4(7, 1) = liqvis
matrix4(8, 1) = airdin
matrix4(9, 1) = airvis
matrix4(10, 1) = ppv
matrix4(11, 1) = psatv
matrix4(12, 1) = ppf
matrix4(13, 1) = psatf
```

Section B-3: Calling-Command for Secondary Breakup

Part A: Declarations

```
Dim Uliquid As Single, Tambient As Single, airdin
As Single, airvis As Double
Dim liqdin As Single, liqsur As Double, liqvis As
Double
Dim k As Double, y As Double, z As Double, aa As
Double, bb As Double
Dim cc As Double, ReAter As Single
Dim step As Single, step2 As Single, right As
Double, right2 As Double, re As Single,
Dim freepath As Double, correction As Double,
Vcrit As Single, Vter As Single
```

Part B: Reading Data

```
Uliquid = matrix1(1, 7)
liqdin = matrix1(2, 7)
liqsur = matrix1(3, 7)
liqvis = matrix1(4, 7)
airdin = matrix1(5, 7)
airvis = matrix1(6, 7)
Tambient = matrix1(7, 7)
For i = 1 To 20010
If matrix1(i, 6) > 0 Then
matrix2(i, 1) = matrix1(i, 1)
matrix2(i, 2) = matrix1(i, 2)
matrix2(i, 3) = matrix1(i, 3)
matrix2(i, 4) = matrix1(i, 6)
End If
Next i
```

Part C: Calculating Critical Velocity

```
For i = 1 To 20010
If matrix2(i, 4) > 0 Then
k = 24 * airvis * airdin
y = 3.6 * (airdin ^ 1.687) * ((matrix2(i, 3) /
1000000) ^ 0.687) * (airvis ^ 0.313)
z = 8 * liqsur * airdin
step = 0.01
Vcrit = 0
For s = 1 To 150000
right = (k * Vcrit) + (y * (Vcrit ^ 1.687))
If right < z Then
Vcrit = s * step
End If
Next s
re = airdin * Vcrit * (matrix2(i, 3) / 1000000) /
airvis
If re > 1000 Then
Vcrit = ((18.18 * liqsur) / (airdin * (matrix2(i, 3) /
1000000))) ^ 0.5
End If
matrix2(i, 5) = Vcrit
End If
Next i
```

Part D: Calculating Terminal Velocity

```
For i = 1 To 20010
If matrix2(i, 4) > 0 Then
freepath = 0.0664 * (Tambient / 293) * ((1 + (110 /
293)) / (1 + (110 / Tambient)))
correction = 1 + ((freepath / matrix2(i, 3)) * (2.34 +
(1.05 * Math.Exp((0.61 - 1) * matrix2(i, 3) /
freepath))))
Vter = (liqdin - airdin) * 9.81 * correction *
((matrix2(i, 3) / 1000000) ^ 2) / (18 * airvis)
ReAter = airdin * Vter * matrix2(i, 3) / (airvis *
1000000)
If ReAter > 1 Then
aa = 72 * airvis * airdin
bb = 10.8 * (airvis ^ 0.313) * (airdin ^ 1.687) *
((matrix2(i, 3) / 1000000) ^ 0.687)
cc = 4 * liqdin * 9.81 * ((matrix2(i, 3) / 1000000) ^
2) * airdin
step2 = 0.01
Vter = 0
For v = 1 To 25000
right2 = (aa * Vter) + (bb * (Vter ^ 1.687))
If right2 < cc Then
Vter = v * step
End If
Next v
ReAter = airdin * Vter * matrix2(i, 3) / (airvis *
1000000)
End If
If ReAter > 1000 Then
Vter = (29.7272 * liqdin * matrix2(i, 3) / (airdin *
1000000)) ^ 0.5
End If
matrix2(i, 6) = Vter
End If
Next i
```

Part E: Secondary Disintegration

```
For i = 1 To 20010
If matrix2(i, 4) > 0 Then
matrix2(i, 7) = Uliquid
End If
Next i
For i = 1 To 20010
If matrix2(i, 5) < matrix2(i, 7) And matrix2(i, 5) > 0
Then
matrix2(i, 8) = ((6.2 * (liqvis ^ 0.5) * ((matrix2(i, 3)
/ 1000000) ^ 0.5)) / ((liqdin ^ 0.25) * (airdin ^ 0.25)
* ((matrix2(i, 7)) ^ 0.5))) * 1000000
matrix2(i, 9) = matrix2(i, 8) * 1.2
matrix2(i, 10) = matrix2(i, 9) * 3.15
End If
Next i
```

```
For i = 1 To 20010
If matrix2(20011 - i, 10) > 0 Then
For v = 1 To 20010
If matrix2(20011 - i, 10) > matrix2(v, 2) Then
matrix2(v, 4) = matrix2(v, 4) + (((1 - Math.Exp(-
0.693 * ((matrix2(v, 2) / matrix2(20011 - i, 9)) ^
2))) - (1 - Math.Exp(-0.693 * ((matrix2(v, 1) /
matrix2(20011 - i, 9)) ^ 2)))) * matrix2(20011 - i,
4))
End If
If matrix2(20011 - i, 10) <= matrix2(v, 2) And
matrix2(20011 - i, 10) > matrix2(v, 1) Then
matrix2(v, 4) = matrix2(v, 4) + (((1 - Math.Exp(-
0.693 * ((matrix2(20011 - i, 10) / matrix2(20011 - i,
9)) ^ 2))) - (1 - Math.Exp(-0.693 * ((matrix2(v, 1) /
matrix2(20011 - i, 9)) ^ 2)))) * matrix2(20011 - i,
4))
End If
Next v
End If
Next i
For i = 1 To 20010
If matrix2(i, 8) > 0 Then
matrix2(i, 4) = 0
End If
Next i
For i = 1 To 20010
matrix2(i, 8) = 0
matrix2(i, 9) = 0
Next i
```

Section B-4: Calling-Command for 1st meter of Free-Falling

Part A: Declarations

```
Dim Tliquid As Single, Tambient As Single, liq As
Byte, VMw As Single
Dim fallH As Single, ppv As Single, psatv As
Single
Dim liqdin As Single, liqsur As Double, liqvis As
Double, airdin As Single
Dim airvis As Double, ppf As Single, psatf As
Single
Dim distance1 As Single, flow As Single
Dim vcount As Double, xcount As Double, tcount
As Double, vapp As Single
Dim rynold As Single, dragco As Single
Dim ttotal As Single, vfinal As Single, adrag As
Single, atotal As Single
Dim v As Single, x As Single
Dim tconst As Double, xconst As Double, breekup
Dim dv, molar As Single, R As Single, saturated As
Single, partial As Single
Dim sr As Single
Dim Tfilm As Single, Reevap As Single, scevap As
Single, dreal As Double
Dim rynoldm As Single, adragm As Single, dinvis
As Double, evap1 As Double
Dim evap2 As Double
```

Part B: Reading Data

```
fallH = matrix2(1, 25)
airdin = matrix2(2, 25)
airvis = matrix2(3, 25)
liqdin = matrix2(4, 25)
liqsur = matrix2(5, 25)
liqvis = matrix2(6, 25)
Tliquid = matrix2(7, 25)
Tambient = matrix2(8, 25)
VMw = matrix2(9, 25)
liq = matrix2(10, 25)
psatv = matrix2(11, 25)
psatf = matrix2(12, 25)
ppv = matrix2(13, 25)
ppf = matrix2(14, 25)
distance1 = matrix2(15, 25)
flow = matrix2(16, 25
```

Part C: Calculating Droplets Acceleration/Deceleration

```
For i = 1 To 20010
If matrix3(i, 5) > 0 Then
If matrix3(i, 6) >= matrix3(i, 7) Then
matrix3(i, 8) = 11
Else
matrix3(i, 8) = 22
End If
End If
Next i
For i = 1 To 20010
If matrix3(i, 8) = 11 Then
vcount = matrix3(i, 7)
tcount = 0
xcount = 0
If matrix3(i, 6) < matrix3(i, 5) Then
vapp = 0.95 * matrix3(i, 6)
End If
If matrix3(i, 5) < (0.95 * matrix3(i, 6)) Then
vapp = matrix3(i, 5)
End If
If matrix3(i, 5) < matrix3(i, 6) And matrix3(i, 5) >
(0.95 * matrix3(i, 6)) Then
vapp = 0.95 * matrix3(i, 5)
End If
rynoldm = (airdin * (matrix3(i, 3) / 1000000)) /
airvis
adragm = (3 * airdin) / (4 * liqdin * (matrix3(i, 3) /
1000000))
For v = 1 To 1000
If xcount < distance1 And vcount < vapp Then
rynold = rynoldm * vcount
If rynold < 1 Then
dragco = 24 / rynold
End If
If rynold >= 1 And rynold < 1000 Then
dragco = (24 / rynold) * (1 + (0.15 * (rynold ^
0.687)))
End If
If rynold >= 1000 Then
dragco = 0.44
End If
adrag = adragm * dragco * (vcount ^ 2)
atotal = 9.81 - adrag
v = atotal * 0.01
x = (vcount * 0.01) + (0.5 * atotal * 0.0001)
vcount = vcount + v
xcount = xcount + x
tcount = tcount + 0.01
End If
Next v
If xcount >= distance1 Then
ttotal = tcount
vfinal = vcount
tconst = 0
xconst = 0
breekup = 3
End If
If vcount >= vapp And matrix3(i, 6) < matrix3(i, 5)
Then
xconst = distance1 - xcount
tconst = xconst / matrix3(i, 6)
ttotal = tcount + tconst
```

```
vfinal = matrix3(i, 6)
breekup = 7
End If
If vcount >= vapp And matrix3(i, 6) >= matrix3(i,
5) Then
xconst = 0
tconst = 0
ttotal = tcount
vfinal = matrix3(i, 5)
breekup = 10
End If
matrix3(i, 9) = tcount
matrix3(i, 10) = xcount
matrix3(i, 11) = tconst
matrix3(i, 12) = xconst
matrix3(i, 13) = ttotal
matrix3(i, 14) = vfinal
matrix3(i, 15) = breekup
End If
If matrix3(i, 8) = 22 Then
If matrix3(i, 3) < 100 Then
matrix3(i, 9) = 0
matrix3(i, 10) = 0
matrix3(i, 11) = distance1 / matrix3(i, 6)
matrix3(i, 12) = distance1
matrix3(i, 13) = matrix3(i, 11)
matrix3(i, 14) = matrix3(i, 6)
matrix3(i, 15) = 7
End If
If matrix3(i, 3) > 100 Then
vcount = matrix3(i, 7)
tcount = 0
xcount = 0
vapp = 1.2 * matrix3(i, 6)
rynoldm = (airdin * (matrix3(i, 3) / 1000000)) /
airvis
adragm = (3 * airdin) / (4 * liqdin * (matrix3(i, 3) /
1000000))
For n = 1 To 1000
If xcount < distance1 And vcount > vapp Then
rynold = rynoldm * vcount
If rynold < 1 Then
dragco = 24 / rynold
End If
If rynold >= 1 And rynold < 1000 Then
dragco = (24 / rynold) * (1 + (0.15 * (rynold ^
0.687)))
End If
If rynold >= 1000 Then
dragco = 0.44
End If
adrag = adragm * dragco * (vcount ^ 2)
atotal = 9.81 - adrag
v = atotal * 0.001
x = (vcount * 0.001) + (0.5 * atotal * 0.000001)
vcount = vcount + v
xcount = xcount + x
tcount = tcount + 0.001
End If
Next n
If xcount >= distance1 Then
ttotal = tcount
vfinal = vcount
tconst = 0
xconst = 0
breekup = 3
End If
If vcount <= vapp Then
xconst = distance1 - xcount
tconst = xconst / matrix3(i, 5)
ttotal = tcount + tconst
vfinal = matrix3(i, 6)
breekup = 7
End If
matrix3(i, 9) = tcount
matrix3(i, 10) = xcount
matrix3(i, 11) = tconst
matrix3(i, 12) = xconst
matrix3(i, 13) = ttotal
matrix3(i, 14) = vfinal
matrix3(i, 15) = breekup
End If
End If
```

Part D: Droplets Disintegration

```
For m = 1 To 20010
If matrix3(i, 15) = 10 Then
matrix3(i, 16) = ((6.2 * (liqvis ^ 0.5) * ((matrix3(i,
3) / 1000000) ^ 0.5)) / ((liqdin ^ 0.25) * (airdin ^
0.25) * (matrix3(i, 14) ^ 0.5))) * 1000000
matrix3(i, 17) = matrix3(i, 16) * 1.2
matrix3(i, 18) = matrix3(i, 17) * 3.15
End If
Next m
For f = 1 To 20010
If matrix3(20011 - f, 18) > 0 Then
For R = 1 To 20010
If matrix3(20011 - f, 18) > matrix3(R, 2) Then
matrix3(R, 4) = matrix3(R, 4) + (((1 - Math.Exp(-
0.693 * ((matrix3(R, 2) / matrix3(20011 - f, 17)) ^
2))) - (1 - Math.Exp(-0.693 * ((matrix3(R, 1) /
matrix3(20011 - f, 17)) ^ 2)))) * matrix3(20011 - f,
4))
End If
If matrix3(20011 - f, 18) <= matrix3(R, 2) And
matrix3(20011 - f, 18) > matrix3(R, 1) Then
matrix3(R, 4) = matrix3(R, 4) + (((1 - Math.Exp(-
0.693 * ((matrix3(20011 - f, 18) / matrix3(20011 - f,
17)) ^ 2))) - (1 - Math.Exp(-0.693 * ((matrix3(v, 1) /
matrix3(20011 - f, 17)) ^ 2)))) * matrix3(20011 - f,
4))
End If
Next R
End If
Next f
For p = 1 To 20010
If matrix3(i, 18) > 0 Then
matrix3(i, 4) = 0
matrix3(i, 5) = 0
matrix3(i, 6) = 0
matrix3(i, 7) = 0
matrix3(i, 8) = 0
matrix3(i, 9) = 0
matrix3(i, 10) = 0
matrix3(i, 11) = 0
matrix3(i, 12) = 0
matrix3(i, 13) = 0
matrix3(i, 14) = 0
matrix3(i, 15) = 0
matrix3(i, 16) = 0
matrix3(i, 17) = 0
matrix3(i, 18) = 0
End If
Next p
```

Part E: Droplets Evaporation

```
dv = 0.0000002581 * Tliquid
molar = VMw / 1000
R = 8.31
If liq = 1 Then
```

```
saturated = psatv
partial = ppv
sr = ppv / psatv
Else
saturated = psatf
partial = ppf
sr = ppf / psatf
End If
If sr < 0.95 Then
Tfilm = ((6.65 + (0.345 * Tambient) + (0.0031 *
(Tmbient ^ 2))) * (sr - 1)) / (1 + ((0.082 + (0.00782
* Tambient)) * (sr)))
Else
Tfilm = Tambient
End If
scevap = airvis / (airdin * dv)
dinvis = airdin / airvis
evap1 = (4 * dv * molar / (liqdin * R)) * ((saturated
/ Tambient) - (partial / Tfilm))
evap2 = 0.276 * (scevap ^ 0.3333)
For g = 1 To 20010
If matrix3(i, 4) > 0 Then
Reevap = dinvis * matrix3(i, 14) * (matrix3(i, 3) /
1000000)
matrix3(i, 19) = (evap1 * 1000000 / matrix3(i, 3)) *
(1 + (evap2 * (Reevap ^ 0.5)))
dreal = (matrix3(i, 3) / 1000000) - (matrix3(i, 19) *
matrix3(i, 13))
If dreal < 0 Then
matrix3(i, 20) = 0
Else
matrix3(i, 20) = dreal * 1000000
End If
Vapour Volume Fraction Of The Droplet
matrix3(i, 21) = ((matrix3(i, 3) ^ 3) - (matrix3(i, 20)
^ 3)) / (matrix3(i, 3) ^ 3)
Vapour Volume Fraction Of The Liquid
matrix3(i, 22) = matrix3(i, 21) * matrix3(i, 4)
New Droplet Size Volume Fraction
matrix3(i, 23) = matrix3(i, 4) - matrix3(i, 22)
End If
Next g
Next i
```

Section B-5: Calling-Command for Remaining falling meters.

Part A: Declarations

```
Dim Tliquid As Single, Tambient As Single, liq As
Byte, VMw As Single
dim fallH As Single, ppv As Single, psatv As
Single, liqdin As Single
Dim liqsur As Double, liqvis As Double, airdin As
Single, airvis As Double
Dim ppf As Single, psatf As Single, distance1 As
Single, flow As Single
Dim vcount As Double, xcount As Double, tcount
As Double, vapp As Single
Dim rynold As Single, dragco As Single, ttotal As
Single, vfinal As Single
Dim adrag As Single, atotal As Single, v As Single,
x As Single, tconst As Double
Dim, xconst As Double, breakup, dv, molar As
Single, R As Single, saturated As Single
Dim partial As Single, sr As Single, Tfilm As
Single, Reevap As Single
Dim, dreal As Double, scevap As Single, rynoldm
As Single, adragm As Single
Dim, dinvis As Double, evap1 As Double, evap2 As
Double
```

Part B: Reading Data

```
For i = 1 To 20010
matrix3(i, 4) = matrix2(i, 24)
matrix3(i, 7) = matrix2(i, 14)
matrix3(i, 8) = 0
matrix3(i, 9) = 0
matrix3(i, 10) = 0
matrix3(i, 11) = 0
matrix3(i, 12) = 0
matrix3(i, 13) = 0
matrix3(i, 14) = 0
matrix3(i, 15) = 0
matrix3(i, 16) = 0
matrix3(i, 17) = 0
matrix3(i, 18) = 0
matrix3(i, 19) = 0
matrix3(i, 20) = 0
matrix3(i, 21) = 0
matrix3(i, 22) = 0
matrix3(i, 23) = 0
matrix3(i, 24) = 0
Next i
fallH = matrix2(1, 25)
airdin = matrix2(2, 25)
airvis = matrix2(3, 25)
liqdin = matrix2(4, 25)
liqsur = matrix2(5, 25)
liqvis = matrix2(6, 25)
Tliquid = matrix2(7, 25)
Tambient = matrix2(8, 25)
VMw = matrix2(9, 25)
liq = matrix2(10, 25)
psatv = matrix2(11, 25)
psatf = matrix2(12, 25)
ppv = matrix2(13, 25)
ppf = matrix2(14, 25)
distance1 = matrix2(15, 25)
flow = matrix2(16, 25)
```

Part C: Calculating Droplets Acceleration/Deceleration

```
For i = 1 To 20010
If matrix3(i, 5) > 0 Then
If matrix3(i, 6) > matrix3(i, 7) Then
matrix3(i, 8) = 11
End If
If matrix3(i, 6) < matrix3(i, 7) Then
matrix3(i, 8) = 22
End If
If matrix3(i, 6) = matrix3(i, 7) Then
matrix3(i, 8) = 33
End If
End If
Next i
For i = 1 To 20010
If matrix3(i, 8) = 11 Then
vcount = matrix3(i, 7)
tcount = 0
xcount = 0
If matrix3(i, 6) < matrix3(i, 5) Then
vapp = 0.95 * matrix3(i, 6)
End If
If matrix3(i, 5) < (0.95 * matrix3(i, 6)) Then
vapp = matrix3(i, 5)
End If
If matrix3(i, 5) < matrix3(i, 6) And matrix3(i, 5) >
(0.95 * matrix3(i, 6)) Then
vapp = 0.95 * matrix3(i, 5)
End If
rynoldm = (airdin * (matrix3(i, 3) / 1000000)) /
airvis
```

```
adragm = (3 * airdin) / (4 * liqdin * (matrix3(i, 3) / 1000000))
For v = 1 To 1000
If xcount < distance1 And vcount < vapp Then
rynold = rynoldm * vcount
If rynold < 1 Then
dragco = 24 / rynold
End If
If rynold >= 1 And rynold < 1000 Then
dragco = (24 / rynold) * (1 + (0.15 * (rynold ^ 0.687)))
End If
If rynold >= 1000 Then
dragco = 0.44
End If
adrag = adragm * dragco * (vcount ^ 2)
atotal = 9.81 - adrag
v = atotal * 0.01
x = (vcount * 0.01) + (0.5 * atotal * 0.0001)
vcount = vcount + v
xcount = xcount + x
tcount = tcount + 0.01
End If
Next v
If xcount >= distance1 Then
ttotal = tcount
vfinal = vcount
tconst = 0
xconst = 0
breekup = 3
End If
If vcount >= vapp And matrix3(i, 6) < matrix3(i, 5) Then
xconst = distance1 - xcount
tconst = xconst / matrix3(i, 6)
ttotal = tcount + tconst
vfinal = matrix3(i, 6)
breekup = 7
End If
If vcount >= vapp And matrix3(i, 6) >= matrix3(i, 5) Then
xconst = 0
tconst = 0
ttotal = tcount
vfinal = matrix3(i, 5)
breekup = 10
End If
matrix3(i, 9) = tcount
matrix3(i, 10) = xcount
matrix3(i, 11) = tconst
matrix3(i, 12) = xconst
matrix3(i, 13) = ttotal
matrix3(i, 14) = vfinal
matrix3(i, 15) = breekup
End If
If matrix3(i, 8) = 22 Then
If matrix3(i, 3) < 100 Then
matrix3(i, 9) = 0
matrix3(i, 10) = 0
matrix3(i, 11) = distance1 / matrix3(i, 6)
matrix3(i, 12) = distance1
matrix3(i, 13) = matrix3(i, 11)
matrix3(i, 14) = matrix3(i, 6)
matrix3(i, 15) = 7
End If
If matrix3(i, 3) > 100 Then
vcount = matrix3(i, 7)
tcount = 0
xcount = 0
vapp = 1.2 * matrix3(i, 6)
rynoldm = (airdin * (matrix3(i, 3) / 1000000)) / airvis
adragm = (3 * airdin) / (4 * liqdin * (matrix3(i, 3) / 1000000))
For n = 1 To 1000
If xcount < distance1 And vcount > vapp Then
rynold = rynoldm * vcount
If rynold < 1 Then
dragco = 24 / rynold
End If
If rynold >= 1 And rynold < 1000 Then
dragco = (24 / rynold) * (1 + (0.15 * (rynold ^ 0.687)))
End If
If rynold >= 1000 Then
dragco = 0.44
End If
adrag = adragm * dragco * (vcount ^ 2)
atotal = 9.81 - adrag
v = atotal * 0.001
x = (vcount * 0.001) + (0.5 * atotal * 0.000001)
vcount = vcount + v
xcount = xcount + x
tcount = tcount + 0.001
End If
Next n
If xcount >= distance1 Then
ttotal = tcount
vfinal = vcount
tconst = 0
xconst = 0
breekup = 3
End If
If vcount <= vapp Then
xconst = distance1 - xcount
tconst = xconst / matrix3(i, 6)
ttotal = tcount + tconst
vfinal = matrix3(i, 6)
breekup = 7
End If
matrix3(i, 9) = tcount
matrix3(i, 10) = xcount
matrix3(i, 11) = tconst
matrix3(i, 12) = xconst
matrix3(i, 13) = ttotal
matrix3(i, 14) = vfinal
matrix3(i, 15) = breekup
End If
End If
If matrix3(i, 8) = 33 Then
matrix3(i, 9) = 0
matrix3(i, 10) = 0
matrix3(i, 11) = distance1 / matrix3(i, 6)
matrix3(i, 12) = distance1
matrix3(i, 13) = matrix3(i, 11)
matrix3(i, 14) = matrix3(i, 6)
matrix3(i, 15) = 7
End If
```

Part D: Droplets Disintegration

```
For m = 1 To 20010
If matrix3(i, 15) = 10 Then
matrix3(i, 16) = ((6.2 * (liqvis ^ 0.5) * ((matrix3(i, 3) / 1000000) ^ 0.5)) / ((liqdin ^ 0.25) * (airdin ^ 0.25) * (matrix3(i, 14) ^ 0.5))) * 1000000
matrix3(i, 17) = matrix3(i, 16) * 1.2
matrix3(i, 18) = matrix3(i, 17) * 3.15
End If
Next m
```

```
For f = 1 To 20010
If matrix3(20011 - f, 18) > 0 Then
For R = 1 To 20010
If matrix3(20011 - f, 18) > matrix3(R, 2) Then
matrix3(R, 4) = matrix3(R, 4) + (((1 - Math.Exp(-
0.693 * ((matrix3(R, 2) / matrix3(20011 - f, 17)) ^
2))) - (1 - Math.Exp(-0.693 * ((matrix3(R, 1) /
matrix3(20011 - f, 17)) ^ 2)))) * matrix3(20011 - f,
4))
End If
If matrix3(20011 - f, 18) <= matrix3(R, 2) And
matrix3(20011 - f, 18) > matrix3(R, 1) Then
matrix3(R, 4) = matrix3(R, 4) + (((1 - Math.Exp(-
0.693 * ((matrix3(20011 - f, 18) / matrix3(20011 - f,
17)) ^ 2))) - (1 - Math.Exp(-0.693 * ((matrix3(v, 1) /
matrix3(20011 - f, 17)) ^ 2)))) * matrix3(20011 - f,
4))
End If
Next R
End If
Next f
For p = 1 To 20010
If matrix3(i, 18) > 0 Then
matrix3(i, 4) = 0
matrix3(i, 5) = 0
matrix3(i, 6) = 0
matrix3(i, 7) = 0
matrix3(i, 8) = 0
matrix3(i, 9) = 0
matrix3(i, 10) = 0
matrix3(i, 11) = 0
matrix3(i, 12) = 0
matrix3(i, 13) = 0
matrix3(i, 14) = 0
matrix3(i, 15) = 0
matrix3(i, 16) = 0
matrix3(i, 17) = 0
matrix3(i, 18) = 0
End If
Next p
```

Part E: Droplets Evaporation

```
dv = 0.0000002581 * Tliquid
molar = VMw / 1000
R = 8.31
If liq = 1 Then
saturated = psatv
partial = ppv
sr = ppv / psatv
Else
saturated = psatf
partial = ppf
sr = ppf / psatf
End If
If sr < 0.95 Then
Tfilm = ((6.65 + (0.345 * Tambient) + (0.0031 *
(Tmbient ^ 2))) * (sr - 1)) / (1 + ((0.082 + (0.00782
* Tambient)) * (sr)))
Else
Tfilm = Tambient
End If
scevap = airvis / (airdin * dv)
dinvis = airdin / airvis
evap1 = (4 * dv * molar / (liqdin * R)) * ((saturated
/ Tambient) - (partial / Tfilm))
evap2 = 0.276 * (scevap ^ 0.3333)
For g = 1 To 20010
If matrix3(i, 4) > 0 Then
Reevap = dinvis * matrix3(i, 14) * (matrix3(i, 3) /
1000000)
matrix3(i, 19) = (evap1 * 1000000 / matrix3(i, 3)) *
(1 + (evap2 * (Reevap ^ 0.5)))
dreal = (matrix3(i, 3) / 1000000) - (matrix3(i, 19) *
matrix3(i, 13))
If dreal < 0 Then
matrix3(i, 20) = 0
Else
matrix3(i, 20) = dreal * 1000000
End If
Vapour Volume Fraction of The Droplet
matrix3(i, 21) = ((matrix3(i, 3) ^ 3) - (matrix3(i, 20)
^ 3)) / (matrix3(i, 3) ^ 3)
Vapour Volume Fraction of The Liquid
matrix3(i, 22) = matrix3(i, 21) * matrix3(i, 4)
New Droplet Size Volume Fraction
matrix3(i, 23) = matrix3(i, 4) - matrix3(i, 22)
End If
Next g
Next i
```

Section B-6: Calling-Command for Droplets Splashing.

Part A: Declarations

```
Dim matrix13(1 To 40010, 1 To 7) As Double
Dim matrix14(1 To 40010, 1 To 6) As Double
Dim matrix15(1 To 40010, 1 To 6) As Double
Dim st As Double, st2 As Double, st3 As Double,
steep2 As Double
Dim steep3 As Double, steep4 As Double, addition
As Double
```

Part B: Estimating Probability of Splashing

```
liqdin = matrix3(4, 25)
liqsur = matrix3(5, 25)
liqvis = matrix3(6, 25)
For i = 1 To 20010
If matrix3(i, 4) > 0 Then
matrix13(i, 1) = matrix3(i, 3) / 1000000
matrix13(i, 2) = matrix3(i, 24)
matrix13(i, 3) = matrix3(i, 14)
matrix16(i, 25) = matrix3(i, 25)
End If
Next i
For i = 1 To 20010
matrix13(i, 4) = (matrix13(i, 3) ^ 2) * liqdin *
matrix13(i, 1) / liqsur
matrix13(i, 5) = matrix13(i, 3) * liqdin * matrix13(i,
1) / liqvis
Next i
For i = 1 To 20010
matrix13(i, 7) = (matrix13(i, 4) ^ 0.5) * (matrix13(i,
5) ^ 0.25)
Next i
For i = 1 To 20010
If matrix13(i, 7) > 57.7 Then
matrix13(i, 6) = (matrix13(i, 1) * 4.23 * (((9 + ((2 *
matrix13(i, 4) * (matrix13(i, 4) + 12)) / matrix13(i,
5))) ^ 0.5) + 3)) / (matrix13(i, 4) + 12)
End If
Next i
```

Part C: Calculating Size Distribution of Generated Droplets

```
For R = 1 To 20010
matrix14(R, 1) = matrix13(R, 1)
matrix15(R, 1) = matrix13(R, 1)
Next R
For i = 1 To 20010
If matrix13(20011 - i, 6) > 0 Then
For k = 1 To 20010
matrix14(k, 2) = 0
matrix14(k, 3) = 0
```

```
matrix14(k, 4) = 0
matrix14(k, 5) = 0
matrix14(k, 6) = 0
Next k
For n = 1 To 20010
matrix14(n, 2) = matrix13(20011 - i, 6)
matrix14(n, 3) = matrix13(20011 - i, 2)
Next n
For v = 1 To 20010
If matrix14(v, 1) > 0 Then
st = Math.Log(matrix14(v, 1) / matrix14(v, 2))
st2 = st - 0.1666
st3 = st2 ^ 2
steep2 = Math.Exp((1 - 4) * st3)
steep3 = 0.977205 * steep2
steep4 = matrix14(v, 1)
matrix14(v, 4) = steep3 / steep4
End If
Next v
addition = 0
For z = 1 To 20010
addition = addition + matrix14(z, 4)
Next z
For L = 1 To 20010
matrix14(L, 5) = matrix14(L, 4) / addition
matrix14(L, 6) = matrix14(L, 5) * matrix14(L, 3)
Next L
For s = 1 To 20010
matrix15(s, 2) = matrix15(s, 2) + matrix14(s, 6)
Next s
End If
Next i
For i = 1 To 20010
matrix15(i, 3) = matrix13(i, 4)
matrix15(i, 4) = matrix13(i, 5)
matrix15(i, 5) = matrix13(i, 7)
matrix15(i, 6) = matrix13(i, 6)
Next i
For i = 1 To 20010
matrix16(i, 1) = matrix15(i, 1)
matrix16(i, 2) = matrix15(i, 2)
matrix16(i, 3) = matrix15(i, 3)
matrix16(i, 4) = matrix15(i, 4)
matrix16(i, 5) = matrix15(i, 5)
matrix16(i, 6) = matrix15(i, 6)
Next i
```

Section B-7: Sub-Command for Clearing Results

```
Form2.Text1.Text = ""
Form2.Text2.Text = ""
Form2.Text3.Text = ""
Form2.Text4.Text = ""
Form2.Text5.Text = ""
Form2.Text6.Text = ""
Form2.Text7.Text = ""
Form2.Text8.Text = ""
Form2.Text9.Text = ""
Form2.Text10.Text = ""
Form2.Text11.Text = ""
Form2.Text12.Text = ""
Form2.Text13.Text = ""
Form3.Text1.Text = ""
Form3.Text2.Text = ""
Form3.Text3.Text = ""
Form3.Text4.Text = ""
Form3.Text5.Text = ""
Form3.Text6.Text = ""
Form3.Text7.Text = ""
For i = 0 To 8
Form4.Text1(i) = ""
Next i
For i = 0 To 14
Form5.Text1(i) = ""
Next i
For i = 1 To 20010
For v = 1 To 126
matrix5(i, v) = 0
Next v
Next i
```

Section B-8: Sub-Command for Clearing All Data

```
Text1.Text = ""
Text2.Text = ""
Text3.Text = ""
Text4.Text = ""
Text5.Text = ""
Text6.Text = ""
Text7.Text = ""
Combo1.Text = ""
Form2.Text1.Text = ""
Form2.Text2.Text = ""
Form2.Text3.Text = ""
Form2.Text4.Text = ""
Form2.Text5.Text = ""
Form2.Text6.Text = ""
Form2.Text7.Text = ""
Form2.Text8.Text = ""
Form2.Text9.Text = ""
Form2.Text10.Text = ""
Form2.Text11.Text = ""
Form2.Text12.Text = ""
Form2.Text13.Text = ""
Form3.Text1.Text = ""
Form3.Text2.Text = ""
Form3.Text3.Text = ""
Form3.Text4.Text = ""
Form3.Text5.Text = ""
Form3.Text6.Text = ""
Form3.Text7.Text = ""
For i = 0 To 8
Form4.Text1(i) = ""
Next i
For i = 0 To 14
Form5.Text1(i) = ""
Next i
For i = 1 To 20010
For v = 1 To 126
matrix5(i, v) = 0
Next v
Next i
```

Section B-9: Sub-Command for Printing

```
Dim Book As Excel.Workbooks
Dim Wsheet As Excel.Worksheet
'Dim RngWSheet As Excel.Range
FileName = "d:\THE MODEL
PROGRAM\RESULTS.xls"
Set appxl = CreateObject("Excel.Application")
Set Book = appxl.Workbooks
Set Wsheet = Book.Add.Worksheets(1)
'Set rngWSheet = Wsheet.Cells
appxl.Visible = True
PRINTING INPUTS
Wsheet.Cells(1, 1) = "INPUTS:-"
Wsheet.Cells(1, 9) = "Dimensionless factors"
Wsheet.Cells(2, 1) = "pipe diameter(mm)="
Wsheet.Cells(2, 2) = Val(Text1.Text)
Wsheet.Cells(2, 3) = "liquid velocity(m/s)="
Wsheet.Cells(2, 4) = Val(Text2.Text)
Wsheet.Cells(2, 5) = "release height(m)="
```

```
Wsheet.Cells(2, 6) = Val(Text3.Text)
Wsheet.Cells(3, 1) = "liquid type"
Wsheet.Cells(3, 2) = Val(Form4.Text1(9).Text)
Wsheet.Cells(3, 3) = "Liquid Temp C ="
Wsheet.Cells(3, 4) = Val(Text4.Text)
Wsheet.Cells(3, 5) = "Ambient Temperature C ="
Wsheet.Cells(3, 6) = Val(Text5.Text)
Wsheet.Cells(4, 1) = "Humidity(%)= "
Wsheet.Cells(4, 2) = Val(Text6.Text)
Wsheet.Cells(4, 3) = "fuel vapour saturation(%) = "
Wsheet.Cells(4, 4) = Val(Text7.Text)
Dimentionless Factors
For i = 1 To 3
Wsheet.Cells(i + 1, 9) = Form5.Label3(i +
7).Caption
Wsheet.Cells(i + 1, 10) = Val(Form5.Text1(i +
7).Text)
Next i
For i = 1 To 4
Wsheet.Cells(i + 1, 11) = Form5.Label3(i +
10).Caption
Wsheet.Cells(i + 1, 12) = Val(Form5.Text1(i +
10).Text)
Next i
Printing Main Titles
Wsheet.Cells(5, 1) = "RESULTS:-"
Wsheet.Cells(6, 2) = "PHYSICAL"
Wsheet.Cells(6, 3) = "PROPERTIES"
Wsheet.Cells(6, 6) = "BREAKUP"
Wsheet.Cells(6, 7) = "CHARACTERISTICS"
Wsheet.Cells(6, 10) = "VAPOUR"
Wsheet.Cells(6, 11) = "GENERATION"
Wsheet.Cells(6, 13) = "AIR"
Wsheet.Cells(6, 14) = "DENSITY"
Wsheet.Cells(6, 15) = "AND"
Wsheet.Cells(6, 16) = "PRESSURE"
Wsheet.Cells(6, 17) = "DETAILS"
Wsheet.Cells(6, 18) = "AIR"
Wsheet.Cells(6, 19) = "VISCOSITY"
Wsheet.Cells(6, 20) = "DETAILS"
Printing Air Density Details
Wsheet.Cells(7, 13) = Form2.Label5(11).Caption
Wsheet.Cells(8, 13) = Form2.Label5(2).Caption
Wsheet.Cells(9, 13) = Form2.Label5(0).Caption
Wsheet.Cells(10, 13) = Form2.Label5(1).Caption
Wsheet.Cells(11, 13) = Form2.Label5(3).Caption
Wsheet.Cells(12, 13) = Form2.Label5(4).Caption
Wsheet.Cells(7, 16) = Form2.Label5(5).Caption
Wsheet.Cells(8, 16) = Form2.Label5(7).Caption
Wsheet.Cells(9, 16) = Form2.Label5(6).Caption
Wsheet.Cells(10, 16) = Form2.Label5(8).Caption
Wsheet.Cells(11, 16) = Form2.Label5(9).Caption
Wsheet.Cells(12, 16) = Form2.Label5(10).Caption
Wsheet.Cells(7, 14) = Val(Form2.Text1.Text)
Wsheet.Cells(8, 14) = Val(Form2.Text2.Text)
Wsheet.Cells(9, 14) = Val(Form2.Text3.Text)
Wsheet.Cells(10, 14) = Val(Form2.Text4.Text)
Wsheet.Cells(11, 14) = Val(Form2.Text5.Text)
Wsheet.Cells(12, 14) = Val(Form2.Text6.Text)
Wsheet.Cells(7, 17) = Val(Form2.Text7.Text)
Wsheet.Cells(8, 17) = Val(Form2.Text8.Text)
Wsheet.Cells(9, 17) = Val(Form2.Text9.Text)
Wsheet.Cells(10, 17) = Val(Form2.Text10.Text)
Wsheet.Cells(11, 17) = Val(Form2.Text11.Text)
Wsheet.Cells(12, 17) = Val(Form2.Text12.Text)
Printing Air Vicosity Details
Wsheet.Cells(7, 18) = Form3.Label5(11).Caption
Wsheet.Cells(8, 18) = Form3.Label5(0).Caption
Wsheet.Cells(9, 18) = Form3.Label5(1).Caption
Wsheet.Cells(10, 18) = Form3.Label5(2).Caption
Wsheet.Cells(11, 18) = Form3.Label5(3).Caption
Wsheet.Cells(12, 18) = Form3.Label5(4).Caption
Wsheet.Cells(7, 19) = Val(Form3.Text1.Text)
Wsheet.Cells(8, 19) = Val(Form3.Text2.Text)
Wsheet.Cells(9, 19) = Val(Form3.Text3.Text)
Wsheet.Cells(10, 19) = Val(Form3.Text4.Text)
Wsheet.Cells(11, 19) = Val(Form3.Text5.Text)
Wsheet.Cells(12, 19) = Val(Form3.Text6.Text)
Printing Physical Properties
For i = 0 To 4
Wsheet.Cells(i + 7, 1) = Form4.Label1(i).Caption
Wsheet.Cells(i + 7, 2) = Val(Form4.Text1(i).Text)
Next i
For i = 0 To 3
Wsheet.Cells(i + 7, 3) = Form4.Label1(i +
5).Caption
Wsheet.Cells(i + 7, 4) = Val(Form4.Text1(i +
5).Text)
Next i
Printing Primary Breakup
For i = 0 To 3
Wsheet.Cells(i + 7, 5) = Form5.Label3(i).Caption
Wsheet.Cells(i + 7, 6) = Val(Form5.Text1(i).Text)
Next i
For i = 4 To 7
Wsheet.Cells(i + 3, 7) = Form5.Label3(i).Caption
Wsheet.Cells(i + 3, 8) = Val(Form5.Text1(i).Text)
Next i
Printing Vapour Generation
Wsheet.Cells(7, 9) = "Vapour in 1st meter"
Wsheet.Cells(8, 9) = "Vapour in 2nd meter"
Wsheet.Cells(9, 9) = "Vapour in 3rd meter"
Wsheet.Cells(10, 9) = "Vapour in 4th meter"
Wsheet.Cells(11, 9) = "Vapour in 5th meter"
Wsheet.Cells(7, 11) = "Vapour in 6th meter"
Wsheet.Cells(8, 11) = "Vapour in 7th meter"
Wsheet.Cells(9, 11) = "Vapour in 8th meter"
Wsheet.Cells(10, 11) = "Vapour in 9th meter"
Wsheet.Cells(11, 11) = "Vapour in 10th meter"
For i = 1 To 5
Wsheet.Cells(i + 6, 10) = matrix5(i, 125)
Next i
For i = 1 To 5
Wsheet.Cells(i + 6, 12) = matrix5(i + 5, 125)
Next i
Printing Table Titles
Wsheet.Cells(14, 21) = "Ave diameter "
Wsheet.Cells(14, 22) = "Crit Vel "
Wsheet.Cells(14, 23) = "Term Vel "
Wsheet.Cells(14, 24) = "Fraction(Prim) "
Wsheet.Cells(14, 25) = "U liq "
Wsheet.Cells(14, 26) = "Dmax sec "
Wsheet.Cells(14, 27) = "Fraction(Sec) "
For i = 0 To 9
Wsheet.Cells(14, (28 + (11 * i))) = "ACC/DEC time "
Wsheet.Cells(14, (29 + (11 * i))) = "ACC/DEC Dis "
Wsheet.Cells(14, (30 + (11 * i))) = "falling time "
Wsheet.Cells(14, (31 + (11 * i))) = "V final "
Wsheet.Cells(14, (32 + (11 * i))) = "Frac "
Wsheet.Cells(14, (33 + (11 * i))) = "Dd/Dt "
Wsheet.Cells(14, (34 + (11 * i))) = "D real "
Wsheet.Cells(14, (35 + (11 * i))) = "Vap frac/drop "
Wsheet.Cells(14, (36 + (11 * i))) = "Vap Frac "
Wsheet.Cells(14, (37 + (11 * i))) = "Liq Frac "
Wsheet.Cells(14, (38 + (11 * i))) = "Final Frac "
Next i
Wsheet.Cells(14, 138) = "Ddrop "
Wsheet.Cells(14, 139) = "Frac splash "
```

```
Wsheet.Cells(14, 140) = "We "
Wsheet.Cells(14, 141) = "Re "
Wsheet.Cells(14, 142) = "K splash "
Wsheet.Cells(14, 143) = "D mean  "
Printing Table of Results
For i = 1 To 20010
For v = 1 To 125
If matrix5(i, 1) > 0 Then
Wsheet.Cells(i + 15, v + 20) = matrix5(i, v)
End If
Next v
Next i
Wsheet.SaveAs (FileName)
Book.Close
```

Appendix C

Appendix C1. Damage Estimates for Common Structures Based on Overpressure (Crowl, 2003)

Over Pressure (kPa)	Damage Effect
0.14	Annoying noise (137 dB if of low frequency 10–15 Hz)
0.21	Occasional breaking of large glass windows already under strain
0.28	Loud noise (143 dB), sonic boom, glass failure
0.69	Breakage of small windows under strain
1.03	Typical pressure for glass breakage
2.07	"Safe distance" (probability 0.95 of no serious damage below this value) - projectile limit, some damage to house ceilings, 10% window glass broken
2.76	Limited minor structural damage
3.4–6.9	Large and small windows usually shattered; occasional damage to window frames
4.8	Minor damage to house structures
6.9	Partial demolition of houses, made uninhabitable
6.9–13.8	Corrugated asbestos shattered, corrugated steel or aluminium panels, fastenings fail, followed by buckling, wood panels (standard housing) fastenings fail, panels blown in
9.0	Steel frame of clad building slightly distorted
13.8	Partial collapse of walls and roofs of houses
13.8–20.7	Concrete or cinder block walls, not reinforced, shattered
15.8	Lower limit of serious structural damage
17.2	50% destruction of brickwork of houses
20.7	Heavy machines (3000 lb) in industrial building suffered little damage, steel frame building distorted and pulled away from foundations.
20.7–27.6	Frameless, self-framing steel panel building demolished, rupture of oil storage tanks
27.6	Cladding of light industrial buildings ruptured
34.5	Wooden utility poles snapped, tall hydraulic press (40,000 lb) in building slightly damaged
34.5–48.2	Nearly complete destruction of houses
48.2	Loaded, lighter weight (British) train wagons overturned
48.2–55.1	Brick panels, 8–12 in. thick, not reinforced, fail by shearing or flexure
62.0	Loaded train boxcars completely demolished
68.9	Probable total destruction of buildings, heavy machine tools (7,000 lb)
2068	Limit of crater lip